N° d'ordre : 3678

THÈSE

PRESENTEE A

L'UNIVERSITÉ BORDEAUX I

ECOLE DOCTORALE DES SCIENCES CHIMIQUES

par **Sandrine Duluard**

POUR OBTENIR LE GRADE DE

DOCTEUR

Spécialité : Physico-chimie de la matière condensée.

STUDY AND SET-UP OF IONIC LIQUID BASED ELECTROLYTIC MEMBRANES FOR FLEXIBLE ELECTROCHROMIC DEVICES

Soutenance prévue le 21 novembre 2008

Après avis de :

A. Rougier, Université d'Amiens　　　　　　　　　*Rapporteur*

M. Subramanian, Oregon State University　　　　*Rapporteur*

C. Biver, Essilor International

G. Campet, CNRS-ICMCB

C. Delmas, CNRS-ICMCB

M.-H. Delville, CNRS-ICMCB

U. Posset, Fraunhofer Institute

L. Servant, Université Bordeaux 1

-2008-

We must learn to live together as brothers or perish together as fools

Nous devons apprendre à vivre ensemble comme des frères,

sinon nous mourrons ensemble comme des idiots

Martin Luther King, 1964

Acknowledgements / Remerciements
Introduction
List of symbols, abbreviations and acronyms
List of main products

Acknowledgements

I am very pleased to thank all the people who contributed to the achievement of my Ph-D.

First of all, I want to deeply thank Marie-Hélène Delville and Guy Campet, my supervisors. They gave me confidence to pursue this project and helped me to fulfil my objectives. I want to underline that I deeply appreciated their support both from professional and personal points of view. Their complementary knowledge and vision of the work contributed a lot to enrich this project.

I thank Mr. Delmas, director of the ICMCB who introduced me to my supervisors and who welcomed me in the laboratory. I am grateful that he judged my work as chairman of the jury and for his support in our actions for the students and staffs associations.

I also thank the jury members for having accepted to judge my work and especially Mrs Aline Rougier, University of Amiens, and Mr. Mas Subramanian, Oregon State University, the referees. It was an honour for me to benefit from your advices.

I want to express my profound gratitude to Mr. Jean-Claude Lassègues for is highly appreciated scientific contribution to this work and for its explanations on electrolytic membranes properties, especially in the light of Raman experiments. I thank Joseph Grondin who performed the experiments with great enthusiasm. I want also to thank Laurent Servant, who participated to the jury, and Suzanne Joiret, who both participated to the reflections on the subject.

Many thanks also to Isabelle Pianet, from the ISM, who introduced me to the PGSE-NMR technique and Axelle Grélard who allowed me to complementary measurements at IECB. I greatly appreciated your warm welcome and your assistance in the execution and analysis of the experiments.

I am also grateful to Fabrice Mauvy, Mario Maglione and Reyniault Van der Muhl from ICMCB who helped for the realization of temperature dependent impedance spectroscopy experiments.

Remerciements

J'ai le plaisir de remercier tous ceux qui ont contribué à la réalisation de mon travail de thèse. Si toutefois j'oubliais quelqu'un je le prie de bien vouloir m'en excuser.

Tout d'abord, je remercie de tout coeur Marie-Hélène Delville et Guy Campet, mes directeurs de thèse. Ils m'ont fait confiance pour mener ce projet et m'ont permis d'accomplir mes objectifs. J'ai beaucoup apprécié leur soutien tant du point de vue professionnel que personnel. Ils ont su chacun à leur manière, par leur connaissances complémentaires et leur manières de travailler contribuer à enrichir ce travail.

Je veux aussi remercier M. Delmas directeur de l'ICMCB pour m'avoir accueilli au laboratoire et m'avoir présenté à mes futurs directeurs de thèse. Je lui suis reconnaissante d'avoir pris le temps de juger mon travail en tant que président du jury.

Je remercie également les membres du jury pour avoir accepté de juger mon travail et plus particulièrement Mme Aline Rougier, de l'université d'Amiens, et M. Mas Subramanian, de l'Oregon State University, les deux rapporteurs de ces travaux. C'est un honneur pour moi de bénéficier de vos conseils.

J'adresse également mes remerciements les plus sincères à Jean-Claude Lassègues pour son importante contribution scientifique à ce travail, pour ses explications sur le fonctionnement des membranes électrolytiques à la lumière notamment des expériences de spectroscopie Raman. Je remercie Joseph Grondin qui a réalisé les manipulations avec beaucoup d'enthousiasme. J'aimerais aussi mentionner les contributions de Laurent Servant, qui faisait partie du jury, et Suzanne Joiret, qui bien que n'ayant pas débouché sur des manipulations dans le temps imparti ont participé à la réflexion.

Je tiens aussi à remercier Isabelle Pianet, de l'ISM, pour nous avoir présenté la technique de PGSE-NMR et Axelle Grélard qui nous a permis de compléter ces résultats par des mesures à l'IECB. J'ai beaucoup apprécié votre accueil chaleureux ainsi que pour votre aide précieuse pour la réalisation et l'analyse des données.

Introduction

The history of electrochromism (change of colour by application of an electrical current or potential) dates back from the nineteenth century. The last twenty years have seen an increasing research effort in this area and the emergence of a few commercial applications. Electrochromic devices can be darkened or lightened electronically. This capability gives the opportunity to control the amount of daylight or solar heat passing through a window or through a lens.
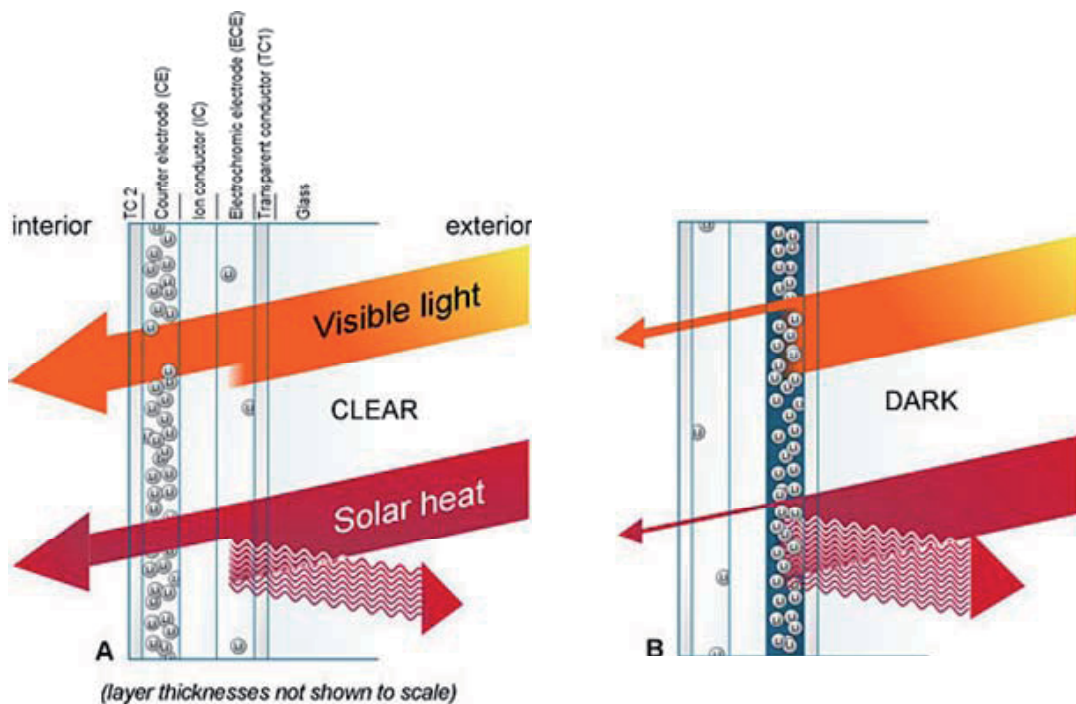
Diagram of a typical electrochromic coating[1].

Electrochromic devices (ECDs) can be used as automatically dimmed rear-view mirror; this is so far the biggest success of ECDs with several millions of pieces sold around the world by Gentex. They are also very valuable as energy-saving devices in buildings or cars, mostly for electrochromic devices with switchable infrared absorbance. In the area of visible sunlight modulation, the topic of this thesis, Saint-Gobain released an electrochromic sunroof that change colour from colourless to blue, however this device is up to now limited to luxury cars because of its high cost.

---

[1] http://windows.lbl.gov/comm_perf/Electrochromic/ec_tech.html

The Gentex's and Saint-Gobain's types of ECDs have relatively large power consumption due to the non bi-stability of the colouration in the first case and to the use of too low colouration efficiency (colour obtained for a given electrical charge) materials in the second case. Moreover, for low cost devices and for nomad applications such as ophthalmic lenses or textiles, the development of systems that consume less energy for both their manufacture and operation is mandatory. Therefore, the choice of bi-stable systems with high colouration efficiency seems very relevant. Furthermore, for ophthalmic lenses, the electrochromics have not drilled so far for two reasons: the excessive power consumption as discussed before but also the non neutral colour of the coloured state since the prototypes were blue.

The challenges in fabricating electrochromic windows lie in achieving low costs, high durability, and practical sizes. These observations have motivated the financial support by the European Commission of the Nanoeffects project that aimed at preparing electrochromic devices that are:

- low cost

- low energy consuming for both their manufacture and their operation

- prepared on plastic substrates, flat or curved, rigid or flexible

- long life

- neutrally coloured (brown or grey)

The Nanoeffects consortium ranged from basic to applicative work as it gathered both public research centres with expertise in the various elements of electrochromic systems and industrialists interested in the integration of this technology in ophthalmic lenses, automotive or textiles. In this manuscript, both basic elements on electrolytes and applied studies on the behaviour of EC materials and the preparation of electrochromic devices will be found.

It will begin with an overview of the advantages and drawbacks of some competitive technologies and an introduction on the operating principle of electrochromic devices and of their important parameters. The state of the art on both electrolytes and electrochromic materials will help to determine what the most interesting materials to fulfil the specifications are.

The materials chosen as a result of this survey are:

- Substrate: flexible polyethylene terephtalate (PET) film (and rigid Essilor's lens and borosilicate glass for studies)

- Transparent conductive layer: indium tin oxide (ITO) (on PET, ophthalmic lens or glass) or fluorine tin oxide (FTO) (exclusively on glass)

- Electrolyte: fluorinated ionic liquid (1-butyl-3-methylimidazolium hexa-fluorophosphate (BMIPF$_6$) and 1-butyl-3-methylimidazolium bis (trifluoromethanesulfonyl) imide (BMITFSI)) gelified by a polymer

- Material for cathodic colouration: Poly(3,4-ethylenedioxythiophene) (PEDOT), blue, with a colour modifier to obtain neutral colour

- Material for anodic colouration: Prussian Blue (PB)

- Colourless electroactive material: indium hexacyanoferrate (InHCF)

The thesis will focus in particular on:

- ❑ The preparation and study of jellified ionic liquid electrolytes (Chapter II)
- ❑ The preparation and study of electrochromic materials: PEDOT, BP and InHCF (Chapter III)
- ❑ The preparation and study of complete devices (Chapter IV).

Other aspects of the Nanoeffects project, including colour modification to get neutral colour and improvement of the bleached state of PEDOT, were studied by other partners in the consortium and will not be detailed here.

We will find in chapter II, studies on the effect of adding a lithium salt in ionic liquid based electrolytes as well as their jellification with PMMA. In particular, thermo-mechanical properties (glass transition temperature), optical quality, ionic conductivity and nature of the interactions in these mixtures are detailed.

In Chapter III, methods for electrochromic materials deposition are detailed: electrochemical deposition for PEDOT, BP and InHCF, in-situ chemical polymerisation of EDOT and PEDOT dispersion deposition. The characteristics of such films in ionic liquid based liquid electrolytes will be given.

In Chapter IV, the method for preparing full EC devices is described. The characteristics of these systems and in particular the influences of the electrical conductivity of the substrates and of the jellification of the electrolytes will be particularly described.
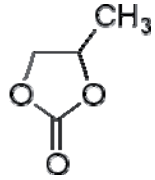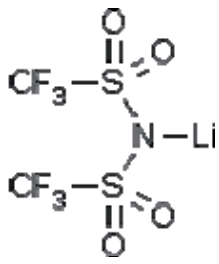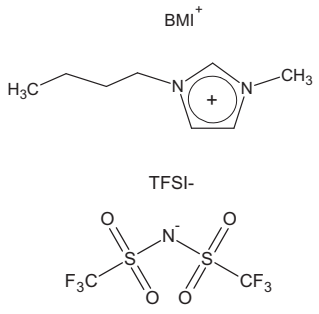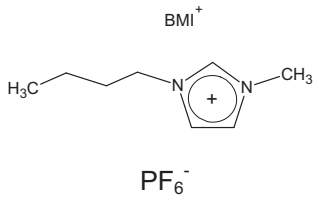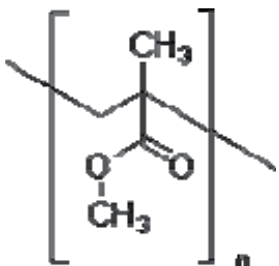
Finally we will conclude and give prospects for the applications of this work.

List of symbols, abbreviations and acronyms

$\Omega/\square$	Ohm per square, unit of sheet resistance
Λ	Molar conductivity
cm^2/C	Centimetre square per coulomb, unit of colouration efficiency
S	Siemens
σ	Conductivity
A	Absorbance
BMI	1-butyl-3-methylimidazolium
EMI	1-ethyl-3-methylimidazolium
$BMIPF_6$	1-butyl-3-methylimidazolium hexafluorophosphate
BMITFSI	1-butyl-3-methylimidazolium bis(trifluoromethanesulfonyl)imide
CE	Colouration Efficiency
CPE	Composite Polymer Electrolyte
CR	Contrast Ratio
CRPP	Centre de Recherche Paul Pascal
CVD	Chemical Vapour Deposition
DSC	Differential Scanning Calorimetry
D_x	Diffusion coefficient of x
EC	Electrochromic
ECD	Electrochromic device
EDOT	3,4 ethylene dioxythiophene
EIS	Electrochemical Impedance Spectroscopy
EP	Electropolymerization
FTIR-ATR	Fourier Transform InfraRed - Attenuated Total Reflectance
FTO	SnO_2:F
ICMCB	Institut de Chimie de la Matière Condensée de Bordeaux
IL	Ionic Liquid
InHCF	Indium hexacyanoferrate
ISP	In-Situ Polymerization
ITO	In_2O_3:Sn
ITZO	In_2O_3:Sn,Zn
LCA	Lyfe Cycle Assessment
MMA	Methyl methacrylate
NMR	Nuclear Magnetic Resonance
PB	Prussian Blue
PC	Propylene carbonate
PEDOT	Poly(3,4 ethylene dioxythiophene)
PEO	Poly(ethylene oxide)
PET	Poly(ethylene terephtalate)
PGSE	Pulsed Gradient Spin Echo
PSS	Poly(styrene sulfonate)
PTFE	Poly(tetrafluoroethylene)

PVD	Physical Vapour Deposition
Q	Electrical charge
RTIL	Room Temperature Ionic Liquid
SCE	Saturated Calomel Electrode
SPE	Solid Polymer Electrolyte
TBAP	Tetrabutyl ammonium perchlorate
TCO	Transparent Conductive Oxide
TFSI$^-$	Bis(trifluoromethanesulfonyl)imide
Tg	Glass transition temperature
Tos	Tosylate
VTF	Vogel-Tammann-Fulcher
XRD	X-Ray Diffraction

List of main products

Name	Abbreviation	Formula	M (g/mol)
4-Methyl-1,3-dioxolan-2-one	PC		102.1
Bis(trifluoromethylsulfonyl)imide lithium salt	LiTFSI		287.1
Lithium perchlorate	LiClO$_4$	LiClO$_4$	106.4
1-Butyl-3-methylimidazolium bis(trifluoromethylsulfonyl)imide	BMITFSI		419.4
1-Butyl-3-methylimidazolium hexafluorophosphate	BMIPF$_6$		284.2
Iron(III) chloride hexahydrate	FeCl$_3$. 6 H$_2$O	FeCl3. 6 H2O	270.3
Potassium hexacyanoferrate (III)	K$_3$Fe(CN)$_6$	K$_3$Fe(CN)$_6$	329.2
Poly(methyl methacrylate)	PMMA 1		Mw= 96000 Mn= 48000

Chapter I. Electrochromic devices: context, objectives and state of the art

I. 1. *Context of the study*

I. 1. 1. Light modulation devices

Studies on electrochromic (EC) devices enter into the scope of the more general "light modulation" research field. EC devices have a special insight in light colouration and intensity modulation. This function is traditionally fulfilled by movable curtains or light filters films. However, active shading devices are looked at for progressive and automatic light intensity modulation. They also maintain transparency during shading which is not the case of curtains. This particularly concerns eye wear industry and car windows applications, even though their use for building applications has also been developed. Other techniques than electrochromics could be used for the same function including mainly photochromics and liquid crystal devices. These three technologies will be briefly described and compared in this paragraph. Electrochromism will be presented in more details latter on.

I. 1. 1. 1. Electrochromism

Electrochromism is the reversible change of a chemical species between two redox states with distinguishable absorption spectra, such redox change being induced by application of an electrical current or a potential difference.[1] An electrochromic device behaves like a thin film battery that changes colour depending whether the battery is charged or discharged; two redox couples must be involved in between the two electrodes to ensure the working of the device, one species being oxidized while the other one is reduced.

The switching is generally fast for both colouration and bleaching. Times from less than one second to a few seconds, depending on the nature of the constituent of the electrochromic system, are classical. Larger devices (sunroof, windows) may have switching times increasing up to a few minutes.

This is represented by the following equation where B (Bleached) can be organic or inorganic. B (Bleached) and C (Coloured) are the two forms of a redox couple. The following two configurations can be found: B oxidised state / C reduced state or C oxidised state /B reduced state.

$$B_{\text{Bleached}} \underset{\text{Potential 2. fast}}{\overset{\text{Potential 1. fast}}{\rightleftharpoons}} C_{\text{Coloured}}$$
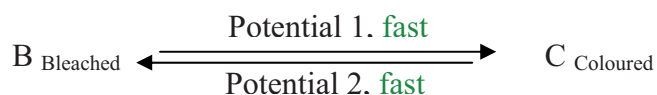
If both couples form insoluble films upon colouration, the system is bi-stable. On the contrary if one at least of the species is soluble, recombination between oxidised and reduced species takes place, the system is self-bleached and a constant application of current is required to maintain the colouration.

I. 1. 1. 2. Photochromism

Photochromism is the reversible change of a chemical species between two states with distinguishable absorption spectra, such a change being induced in at least one direction by the action of electromagnetic radiations[2].The inducing radiation is generally in the ultraviolet or visible range, and the change in the absorption spectra appears in the visible or near infrared regions. The reverse reaction is generally thermally induced, though it can sometimes be photochemical. The colouration takes a few seconds to tens of seconds depending on the nature of the photochromic species; however the reverse reaction is often longer: a few minutes to tens of minutes.

This can be represented by the following equation:

$$B_{Bleached} \underset{\Delta.\ slower}{\overset{h\nu.\ fast}{\rightleftarrows}} C_{Coloured}$$
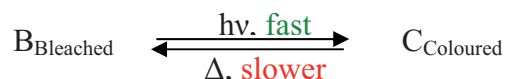
Commonly, state C is thermodynamically less stable than B.

The Transition[®] photochromic lenses are the most widely known application of photochromic materials (Figure I.1).

Figure I.1: Transitions[®] photochromic lenses

I. 1. 1. 3. Liquid crystal based devices

Liquid crystal based devices can reversibly change between two states with different absorption spectra depending on the orientation of the liquid crystal species as compared to light orientation.[3] The liquid crystal orientation is modified by applying an electrical field.

Colouration and bleaching times are very fast, as demonstrated by their widely spread use as displays. The required potentials are rather high, in the range of 10 V and the electrical field must be applied continuously to maintain the colouration.

Liquid crystals can be anchored on the electrodes (the corresponding devices are called LCD: Liquid Crystal Displays) or suspended in a polymer matrix in between two electrodes (SPD: Suspended Particles Devices)[4], the latter case simplifies the preparation of the device but leads to a diffuse state.

Due to defaults in the orientation of the liquid crystal species, the bleached state is not fully transparent. This is a major drawback for application that requires high colourlessness in the bleached state as for ophthalmic application.

I. 1. 1. 4. Light modulation devices: summary

The main characteristics for these three light modulation devices are summarized in Table I.1.

Property	ECD	Photochromic	Twisted Liquid crystal	SPD
Bleached state	**OK**	**OK**	NOK (intrinsic)	NOK(intrinsic)
Transparency	**OK**	**OK**	OK	NOK
Contrast	**OK**	**OK**	OK	OK
Colouration time	**OK**	**OK**	OK	OK
Bleaching time	**OK**	NOK	OK	OK
Colouration controller	**Electricity**	Environment (UV, T°C)	**Electricity**	**Electricity**
Bi-stability	**YES** or NO	n/a	NO	NO
Required voltage	**1-2 V**	n/a	10 V	10 V
Required intensity	1-10 mA/cm²	n/a	**n/a**	**n/a**
Layers	Electrode/EC1/ electrolyte/EC2/E lectrode	Photochromic layer	Electrode/film /liquid crystal/film /Electrode	Electrode / liquid crystal in a matrix/Electrode

Table I.1: Summary of the main characteristics of electrochromic devices (ECD), photochromic devices, twisted liquid crystal and suspended particle device (SPD).

Photochromic devices benefit from high colourlessness of the bleached state, good contrast ratio and colouration rates. However, the too slow bleaching speed and the dependence of the colouration on non controllable parameters such as sun light intensity and

external temperature are problematic. It is valuable to develop active systems such as electrochromic and liquid crystal based devices. ECD have been identified as being able to gather the advantages of both photochromic and liquid crystal devices: high colourlessness of the bleached state, good contrast ratio, high colouring and bleaching rates and transparency.

I. 1. 2. Electrochromism developments

The term "electrochromism" was first introduced in 1961 by Platt[5]. In 1969, Deb demonstrated the reversible colouration by UV-irradiation or electrical potential of thin films of tungsten trioxide WO_3.[6] This electrochromic material became one of the most widely studied and industrially used.

The French glass manufacturer, Saint-Gobain, proposed its first generation of EC smart windows in 1985. They were based on inorganic electrochromic layers (WO_3, IrO_x) and a proton-conducting solid polymer electrolyte; however, their fabrication, initially intended for building industry, had to be stopped in 1995 due to lack of long term durability. More recently, they have been working on a new all-solid type electrochromic prototype. These systems show rather high contrasts (transmissions from 1% to 16% or from 4% to 40% depending on the prototypes) with reasonable switching rates (50-100 s to reach 80% of the total coloration for 30*30 cm² devices). Saint-Gobain developed a special ECD encapsulation process to provide high durability to these systems[7]. Due to their high cost, the commercial development of such devices is directed toward niche market as Ferrari SuperAmerica roof-car (see Figure I.2) and possibly Airbus A 380 aircrafts windows.

Figure I.2: Ad from Saint Gobain at the release of their second generation of electrochromic devices on the Ferrari SuperAmerica (2005).

In 1987, Gentex industrialised an electrochromic rear-view mirror (see Figure I.3) based on liquid electrochromic species, the modified viologens[8]. It has been a commercial success with about 100 million pieces sold all-over the world. Rear-view mirrors market

totalised US $ 2.5 billion in 2003, sales amount of EC rear-view mirrors reached $500 M in 2006. Gentex-PPG Aerospace also developed ECDs that could be used as windows for the Boeing 787 Dreamliner.

Figure I.3 : Gentex auto-dimming rear-view mirrors

Efforts are now devoted by several manufacturers and research centres to reduce the cost of ECDs. For example, Bekaert is developing a roll-to-roll process with low temperature processing and high deposition rates in order to produce inorganic monolithic electrochromic devices, based on WO_3, and polymer substrates. Their target is a decrease of the price down to 100 €/m². The actual costs are about 1,500 €/pair for smart sunglasses, 800 €/m² for smart windows. As developed latter on, lowering the cost of ECDs is also an attribution of the Nanoeffects project.

For more details on electrochromism developments see reference 9 released in 2007 and International Meeting on Electrochromism proceedings.

I. 1. 3. The Nanoeffects project

The Specific Targeted Research European Project (STREP) **Nanoeffects** is supported by the European Community and deals with **Nano**composites with High Colouration **Eff**iciency for **E**lectro**C**hromic Smart Plastic Devices. This project gathered, during three and an half years (2004-2007), 12 teams from public and private research all over Europe and one partner from Canada with a common objective: the study and set-up of low cost electrochromic devices. The map shown below (Figure I.4) summarizes the location and skills of each partner. The competences of the consortium include material, films and devices preparation and characterisation.

7
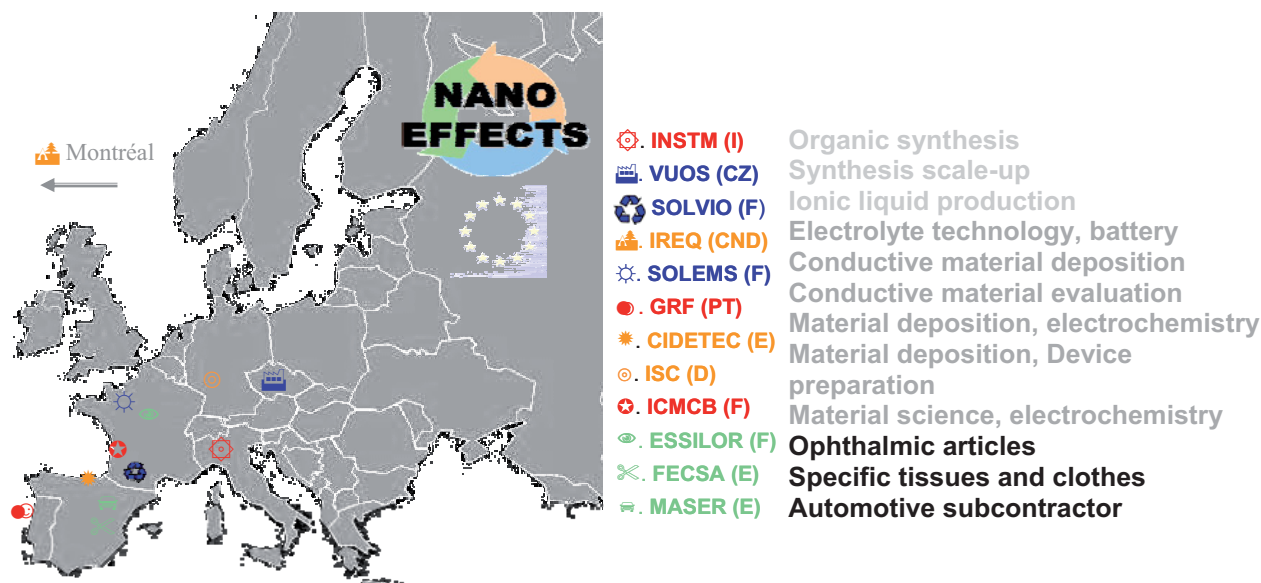
Figure I.4: From raw material synthesis to system set-up and preparation to industrial applications

The goal of the Nanoeffects project is the development of all-plastic ECD prototypes presenting the following specifications:

- Cost-effectiveness
- Low energy consumption both for fabrication and functioning
- Reasonable switching times (15 s. for small devices (50 cm²), 2 min for larger devices (2 500 cm²))
- Cycle lifetime $\geq 10^5$
- Operating temperature range -20 °C to 60 °C,
- Nearly no performance loss after 1 year at ambient exposure and 200 h Suntest$^{®}$

To fulfil this aim, the insight has been put towards:

- Low energy consuming and plastic compatible deposition processes (< 130°C, applicable on a broad variety of plastic substrates PET, PMMA, CR39$^{®}$).
- EC materials with high coloration efficiencies (> 120 cm²/C)
- New hydrophobic polymer electrolyte with optimised stability against humidity

ICMCB work was dealing with counter electrode, hydrophobic electrolyte, preparation and characterisations of complete devices.

I. 1. 4. Interest of plastic substrates

In the scope of the Nanoeffects project, an insight has been put forward on the use of plastic substrates. This choice is motivated by at least three reasons:

- Lower cost of plastic substrates (raw material and handling) as compared to glass ones

- Adaptability of the EC technology developed on plastic to eyewear lenses (such as polycarbonate)

- Possibility to preparation flexible devices

- Possibility to adapt EC devices prepared on flexible plastic substrates on existing windows and on curved surfaces by retrofit (see Figure I.5).

Figure I.5 : Illustration of the lamination of an EC device prepared on flexible plastic on a flat substrate. This substrate could be curved, flexible, etc.

- Possibility to replace ECDs in case of failure. This is of particular great interest for building industry since a long warranty is required (minimum 10 years in France, 20 years in USA).

Indirectly, plastic substrate requires the use of low temperature material deposition procedures (T max = 120°C) which is energetically beneficial and enters into the specifications of the Nanoeffects project i.e. low energy consumption.

I. 1. 5. ECD for lowering energy consumption

The energetic resources being physically limited on the Earth, efforts towards lowering of energy consumption are mandatory. Electrochromic devices can help to regulate our energy consumption for example in building or in cars by adapting incident light transmitted through windows depending on the weather conditions, IR modulation is the most valuable for this application. The determination of the energetic benefit of such devices requires a complete life cycle assessment (LCA) (fabrication, life time, waste recycling and storage). Energy saving must be done at each step of the process from the fabrication to the

functioning of the devices and finally its recycling. These efforts are encouraged by the European commission as for example through the Nanoeffects project. Energetic analyses of EC devices during their life time are studied by the National Renewable Energy Laboratory (NREL) in the US. NREL also makes available on internet a database, the LCI 'Life-Cycle inventory' that gives inputs for the preparation of Life-Cycle Assessment (LCA) for example for EC devices. Quantified results are expected for the type of devices we used in this project, since the LCA aspect will be addressed within the European project Innoshade that has begun in September, 2008.

I. 2. *Electrochromism principle and key parameters*

I. 2. 1. Electrochromism principle

An electrochromic material is a material which exhibits an optical absorption band in the visible region in one of its two oxidation states. It is generally related to the presence of a mixed redox state of the metallic centre for M_xO_y or to highly conjugated systems of conductive polymers. By extension, this definition includes materials having a modulation of their IR- reflectivity upon electrochemical reaction.[1] The term electrochemichromism is sometimes used for such systems however the general term 'electrochromism' will be preferred in the following for sake of simplicity.

An electrochromic device (ECD) is designed like a micro-battery, i.e. composed of a working electrode, a counter-electrode and an electrolyte in thin-film forms. The working and counter electrodes are generally based on electrochromic materials with complementary colourations (namely colouring upon reduction and oxidation respectively). The working principle of an electrochromic device (ECD) is represented in Figure I.6. It is made of five components: two transparent conductive substrates, two electro-active materials (EC1 and EC2) one at least being electrochromic and an electrolyte.

Upon application of an electrical current, one of the electro-active materials is reduced while the other is oxidised leading to a change in colouration (at least for one of them). In consequence, the system switches from the bleached state to the coloured state and the other way around. In order to get a system able to switch from a fully bleached to a fully coloured state, two conditions are mandatory: the two materials must have colourless bleached states

and complementary colourations (one is coloured in reduction(EC1), the other in oxidation (EC2) in Figure I.6).
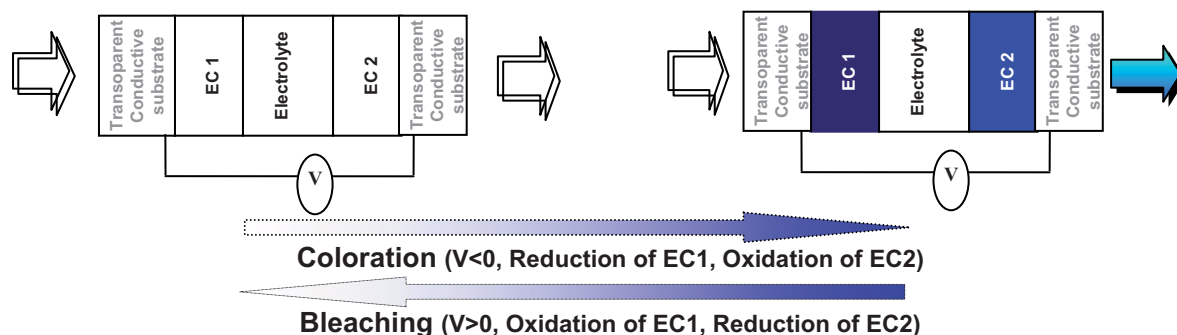
Figure I.6 : Working-principle of an ECD (electrochromic device).

The material with the highest colouration efficiency is called the primary electrochromic species, and, by convention, it is attached to the working electrode. In some cases, the counter-electrode can be simply an ion storage material without electrochromic activity. The two materials are separated by an ionic conductor layer which must also have a negligible electronic conductivity to avoid short circuit and to get a high 'memory-effect' i.e. the conservation of the optical properties under open-circuit conditions.

I. 2. 2. Types of ECD

Three types of EC material are distinguished:

- Types I: soluble molecules. Viologens are the most known, lots of other dyes can be used (cf. I. 3. 3. 2.).

$$EC_{bleached} \text{ liquid} \rightarrow EC_{coloured} \text{ liquid}$$
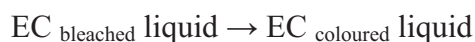
- Type II: soluble molecules that form a solid film upon colouration. For instance, silver salts [9] or some bipyridinium salts, e.g. heptyl viologen[10] can be used.

$$EC_{bleached} \text{ liquid} \rightarrow EC_{coloured} \text{ solid}$$
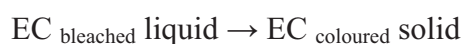
- Type III: solid electrochromic film. This can be for example inorganic or polymer electrochromic materials in thin-film form, namely transition metal oxides, Prussian blue, conducting polymers, etc (cf I. 3. 3. , Table I.7, Table I.8, Table I.10).

$$EC_{bleached} \text{ solid} \rightarrow EC_{coloured} \text{ solid}$$
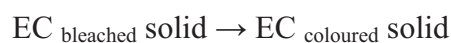
I. 2. 3. Important parameters

The key parameters of electrochromic devices include[1]:

- contrast ratio (colour change),
- colouration efficiency (colouration obtained as compared to the electrical charge involved),
- switching time (rate of colouration and bleaching)
- write-erase efficiency, long term cycling (evolution of the colouration and bleaching properties with cycles)

I. 2. 3. 1. Contrast ratio

The quantitative measure of the intensity of the colour change in an ECD is commonly measured by the contrast ratio CR.

$$CR = \frac{R_0}{R_x}$$

where R is the intensity of light diffusively reflected R_x from the coloured state and R_0 from the bleached state, the EC material being deposited on a diffuse white back plate. For commodity in the case of transmissive devices, we will use the following definition:

$$CR = \frac{T_0}{T_x}$$

where T_x is the intensity of light transmitted through the coloured state and T_0 is the intensity of light transmitted through the bleached state, the reference being the air.

Contrast ratio (CR) can refer either to a specific wavelength or to the overall white light. A CR higher than 5 is compulsory for effective sun shading.

I. 2. 3. 2. Colouration efficiency

The colouration efficiency (η) is the optical absorbance change (ΔA) obtained for a certain amount of injected charge per unit area (Q) (assuming no side electrochemical reactions).

$$\eta = \frac{\Delta A}{Q} \quad (cm^2/C)$$

η may be regarded as the electrode area that is coloured with an absorbance of 1 and a charge of 1 C, it is arbitrarily designated as positive for cathodically induced colouration and negative for anodic colour formation.

If η_p is the colouration efficiency of the primary electrochromic material and η_s that of the secondary, the colouration efficiency of the complete ECD η_t is obtained as:

$$\eta_t = \eta_p - \eta_s$$

Colouration efficiencies are generally higher for organic materials than for inorganic ones because of their higher molar absorptions.

I. 2. 3. 3. Write-Erase efficiency

The write-erase efficiency is the percentage of the originally formed colouration that can be subsequently electro-bleached.

For all-liquid electrochromic systems (with type I EC materials and liquid electrolyte), the bleaching of the ECD requires that all the coloured material that has diffused in the liquid electrolyte diffuses back to the electrode. These systems generally have poor write-erase efficiency and so suffer from colour segregation effects [9] Various approaches to overcome this drawback due to liquid systems have been found[9]. One of the most widespread consists in using solid devices (type III EC material). Redox chromophores can also be attached to supporting semiconductor electrodes[11] or the cathodic and anodic chromophores coupled to each other[12]. Another approach consists in having a colourless species soluble in solution that will precipitate onto the electrode upon electron transfer, thereby depositing a metallic or coloured film (type II EC material).

I. 2. 3. 4. Response time

The response time τ is the time required for an ECD to colour from its bleached state (and vice versa). Different methods to calculate τ are available, leading to difficulties to compare published data. In the present study, τ will be defined as the time required to obtain 90% of coloration (90% of the final coloration value); the conditions of measurements will be detailed.

Electrochromic displays that could be produced generally had response times in the order of a few seconds which is much longer than for LCDs (Liquid Crystal Displays)[13] or

CRTs (Cathode Ray Tubes).[14] This is due to the necessary diffusion either of the charged species throughout the film for solid electrochromic materials (type II and III) or of the electrochromic species to the electrode for all-solution systems (type I). However, in the case of light transmission modulation devices, switching times of a few seconds are largely acceptable.

I. 2. 3. 5. Cycle life

When an ECD is repeatedly cycled between its coloured and bleached states, device failure eventually occurs resulting from physical changes in solid phases or from chemical side reactions. The life-time highly decreases if strong changes in electrode composition occur during cycling, so that it can be preferable not to switch the ECDs at their maximum capacity.

For the US market (ASTM E2141_02), the life-time assessment includes tests at 90°C in solar radiation, 50,000 colouring/bleaching cycles, and operating range temperatures from -55°C to 95°C. In our case, most of the tests were limited to 1,000 cycles at room temperature except for some of them which were tested up to 25,000 cycles due to equipment availability.

I. 3. *State of the art*

Due to the large field of materials covered by electrochromic devices (from conductive substrates to electrolytes and to electrochromic materials), the state-of-the-art will give general information and references will be inserted for the reader who wishes to go further in details.

I. 3. 1. Conductive substrates for ECDs

For transmissive ECDs, current collectors, in addition to be electronic conductors, must also be as transparent and colourless as possible, in the visible wavelength domain. Several kinds of systems have been studied. The most used are Transparent Conductive Oxides (TCO).[15] Metallic grids are sometimes used [16]. Conductive polymers are also candidates but they have lower optical and electronic properties.[17]

TCO thin films are generally based on In_2O_3:Sn (ITO), and SnO_2:F (FTO). ITO can be deposited as thin films on either glass substrates or plastic substrates whereas FTO can be up

to now only deposited on glass. The industrial deposition techniques commonly used are PVD for ITO and CVD for FTO (for Physical and Chemical Vapor Deposition respectively). Many other TCOs are known, but mostly on a laboratory scale. For example, recent studies performed at the ICMCB showed the interest of ITZO (indium oxide co-doped with tin and zinc) for high conductivity on plastic substrates.

I. 3. 1. 1. Key parameters for transparent conductors

The key parameters for transparent conductors are a high transparency in the visible range and low sheet resistance. The sheet resistance (resistivity of the conductive material divided by its thickness) must be as low as possible. However thick films are not any more fully transparent (metals are reflective and TCOs are partially reflective and slightly absorbent) and suffer from lack of adhesion. An optimum must be found for each application.
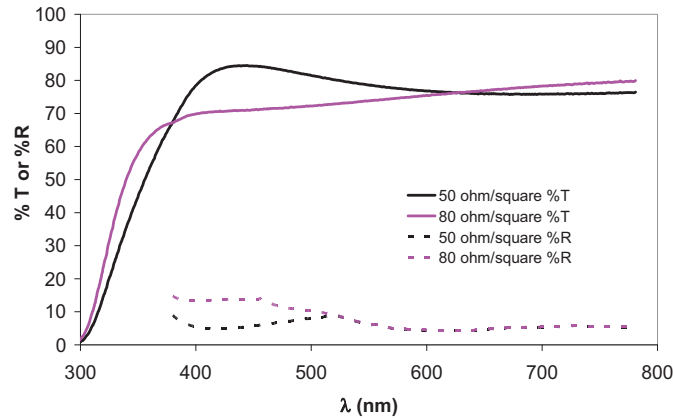
Figure I.7 : Transmittance and Reflectance of ITO films deposited with resistivity of 50 ohm/square and 80 ohm/square.[18]

I. 3. 1. 2. Properties of the TCOs used in this study

The 'sheet resistances' of TCOs are given in Table I.2.

TCO	Substrate	Sheet resistance ($\Omega/\square$)	Supplier
FTO	Glass	13	Solems (F)
ITO	Glass	20	Solems (F)
ITO	PET	45-80	Bekaert (B)
ITO	Ophthalmic lenses	60	Solems-Essilor (F)

Table I.2 : Sheet resistance of the TCO-substrates used in the study in order to have an average optical transmission in the visible of at least 80%. The deposition technique is PVD (DC sputtering) for ITO and CVD for FTO.

The use of plastics limits the temperature that can be used (120°C for PET, 70°C for Orma). ITO sputtered on large area PET with reasonable mechanical resistance is commercially available (e.g. Bekaert Company).

I. 3. 2. Electrolytes

Electrochemical studies were historically performed in water based electrolytes, mainly due to their high ionic conductivity. However, water is electrochemically active at rather low potential (1.23 eV are sufficient to split water molecules into hydrogen and oxygen) so that the electrochemical window available for electrochromic reactions is restricted ($\leq$ 1.23V). On the contrary, the use of electrochemically inert solvents such as propylene carbonate or acetonitrile with an additional salt to ensure the ionic conduction has been found to widen the electrochemical window above 3V; the use of ionic liquid increases it up 4V.

We will focus our work on lithium (Li^+) conductive electrolytes. The general specifications for an electrolyte will first be presented; then, different types of lithium conductive electrolytes, as well as the newly used ionic liquid based lithium-conducting electrolytes, will be described.

I. 3. 2. 1. Electrolyte performances

The major parameters for electrolytes are their ionic conductivity, electrochemical windows, and transference numbers of the ion of importance for the electrochemical reactions.

I. 3. 2. 1. i. Ionic conductivity

Ionic conductivity σ_i is defined for ionic species i by:

$$\sigma_i = C_i \, |z_i| \, F \, \mu_i$$

where z_i is the charge of the ionic specie i, F is the Faraday constant and μ_i is the mobility of species i[19]. C_i is the molar concentration of charge carriers.

The global ionic conductivity σ of an electrolyte with different mobile species denoted i, is given by:

$$\sigma = \Sigma\ \sigma_i = \Sigma\ C_i\ |z_i|\ F\ \mu_i$$

It is also defined as the reciprocal of the proper resistance of the electrolyte, R_p, and can be obtained by calculating:

$$\sigma = \frac{d}{R_p A}$$

where d is the electrolyte thickness and A its average area.

For practical applications requiring high colouration and bleaching rates, ionic conductivity should ideally be close to or higher than 10^{-4} S.cm^{-1} on the whole range of operating temperatures (-20°C to 60°C for building and car-window applications notably). [20]

I. 3. 2. 1. ii. Electrochemical window

The electrochemical window is the range of potential available in the electrolyte without degradation of the supporting electrolyte itself. The maximum (respectively minimum) potential is determined by the potential at which the reaction of oxidation (respectively reduction) of the electrolyte occurs. These potentials are measured using cyclic voltammetry. To ensure the stability of the devices upon cycling, the range of potentials used to cycle the ECD must obviously be included in the electrochemical window of the electrolyte.

I. 3. 2. 1. iii. Transference number

The transference number or transport number t is the fraction of the total current that is carried by a given ion. The transference number definition based on diffusion coefficients for the cations A_i (t_+) and for the anions B_j (t_-), are given by:

$$t_{A_i^+} = \frac{D^{A_i^+}}{\sum\limits_{ij} D} \ ; \qquad t_{B_j^-} = \frac{D^{B_j^-}}{\sum\limits_{ij} D}$$

The higher the transference number, the higher the relative ion displacement. A right performance of the device is favoured by a transference number as high as possible for the ions that are reversibly inserted in the EC films.

I. 3. 2. 1. iv. Chemical properties

Moreover, for safety and stability purpose, the chemical stability towards the electrodes and the thermal stability have to be taken into account. Flammable and toxic products will be preferably avoided.

To facilitate recycling, the electrolyte should be easily removed from the electrodes. For example, the use of thermoplastics allows the separation of the device components thanks to a simple heating step.

I. 3. 2. 2. Lithium conductive electrolytes: state-of-the-art

We have limited our study to Li^+ conducting electrolytes. This chapter briefly reviews the available lithium conducting electrolytes from liquid electrolytes, to soft and hard polymer electrolytic membranes, and finally inorganic solid electrolytes.

I. 3. 2. 2. i. Liquid electrolytes

Conventional lithium conductive liquid electrolytes are based on lithium salts, e.g. $LiClO_4$, $LiAsF_6$, $LiPF_6$, $LiBF_4$, $LiPF_3(CF_2CF_3)_3$, $LiBC_4O_8$, $LiCF_3SO_3$, $LiC(CF_3SO_2)_3$, $LiN(CF_3SO_2)_2$, $LiN(SO_2CF_2CF_3)_2$ dissolved in non aqueous organic solvents: carbonates (e.g. ethylene carbonate (EC), propylene carbonate (PC), dimethyl carbonate (DMC)), esters (e.g. methyl acetate, methyl formate), cyclic ethers (e.g. dioxane, tetrahydrofuran), lactones (e.g. gamma butyrolactone (GBL)) or aliphatic ethers (e.g. dimethyl ether (DME)). Such electrolytes are commonly used for lithium-ion batteries.

They show conductivity of about 10 mS/cm at ambient temperature and can operate between -20°C and 60°C. This conductivity is lower than that of aqueous electrolytes that can reach 700 mS/cm. (cf.Table I.3). Such liquid lithium conductive electrolytes generally exhibit high volatility, high flammability and most of all rather high toxicity.

Electrolyte	Solvent	Conductivity [mS/cm]	Application	Reference
H_2SO_4 (30 wt.%)	H_2O	730	Lead-acid battery	21
KOH (29.4 wt.%)	H_2O	540	Alkaline battery	21
NH_4Cl (25 wt.%)	H_2O	400	Leclanché battery	21
$LiN(CF_3SO_2)_2$ (1 mol/dm3)	EC + DME (1:1)	13	Lithium-ion battery	22
$LiN(CF_3SO_2)_2$ (1 mol/dm3)	EC + DC (1:1)	6.5	Lithium-ion battery	21
$LiCF_3SO_3$ (1 mol/dm3)	EC + DME (1:1)	8.3	Lithium-ion battery	22
$LiPF_6$ (1 mol/dm3)	EC + DME (1:1)	16.6	Lithium-ion battery	22

Table I.3 : Examples of conductivity of classically used electrolytes in various electrochemical applications

I. 3. 2. 2. ii. Polymer lithium conductive electrolytes[23,24]

The use of polymer electrolytes is beneficial from safety points of view as it decreases the probability of internal shorting between the electrodes and prevents the leakage of the electrolyte[25]. Their development has gone through different stages: (i) dry solid polymer electrolytes, (ii) plasticized/gel polymer electrolytes, iii) inorganic filled composite polymer electrolytes.

Dry solid polymer electrolyte (SPE)

In SPE, a polymer is used as a solvent of the lithium salt; no organic solvent is added. Polyethylene oxides (PEO) are known to be the first and most widely investigated polymers for SPE[26]. The ionic conductivity in PEO-LiX (LiX: lithium salt) complexes has been discovered by Fenton et al.[27] in 1973. The conductivity of these systems is very low, generally lower than 10^{-6} S/cm at room temperature[28]. For some practical applications such as lithium batteries[29] an additional heating up to around 60°C is required to lower the resistivity[30]. PEO-lithium salt complexes exhibit a multiphase nature: a salt-rich crystalline phase, a pure PEO crystalline phase and an amorphous phase with dissolved salt. In the early history of SPEs, the ion transport inside the crystalline PEO-helices was believed to be the major contribution[31]. It has later been shown that the ionic conduction in SPE takes place primarily in the amorphous phase[32], the conduction mechanism is based on the creation of free volume in this phase due to polymer chains dynamics.

Other polymers were also studied, for example polyethylenesuccinate[33], cross-linked polyurethane/acrylate polymer[34]. Some experimental results did not fit with the PEO conduction model based on a conduction mostly located in the amorphous phase. The conduction in the crystalline region had to be taken into account and showed that, above the transition glass temperature, ionic conductivity in the static, ordered environment of the crystalline phase can be higher than that of the amorphous one[35]. The conductivity of these systems was of the order of 10^{-4} S/cm.

Plasticized polymer electrolytes

Plasticized polymer electrolytes are liquid electrolytes gelified by polymers or, from another point of view, a polymer that is plasticized by a liquid. These electrolytes are a combination of a liquid electrolyte with a polymer host, so that they can benefit from both the cohesive properties of solids and the diffusive property of liquids. The polymer/liquid system can be monophasic or multiphasic depending on whether the interactions between the polymer and the liquid are strong or not. A compromise needs to be found between the increase in ionic conductivity and the decrease in mechanical strength while plasticization occurs.

Plasticization has notably been used to lower the operating temperature of Li-conducting membranes. The most common approach consisted in adding low molecular weight liquid plasticizers e.g. cyclic or aliphatic carbonates to the PEO-lithium salt solid polymer electrolyte. Plasticization with the liquid electrolyte $LiClO_4$/PC of the PEO based lithium conductive membranes led to technological applications in the early 1980s [36]. Another approach consisted in plasticizing non lithium conductive polymers such as PAN, PMMA, PVC or PVdF by lithium conductive liquid electrolytes. The poly(acrylonitrile) (PAN) based electrolytes plasticized with $LiClO_4$/PC liquid electrolyte were the most promising as they exhibit exceptional ionic conductivity of the order of 1 mS/cm at ambient temperature, appreciable transference number of 0.6 for lithium and a rather wide electrochemical stability window (about 4 V)[37]. However, their use in lithium metal-based batteries was impossible due to their chemical reactivity towards lithium metal electrode[38]. Membranes with poly(vinyl chloride) (PVC) have been shown to offer poor ionic conductivity[39]. Poly(methylmethacrylate) (PMMA) plasticized with propylene carbonate has been successfully used as electrolyte for lithium batteries[40]. The mechanical strength of the PMMA

electrolyte was increased by blending with PVC[41]. PMMA is transparent, colourless and has been found compatible with ionic liquids[42,43]. Poly-(vinylidene fluoride) (PVdF) has appealing properties, such as a reasonably high dielectric constant of 8.4 which assists the ionisation of the salt providing higher charge carrier density, and a high electrochemical stability window due to the presence of strong electron-withdrawing functional groups which increase the anodic stability[44]. However, these fluorinated polymers have poor interfacial properties. Moreover in the case of lithium batteries, the reaction between lithium and fluorine resulted in the formation of LiF which is detrimental for safety considerations. The use of copolymers, with amorphous parts that would favour the entrapment of a liquid electrolyte and crystalline parts to ensure the mechanical property, is expected to increase polymer electrolytes performances. Poly(vinylidene fluoride-hexa fluoropropylene) (PVdF-HFP) (88:12) mixtures with a HFP amorphous phase and a PVdF crystalline phase have been identified as interesting candidates; their study is in progress[45].

PAN and PVdF systems do not exhibit significant interactions between the polymer and the liquid[46] which can easily flow from the polymer (for example due to temperature increase, pressure applied on the membrane, etc.). This multiphasic configuration has been used by the Bellcore's group. Their processing consists in first preparing a micro-porous pure polymeric membrane which is then soaked in the liquid electrolyte[47]. The conductivity is ensured by the liquid present in the micro-pores so that it is expected to be relatively high. Moreover, from a process point of view, the system requires moisture-free atmosphere only at the final step of soaking of the membrane and assembling of the complete devices, which is interesting for simplification of the process.[48] The rate capability of these membranes is generally rather low[49,50,51]; however for some industrial application such technique has been found beneficial.

Composite polymer electrolytes (CPE)

Composite polymer electrolytes consist in adding an inorganic material to the polymer-gel electrolyte. This combination is expected to improve mechanical and electrochemical properties of the gel electrolyte and to provide higher electrolyte/electrode compatibilities and safety than polymer gelified electrolytes[52].

One of the most promising ways is the addition of ceramic fillers in the gel electrolyte[52]. These fillers can be ionic conductive as zeolites[53] or ionites[54] (e.g. Li_2N, $LiAl_2O_3$) or neutral

as Al_2O_3, SiO_2, MgO [55]. Their effect is highly dependant on their particle size and characteristics. It has been well established that this ceramic filler addition enhanced the degree of amorphisation of the polymer chain or hindered crystallization, leading to higher ionic conductivity[52]. Moreover, the localization of filler molecules in the vicinity of the coordination sphere of Li^+ cation has the effect of decreasing the fraction of ion pairs and aggregates.[56]

I. 3. 2. 2. iii. Inorganic solid lithium conductive electrolytes

Inorganic solid lithium conductive electrolytes can be 2D layered materials such as Li_3N, Li-β-alumina or 3D materials e.g. $Li_{14}ZnGe_4O_{16}$, $(Li,La)TiO_3$, $Li_{1.3}Ti_{1.7}Al_{0.3}(PO_4)_3$ and $xLi_2O:yP_2O_5:zPON$ (LiPON, PON: phosphorous oxynitride). Their critical properties are reported in Table I.4.

Solid Electrolyte	Conductivity (RT) [S/cm]	Remarks	Reference
Li_3N	$2\text{-}4\ 10^{-4}$	Low decomposition voltage (0.44V at RT)	57
Li-β-alumina	$3\ 10^{-3}$	Highly hygroscopic	58
LISICON type e.g. $Li_{14}ZnGe_4O_{16}$	10^{-6}	Decrease with time, CO_2 sensitive	59
Thio-LISICON type e.g. $Li_{4-x}Ge_{1-x}P_xS_4$	up to $2.2\ 10^{-3}$	Electrochemical stability (> 5V) Thermal stability (up to 500°C)	60
Perovskite (ABO_3) type A-site-deficient $(Li, La)TiO_3$ e.g. $Li_{3x}La_{(2/3)-x}\square_{(1/3)-2x}TiO_3$	$1.5\ 10^{-3}$	Ti^{4+} reduction	61
NASICON-type e.g.$Li_{1.3}Ti_{1.7}Al_{0.3}(PO_4)_3$	$1.\ 10^{-5}$	Ti^{4+} reduction, high temperature for preparation, difficulties in lithium content control	62
LiPON	$3.3\ 10^{-6}$	Moderate conductivity	63
$Li_5La_3M_2O_{12}$ (M = Nb, Ta) and Li_6ALaM_2O12 (A = Ca, Sr, Ba; M = Nb, Ta)	10^{-5}	Electrochemical stability (>6V) Chemical stability towards lithium batteries materials (as $LiCoO_2$, $LiMn_2O_4$, $LiNiO_2$, $Li_2MMn_3O_{8)}$	64

Table I.4 : Properties of the most studied inorganic solid electrolytes[64]

Ionic conductivity of inorganic compounds is generally low as compared to liquid or polymeric ones. Moreover, some of them suffer from the easy reduction of Ti^{4+} to Ti^{3+} that leads to undesirable electronic conduction preventing application as electrolyte[63]. Electrochemical instability and chemical instability towards water or CO_2 are also

detrimental. The stability towards the materials used at the electrodes is also important. So far, lithium conductive inorganic compounds with both rather high ionic conductivity and high stability were mainly found in the thio-LiSICON family[64].

An advantage of solid electrolytes is their mechanical strength in solid devices, but the can be non flexible and may require high preparation temperature, which make them not easily compatible with plastic substrates.

I. 3. 2. 3. Ionic liquids as electrolytes

Ionic liquids are molten salts liquid at room temperature (<100°C). They have been recently used for electrochemical applications due to their large electrochemical window and ionic conductivity.[65] We will first describe what an ionic liquid is and then detail the interests of such molecules as potential electrolytes for EC devices.

I. 3. 2. 3. i. Ionic liquids

Whereas classical electrolytic solutions described above are obtained by dissolution of a salt in a medium (molecular solvent, polymer), the direct melting down of salts leads to solutions with high concentration of ions. These salts are called molten salts and have been extensively used in practical applications such as batteries and fuel cells but their operating temperatures were in general in the 400°C to 700°C range, which is not applicable for our application. However, more recently, salts with a low melting point (RT or at the maximum 100°C in the extended definition) have been developed, they are called RTILs (Room Temperature Ionic Liquids).

RTILs can be based on quaternary ammonium cations such as tetralkylammonium $[R_4N]^+$, on cyclic amines both aromatic (pyridinium, imidazolium) and on saturated (piperidinium, pyrrolidinium), sulfonium $[R_3S]^+$ or phosphonium $[R_4P]^+$. Possibilities for anions are numerous: $[F]^-$, $[Cl]^-$, $[Br]^-$, $[BF_4]^-$, $[PF_6]^-$, $[AsF_6]^-$ $[N(CN)_2]^-$, $[CF_3SO_3]^-$, $[C_4F_9SO_3]^-$, $[CF_3CO_2]^-$, $[N(CF_3SO_2)_2]^-$, $[N(C_2F_5SO_2)_2]^-$, $[C(CF_3SO_2)_3]^-$, $[CF_3CONCF_3SO_2]^-$.[65]

They show physicochemical properties identical to those of high temperature molten salts, but their liquid properties at room temperature make their handling much easier than that of classical high temperature molten salts. Their use as electrolytes has been the object of

extended studies within the last years; the increasing number of publications in this field is eloquent. Singular properties of ionic liquids are summarized in Table I.5.

Property	Practical interest
Low melting point	Liquid at ambient temperature Wide usable temperature range
Non – volatility	Thermal stability Nonflammability
Composed by ions	High ion density High ionic conductivity
Organic ions	Various kind of salts, unlimited combinations Designable

Table I.5 : Basic characteristics of organic room temperature ionic liquids[65]

Nowadays, most of the interests in ionic liquids are dedicated to the design of new solvents for various applications (general chemistry reactions, catalysis…) including electrochemical applications. One of the advantages that have been highlighted is the possibility to recycle these solvents after use thanks to their non–volatility. Then they are more environment friendly at the express condition to be recycled. For some of them, including 1-Butyl-3-methylimidazolium bis (trifluoromethanesulfonyl) imide (BMITFSI), the toxicity is not negligible. Ionic liquids are expected to reach more and more fields of the chemistry notably due to the REACH legislation (Registration, Evaluation and Authorization of Chemicals) specifications.

Moreover, due to the huge possibilities offered by organic synthesis, ionic liquid properties can be tuned by simply modifying their composition. For example, by choosing the right counter anion (BF4, TFSI), ionic liquids can be hydrophobic.

I. 3. 2. 3. ii. Ionic liquids as electrolytes

An extensive data collection on electrochemical properties of ionic liquids has been performed by Galiński et al.[21]; the most important parameters for their use as electrolytes are described: ionic conductivity, transference numbers, electrochemical window, as well as physical and chemical properties such as melting point, observed temperature of solidification, density, and viscosity.

We have chosen to work with two ionic liquids: 1-Butyl-3-methylimidazolium hexafluorophosphate and 1-Butyl-3-methylimidazolium bis (trifluoromethanesulfonyl) imide

i.e. BMIPF$_6$ and BMITFSI respectively (see Table I.6). They are liquid at room temperature, offer a large electrochemical window (4.4 V) and benefit from resistance to moisture in the case of TFSI⁻ anion.
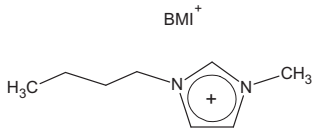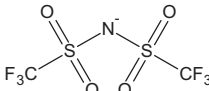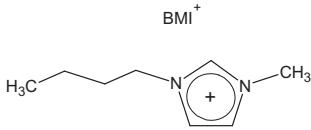
Name	Cation	Anion	Viscosity (mPa.s, 25°C)	Ionic conductivity (mS.cm⁻¹, 30°C)
BMITFSI	BMI⁺	TFSI⁻	50	3.79
BMIPF$_6$	BMI⁺	PF$_6^-$	56	3.77

Table I.6 : Chemical formula of BMITFSI and BMIPF6 ionic liquids, as well as their viscosity at 25°C and ionic conductivity at 30°C.

An ionic liquid (IL) can be used as electrolyte without additional salt since it is intrinsically ionic conductive. However, it is sometimes necessary for applications requiring the presence of a specific ion, such as lithium insertion based devices, to add a salt. It is then preferable to use a lithium salt with a common anion (ex: LiTFSI in BMITFSI).

The gelification of IL has been performed, with PVdF-HFP[66], with MMA polymerized in-situ[67], with PAN [68]. Another approach was developed by Vioux et al. and consists in preparing ionogels i.e. ionic liquid confined in a silica matrix. These solid state electrolytes benefit from a liquid-like behaviour even at temperature lower than that of the crystallisation of the IL.[69]

I. 3. 3. Electrochromic materials

After the brief review of materials usable as transparent conductive substrates and electrolytes for EC devices, we will now focus on the electrochromic layers, i.e. electroactive materials that exhibit colour change upon electrochemical charge or discharge. Both inorganic and organic EC materisl will be reviewed here. For more precise information please refer to general and specific reviews.[1,9, 70]

I. 3. 3. 1. Inorganic electrochromic materials

Films based on inorganic materials exhibit high mechanical resistance and durability. The possibilities they offer in terms of electrochromic materials are summarized in Table I.7 for oxides and Table I.8 for non-oxide compounds.

Oxide	Colouration Cathodic (C) or Anodic (A)	Oxidized	Reduced	Colouration efficiency : η (cm²/C)	Ref.
WO_3	C	**Colourless**	Blue	42 (650 nm) to 115(633 nm)	71, 72
TiO_2	C	**Colourless**	Blue	5	73
LixCoO2	A	Deep Blue	**Blue**	-10	74
MoO_3	C	**Colourless**	Blue	77 (700 nm)	75
V_2O_5	C	**Pale Yellow**	Pale blue	-15 (600 nm)	76
"IrO_x"	A	Blue/Grey	**Colourless**	-30	77
Nb_2O_5	C	**Colourless**	Brown	<12	78
"NiO"	A	Brown/black	**Colourless**	-36 (640nm)	79
"$Li_{0.5}Ni_{0.5}O$"	A	Brown	**Pale brown**	-40 (650 nm)	80
InO_2:Sn	C	**Colourless**	Brown	irreversible	81

Table I.7 : Properties of the most studied electrochromic inorganic metal oxide materials. The colouration efficiency values are highly dependent on the measurement conditions, they are given here as approximate indicators.

Inorganic non-oxide	Colouration	Oxidized state	First reduction	Second reduction	η (cm²/C)	Ref
Metals (Zn, Bi, Ag)	C	**Colourless** (in solution)	Black (electrodeposition)	n/a		82
Graphite	C/A	Golden Yellow - Light green- Deep Blue - Brassy Black				83
Lutetium bis(phtalocyanine)	C/A	Red - Yellow- Green – Light Blue – Blue –Violet				84
Prussian Blue FeHCF	C/A	Light Yellow	Blue	**Colourless**	88.8	85
Prussian Blue analogues:						
CuHCF	C/A	Yellow	Red-brown	n/a		86
PdHCF	C/A	Orange	Green	n/a		86
CoHCF	C/A	Violet	Green	n/a		87
NiHCF	C/A	Yellow	Grey	n/a		87
VHCF	C/A	Blue-green	Yellow	n/a		88
InHCF	A	Yellow	**Colourless**	n/a		89

Table I.8 : Properties of the most studied electrochromic inorganic non oxide materials. The colouration efficiency values are highly dependent on the measurement conditions; they are given here as approximate indicators.

Within the inorganic electrochromic materials, WO_3 is the most studied and used. It presents a blue colouration such as other oxides TiO_2, LixCoO2, MoO_3, V_2O_5, or IrO_5. Only Ni and Nb oxides exhibit a different colouration that is interestingly brown.

The coloration efficiencies of inorganic oxide electrochromic materials are rather low, in the range of tens cm²/C; therefore, ECDs based on such films require high electrical power input

to reach the desired optical contrast. Their colouration-bleaching kinetic is also limited; indeed, the ion diffusion in and from the films is generally the limitative step; the influence of the film texture, particularly its porosity, and the counter ion nature are primordial and have been widely reported.[70]

Table I.7 also indicates that oxides based on Ti, Ni, Nb, Mo, W and Ir can be fully colourless in their bleached state. The other oxides showing residual absorbance can't be used as far as totally bleached devices are required (for ophthalmic applications). Mixed oxide systems have also been studied. In the case of Mo and W mixed oxides, small increase in coloration efficiencies and switching speed have been observed.[70] In_2O_3 shows a very poor reversibility and cannot be used as an electrochromic compound. However, its use as conductive substrate (once doped with Sn^{4+}) is widely spread, a deterioration of its conductive properties due to irreversible electrochemical reduction of tin (leading to colour centres) can be detected by the formation of a brown colouration (at -1.6 V/NHE). Inorganic electrochromic devices based on reversible metal electrodeposition seems to be the most promising inorganic system since the bleached state is fully colourless and the coloured state is highly coloured and gives nearly opaque films. However, reversible electrodeposition of metals on large surface devices is not demonstrated. Graphite suffers from no colourlessness in the bleached state. Lutetium bis-phtalocyanines can be prepared as films or used in solution. Many prototypes based on this material have been prepared, due to its high memory effect[90], but the film disintegration caused by repeated anion insertion-extrusion and slow response time are its limitations. Phtalocyanines with other metals or modified phtalocyanines have been prepared; detailed information can be found in ref 84.

The family of the hexacyanoferrates offers in some interesting cases a total colourlessness in the bleached state; that is for instance the case of Prussian Blue (PB) and InHCF. The coloration efficiency of PB is in the same range (88.8 cm²/C) as that of the most efficient oxides (Table I.7 and Table I.8). InHCF is a nearly colourless electroactive material, which could be advantageously used in some EC devices.

I. 3. 3. 2. Organic electrochromic materials

A large number of electrochromic organic dyes and derivatives are known. They include bipyridinium systems, carbazoles, methoxybiphenyl, quinones, diphenylamine, pyrazolines etc (Table I.9) [91]. Extensive literature reports on bipyridinium compounds and particularly on 1,1'-dimethyl-4,4'-bipyridinium, also called 'methyl viologen'.[92]

They can be used either as such by solubilising in the electrolytic solution or as solid films after polymerisation or grafting onto an appropriate substrate.

Organic compound	Col.	Oxidized		Reduced	CE (cm²/C)	Ref
Viologens: **Bipyridilium (bipm)**	C	**Bipm2+**	**Bipm+•**	**Bipm**	(170 *)	93
R=alkyl	C	**Colourless**	Blue/violet	Weak colour		
R= aryl	C	**Colourless**	Green	Weak colour		
Diphenylamine	C					94
p-phenylene diamine	C	**Colourless**		Highly coloured		
xylated N,N,N',N'-tetramethyl-p-phenylene diamine	C	**Colourless**		Blue / Blue/green		
Tetracyanoquinodimethane (TCNQ)	C	**Colourless**		Blue		95
Carbazole	A	**Carbazole+•**		**Carbazole**		96
R=H	A	Dark green		**Colourless**		
R=ethyl	A	Green		**Colourless**		
R=phenyl	A	Iridescent		**Colourless**		
Violene: **Methoxybiphenyl type**	A	Blue or green		**Colourless**		97
Quinones types	A	RQ		RQ-•		98
		≈ colourless		Blue, Pink, Yellow, Red		
Pyrazoline compounds	A	Green or Red		Yellow		99

Table I.9 : Properties of the most studied organic electrochromic materials
* for material tethered on TiO$_2$ structured elecrodes[100]

In liquid systems, spontaneous redox reactions between the redox species formed at the cathode and the anode take place since the species can diffuse toward one another. These systems do not have memory effect, and suffer from segregation of the molecules and bad write-erase efficiency. To improve that, the molecules can be tethered to the electrodes or to an electronically conductive structured host material (such as nanostructured n-type TiO$_2$[100]); immobilization of the species within a gel or membrane electrolyte was also carried out.[101] Another possibility is to use molecules that form a film once reduced or oxidized. For example, 1,1'-diheptyl-4,4'-bipyridilium (heptyl viologen) forms a durable film at the electrode. This approach has been used, notably by Philips laboratories[102].

Organic materials also include solid films formed by polymerization of molecules; most often the solid organic materials used for electrochromic applications are conductive polymers.[103] As opposed to the inorganic solid materials listed in Table I.7and Table I.8, they have very high colouration efficiencies (hundreds of cm²/C). They can be anodically or cathodically coloured. They combine high flexibility and good mechanical resistance and are very attractive candidates for electrochromic applications.

As shown in Table I.10, most of the electrochromic polymers[104] suffer from a residual colour in the bleached state; it is expected that this point could be improved by playing on the polymer structure[105].

Electrochromic polymers	Colouration Cathodic (C) or Anodic (A).	Oxidized	Reduced	CE (cm²/C)	Ref
Poly(thiophene):					104
R1=R2 =H	C/A	Blue	Red		
R1= CH3	C /A	Deep Blue	Red		
R1=R2=CH3	C/A	Dark Blue	Pale Brown		
R1= Ph	C/A	Green Blue	Yellow		
R1=R2= Ph	C/A	Blue/Grey	Yellow		
PEDOT (polyethylenedioxithiophene)	C	Pale Blue	Dark Blue	183	
Poly(aniline)	A	Blue/dark Yellow/Green /Yellowish			104
Poly(pyrrole)	A	Blue/violet	Yellow/Green		104

Table I.10 Properties of the most studied electrochromic polymers

I. 3. 3. 3. Choice of the electrochromic materials for Nanoeffects

The Nanoeffects project aimed at preparing large devices, so that materials for which the deposition on large surface is demonstrated have been preferred. Metals were discarded because electrochromism of metals is difficult to be obtained on large surface on plastics. The use of small organic molecules was also avoided since they require to be tethered onto the structured electrodes (for example TiO_2) to avoid segregation and to give a bistable system, the use of flexible polymer film was preferred.

Nanoeffects specifications also orientate the study towards materials that need low energy for both deposition and operation, so that materials compatible with low temperature deposition and with high-colouration efficiency are needed. Lots of inorganic films are more easily prepared at high temperature and colouration efficiencies of inorganic films are rather low (as compared to electrochromic polymers or liquids), so that inorganic films were not considered as interesting primary electrochromic materials.

Organic electrochromic polymers have attracted our attention due to their easy handling, high flexibility, and processability even on plastic substrates. Large surface depositions are known for PEDOT as shown by the PEDOT films sold by Agfa under the

trademark Orgacon RTM. Other electrochromic polymers such as, polyaniline have interesting properties; but their deposition on large substrate is not demonstrated. Moreover PEDOT shows reasonably high electronic conductivity ($\sim 10^{-3}$ S.cm^{-1}), electrochemical stability, very high colouration efficiencies (e.g. 183 cm²/C, see Table I.10). So that PEDOT reveals to be a primary electrochromic material of choice. The choice however implied to work on the major drawbacks of PEDOT:

-   residual blue colouration in the bleached state,
-   lack of adhesion on certain substrates
-   blue coloured state.

The final choice of electrochromic layers was the following:

-   Coloured reduced state (working electrode): PEDOT and its derivatives mainly chosen to improve both colouration efficiency and mechanical properties
-   Coloured oxidised state (counter electrode): Prussian blue and derivative films whose capacities are easily adaptable.

With this respect, ICMCB was in charge of the counter electrode with completely colourless bleached state. This includes compounds such as Prussian Blue and a Prussian Blue analogue InHCF.

-   Prussian Blue can be deposited with controllable capacities (up to 12 mC/cm²) by electrodeposition on large-area conductive substrate
-   InHCF, a Prussian Blue analogue, has the other advantage of being a colourless ion-storage layer and would simplify the set-up of the devices. The preparation of InHCF on large surfaces is however still to be studied.

I. 4. *Conclusion*

For the targeted applications by the consortium Nanoeffects (ophthalmic glasses, car glazing, textiles), the use of plastic substrates, for rigid or flexible devices is essential. The best transparent conducting film for this type of substrate is ITO (indium tin oxide) since FTO

(fluorine-doped tin oxide) has not yet been industrially deposited on plastic substrates. The deposit of ITO on particular substrates usefull for the Nanoeffects project (e.g. ophthalmic lenses Orma by Essilor) was developed by Solems. The electrolyte must have a rather high ionic conductivity, be flexible, and avoid the problems of leakage. As opposed to solid electrolytes, those containing polymer are flexible and can reach rather large conductivities (> 10^{-4} S/cm) even when prepared at low temperature (temperature compatible with plastics). The selected electrolytic liquid contains ionic liquid. These liquids are intrinsically ionic conducting and offer a broad electrochemical window, and for some of them a hydrophobic character which protects the system from moisture. The gelification of these liquids is carried out with PMMA, known as a transparent and colourless polymer compatible with imidazilium-based ionic liquids and electrochemically stable. As detailed above the selected electrochromic materials are PEDOT and its derivatives and Prussian blue and its derivative containing indium (InHCF).

PEDOT-based films have an appreciable contrast ratio (CR=4) as soon as a capacity of only 3 mC/cm² is reached. Therefore, systems with capacity around 3 mC/cm² will be studied in the following.

References

[1] P.M.S. Monk, R.J. Mortimer and D.R. Rosseinsky, *Electrochromism : Fundamentals and applications*, **1995**, VCH (ed.).

[2] H. Dürr, H. Bouas-Laurent, In Photochromism: Molecules and Systems; Eds.; Elsevier: Amsterdam, 1990.

[3] I.C. Koo, Y. R. Shen, *Opt. Eng*. **1985**, *24*, 579.

[4] E. Land, US Patent 1955923, **1934,** Light valve and method of operation.

[5] J.R. Platt, *J. Chem. Phys.* **1961**, 34, 862.

[6] S.K. Deb, *Applied Optics Suppl. 3*, **1969**, 192.

[7] P. Letocart, Saint-Gobain, IME7, **2006.**

[8] R.J. Mortimer, *Electrochimica Acta* **1999**, 44(18), 2971.

[9] P.M.S. Monk, R.J. Mortimer, D.R. Rosseinsky, *Electrochromism and electrochromic devices*, **2007**, Cambridge University Press (ed.).

[10] C.J. Schoot, J.J. Ponjée, H.T. van Dam, R.A. van Doorn and P.J. Bolwijn, *Appl. Phys. Lett.* **1973**, 23, 64.

[11] F. Campus, P. Bonhoöte, M. Grätzel, S. Heinen, L. Walder, Solar Energy Materials & Solar Cells **1999**, 56, 281.

[12] A. Michaelis, H. Berneth, D. Haarer, S. Kostromine, R. Neigl, R. Schmidt**,** Advances Materials **2001**, 13, 23, 1825.

[13] H. Kawamoto, *Proceedings of the IEEE* **2002**, The History of Liquid-Crystal Displays, vol. 90, 4, 460.

[14] K.F. Braun, 1897

[15] G.J. Exarhos, X.-D. Zhou, *Thin solid films* **2007**, 515, 7025.

[16] M. E. Tadros, J.A. Mason, C.A. Kadoch, *Oxide coated metal grid electrode structure in display devices*, **1994**, US patent 5293546

[17] D.R. Cairns, G.P. Carwford, *Proceedings of the IEEE* **2005**, 93, 8, 1451

[18] From M. Feuillade, Essilor

[19] IUPAC **1974**, *37*, 512.

[20] Nanoeffects specifications

[21] M. Galiński, A. Lewandowski, I. Stępniak, *Electrochimica Acta* **2006,** 51, 5567.

[22] M. Morita, M. Ishikawa, Y. Matsuda, *Lithium Ion Batteries* **1998**, Wiley, 162.

[23] Review on gel polymer electrolytes for lithium batteries, A. M. Stephan, *European Polymer Journal* **2006,** 42, 21.

[24] Review on composite polymer electrolytes for lithium batteries, A. M. Stephan, K.S. Nahm, *Polymer* **2006,** 47, 5952.

[25] F.M. Gray, *Solid polymer electrolytes: fundamentals and technological applications* **1991**,VCH.

[26] P.V. Wright, *Br. Polym. J.* **1975**, 7, 319.

[27] D.E. Fenton, J.M. Parker, P.V. Wright, *Polymer* **1973**, 14, 589.

[28] E. A. Rietman, M. L. Kaplan, R. J. Cava, *Solid State Ionics* **1985**, 17, 1, 67.

[29] Y.G. Andreev, P.G. Bruce, *Electrochimica Acta* **2000**, 45, 1417.

[30] M. Armand, *Adv. Mater.* **1990**, *2*, 278.

[31] M. Armand, J.M. Chabagno, M.J. Duclot, *Fast ion transport in solid* **1979**, Elsevier, 131

[32] C.Berthier, W.Gorecki, M. Minier, M.B. Armand, J.M. Chabaqno, P. Riqaud, *Solid State Ionics* **1983**, 11, 91.

[33] M. Watanabe, M. Rikukawa, K. Sanui, N. Ogata, H. Kato, T. Kobayashi, Z. Ohtaki, *Macromolecules* **1984**, 17, 2902.

[34] T.B. Ren, X.B. Huang, X. Zhao, *Journal of materials science* **2003**, 38, 3007.

[35] Z. Gadjourova, Y.G. Andreev, D.P Tunstall, P.G. Bruce, *Nature* **2001**, *412*, 520.

[36] F.M. Gray, J.R. MacCallum, C.A. Vincent, *Solid State Ionics* **1986**; 18-19, 282.

[37] D. Orbakh *Nonaqueous electrochemistry*, CRC Press, 1999 ISBN 0824773349

[38] Z.X. Wang, B.Y. Huang, H. Huang, L.Q. Chen, R.J. Xue, F.S.Wang, *Electrochimica Acta* **1996**, 41, 1443.

[39] A.M. Sukeshini, A. Nishimoto, M. Watanabe, *Solid State Ionics* **1996**, 86, 385.

[40] O. Bohnke, M. Frand, M. Rezrazi, C. Rousselot, C. Truche, *Solid State Ionics* **1993**, 66, 105.

[41] A.M. Stephan, R.T. Karan, N.G. Renganathan, S. Pitchumani, N. Muniyandi, P. Ramamoorthy, *J. Power Sources* **1999**, 81, 752.

[42] M. Gazard, *Handbook of Conducting Polymers*, vol. 1, **1986**, Marcel Dekker.

[43] M.P. Scott, M. Rahman, C.S. Brazel, *European Polymer Journal*, **2003**, 39, 1947

[44] H.S. Choe, J. Giaccai, M. Alamgir, K.M. Abraham, *Electrochim Acta* **1995**, 40, 2289.

[45] C. Capiglia, Y. Saito, H. Kataoka, T. Kodama, E. Quartarone, P. Mustarelli, *Solid State Ionics* **2000,**131, 291.

[46] N. Treuil, *Synthèse et caractérisation des composants d'un accumulateur au lithium* **1998**, thesis, Université Bordeaux 1, France

[47] J.M. Tarascon, A.S. Goztz, C. Schmutz, F. Shokooki and P.C. Warren, *Solid States Ionics* **1996**, 86, 46.

[48] Y. Saito, H. Kataoka, A.M. Stephan, *Macromolecules* **2001,** 34, 6955.

[49] J.Y. Song, Y.Y. Wang, C.C.Wan, *J. Electrochem. Soc.* **2000**, 147, 3219.

[50] T. Michot, A. Nishimoto, W. Watanabe, *Electrochimica Acta* **2000**, 45, I347.

[51] H. Huang, S.L. Wunder, *J. Electrochem. Soc.* **2001**, 148, A 279.

[52] F. Croce, G.B. Appetecchi, L. Perci, B. Scrosati, *Nature* **1998**, 394, 456.

[53] S.S. Kaarup, K. West, B.C. Zachau, *Solid State Ionics* **1980,** 28, 375.

[54] W. Wieczorek, *Mater Sci Eng B* **1992,** 15, 108.

[55] F. Capuoano, F. Croce, B. Scrosati, *J Electrochem Soc* **1991**, 138, 1918.

[56] C.J. Leo, G.V. Subba Rao, B.V.R. Chowdari, *Solid State Ionics* **2002**, 148, 1-2, 159.

[57] T. Lapp, S. Skaarup, A. Hooper, *Solid State Ionics* **1983**, 11, 97.

[58] J.L. Briant, G.C. Farrington, *J. Electrochem. Soc.* **1981,** 128, 9, 1830.

[59] H.Y.P. Hong, *Mater. Res. Bull.* **1978**, 13, 117.

[60] R. Kanno, M. Murayama, *J. Electrochem. Soc.* **2001**, 148, 7, A742.

[61] X. Yu, J.B. Bates, G.E. Jellison, F.X. Hart, *J. Electrochem. Soc.* **1997**, 144, 524.

[62] a) H. Aomo, E. Sugimoto, Y. Sadaoka, G. Adachi, *J. Electrochem. Soc.* **1989**, 540 ; b) V. Thangadurai, W. Weppner, *Ionics* **2002**, 8, 281.

[63] Y. Inaguma, C. Liquan, M.Itoh, T. Nakamura, T. Uchida, H. Ikuta, W. Wakihara, *Solid State Commun.* **1993,** 86, 689.

[64] V. Thangadurai and W. Weppner, *Ionics* **2006**, 12, 81.

[65] H. Ohno, *Electrochemical aspects of Ionic liquids* **2005**, Wiley.

[66] J. Fuller , A. C. Breda, R. T. Carlin, *Journal of Electroanalytical Chemistry* **1998**, 459, 29.

[67] J.S. Oh, J. D. Park, B.B. Lee, W.J. Kwon, Kim, S.H., S.J. Mun, *Gel polymer electrolyte containing ionic liquid and electrochromic device using the same* **,** US Patent 7411716, Pub. **2008.**

[68] B. Yu, F. Zhou, C. Wang, W. Liu, *European Polymer Journal* **2007,** 43, 6, 2699.

[69] A. Vioux, J. Le Bideau, M.-A. Neouze, F. Leroux, Patent Appl. 2005/007746, WO2857004, **2005**

[70] Granqvist C.G., *Handbook of Inorganic Electrochromic Materials* **1995,** Elsevier Science Pub Co (ed.)

[71] M.L. Hitchmann, *J. Electroanal. Chem.* **1977**, 85, 135.

[72] B.W. Faughnan, R.S. Crandall,P.M. Heyman, *RCA Rev.* **1975**, 36, 177.

[73] P. Baudry, A.C.M. Rodriguez, M.A. Aegerter, L.O. Bulhôes, *J. Non-Cryst. Solids* **1990**, 121, 319.

[74] M. Rubin, K. Von Rottkay, S.-J. Wen, N. Özer, J. Slack, *Solar energy materials and solar cells* **1998**, 54, 49.

[75] R.J. Colten, A.M. Guzman, J.W. Rabalais, *J. Appl. Phys.* **1978**, 49, 1734.

[76] A.I. Gavrilyuk, F.A. Chudnovski, *Sov. Tech. Lett.* **1977**, 3, 69.

[77] W.C. Dautremont-Smith, *Displays* **1982**, 3, 67.

[78] S.F. Cogan, R.H. Rauh, *Solid State Ionics* **1988**, 28-30, 1717.

[79] M. Kitao, S. Yamada, *Proceedings of the International Seminar on Solid State Ionic Devices* **1988**, World Publishing Co., 359.

[80] S. Gottesfeld, *J. Electrochem. Soc*. **1980**, 127, 272.

[81] N.R. Armstrong, A.W.C. Lin, M. Fujihira, T. Kuwana, *Anal. Chem*. **1976**, 48, 741.

[82] J.P. Ziegler, B.M. Howard, *Proc. Electrochem. Soc.* **1994**, 94, 158.

[83] P. Pfluger, H.U. Künzi, H.J. Güntherodt, *Appl. Phys. Lett.* **1979**, 35, 771.

[84] a) G.S.E Collins, D.J. Schriffrin, *J. Electoanal. Chem.* **1982**, 139, 335, b) M.M. Nicholson, F.A. Pizzarello, *J. Electrochem. Soc.* **1979**, 126, 1490 ; c) M.M. Nicholson, F.A. Pizzarello, *J. Electrochem. Soc.* **1981**, 128, 1740.

[85] R.J. Mortimer, D.R. Rosseinski, *J. Elecroanal. Chem.* **1983,** 151, 133.

[86] R.O. Lezna, R. Romagnoli, N.R. de Tacón, K. Rajeshwar, *J. Electroanal. Chem.* **2003,** 544, 101.

[87] P.J. Kulesza, M.A. Malik, J. Shorek, K. Miecznikowski, S. Zamponi, M. Berrettoni, M. Giorgetti, R. Marassi, *J. Electrochem. Soc.* **1999,** 146, 10, 3757.

[88] M.K. Carpenter, R.S. Conell, S.J. Simko, *Inorg. Chem.* **1990,** 29, 845.

[89] P.J. Kulesza, M. Faszynska, *J. Electroanal. Chem.* **1988,** 252, 461.

[90] M.M. Nicholson, F.A. PIzzarello, *J. Electrochem. Soc.* **1981**, 128, 1288.

[91] R.J. Mortimer, R, *Electrochimica Acta* **1999**, 44(18), 2971.

[92] Samat, A.; Guglielmetti, R Encyclopedia of Chemical Technology (5th Edition) (2004), 6 571-587

[93] a) L.A. Summers, *Adv. Hetero. Chem.* **1984**, 35, 281 ; b) A.J. Bard, A. Ledwith and H.J . Shine, *Adv. Phys. Org. Chem.* **1976***, 13, 155 ; c) C.L. Bird and A.T. Kuhn, *Chem. Soc. Rev.* **1981**, 10, 49.

[94] a) A. Watanabe, K. Mori, Y. Iwasaki, Y. Nakamura, S. Niizuma, *Macromolecules* **1987**, 20 ,1793 ; b) L. Michaelis, *Chem. Rev.* **1935,** 16, 243.

[95] G. Inzelt, R.W. Day, J.F. Chambers, *J. Electroanal. Chem.* **1984**, 161, 147.

[96] J.E. Dubois, F. Garnier, G. Tourillon, M. Gazard, *J. Electroanal. Chem.* **1981**, 129, 229.

[97] B. Grant, N.J. Clecak, M. Oxsen, A. Jaffe, G.S. Keller, *J. Org. Chem.* **1980**, 45, 702.

[98] a) A. Desbène-Monvernay, P.C. Lacaze, A. Cherigui, *J. Electroanal. Chem*. **1989**, 260, 75 ; b) J.E. Dubois, A. Desbène-Monvernay, A. Cherigui, P.C. Lacaze, *J. Electroanal. Chem.* **1984**, 169, 157 ; c) M. Yashiro, K.Sato, *Jpn. J. Appl. Phys*. **1981**, 20, 1319 ; d) V.K. Gater, M.D. Liu, M.D. Love and C.R. Leidner, *J. Electroanl. Chem.* **1988,** 257, 133.

[99] F.B. Kaufman, E.M. Engler, *J. Am. Chem. Soc*. **1979**, 101, 547.

[100] R. Cinnsealach, G. Boschloo, S. Nagaraja Rao, D. Fitzmaurice, *Solar energy materials and solar cells* **1998**, 55, 3, 215.

[101] R.J. Mortimer, J.L. Dillingham, *J. Electrochem. Soc.* **1997**, 144, 1549.

[102] C.J. Schoot, J.J. Ponjée, H.T. van Dam, R.A. van Doorn, P.J. Bolwijn, *Appl. Phys. Lett.* **1973**, 23, 64.

[103] R. Mortimer; J. Dyer, L. Aubrey, J.R. Reynolds, *Displays* **2006**, 27, 1, 2.

[104] J. Dyer, L. Aubrey; J.R. Reynolds, *Electrochromism of conjugated conducting polymers***.** Handbook of Conducting Polymers (3rd Edition) **2007**, 1, 20.

[105] L. Groenendaal, F. Jonas, D. Freitag, H. Pielartzik, J.R. Reynolds, *Adv. Mater*. **2000**, 12, 7, 481

Chapter II. Electrolytes based on BMIPF$_6$ and BMITFSI ionic liquids with LiTFSI lithium salt and PMMA polymer

_____

II. 1. Introduction

The electrolyte allows ions movements between the two electrodes in order to provide ions to compensate the charge created by redox reactions taking place at the electrodes. In addition to this first functionality, the electrolyte can advantageously be formulated as an adhesive in order to give mechanical strength to the electrochromic stack (see Figure II.1).

PET 150µm
ITO 0.2µm
EC1 0.3µm
Electrolyte 40 µm
EC2 0.3µm
ITO 0.2µm
PET 150µm
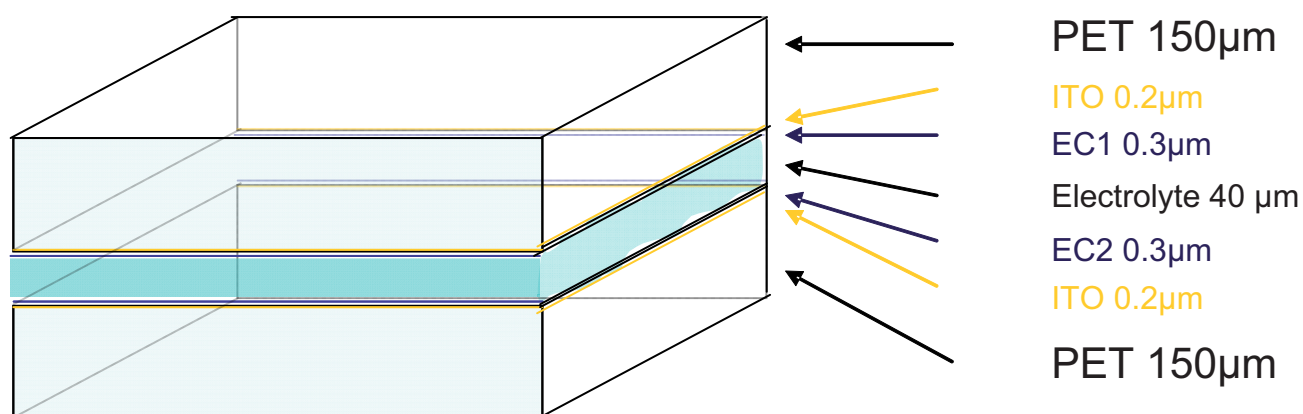
Figure II.1: Complete EC device and the approximate dimensions for each layer of the stack, the electrolyte has a central position.

The electrolyte medium we chose is ionic liquid based. As already discussed, ionic liquids (ILs) benefit from wide electrochemical window, low vapour pressure (meaning low volatility), high thermal stability and rather high ionic conductivity, the later being only one range of order lower than that of classical liquid electrolytes (see chapter I). Moreover, they belong to the so-called 'green chemistry' solvents, meaning that they are environmentally friendly since easily recyclable.

Some of these ILs which contain fluorine atoms, such as 1-butyl-3-methylimidazolium hexafluorophosphate and 1-butyl-3-methylimidazolium bis(trifluoromethanesulfonyl)imide, $BMIPF_6$ and BMITFSI salts respectively, also exhibit a hydrophobic character useful for the long term stability of electrochromic devices.

When used as polymer plasticizers, these ILs give rise to leakage-free, safe membrane electrolytes. Poly(methyl methacrylate) (PMMA) has been chosen as a polymer for its high transparency and colourlessness, high compatibility with the chosen ionic liquids and good electrochemical stability[1,2]. ICMCB and CRPP teams have been the first to patent the use of this kind of electrolytes for electrochromic applications.[3]

In order to assess the main properties (thermo-mechanical properties, ionic conduction, chemical species in presence, etc.) of such liquid and related membrane electrolytes, liquid electrolytes (BMIPF$_6$ and BMITFSI ILs with LiTFSI lithium salt) and the liquid electrolyte – PMMA polymer associations have been analysed in terms of:

- Glass transition temperature using Differential Scanning Calometry (DSC),
- Transparency using UV-Visible spectroscopy
- Crystallinity using X-Ray diffraction (XRD)
- Ionic conductivity using Electrochemical Impedance Spectroscopy (EIS),
- Species in presence and their interactions using Raman and Attenuated Total Reflectance Infrared (ATR-IR) spectroscopies.
- Species diffusion coefficients using Pulsed Gradient Spin Echo Nuclear Magnetic Resonance (PGSE-NMR).

Two types of ionic liquid-based electrolytes were prepared by dissolving the lithium salt, lithium bis(trifluoromethanesulfonyl)imide, LiTFSI, in the following ionic liquid-based solvents : BMIPF$_6$ and BMITFSI (Figure II.2) with different lithium salt molar ratios (x_{LiTFSI} from 0.01 to 0.36). PMMA molecular weights (from 35,000 to 150,000 g/mol) were used. For the Mw = 96,400 g/mol an extensive study has been performed varying the PMMA weight percent from 20 to 50 %.

In a first part, the experimental procedures for the electrolyte preparation will be presented as well as the experiments for characterization listed above. A discussion on the probable structure and ionic interactions within the electrolytes will be included.

II. 2. Electrolyte preparation

II. 2. 1. Products

The two ionic liquids, BMIPF$_6$ and BMITFSI (Figure II.2) were provided by Solvionic, one of the Nanoeffects program partners, with a purity of 99%. For sake of clarity, the results concerning BMIPF$_6$ will be presented in appendix C.

BMITFSI (BMI$^+$ TFSI$^-$)
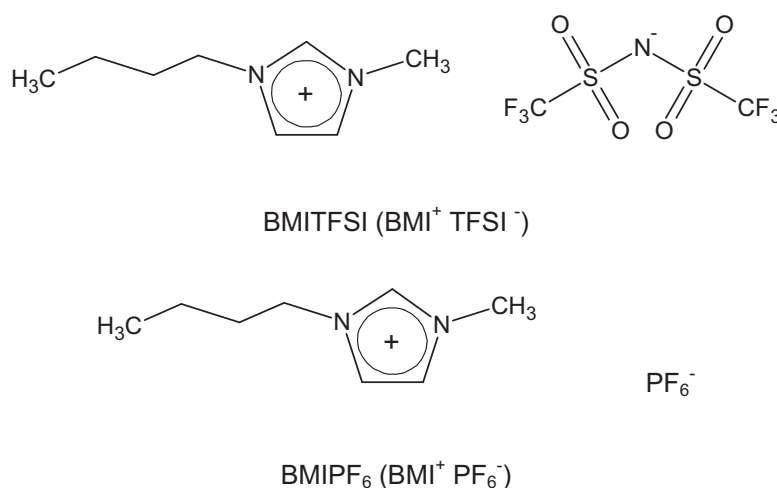
BMIPF$_6$ (BMI$^+$ PF$_6^-$)

Figure II.2: Formula of BMITFSI and BMIPF$_6$

LiTFSI and PMMA are purchased from Aldrich and dried for 2h at 100°C before use. PMMA is provided as beads. Anhydrous butanone, acetone and dichloromethane, used for the ionic liquids and PMMA mixing, are purchased from Aldrich, in a high purity grade, stored under argon and used as received.

All the products are stored and handled in the glove box.

II. 2. 2. Electrolyte preparation procedure

Liquid electrolytes are prepared by dissolving the lithium salt, LiTFSI, in the ionic liquid solvent (either BMIPF$_6$ or BMITFSI). Solutions with LiTFSI molar ratios from 0.00 to 0.17 in BMIPF$_6$ and from 0.00 to 0.36 in BMITFSI have been prepared. The lower solubility of LiTFSI in BMIPF$_6$ prevented the use of concentrations as high as in BMITFSI which has a common anion TFSI$^-$ with the lithium salt. A co-solvent (dichloromethane) was used with BMIPF$_6$ to assist the salt dissolution at room temperature leading to a fully transparent electrolytic solution. Once prepared, these liquid electrolytes were mixed with different

weight ratios of PMMA. Three commercially available PMMA molecular weights (M$_w$) were chosen: 35,000; 96,400 and 150,000 g/mol.

The PMMA is dissolved in solvents such as acetone, dichloromethane, or butanone, and is then added to the ionic liquid based liquid electrolyte in the required proportions (between 20 and 50 wt% of the total final weight). Before deposition, the mixture is stirred during at least one hour until getting a clear and homogeneous solution. The quantities of co-solvent used to plasticize the PMMA (M$_w$ = 96,400 g/mol), are reported in Table II.1. They have been chosen in order to easily cast the solution by doctor-blade and spin-coating techniques. We will note (see Table II.1) that 1 g of PMMA in 5 g of liquid is used in order to achieve the complete swelling of PMMA.

wt%PMMA	m $_{PMMA}$(g)	m liquid electrolyte (x) (g)	m butanone (y) (g)	m liquid (x+y) (g)
20	1	4	1	5
30	1	2,3	2,7	5
40	1	1,5	3,5	5
50	1	1	4	5

Table II.1: Quantities of the different components in order to obtained different wt% of PMMA in the final coated membranes. The given quantity of co-solvent (butanone) must be added in order to get the appropriate viscous solutions suitable for doctor-blade, spin-coating depositions.

The deposition conditions generally used were:

- for spin-coating, a sequence, 30s at 600 rpm ; 30s at 1000 rpm and 2s at 2000 rpm

- for doctor blade, the use of a plain bar and deposition at 2 cm/s with a height of 200 μm.

They were adapted depending on the desired thickness. Once the polymer electrolyte-based solution was deposited, the co-solvent was evaporated by a thermal treatment at 70°C under primary vacuum for 2 hours. By doctor blade, a membrane with an 85 μm thickness is obtained with the 40wt% PMMA solution (for complete devices, further heating under press for the fabrication of complete devices decreases this value to around 40-50 μm).

The various mixtures studied in the following parts are gathered in Table II.2.

wt%PMMA / total	x_{LiTFSI} in BMITFSI	m LiTFSI (g)	$m_{BMITFSI}$ (g)	m_{PMMA} (g)	MMA/Li
0	0	0.000	1	0	0
0	0.03	0.021	1	0	0
0	0.05	0.036	1	0	0
0	0.08	0.060	1	0	0
0	0.36	0.385	1	0	0
20	0.03	0.085	4	1	34
30	0	0.000	2.33	1	n/a
30	0.03	0.049	2.33	1	58
40	0.03	0.032	1.5	1	90
40	0.12	0.140	1.5	1	20
40	0.18	0.225	1.5	1	13
40	0.22	0.290	1.5	1	10
50	0.03	0.021	1	1	135
50	0.12	0.093	1	1	31
50	0.18	0.150	1	1	19
50	0.22	0.193	1	1	15

Table II.2: Different mixtures of electrolytic membranes studied in the following parts. The molar ratio of LiTFSI, *x*, in the solution LiTFSI/BMITFSI are given. The wt% PMMA is the weight percentage of PMMA in the final membrane containing the solution *x* LiTFSI/(1-*x*)BMITFSI and PMMA. The MMA/Li ratio number will be mostly useful for Raman analysis (see below). A molar ratio of 0.36 LiTFSI corresponds to about 0.1M in molar concentration.

II. 3. Thermo-mechanical characterisation

II. 3. 1. DSC measurements

Differential Scanning Calorimetry measurements (see appendix A for more information on this technique) have been performed for BMITFSI and BMIPF$_6$ (appendix C) ILs with and without the lithium salt as well as for their corresponding based electrolytic PMMA based membranes. DSC measurements give information on the glass transition temperature of glassy compounds such as polymers and ionic liquids. Information on the melting point and on the crystalline/amorphous ratio of such compounds is also provided.

II. 3. 1. 1. Effect of the addition of LiTFSI on the transition temperatures of BMITFSI

The DSC measurements were performed for pure IL and ILs having two different Li salt concentrations. The diagram presents both a glass transition around - 87°C and a crystallisation/melting one at higher temperatures, cf. Figure II.3.
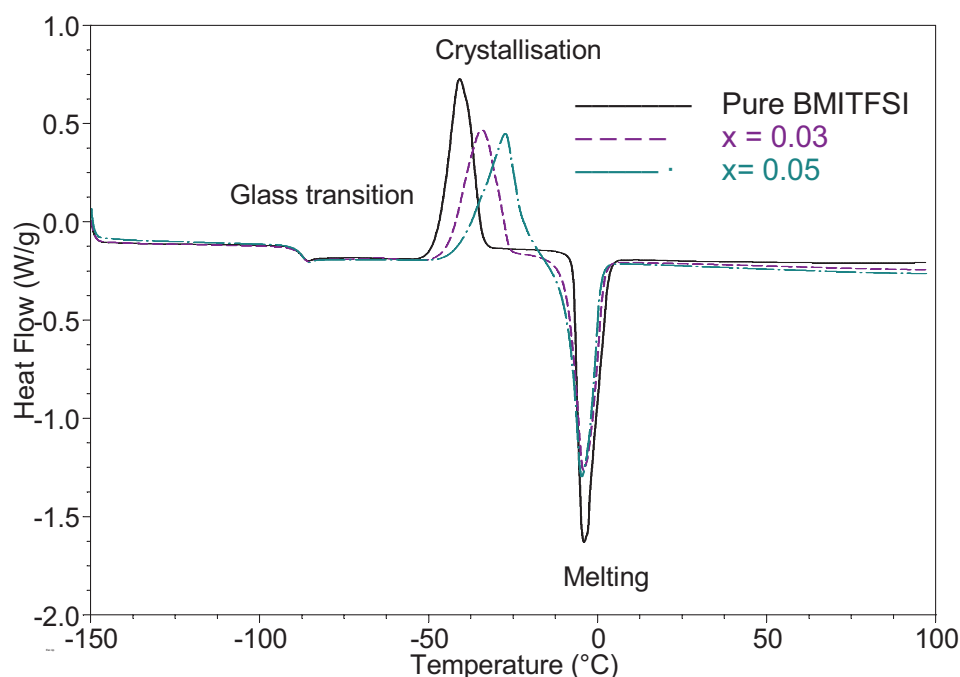
Figure II.3: Evolution of the DSC curves with increasing LiTFSI molar ratios in BMITFSI.

The glass transition (T$_g$) and melting (T$_m$) temperatures have been extracted from the graph and are reported in Table II.3.

x $_{LiTFSI}$	T$_g$ (°C)	T$_m$ (°C)
0	-87.0	-4.1
0.03	-87.3	-4.2
0.05	-87.0	-4.9

Table II.3: DSC analysis of LiTFSI/BMITFSI mixtures, glass transition temperature (T$_g$), and melting temperature (T$_m$)

The glass transition and melting temperatures remain unchanged (-87°C and -4°C) as LiTFSI molar ratio is increased from 0 to 0.05 in BMITFSI (Table II.3).The same trend is observed in BMIPF$_6$ (cf. appendix C).

The crystallisation temperature (T$_c$), crystallisation heat (H$_c$), i.e. area under the crystallisation peak, melting heat (H$_m$), i.e. area under the melting peak, as well as the difference between the melting heat and the crystallisation heat (H') can also be calculated from the DSC curves; they are listed in Table II.4.

The crystallisation temperature shifts towards higher values as LiTFSI molar ratio increases. Crystallisation appears at -41.0°C for pure BMITFSI, versus -34.2°C for x = 0.03 and -27.4°C for x = 0.05. The system needs a higher temperature to self-organize and to crystallize, probably because of the disturbing effect introduced by Li$^+$ cation. Raman

44

spectroscopy[4] will show that this cation is able to coordinate 2 TFSI⁻ anions and generate a BMI⁺[Li(TFSI)$_2$]⁻ cluster-like system which prevents the normal crystallisation of the IL. This could also explain the broad character of this crystallisation.

x_{LiTFSI}	T_c(°C) (K)	H_c (J/g)	H_m(J/g)	H'=H_m-H_c
0	-41.0 (232)	-45.4	55.7	10.3
0.03	-34.0 (239)	-42.6	48	5.4
0.05	-27. 0 (246)	-47.6	48	0.4

Table II.4: DSC analysis of LiTFSI/BMITFSI mixtures, crystallisation temperature (T_c), crystallisation heat (H_c), melting heat (H_m), difference between melting heat and crystallisation heat (H').

Moreover, the difference between the melting heat (area of the melting peak) and the crystallisation heat (area of the crystallisation peak) is positive. It means that the melting peak includes the melting of the crystalline part that has been formed just before (crystallisation peak) and of an additional crystalline part that was already present in the compound. This difference in heat decreases from 10.3 J/g for the pure BMITFSI to 5.4 J/g for x = 0.03 and 0.4 J/g for x = 0.05 indicating that the crystalline part of the ionic liquid before experiment gets smaller as LiTFSI is added showing again that the crystallisation process of the IL is disturbed by the presence of LiTFSI.

II. 3. 1. 2. Effect of the PMMA addition in BMITFSI/LiTFSI/PMMA membranes

The DSC diagrams for 0.03 LiTFSI/ 0.97 BMITFSI with increasing PMMA ratio (0 to 50 wt% of PMMA) are given on Figure II.4.

Despite the presence of two major distinct components (PMMA and BMITFSI) in this system, the polymer electrolytes exhibit a single Tg in this range of composition, and the endothermic peak corresponding to the melting point of BMITFSI vanishes (Figure II.4). Therefore, for all the considered compositions of the ion gels, the systems at temperatures around room temperature are in a rubbery state (temperature higher than T_g) and behave as monophasic compounds.
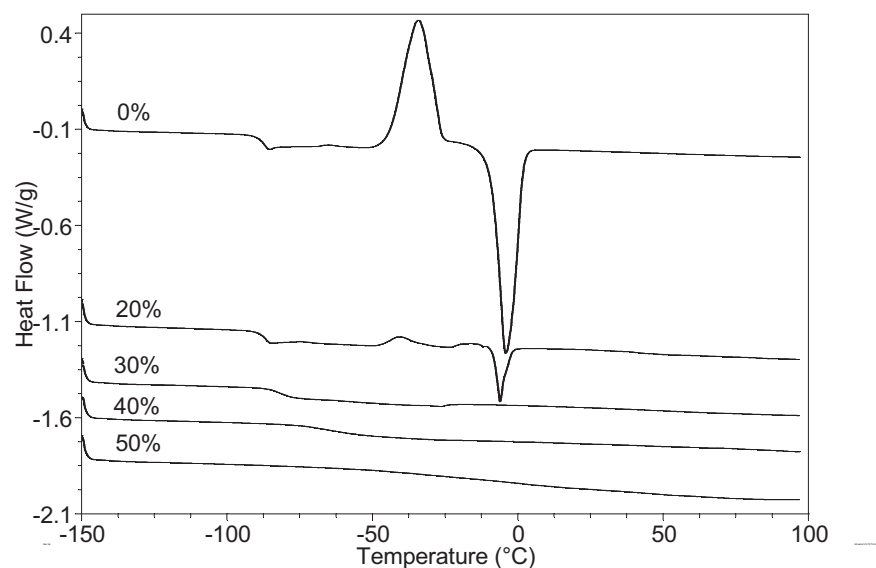
Figure II.4: Variation of the DSC curves with increasing PMMA wt% from 0 to 50 in 0.03 LiTFSI/ 0.97BMITFSI solution.

The glass transition temperatures have been extracted from these graphs and their composition dependence with varying [PMMA]/[0.03LiTFSI-0.97BMITFSI] ratios is presented in Figure II.5.
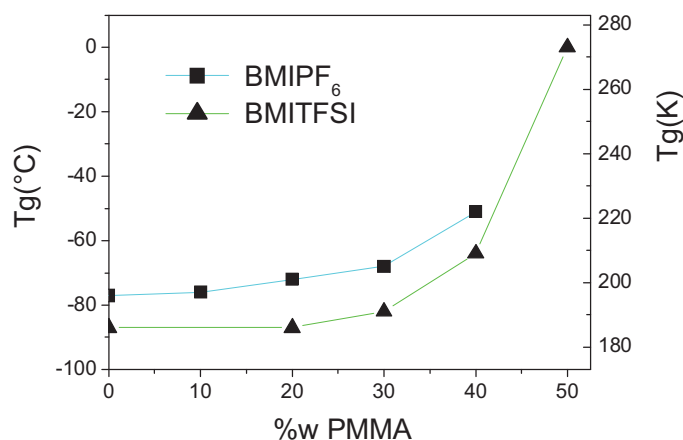
Figure II.5: Variation of the glass transition temperature (Tg) of membranes containing 0.04LiTFSI/0.96BMIPF$_6$ and 0.03LiTFSI/0.97BMITFSI with respect to the PMMA weight percentage (from 0 to 50%) in the membrane.

For comparison, the Tg variation for [PMMA]/[BMIPF$_6$] electrolytes is also reported here. Up to 30% PMMA, the T$_g$ is rather constant and close to the Tg of pure ionic liquid (-87°C for BMITFSI and -77°C for BMIPF$_6$). For higher PMMA contents, Tg dramatically increases (Figure II.5), but still remains much lower than that of PMMA (T$_{g\ PMMA}$ = 103°C).

This dependence of Tg on the composition can be better understood if we consider the equation developed by Fox[5] for compatible polymer/polymer systems and adapted to polymer

plasticized by an ionic liquid[6]. It is based on the additive character of the weight fraction of the two components. If the Tg of the polymer (PMMA) and the ionic liquid (BMITFSI), are represented by Tg_{PMMA} and $Tg_{BMITFSI}$, respectively, the Fox equation is given by equation (II.1):

(II.1) $$1/Tg = w_{BMITFSI}/Tg_{BMITFSI} + w_{PMMA}/Tg_{PMMA}$$
$$\text{with } w_{BMITFSI} + w_{PMMA} = 1$$

where $w_{BMITFSI}$ and w_{PMMA} are the weight fractions of BMITFSI and PMMA respectively, in the systems. The experimental results fit rather well this equation (Figure II.6) for wt% PMMA up to 40%. Therefore, this system of PMMA and BMITFSI/LiTFSI behaves as a compatible system, with interactions between the liquid electrolyte and the polymer; (interactions which will be addressed later on (Raman, ATR-IR measurement)).
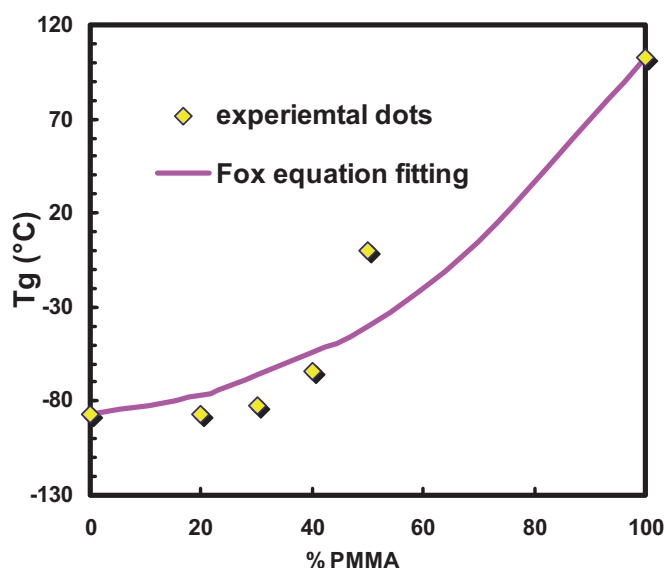
Figure II.6: Variation of the glass transition temperature (Tg) of membranes containing 0.03LiTFSI/0.97BMITFSI with respect to the PMMA weight percentage (from 0 to 50%), and comparison with Fox equation.

The DSC measurements on these membrane electrolytes (Figure II.4) also highlight the disappearing of the crystallisation and melting peaks of the IL with increasing PMMA ratios. The presence of PMMA disturbs the IL crystallisation, as will be shown in the Raman and ATR-IR experiments.

II. 3. 2. Adhesive properties of the membrane electrolyte

Playing with the PMMA/IL ratios allows a fine tuning of the consistency, rheological and adhesive properties of such membranes. As preliminary results, this can be observed by preparing electrolyte membranes of different PMMA ratios in between two plates (for example glass or FTO glass plates) and submitting them to a manual shearing stress. Table II.5 gives the appreciation of the electrolytes in terms of consistency (gel or self-standing membranes) and in terms of adhesive properties.

wt% PMMA	Effect of the manually applied shearing stress	Membrane mechanical properties at RT	Adhesive properties
20		Liquid-gel	Falls apart by simple manual pressure
30		Gel	Falls apart after a few seconds of manual pressure
40		Gel-membrane	Moves after a few tens of seconds of manual pressure
50		Membrane	Does not fall apart manually

Table II.5: Consistency and appreciation of the electrolytic membrane sticking properties (20 to 50 wt% PMMA, 0.03 LiTFSI / 0.97 BMITFSI)

The membranes with 20 and 30 wt% PMMA have a bad adhesion. For 40 to 50 wt% PMMA, a membrane with cohesive properties is formed, leading to much better adhesion properties. This shows again interactions between the PMMA and the liquid since cohesive membranes are obtained (no demixion).

II. 4. Membrane transparency

High transparency of electrolyte-membrane is a fundamental aspect for the Nanoeffects project with regards to the optical specifications from industrial partners such as Essilor (ophthalmic lenses) and Maser (car windows).

Due to the gel consistency of some electrolyte-membranes, the transparency measurements are performed by placing the electrolyte between two glass slides (see appendix A for more information). Measurement corrections must be applied to take into account the refractive index mismatch between glass and air optical indexes, whereas the refractive indexes of glass and electrolyte-membrane are close (see Table II.6). The ratio R of reflected light at an interface under normal incidence is given by:

(II.2) $$R = \left(\frac{n_{verre} - n_{air}}{n_{verre} + n_{air}} \right)^2$$

As two interfaces glass/air are replaced by glass/membrane interfaces, a correction of 8.0 % in transmission must be applied. The refractive indexes of the different components of the membranes are given in Table II.6.

Component	Refractive index (25°C)
Glass	1.513 (Soda Lime, 645 nm)
Air	1.00
PMMA	1.495 (589.3 nm)[7]
BMITFSI	1.427 (wavelength not specified)[8]

Table II.6: Refractive indexes of the components of the membrane.

The membranes all exhibit a very high transparency in the visible range; the worst being at 99 % in transmittance for the 50 wt% PMMA based membrane (Figure II.8 and Figure II.7). Moreover, no haze is visible neither on the solution or membranes up to $x = 0.36$.
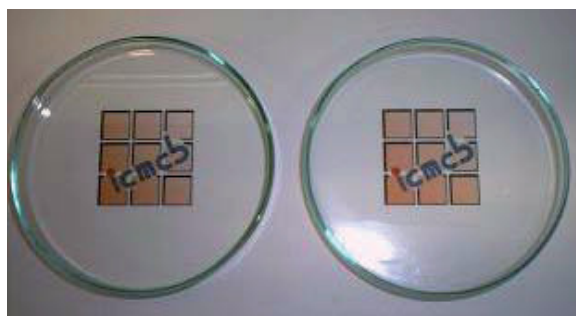
Figure II.7: Two Petri dishes: left hand side with no deposited membrane and right hand side with an electrolytic membrane (0.03 LiTFSI/0.97 BMITFSI) for a PMMA 30 wt %.
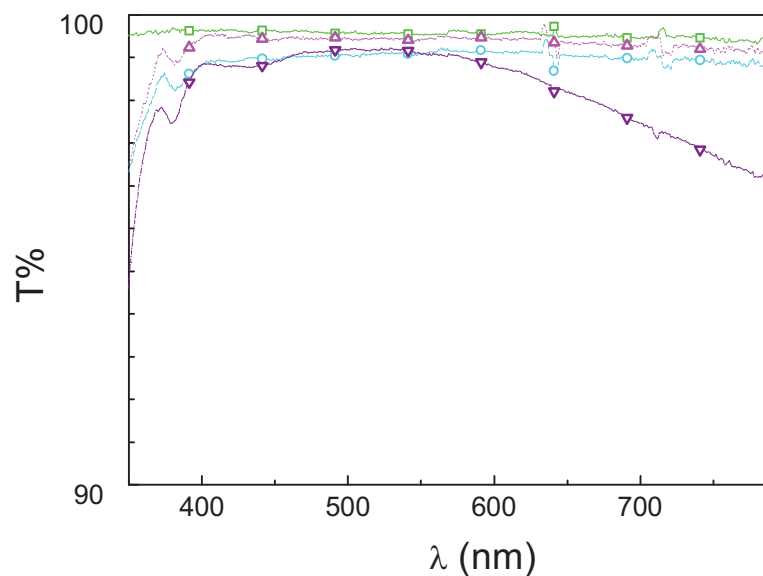
Figure II.8: UV-Visible spectra of electrolytic membranes (0.03 LiTFSI/ 0.97 BMITFSI) deposited in between two glass slides for wt% PMMA: □ 20%, ○ 30%, △ 40%, ▽ 50%.

II. 5. XRD analysis

The XRD diagrams for PMMA and electrolyte membranes with 0.03LiTFSI/0.97BMITFSI and varying PMMA wt% are given in Figure II.9 (for more information see appendix A).
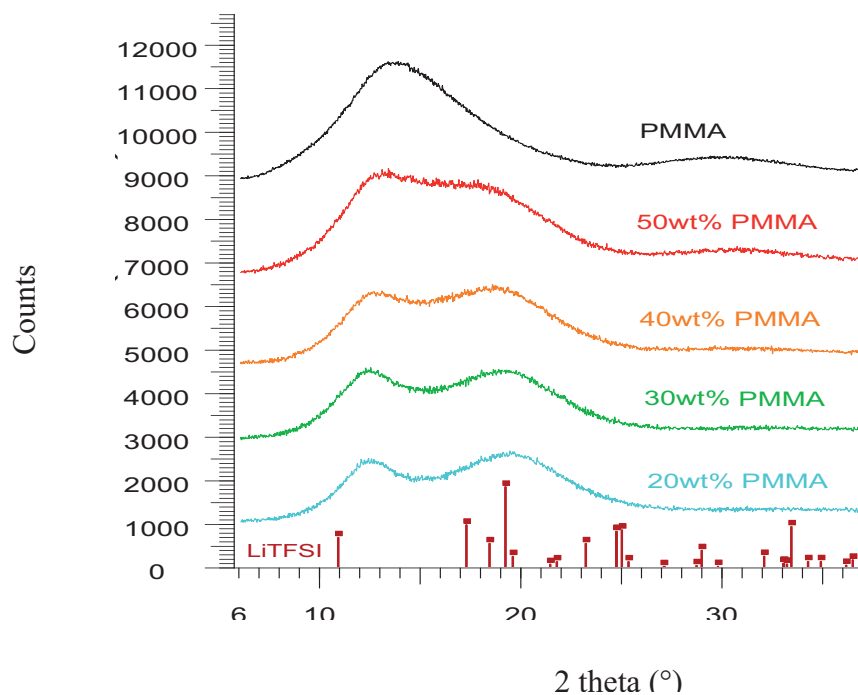
Figure II.9: X-ray diffraction diagram of PMMA (——) and PMMA membranes plasticized with 0.03LiTFSI/0.97BMITFSI for wt% PMMA: 50 wt% (——); 40 wt% (——); 30 wt% (——); 20 wt% (——).

The pure PMMA (Mw =96,400 g/mol) shows two zones of ill-defined crystallisation centred at two-theta 13.6 and 30.14 ° (d = 6.5 and 2.9 Å).

The introduction of increasing amounts of LiTFSI/BMITFSI in the PMMA membranes generates a new broad peak, centred around 20° (Figure II.9). It may account for a local organisation of PMMA probably due to interconnectivity by lithium cations. It is however very difficult at this point to deduce more information with regards to the nature of the respective interactions in the membrane. More information will be obtained from Raman and IR experiments.

II. 6. Homogeneity of deposited membranes

DSC measurements showed that only one glass transition occurs, which is in favour of the miscibility of PMMA with the ionic liquid as already observed in the literature.[9] Raman spectroscopy in the mapping mode has been used to control the homogeneity of the membranes. No change in the Raman spectra is observed when scanning the whole surface of a 2 cm-diameter membrane disc showing that the electrolytes are homogeneous at the scale of Raman spatial resolution i.e. 1 μm. This demonstrates the accuracy of the preparation procedure for electrolyte solutions and films.

II. 7. Ionic conductivity of the electrolytes

II. 7. 1. Electrochemical Impedance Spectroscopy (EIS) principle

Electrochemical Impedance Spectroscopy (EIS) measures the overall conductivity of the electrolytic media, whatever its state: liquid, gel, or membrane. This can be performed at different temperatures and then gives rise to the thermodynamic characteristics of the system.

The fundamental approach of all impedance methods is to apply a small amplitude sinusoidal excitation signal to the system under investigation and measure the response (current or voltage or another signal of interest) (Figure II.10).
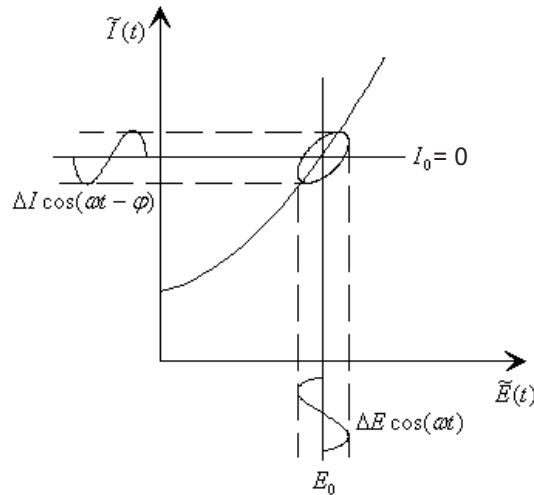
Figure II.10: Principle of EIS, a periodic signal is applied to the sample and the periodic variation of the studied parameter is measured.

By modulating the applied signal frequency from high to low frequencies, the different electrochemical phenomena from the quickest to the slowest can be scanned. The confrontation between experimental data and model electrical circuits leads to parameters such as proper resistance, diffusion, and charging transfer coefficients.

The amplitude of the applied signal is chosen small enough as to remain in the pseudo-linear behaviour range, so that the response is a signal with the same frequency as the excitation signal; only its phase changes.

In the case of an applied sinusoidal potential signal, given by:

(II.3)   **E(t)=E$_0$ cos(ωt)**

The answer signal in terms of current density will be:

(II.4)   **I(t)= I$_0$ cos(ωt+Φ)**

The impedance is calculated as the potential over the current intensity:

(II.5) $$Z(t) = \frac{E(t)}{I(t)} = \frac{E_0 \cos(\omega t)}{I_0 \cos(\omega t + \Phi)} = Z_0 \frac{\cos(\omega t)}{\cos(\omega t + \Phi)}$$

This can be noted in complex notation:

(II.6) $Z(t) = Z' - jZ''$ **with** $Z' = Z_0 \cos \Phi$ **and** $Z'' = Z_0 \sin \Phi$

A usual representation of the impedance is the Nyquist's plot, which consists in reporting the complex plan –Z" as a function of Z'.
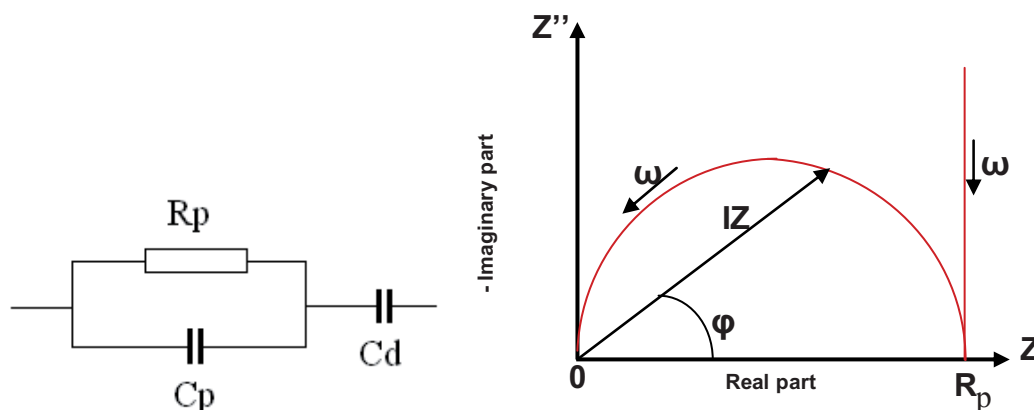
Figure II.11: RpCp electrical circuit with Cd capacity from blocking electrode (a) and associated Nyquist plot (b).

The Nyquist's diagram of an electrolyte sandwiched between two stainless-steel blocking electrodes is given in Figure II.11 a. The equivalent electrical circuit consists in one resistance R_p, one capacitance C_p associated in parallel (the product $R_p C_p$ being the relaxation time, namely the time required for mobile species of the electrolyte to jump from one site to the neighbouring equivalent one) and a capacitance C_d associated in series with the parallel R_p-C_p configuration; C_d represents the accumulation of the mobile species in the electrolyte at the blocking electrodes, which takes place at low frequencies of the excitation signal. Therefore, the Nyquist's plot is composed of a circle at high frequencies due to the R_pC_p circuit and a capacitive vertical slope at low frequencies (see Figure II.11 b).

For more information on EIS technique, see appendix A.

II. 7. 2. EIS measurements procedure

EIS measurements on electrolytes are performed with a HP 4194A Impedance/Gain Phase analyser. The temperature is measured with a platinum resistance thermometer connected to a Keithley 195A digital multimeter. Frequency range (from 100 Hz to 15 MHz) is scanned by measuring the impedance in 200 points per decades of frequencies with 16 measures for each point. The potential amplitude of the entrance signal is 200 mV, the sample is not polarized ($E_{average} = 0.0V$).

The electrolyte is placed in a two-electrode cell, the electrodes being metallic blocking electrodes. In the case of liquid electrolytes, the liquid is placed in a cell made of two pieces

of brass of diameter 2 cm with an internal diameter of 1.8 cm. A constant space of 500 microns in between the two electrodes is ensured by a rigid PTFE O-ring (cf. Figure II.12).

For membranes, the electrolyte solution (membrane dissolved in butanone) is deposited by doctor blade on a stainless steal plate (diameter 2 cm). A PTFE O-ring (t = 100 µm, external diameter = 2 cm, internal diameter = 1.8 cm) is placed on top of the membrane to avoid short circuits between the two metallic electrodes. After butanone evaporation obtained by heating at 70°C for 2h, the second stainless steel plate is placed on top of the electrolyte. The assembly is then heated at 70°C under vacuum until being stuck together.

Top   Cross   Top   Cross

a)   b)
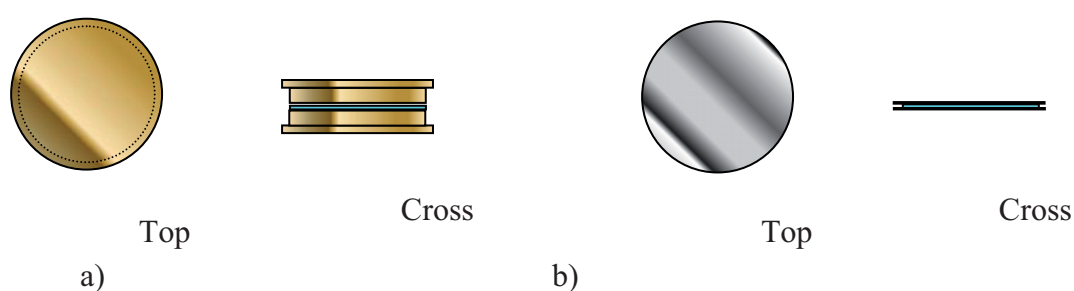
Figure II.12: Schematic view of the two-electrode cell used for EIS measurement for liquid electrolytes (a) and membranes (b)

The current collector of the EIS apparatus is made of brass, a system with a spring ensures the electrical contact between the cell and the current collector.

II. 7. 3. Ionic conductivity results

As for DSC measurements, the study of the variation of the ionic conductivity has been performed for membranes using the two ionic liquids BMITFSI and BMIPF$_6$. For sake of clarity we have chosen to go on presenting the results concerning the BMITFSI system in the following and those for BMIPF$_6$ in appendix C.

The different compositions are given below for both the liquid and the membrane electrolytes:

- liquid electrolytes:
    - BMITFSI with x_{LiTFSI} = 0, 0.03, 0.05, 0.08, 0.1, 0.12, 0.36
- membrane electrolytes :

- BMITFSI / PMMA (0, 30 wt%)
- BMITFSI / x_{LiTFSI} = 0.03, 0.12, 0.18, 0.22 / PMMA (40, 50 wt%)
- BMITFSI / x_{LiTFSI} = 0.03 / PMMA (0, 20, 30, 40, 50 wt%)

II. 7. 3. 1. EIS spectra variation with temperature

The effect of the temperature on the EIS spectra gave the same kind of results for all the compositions. An example for 0.97 BMITFSI / 0.03 LiTFSI (molar ratio) / PMMA = 40 wt% is illustrated in Figure II.13 which represents the classical variation of the impedance spectra with temperature between - 30 °C and + 60 °C. Similar behaviours are observed for LiTFSI/ BMIPF$_6$ electrolytes.
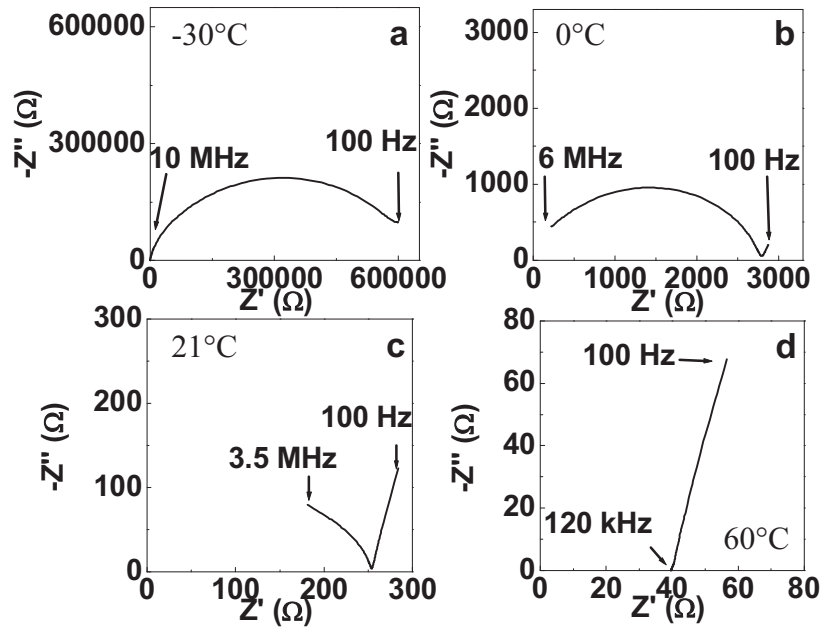
Figure II.13: EIS spectra of a cell containing the gel electrolyte BMITFSI / x_{LiTFSI} = 0.03 / PMMA =40 wt% in between two stainless-steel electrodes for different temperatures : (a) - 30 °C, (b) 0 °C, (c) 21 °C, (d) 60 °C

At low temperature, the impedance spectrum on the whole range of frequencies consists only in a semi-circle. As the temperature increases, a vertical line progressively appears and becomes the only visible signal at higher temperatures. The semi-circle represents a relaxation phenomenon that can be characterized by an average relaxation time τ = RpCp. τ is the time needed by the mobile species to leave their position and reach an empty side

position. At higher temperature, the capacitive behaviour is observed for lower frequencies. Indeed the ions are more mobile and have enough time to reach the metallic electrode before the field changes of sign. Moreover, the observation that the semi-circle centre is not fully centred on the Z' axis shows that different mobile species are in presence but that they have relaxation times and then diffusion coefficients ($D = e\tau/l$ with l the diffusion length of the ionic species) rather similar. This will be confirmed by the NMR study.

Depending on the temperature of measurements, the internal resistance of the electrolyte, Rp, is measured at the intersection between the circle and the Z'-axis or at the intersection of the vertical slope with the Z'-axis.

II. 7. 3. 2. Influence of LiTFSI concentration on IL based liquid electrolyte conductivity.

All the measurements were performed under moisture-free atmosphere in the temperature range from – 30 °C to 60 °C. LiTFSI molar fractions from 0.0 to 0.36 have been tested.

II. 7. 3. 2. i. EIS spectra variation

Figure II.14 shows the variation of the ionic conductivity with the temperature for different lithium salt molar fractions.

The curves at different LiTFSI molar ratios exhibit a similar decrease of σ with temperature. The ionic conductivity of BMITFSI is always the highest among all the measured temperature range and decreases with increasing LiTFSI concentration. At 303 K, the LiTFSI dependent ionic conductivity decreases by a factor of more than 5, from 3.8 mS cm^{-1} for BMITFSI to 0.7 mS cm^{-1} for the LiTFSI/BMITFSI electrolyte (LiTFSI molar ratio from 0 to 0.36).
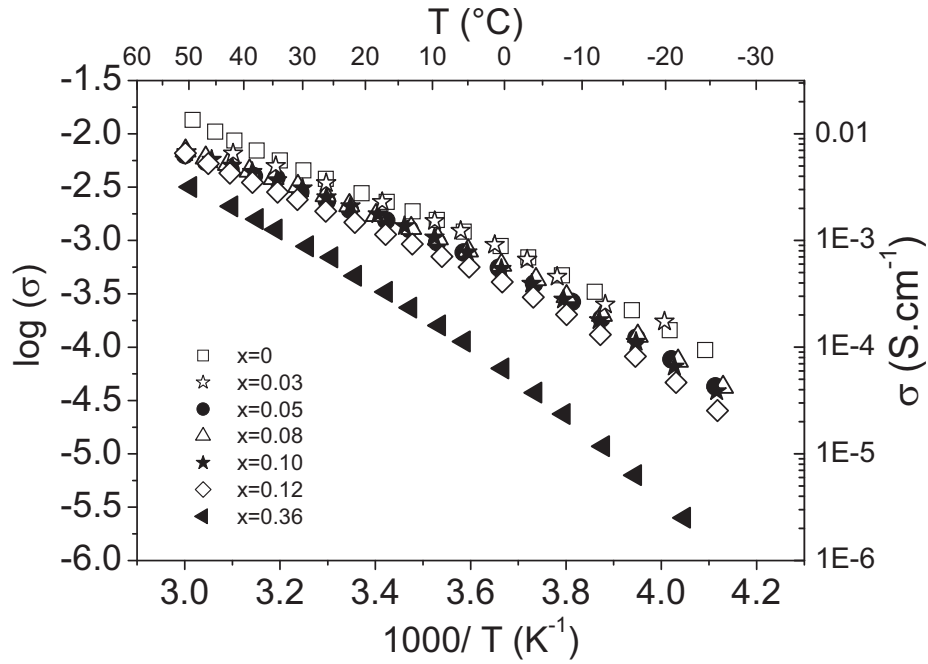
Figure II.14: Temperature dependence of the conductivity σ in the range -30°C - +60°C for BMITFSI solutions with LiTFSI molar fractions *x*: □ 0.0; ☆ 0.03; ● 0.05; △ 0.08; ★ 0.10; ◇ 0.12; ◀ 0.36.

As this will be shown below, this decrease follows the Vogel–Tammann–Fulcher model (VTF) [10,11,12] commonly used for glassy materials (see below).

II. 7. 3. 2. ii. The Vogel–Tammann–Fulcher model

The VTF equation is a modified form of the Arrhenius equation which is used for the temperature dependence of chemical reactions kinetics[13] and for many other parameters describing various processes. [14,15,16,17] The Vogel–Tammann–Fulcher type asymptotic exponential functions can be expressed in the following general form[18]:

(II.7) $$\ln f = \ln f_c - B/R(T - T_c)$$

where *f* is a temperature-dependent property of a system ; *T* and *Tc* are defined as the actual and critical-limit absolute temperatures of the system. Hence, *(T − Tc)* is referred to as the temperature deviation from the critical-limit temperature value. *B* is a pseudo-activation energy (the energy required for a species to move to a neighbouring site of the relevant process). *R* denotes the universal gas constant. *fc* is the high temperature value of the property *f* in the limit when *(T − Tc)*→∞. Eq. (II.7) is essentially a three-parameter empirical equation.

It has been demonstrated by many examples that it can provide a reasonable approximate description of the temperature dependency of various system properties. When $Tc = 0$ K, Eq. (II.7) is the basic Arrhenius equation. Originally, the Vogel–Tammann–Fulcher equation (VTF) had been proposed for the representation of the liquid viscosity based on the free-volume theory, where the free volume is equal to the apparent liquid specific volume minus the total specific volume of all the molecules forming the liquid. The VTF equation is often used to fit the properties of polymers close to their glass transition temperatures. The parameters of this equation are determined using experimental data.

II. 7. 3. 2. iii. The Vogel–Tammann–Fulcher model for conductivity

The temperature dependence of the ionic conductivity of glassy electrolytes close to Tg can well be described by this Vogel-Tamman-Fulcher (VTF) equation:

(II.8)
$$\sigma = \sigma_0 \exp\left[\frac{-B}{R(T - T_0)}\right]$$

where σ_0, B, and T_0 are fitting parameters. σ_0 is assumed to be proportional to the number of charge carriers, it is the conductivity value for high values of T. B is a pseudo-activation barrier, it is related to the critical free volume for transport, generally taken as fixed by the size of the polymer segment for polymer electrolytes and to the material expansion with temperature. As it can be assumed that virtually no long-range molecular movements are observed below Tg, a very good approximation for the T_0 value is: $T_0 = $ Tg - 50 K [18], it is the temperature where the configurational entropy becomes zero. This $T_0 = $ Tg – 50 is generally admitted for salt-polymer complexes[19] and ionic liquids.[20]

The free volume approach can be used to analyse the ionic motion in molten salts, fluids, and polymer electrolytes. This theory has been developed by Cohen and Turnbull.[21] It states that the polymer motion is not mainly thermally activated but essentially occurs by redistribution of the free volume. As the temperature increases, local voids are created by the expansion of the material and polymer segments can move in this free volume.

II. 7. 3. 2. iv. VTF fitting of the EIS curves of LiTFSI / BMITFSI electrolyte

The results of the VTF equation applied to the ionic conductivity are shown in Figure II.15 for one composition and summarized in Table II.7 for the others.
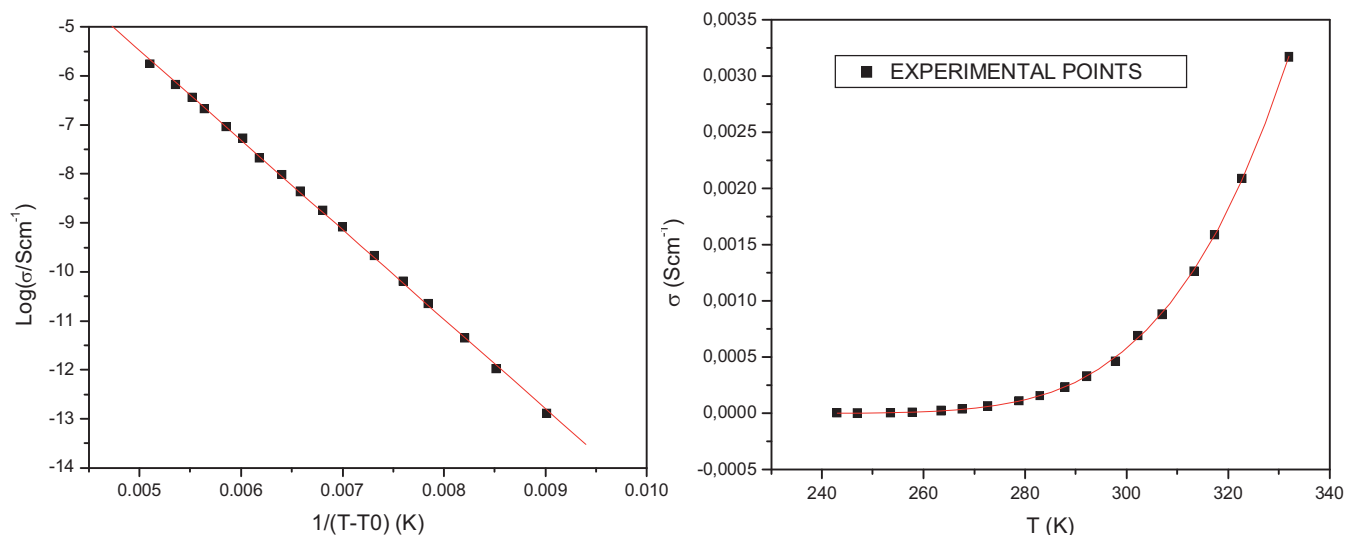
Figure II.15: Temperature dependence simulation of the conductivity σ in the range -30°C - +60°C for a BMITFSI solution with LiTFSI molar fraction of 0.36. a) $\text{Log}(\sigma T) = f(1/(T-T_0))$, b) $\sigma = f(T)$; the red line is the VTF fit.

x LiTFSI (molar ratio)	Tg (°C)	Tg (K)	σ (S.cm^{-1}) T=30°C	σ_0 (S.cm^{-1})	B (K)	T_0 (K) (Tg-50)	R²
0	-87	186	0.00379	4.48	1170	136	0.999
0.03	-87	186	0.00345	2.43	1098	136	0.998
0.05	-87	186	0.00233	2.36	1156	136	0.999
0.08	-87	186	0.00264	4.06	1163	136	0.999
0.1	-87	186	0.00254	3.45	1208	136	0.999
0.12	-87	186	0.00188	3.56	1253	136	0.997
0.36	-87	186	0.00074	38.86	1829	136	0.999

Table II.7: Conductivity data for BMITFSI with various amounts of LiTFSI, Tg values are deduced from DSC measurements (cf. II. 3. 1.) for low concentrations and assumed identical for higher one according to ref.[22].

Figure II.16 is another representation of the results showing the decrease of the conductivity with respect to the Li$^+$ salt concentration in the solution.
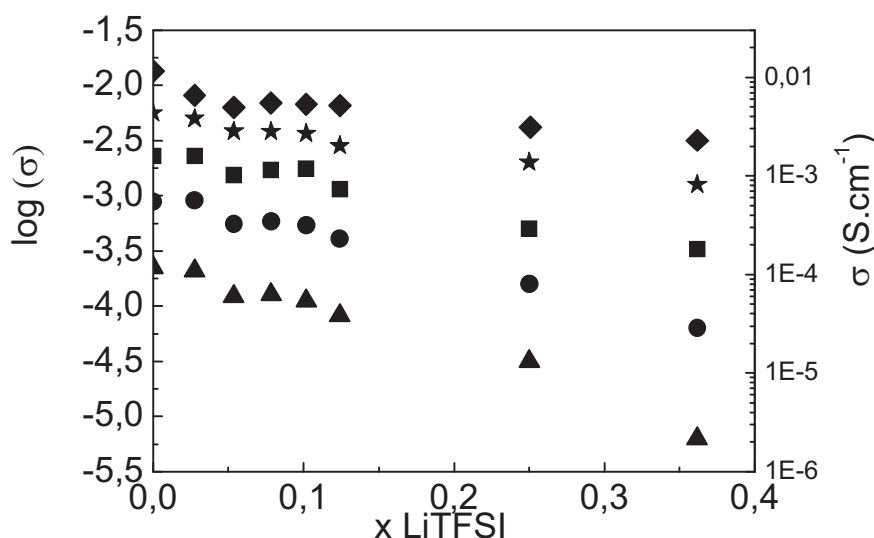
Figure II.16: Variation of the conductivity σ (S.cm^{-1}) of the electrolyte with the LiTFSI in BMITFSI molar fraction (*x*=0 to *x*=0.36) for temperatures: ▲ -20°C; ● 0°C; ■ 20°C; ★ 40°C; ◆ 60°C

As expected, the ionic conductivity of the pure ionic liquid, BMITFSI, is high (3.8.10^{-3} S.cm^{-1} at 30 °C) since ILs are composed of large ions with charges largely delocalized over the whole ion skeleton. Imidazolium aromatic cations have a delocalized positive charge, which promotes weaker interactions with the anion in the case of TFSI$^-$ as compared to PF$_6^-$ (appendix C) and higher conductivity.[23] Whatever the temperature, the conductivity decreases with the addition of Li$^+$ salt at a rate which seems to increase with decreasing temperature (the same trend was difficult to observe for BMIPF$_6$ on the same concentration range because of the very low solubility of LiTFSI in this IL).

The fitting of the experimental points with the VTF model is excellent, as shown by the R^2 values. Generally, such a close correspondence with the VTF equation implies that the ion conduction can be explained in terms of the free volume and configurational entropy theories. From these data it seems that in the Li ratio range between 0 and 0.12, the number of charge carriers (closely related to σ$_0$) is rather constant whereas the activation energy for the motion from one site to the other increases as illustrated in Figure II.17.
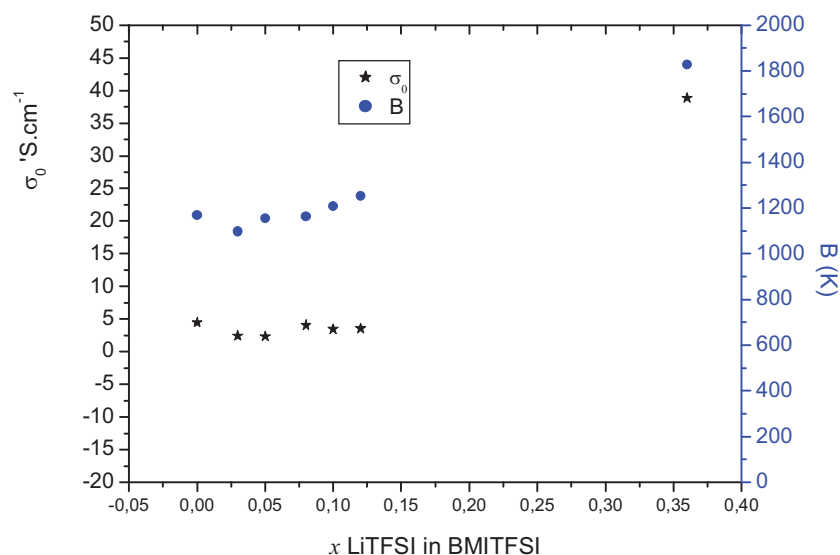
Figure II.17: Variation of σ_0 and B with the amount of Li$^+$ salt in BMITFSI.

To explain these results, we can evidence at least two reasons:

¤ the increase of the viscosity of the solution with the increase of LiTFSI concentration (not measured here) as already observed for LiBF$_4$ in EMIBF$_4$.[22,24.]As opposed to what occurs in classical solvents (propylene carbonate, ethylene carbonate…) in which the viscosity increase is compensated by the strong increase in charge carrier concentration as lithium salt is added (see appendix B for the evolution of ionic conductivity with increasing salt concentration in classical solvents), in ILs the number of charge carrier remains constant.

¤ the potential formation of aggregates or clusters around the lithium cation already observed by Lassègues et al.[25,26] In both cases, (ILs and classical solvents), the conductivity comes from salt dissociation but in the case of ILs, Li$^+$ salt dissociation means consumption of other ions (those of the solvent) to give Li(TFSI)$_2^-$ anions.

The measurement of the conductivity which concerns global phenomena cannot evidence such aggregation phenomena neither the proportion of these ions which are associated and therefore basically neutral and that of those which can serve as charge carriers, therefore more detailed studies such as FTIR, Raman and NMR were undertaken and will be described later on.

II. 7. 3. 3. Ionic conductivities of the BMITFSI/ PMMA membranes

We have shown in the previous section that for 0-0.1 molar ratios of lithium salt (x =0 -0.1), the influence on the decrease of the ionic conductivity is not detrimental. It is not the

case anymore when a polymer (PMMA) is added as exemplified in Figure II.18 which shows on the same graph the response of three samples of BMITFSI containing either Li$^+$ salt (x = 0.03) or PMMA (30 wt%) or both. The conductivity of BMITFSI is also reported for comparison.
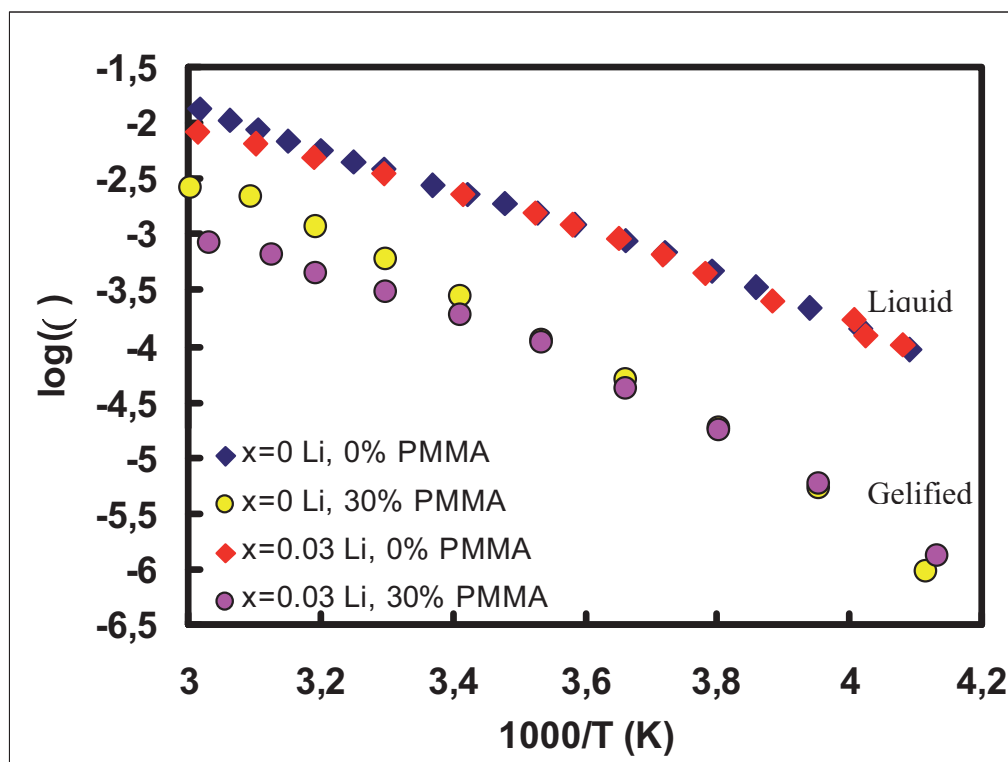
Figure II.18: Temperature dependence of the ionic conductivity σ in the range -30°C - +60°C for BMITFSI (◆), BMITFSI with 30 wt% PMMA (◯), BMITFSI with 0.03 LiTFSI (◆), and BMITFSI with 0.03 LiTFSI and 30 wt% PMMA (◯).

From this graph, it is easy to see that in the absence of the PMMA matrix, the overall conductivity does not change much. However, the addition of 30 wt% PMMA is detrimental for the conductivity by more than one order of magnitude. This decrease in conductivity is as expected, partly due to the decrease of the electrolyte volume as compared to the total volume; since part of the ionic conductive ionic liquid is replaced by non ionic conductive PMMA. However, this cannot explain the whole decrease in conductivity. It is then possible to have an idea of the degree of interaction between the polymer and the ionic liquid by calculating in Table II.8 the ratio of conductivity (σ membrane/ σ liquid) and to compare it with the ratio of volume (V liquid in membrane / V liquid).

%w PMMA	v% liquid	x_{LiTFSI}	Tg (°K)	σ (S.cm^{-1}) T=30°C	$\sigma_{membrane}/\sigma_{liquid}$ (%)
0	100	0	186	0.00379	100
30	60	0	191	0.00060	16
0	100	0.03	186	0.00345	100
30	60	0.03	191	0.00031	9

Table II.8: Glass transition temperature, conductivity, and ratio $\sigma_{membrane}/\sigma_{liquid}$, of BMITFSI jellified by PMMA. The weight % value of liquid in the membrane is 70% corresponding to a 60 % value in volume ($\rho_{BMITFSI}$ = 1.43 kg/L; $\rho_{membrane\ 30\%PMMA/70\%BMITFSI}$ = 1.25 kg/L)

The $\sigma_{membrane}/\sigma_{liquid}$ ratio, 16 % or 9 % depending on the quantity of lithium salt is very low as compared to the 60 % expected for such a membrane without interaction in between the two components. This high difference shows that the membrane electrolytes are not made of an inert PMMA network with ionic liquid imbedded in (like a sponge), but consists in a liquid electrolyte in strong interaction with the polymer matrix. These conductivity results are consistent with the fact that IL and PMMA are compatible and show a single phase as already observed in the DSC measurements of the membrane. This aspect will also be confirmed later on with conductivity results with different wt% of PMMA and with the Raman results.

An even lower value of σ for the Li$^+$ loaded membrane presumes of the implication of this cation in the interaction process. The forthcoming ATR-IR and Raman data will help us to describe the intimate nature of these interactions. The same trends are observed when BMIPF$_6$ is used as an ionic liquid, see appendix C.

The results of the empirical VTF law used to fit the curves for these four soft systems are detailed in Table II.9.

%w PMMA	x_{LiTFSI} in BMITFSI	Tg (K)	σ (S.cm^{-1}) T=30°C	σ_0 (S.cm^{-1})	B (K)	T_0 (K)	R²
0	0	186	0.00379	4.48	1170	136	0.999
30	0	191	0.00060	28.2	1748	141	0.998
0	0.03	186	0.00345	2.43	1098	136	0.999
30	0.03	191	0.00031	1.8	1413	141	0.999

Table II.9: Conductivity of BMITFSI jellified by PMMA, VTF data : σ_0, B, T_0. Tg is measured by DSC.

In the pure IL, the addition of PMMA decreases the overall conductivity despite a large increase of the number of charge carriers. The high compatibility between the polymer and the ionic liquid does improve the charge separation of the ions, and increase the number of charge carriers. On the other hand, the concomitant increase of T_0 and of the energy of

activation (B) is probably due to the interactions in between the polar CO$_2$Me functional groups of the polymer and the ionic species of the IL which induce their overall lower mobility, responsible for the lowering of the conductivity.

The addition of 0.03 molar ratio of lithium salt in pure IL does not modify its ion conductor properties. It is not the case any more in a 30% PMMA membrane. With LiTFSI, a strong decrease of the number of charge carriers as compared to a 30% PMMA Li-free membrane is observed suggesting that the Li$^+$ cation probably acts as a cross linker in between the polymer and the solvent. The motion of the different ionic species remains low, with high activation energy.

As PMMA is added, the macroscopic viscosity of the membrane increases and if high molecular weight polymer are used the effect on viscosity is even stronger. The effect of different molecular weights for PMMA polymer was checked (Mw: 35,000; 96,000 and, 350,000) but did not show great differences as illustrated in Figure II.19.
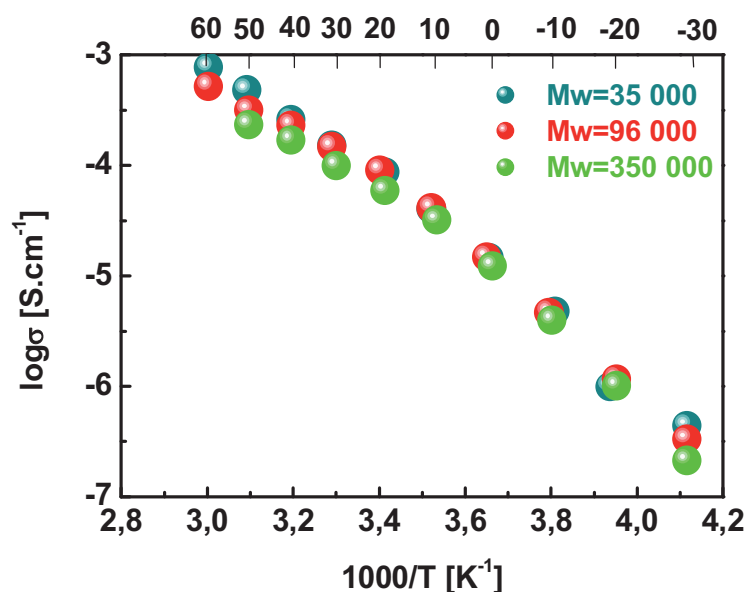
Figure II.19: Temperature dependence of the ionic conductivity σ in the range -30°C – 60°C for different molecular weights of PMMA (30% PMMA membrane**).**

The influence of the macroscopic viscosity on conductivity is low. This result is expected since as discussed by Bruce and Vincent[27] for high molecular weight polymers, conduction mechanisms are mostly related to the microscopic viscosity, i.e. polymer lateral chains mobility. These lateral chains are the same for the different samples since it is in all cases PMMA.

Keeping in mind our objectives of setting-up complete electrochromic devices, we focused our attention on the study of BMITFSI/PMMA polymeric membranes containing various amounts of lithium salt. Our purpose was to determine the best membrane composition, corresponding to our requirements. We shall therefore in the following sections, more precisely examine the influence of the LiTFSI and PMMA ratios on the conductivity properties of the membranes.

II. 7. 3. 3. i. Influence of LiTFSI concentration

For LiTFSI - BMITFSI - PMMA systems, different LiTFSI molar ratios in BMITFSI, x_{LiTFSI}, were tested varying from 0.03 to 0.23 for PMMA concentrations for 30, 40 and 50 wt%. Figure II.20 presents the results for 40 wt% PMMA and Figure II.21 for 50 wt% PMMA respectively.
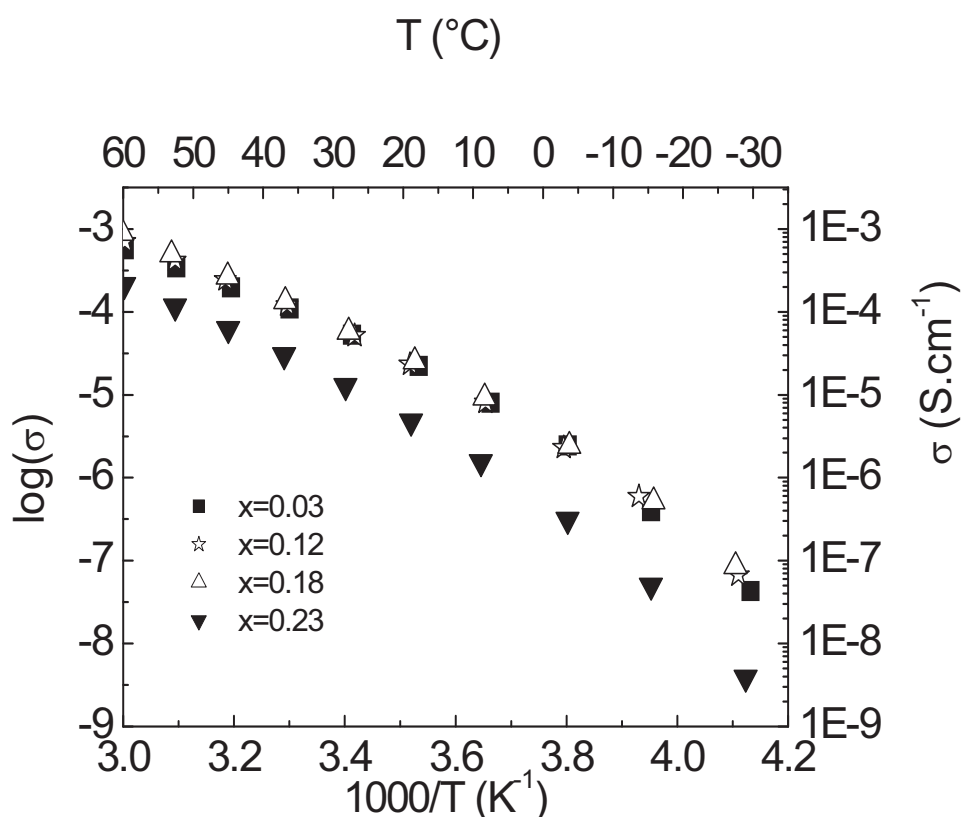
Figure II.20: Temperature dependence of the ionic conductivity σ in the range -30°C - +60°C for membranes consisting of PMMA (40 wt%) and BMITFSI solutions with LiTFSI molar fractions: x_{LiTFSI} = 0.03; 0.12; 0.18 and 0.23.
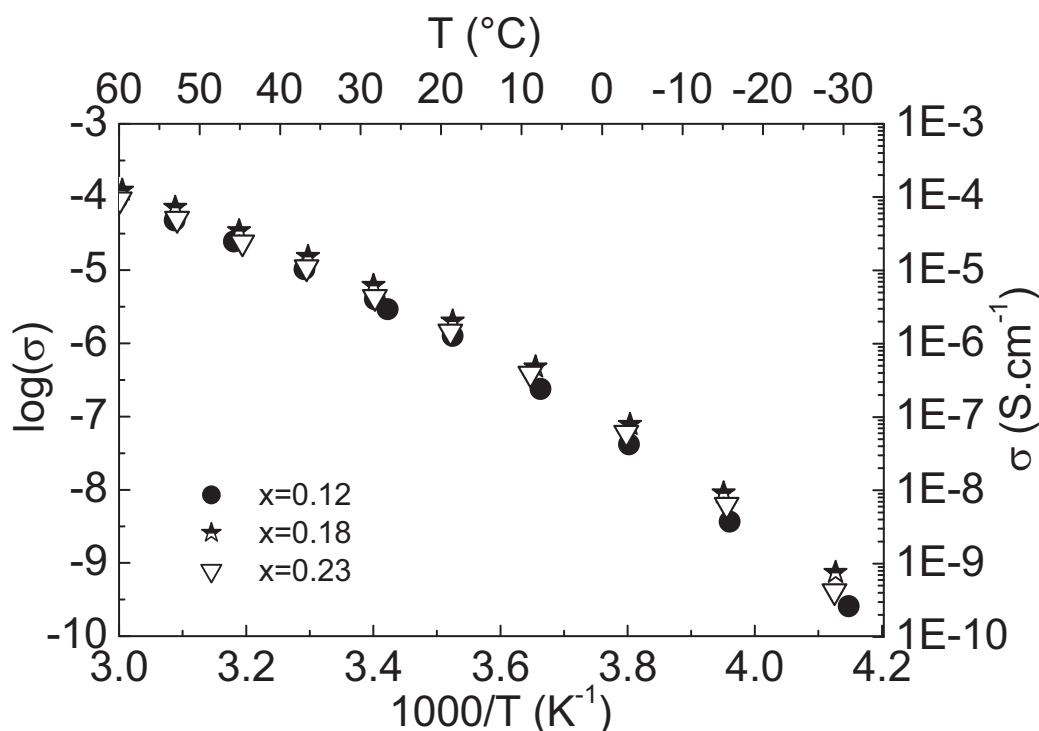
Figure II.21: Temperature dependence of the ionic conductivity σ in the range -30 °C - +60 °C for membranes with 50 wt % PMMA and BMITFSI solutions with LiTFSI molar fractions: 0.12; 0.18 and 0.23.

No change of ionic conductivity is observed for LiTFSI concentrations up to 0.23 as far as the 40% and 50 wt% PMMA electrolytes are concerned, the conductivity is identical whatever the Li$^+$ salt concentration. For x= 0.23 and 40 wt% PMMA in the membrane a decrease of less than one order of magnitude seems to appear. This phenomenon may be a measurement artefact and should be studied more deeply. An increase from 40 to 50% of PMMA in the membrane induces a decrease of one order of magnitude for the conductivity.

The comparison of the variation of the conductivity with respect to the LiTFSI molar ratio, for PMMA ratio of 0, 40 and 50 wt% at room temperature is summarized in Figure II.22. It shows that in the chosen lithium salt and PMMA proportions, the influence of LiTFSI addition on the global conductivity is much weaker (as already observed, see II. 7. 3. 3.) than the effect of PMMA addition. The same trend is observed for BMIPF$_6$ based electrolytes (cf annex 2 Figure 7).
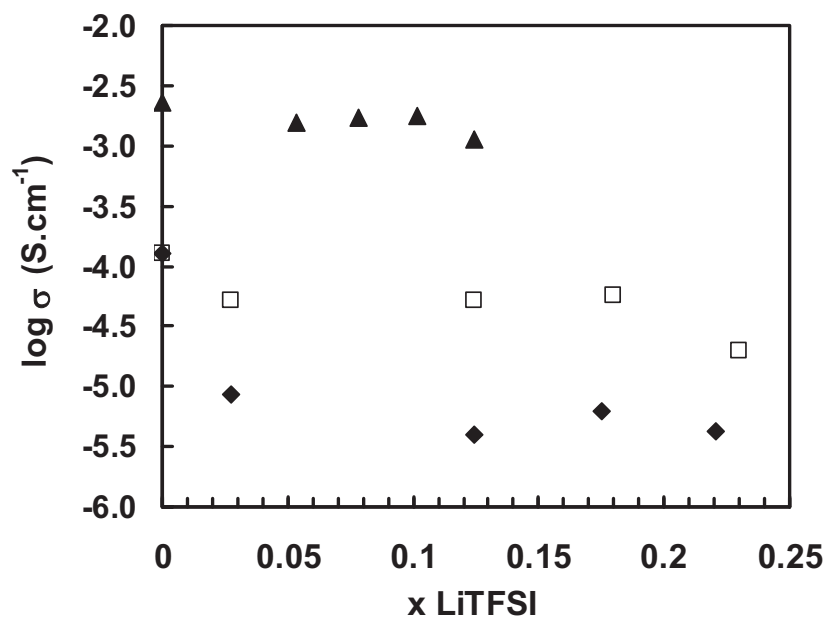
Figure II.22: Variation of the ionic conductivity of the BMITFSI/PMMA membranes with the molar ratio of LiTFSI at 20 °C of: ▲ BMITFSI, □ BMITFSI + 40 wt% PMMA, ◆ BMITFSI + 50 wt% PMMA..

II. 7. 3. 3. ii. Influence of PMMA ratios

The influence of the PMMA ratio has been studied for membranes with $x_{LiTFSI} = 0.03$ to 0.1 in BMITFSI. Results concerning the $x_{LiTFSI} = 0.03$ are presented in Figure II.23.
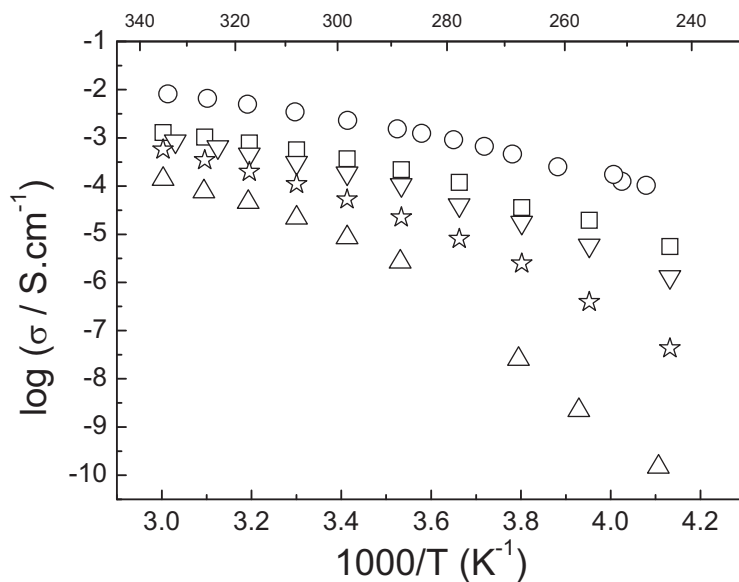
Figure II.23: Temperature dependence of the ionic conductivity σ for BMITFSI electrolytes with LiTFSI molar ratio of $x = 0.03$ and PMMA wt%: ○ 0%; □ 20%; ▽ 30%; ☆ 40%, △ 50%

From this graph it is easy to figure out the impact of the PMMA ratio in the membrane for all the concerned temperatures. At each temperature, the conductivity decreases with the polymer ratio. The plots of the ionic conductivity as a function of 1/T exhibit the usual curved profile for soft systems. The curvature is however increasing with the PMMA ratio giving once more the indication of a strong interaction in between the two components. The conductivity decrease as PMMA is added is presented on Figure II.24.
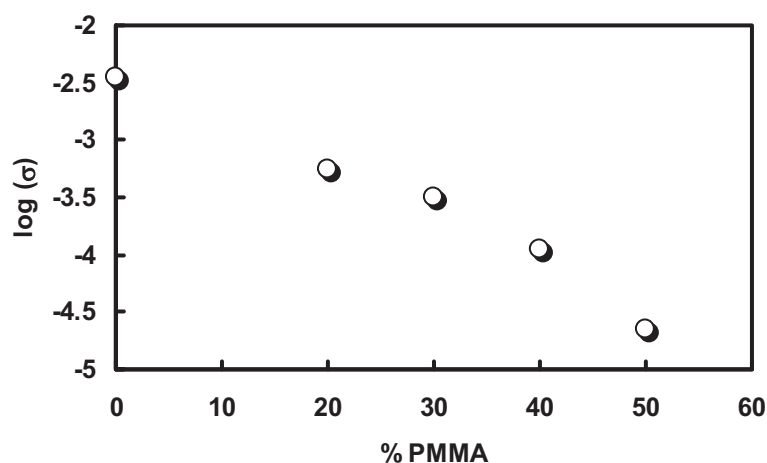
Figure II.24: Variation of log (σ) at 30°C with the wt% of PMMA in the membrane for x = 0.03 in BMITFSI.

This strong interaction is illustrated in Table II.10 and Figure II.25.

% PMMA	x $_{LiTFSI}$	T_g (K)	σ (S.cm^{-1}) T=30°C	σ $_{membrane}$ / σ $_{liquid}$ (%)
0	0.03	186	0.00345	**100**
20	0.03	186	0.00056	**16**
30	0.03	191	0.00031	**9**
40	0.03	209	0.00011	**3**
50	0.03	273	0.000022	**0.6**

Table II.10 : Conductivity of LiTFSI / BMITFSI jellified by PMMA and ratio σ $_{membrane}$/σ $_{liquid}$

Figure II.25 indeed shows in dotted line the normal variation of the conductivity of a mixture of two non-interacting components: an isolating one and an ionic conducting one in different ratios. For comparison, are plotted the results for mixtures of BMITFSI and BMIPF$_6$ ionic liquids with PMMA. The high decrease of conductivity (much higher than the decrease in the proportion of liquid electrolyte LiTFSI-BMITFSI) is directly due to the increase of viscosity and high interactions in between the different species.
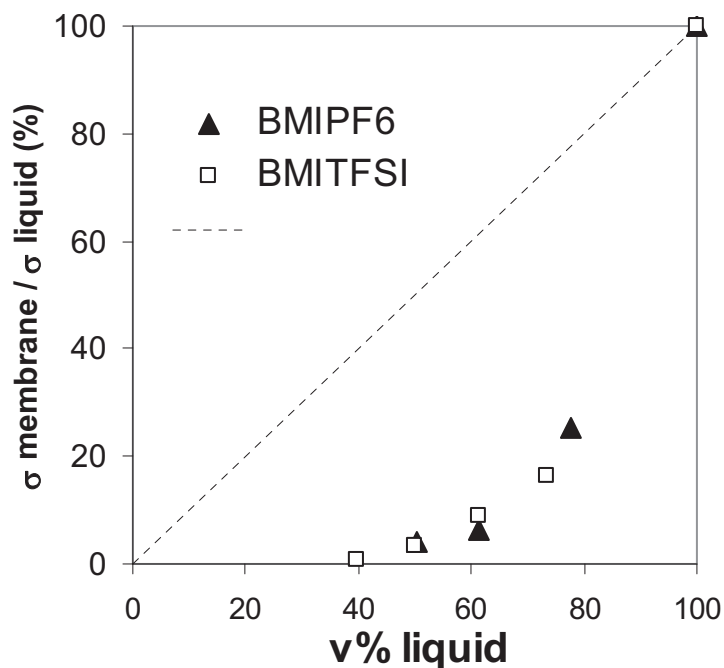
Figure II.25: Variation of σ $_{membrane}$/σ $_{liquid}$ as compared to the volume % of liquid in the membrane for x LiTFSI = 0.03.

II. 7. 3. 4. VTF fits of the ionic conductivities

We performed the VTF fit of all these membranes and the results are gathered in Table II.11 and Table II.12.

Results from Table II.11 clearly show that for a given amount of lithium salt, the increase of the PMMA ratio does not really modify the number of charge carriers except for 50% PMMA. The energy of activation B increases with the viscosity of the mixture, but once more, there is a modification of the membrane behaviour for 50% PMMA.

% PMMA	x $_{LiTFSI}$	T_g (K)	σ (S.cm^{-1}) T= 30°C	$σ_0$ (S.cm^{-1})	B ((K)	T_0 (K)	R²
0	0.03	186	3.45 10^{-3}	**2.43**	**1098**	136	0.999
20	0.03	186	5.63 10^{-4}	**1.35**	**1308**	136	0.999
30	0.03	191	3.1 10^{-4}	**1.8**	**1413**	141	0.999
40	0.03	209	3.08 10^{-4}	**3.5**	**1496**	159	0.999
50	0.03	273	2.19 10^{-5}	**0.01**	**500**	223	0.999

Table II.11 : Conductivity of 0.03 LiTFSI / 0.97 BMITFSI gelified by PMMA, VTF data: $σ_0$, B, T_0

In order to understand this difference of behaviour of the 50% PMMA membrane, we undertook a systematic study of the variation of lithium salt concentration in these two membranes: 40% and 50%. Results are shown in Table II.12 .

% PMMA	x_{LiTFSI}	T_g (K)	σ (S.cm^{-1}) T=30°C	σ_0 (S.cm^{-1})	B ((K)	T_0(K)	R²
40	0.03	209	3.08 10^{-4}	3.5	1496	159	0.999
40	0.12	209	1.20 10^{-4}	4.01	1505	159	0.999
40	0.18	209	1.34 10^{-4}	4.42	1501	159	0.999
40	0.23	209	3.03 10^{-5}	4.71	731	159	0.999
50	0.03	273	2.19 10^{-5}	0.01	505	223	0.999
50	0.12	273	1.03 10^{-5}	0.05	697	223	0.999
50	0.18	273	1.54 10^{-5}	0.044	646	223	0.999
50	0.23	273	1.09 10^{-5}	0.038	663	223	0.999

Table II.12: Conductivity of LiTFSI / BMITFSI jellified by 40% and 50% PMMA, VTF data: σ_0, B, T_0 .

From these results, it really seems that there is a gap in between these two concentrations, gap which probably illustrates a change in the intimate structure of the membrane and possibly a different diffusion mechanism of ions throughout the membrane. Indeed, $\sigma_{30°C}$ goes on decreasing for 40% while it is rather constant for 50%; the number of charge carriers is divided by 100. The energy of activation is higher in 40% PMMA by a factor of around 2.3 except for $x = 0.23$. This difference can be explained if we consider that as illustrated in Figure II.26, up to 40 % PMMA in the membrane, the working range of temperature (-30°C-+60°C) remains over the glass transition, but not any more for 50% PMMA ($T_g = 0°C$). In the first case the ions motion obeys the so-called assisted transport model with characteristics closer that those of rubbery phase, so does the 50% membrane when above T_g.
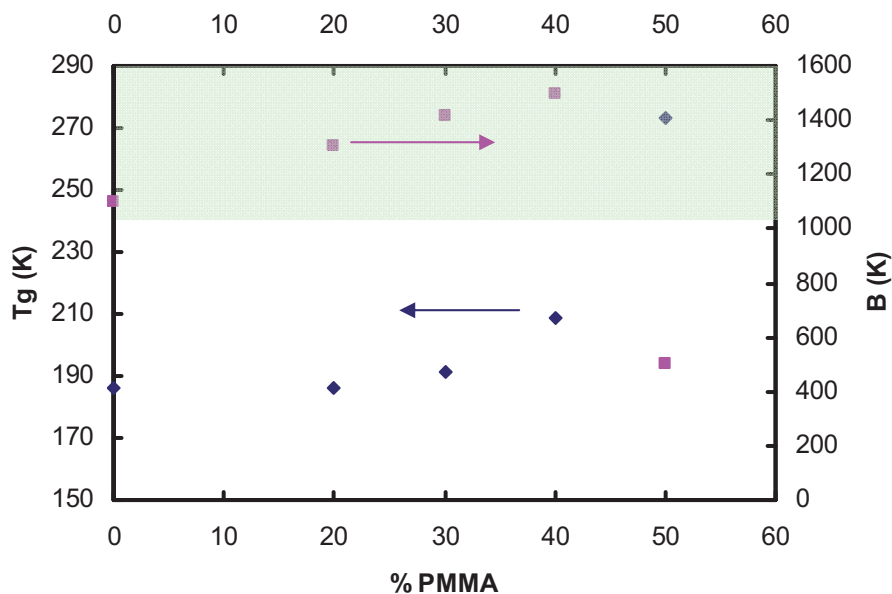
Figure II.26: Evolution of Tg and B with the wt% of PMMA in the membrane. Zone of working temperature.

A close inspection of the 50% membrane shows the results given in Figure II.27. Clearly the whole experimental data set cannot be fitted correctly with neither the classical Arrhenius law nor the VTF one (Figure II.27 a (red line) and b (green or blue line)).
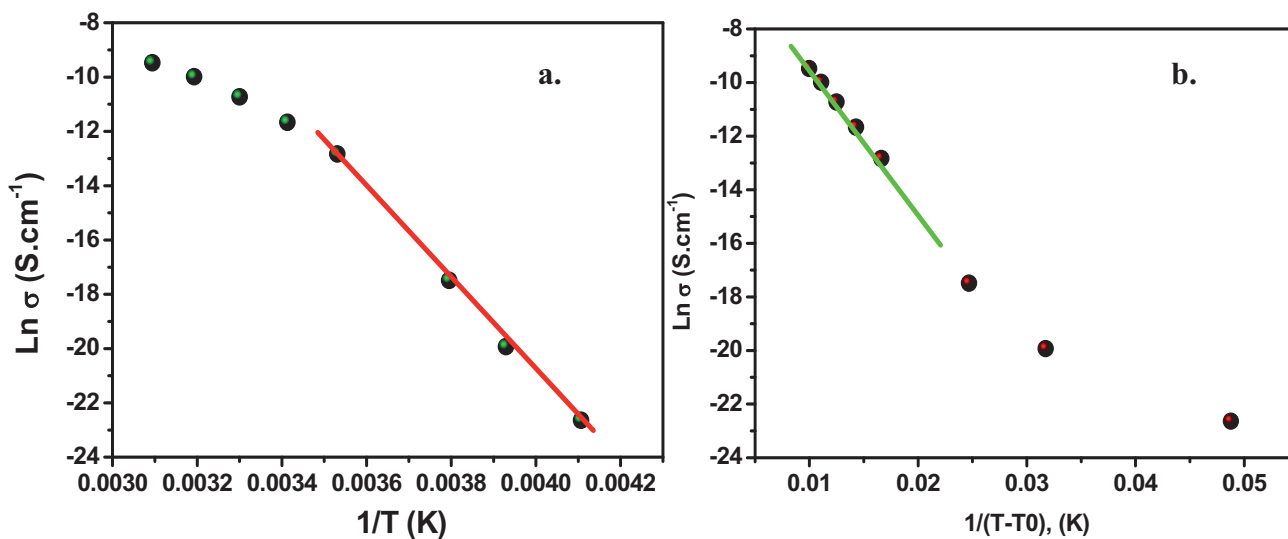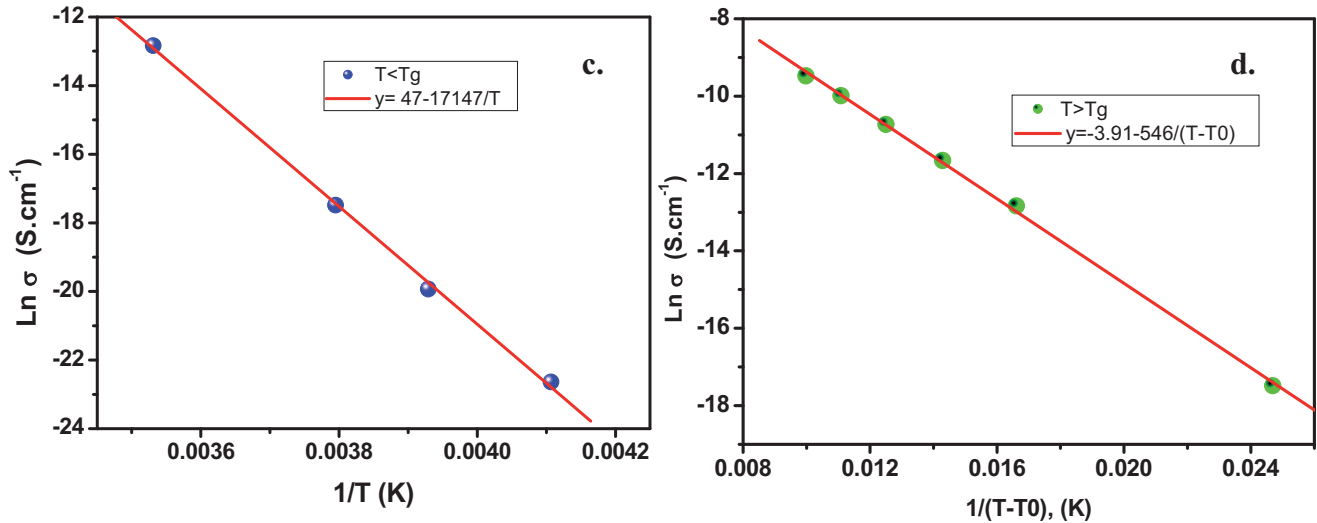
Figure II.27: attempts to fit experimental points with a) a law in 1/T, b) a law in 1/(T-T0) and c) and d) a sum of the two taking into account the value of Tg.

However, we can perfectly fit the experiment considering that Tg separates two behaviours of the membrane: one for T<Tg with the characteristics of a solid (Arrhenius fit) and the other with those of a rubbery system (VTF fit) (Figure II.27 a, b (green and blue lines) and c,d (red line)).

Therefore as a conclusion of this study we can mention that:

◎ Membranes based on mixtures of a LiTFSI/BMITFSi electrolytes with different ratios of PMMA can serve as plasticized polymer electrolytes for electrochromic devices.

◎ Their conductivity is high enough for such applications.

◎ The addition of lithium salt in the IL increases its overall viscosity decreasing the conductivity

◎ However, the introduction of PMMA has a much more detrimental effect, however up to 40% PMMA, the specification σ >10^{-4}S/cm is respected.

These data give information at the macroscopic level. That's the reason why these membranes were also studied by ATR-IR and Raman spectroscopy in order to have a deeper insight in the nature of the interactions at the molecular level.

II. 8. ATR-IR and Raman study

Fourier transform infrared–attenuated total reflectance (FTIR-ATR) and Raman spectroscopy are experimental techniques allowing the determination of some of the interactions between species.

IR spectra are recorded using a Nicolet Nexus spectrometer with a resolution of 4 cm^{-1} and a single reflection diamond ATR system (Specac) that limits the transparency at low wavenumbers to ~ 600 cm^{-1}. For Raman experiments, the ionic liquids or membranes are transferred into a Linkam TMSG600 stage flushed with argon and equipped with a glass window. Spectra are recorded, as previously described,[4] with a Labram 1B Jobin-Yvon spectrometer, an incident wavelength of 632.8 nm and a resolution of 3 cm^{-1} (for more information see Appendix A).

II. 8. 1. ATR / IR and Raman spectra

The ATR-FTIR and Raman spectra of pure PMMA, LiTFSI dissolved in PMMA, (1-x)(BMITFSI), x LiTFSI ionic liquid with x = 0.23 and PMMA plasticized by this ionic liquid are shown in Figure II.28 and Figure II.29, respectively.

The vibrational assignments of PMMA[28-29], of LiTFSI dissolved in a solvent or a polymer[30-4], of BMI and TFSI based ionic liquids[31], are available in the literature.
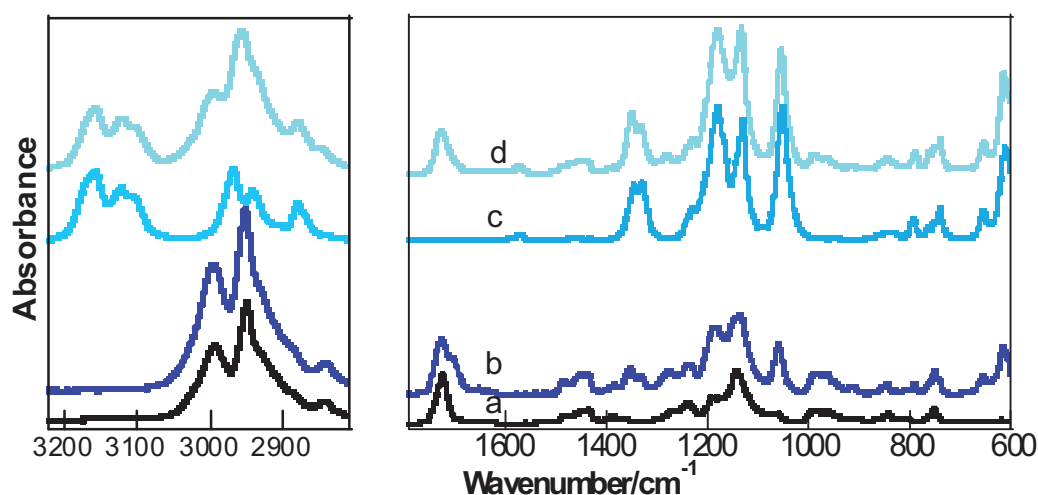
Figure II.28: ATR-IR spectra at room temperature of PMMA: (a), of a LiTFSI/PMMA blend with MMA/Li = 9.5: (b), of the 0.77(BMITFSI),0.23 LiTFSI ionic liquid: (c) and of PMMA (40 wt%) plasticized by 0.77(BMI-TFSI),0.23 LiTFSI: (d). The intensities between 3200 and 2800 cm^{-1} have been amplified by a factor of about 20.
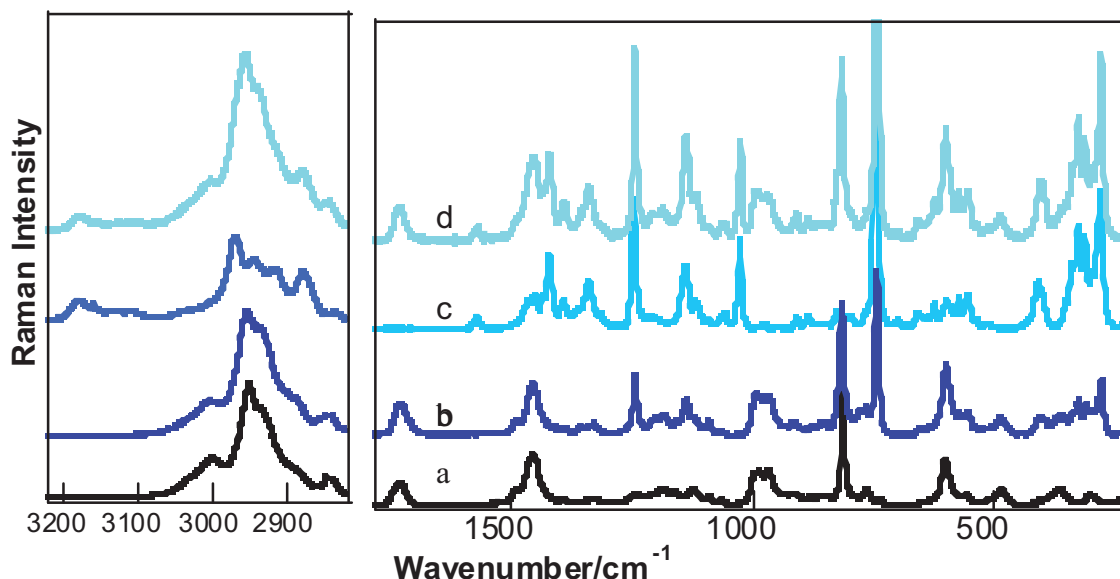
Figure II.29: Raman spectra at room temperature of PMMA: (a), of a LiTFSI/PMMA blend with MMA/Li = 9.5: (b), of the 0.77(BMI-TFSI),0.23 LiTFSI ionic liquid: (c) and of PMMA (40 wt%) plasticized by 0.77(BMI-TFSI),0.23 LiTFSI: (d).

PMMA has been extensively studied with respect to its tacticity and adhesive properties, using the IR absorptions due to the C=O stretching vibration around 1730 cm^{-1} and the vibrations of the COCH$_3$ group between 1300 and 1100 cm^{-1}.[28] Unfortunately, intense BMI$^+$ and TFSI$^-$ features take place in this latter spectral region. On the contrary, the region of C=O vibration around 1730 cm^{-1} is free from contributions of BMI$^+$ or TFSI$^-$; this band is influenced by the C=O coordination state.

The BMI$^+$ cation is characterized by imidazolium CH stretching vibrations situated in the 3200-3050 cm^{-1} region that do not overlap with any other feature of PMMA or TFSI$^-$ (Figure II.28 c,d). The presence of four BMI$^+$ conformers, from the combination of gauche (G) and anti (A) sequences of the butyl C-C bonds, has been correlated in the BMIBF$_4$ IL with four unique Raman modes at 808 (GG), 825 (GA), 883 (AG) and 905 cm^{-1} (AA), with respective populations of 0.08, 0.48, 0.17 and 0.28 at room temperature.[31] A similar equilibrium can be observed in BMITFSI (see below), but in plasticized PMMA an intense band of the polymer at 815 cm^{-1} partly hides this region (Figure II.29d).[32]

The conformational state of the TFSI$^-$ anion can also be determined by Raman spectroscopy using a series of deformation modes situated in the 360-260 cm^{-1} region, that produce separated features for the *transoid* and *cisoid* conformers.[29] In this region, the contributions of BMI$^+$ and PMMA are negligibly small (Figure II.29).

Similarly, BMI$^+$ or PMMA are transparent in the 730-760 cm^{-1} region where the most intense line of TFSI$^-$ is observed. This line, due to an overall anion expansion and contraction, is rather insensitive to the anion conformational state, but is significant of the formation of ion-pairs by a line at ~748 cm^{-1} near the 740-742 cm^{-1} component of the "free" anions. [33]

The bands that will be useful for the Raman and IR spectra interpretation of LiTFSI-BMITFSI-PMMA mixtures are summarized in the following table:

Compound	Origin	Wavelength (cm^{-1})	Information
PMMA	C=O stretching vibration	1730-1700	Coordination of C=O
BMI$^+$	Imidazolium C-H stretching vibration	3200-3050	Imidazolium presence
BMI$^+$	Butyl C-C	1100-800	BMI conformers
TFSI$^-$	Anion deformation	360-260	Transoïd / cisoïd conformation
TFSI$^-$	Anion expansion / contraction	730-760	Ion-pairing

Table II.13 : Principal bands useful for the Raman-IR interpretation for LiTFSI-BMITFSI-PMMA mixtures

II. 8. 2. Determination of TFSI- "free" anion and ion pair populations

As the Raman activity of the overall anion expansion and contraction of TFSI$^-$ vibration (around 740 cm^{-1}) is unchanged from the "free" to the coordinated state, the population of the TFSI$^-$ anions can be directly derived from the integrated areas of the two components, at ~748 cm^{-1} for ion-pairs (coord.) and at 740-742 cm^{-1} for "free" anions :

(II.9) $$P[\text{coord. anions}] = A_{748}/(A_{742} + A_{748})$$

II. 8. 3. Determination of C=O "free" and C=O coordinated populations

The interaction of the lithium ion with the ester groups of PMMA has been shown to occur essentially with the carbonyl oxygen.[28,29,34,35] The IR spectra in the region of the C=O stretching vibrations exhibit a band at 1730-1728 cm^{-1} due to the "free" C=O groups and another band at 1715-1707 cm^{-1} characteristic of coordinated C=O groups.

The integrated areas of these two components are related to the concentrations of the free and coordinated C=O groups and can be evaluated by fitting with the Beer-Lambert law:

(II.10) $\qquad A_{1728} = \varepsilon\,(\nu C=O)_{free}.c(C=O_{free}).d$

(II.11) $\qquad A_{1711} = \varepsilon\,(\nu C=O)_{coord}.c(C=O_{coord}).d$

where $\varepsilon\,(\nu C=O)$ are molar absorption coefficients, $c(C=O)$ concentrations and d is the ATR penetration depth.

It follows that the population of coordinated C=O groups

(II.12) $\qquad P(C=O_{coord}) = c\,(C=O_{coord.})\,/\,[c\,(C=O_{coord.}) + c\,(C=O)_{free}]$

is given by:

(II.13) $\qquad P(C=O_{coord.}) = A_{1711}/(R_{IR}.A_{1728} + A_{1711})$

$\qquad\qquad$ with $R_{IR} = \varepsilon\,(\nu C=O)_{coord}\,/\,\varepsilon\,(\nu C=O)_{free}$

For a given polymer electrolyte obtained by dissolving LiTFSI in PMMA or by plasticizing PMMA by a $(1\text{-}x)$(BMI-TFSI),xLiTFSI ionic liquid based electrolyte, it is possible to define the total number of C=O groups per lithium or, equivalently, the number of polymer repeat units per lithium, MMA/Li. The average number of C=O coordinating a single lithium ion is then:

(II.14) $\qquad C=O_{coord}/Li = P(C=O_{coord}).(MMA/Li)$

One key parameter in this series of equations is R_{IR} used in (II.13) to define the population $P(C=O_{coord})$ and it is not accurately known. Some authors have either adopted the simple hypothesis of R_{IR} equal to unity,[28,36] or used a value of 1.5[29,37]. This latter value is predicted by *ab initio* calculations of the coordination of Li$^+$ with the C=O groups of methyl isobutyrate, in contrast with a R_{Raman} ratio of 0.74 for the Raman activity.[35] We have treated the IR results using the two values of 1 and 1.5 for R_{IR}.

II. 8. 4. Li$^+$ solvation in (1-*x*)(BMI-TFSI),*x*LiTFSI ionic liquids

Typical spectra are reported in Figure II.30 to illustrate the respective contributions of the BMI$^+$ cation and TFSI$^-$ anion and to identify characteristic features for each ion. The anion has no Raman bands above 1400 cm^{-1} (Figure II.30a) and its vibrational assignment has been thoroughly studied.[25,4,30] Detailed vibrational assignments of the BMI$^+$ cation have also been established recently.[31] Imidazolium CH stretching vibrations are situated in the 3200-3050 cm^{-1} region, well separated from the stretching vibrations of the methyl and methylene groups situated in the 3000-2800 cm^{-1} region (Figure II.30b,c). Well separated cation lines are also observed in the 1600-1400 and 1100-800 cm^{-1} regions.[32]
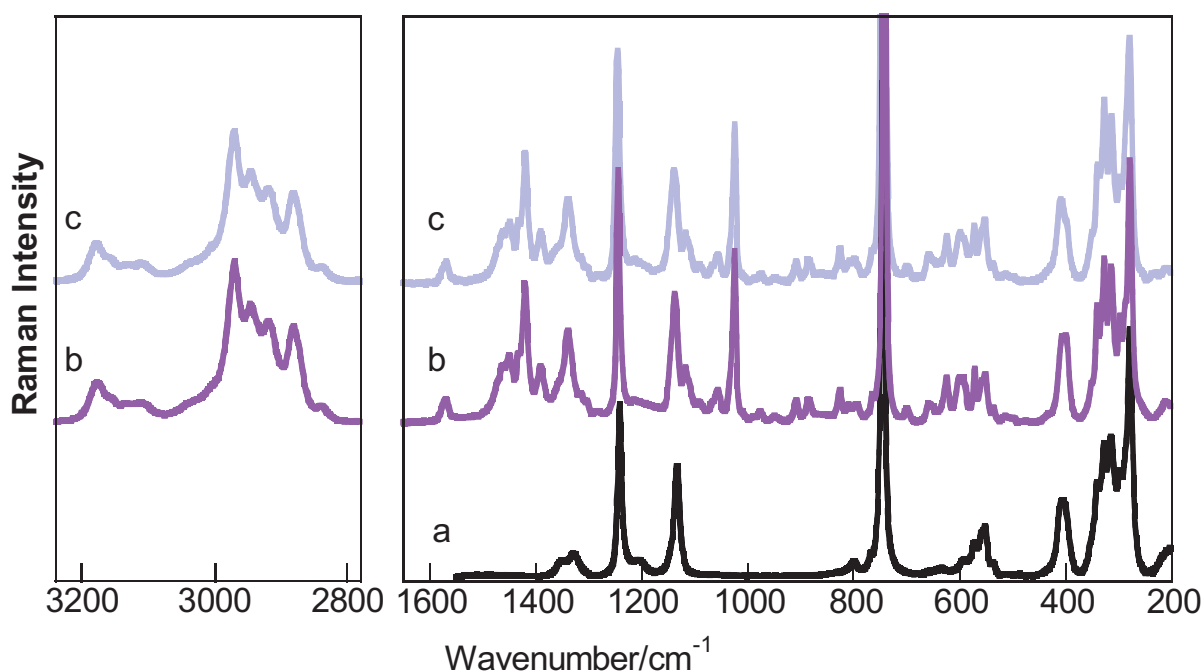
Figure II.30: Raman spectra at 298 K of an aqueous solution of LiTFSI (a), of the ionic liquid BMITFSI (b), and 0.77(BMITFSI),0.23LiTFSI (c).

In the 1100-800 cm^{-1} region, the presence of four BMI$^+$ conformers, coming from the combination of gauche (G) and anti (A) sequences, produces four unique Raman modes at 808 (GG), 825 (GA), 883 (AG) and 905 cm^{-1} (AA), with respective populations of 0.08, 0.48, 0.17 and 0.28 at room temperature in BMI-BF$_4$.[25] A similar equilibrium can be observed in the (1-*x*)(BMITFSI),*x*LiTFSI ionic liquids (Figure II.31).
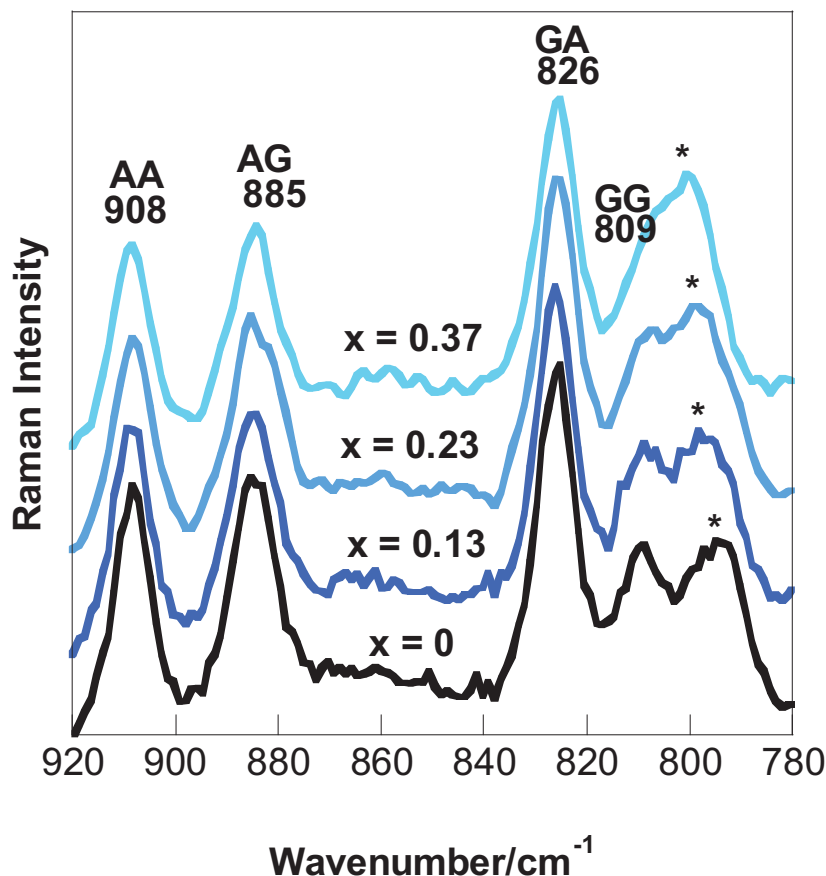
Figure II.31: Raman spectra of (1-x)BMITFSI,xLiTFSI ionic liquids at 298 K. The asterisk indicates a band of the anion, all the other bands being due to the indicated BMI$^+$ conformers.

The relative intensity of the four components, observed here at 809, 826, 885 and 908 cm^{-1}, is hardly changed when x increases. Therefore, the population of the four conformers is roughly the same in BMITFSI as in BMIBF$_4$ and the BMI$^+$ conformational state is practically unmodified from x = 0 to 0.37.

When a lithium salt is added in the ionic liquid leading to compositions x with 0 < x < 0.4, the coexistence of "free" anions characterized by a Raman component at 742 cm^{-1} and of ion-paired anions characterized by a component at 748 cm^{-1} is illustrated in Figure II.32.

The two components have been fitted, with respect to x, using mixed Gaussian/Lorentzian profiles with a proportion of Lorentzian imposed to 60% in order to measure the proportion of "free" and associated TFSI. The results reported in Figure II.33 are quite similar to those previously obtained for (1-x)(EMI-TFSI),xLiTFSI, where EMI is 1-ethyl-3-methyl-imidazolium[25]: the population of "free" anions decreases linearly with a slope of -2, confirming that the lithium is essentially involved in [Li(TFSI)$_2$]$^-$ anionic clusters. For

example, for the $x = 0.23$ composition, 41.5% of the anions are found to be coordinated. If they were all involved in $[Li(TFSI)_2]^-$, 44% would be coordinated. Therefore, the equilibrium:

(II.15) $(1-x)(BMI\text{-}TFSI) + x\ LiTFSI \leftrightharpoons x[Li(TFSI)_2]^- + (1 - 2x)\ TFSI^- + (1 - x)\ BMI^+$
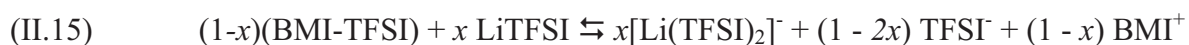
can be considered as completely displaced to the right at room temperature for $x < 0.23$. Above this value, other kinds of ionic associations may contribute, as shown by the small deviation from the line of slope -2 at $x = 0.37$ in Figure II.33.
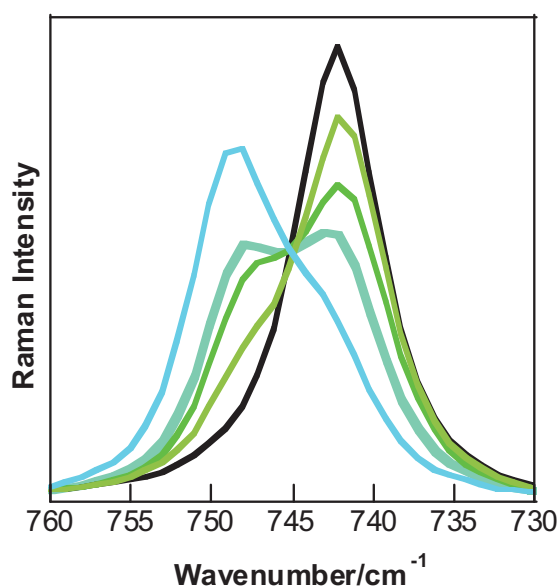
Figure II.32: Raman spectra of $(1-x)(BMI\text{-}TFSI),x\text{LiTFSI}$ ionic liquids for $x = 0$ (black), 0.08, 0.18, 0.22 and 0.36 (blue) by order of decreasing intensity at 742 cm^{-1} and of increasing intensity at 748 cm^{-1}, respectively. For a convenient comparison, all the spectra were normalized with respect to their total intensity integrated between 775 and 717 cm^{-1}.
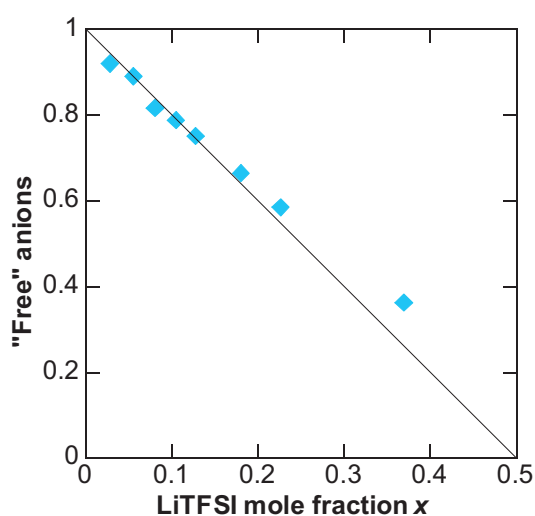
Figure II.33: Population of 'free" TFSI$^-$ anions in $(1-x)(BMI\text{-}TFSI),x\text{LiTFSI}$ ionic liquids evaluated from the fraction of intensity contained in the 742 cm^{-1} component of Figure II.32. A theoretical line of slope -2 is drawn for comparison.

VTF fits of EIS measurements show that the number of charge carriers remains constant in x LiTFSI - (1-x) BMITFSI mixtures up to x = 0.12 (see Figure II.17) which is in accordance with the implication of LiTFSI in [Li(TFSI)$_2$] clusters as demonstrated by Raman spectroscopy. Moreover, for x = 0.37, the number of charge carriers is found to increase (EIS), which can be related to the excess of free TFSI anions observed by Raman spectroscopy.

According to the Raman spectra in the 360-260 cm^{-1} region (Figure II.34), the conformational equilibrium of the anion between the *transoid* (C$_2$) and *cisoid* (C$_1$) forms seems to be slightly displaced towards C$_1$ when x increases, as already observed with the EMI homologue (Figure II.35). One can infer that the anion adopts a *cisoid* conformation in the [Li(TFSI)$_2$]$^-$ anionic clusters.
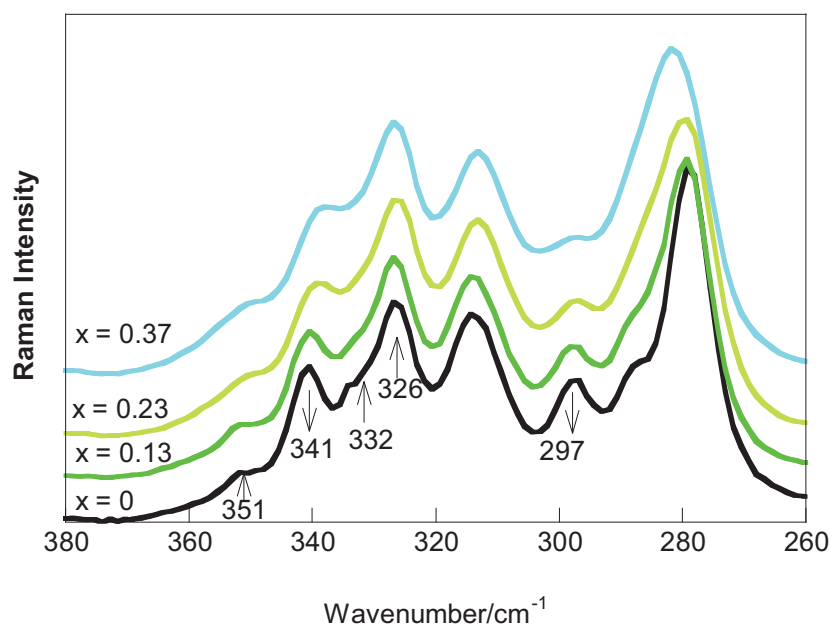
Figure II.34: Raman spectra of (1-x)BMITFSI,xLiTFSI ionic liquids at room temperature in the 360-260 cm^{-1} region.
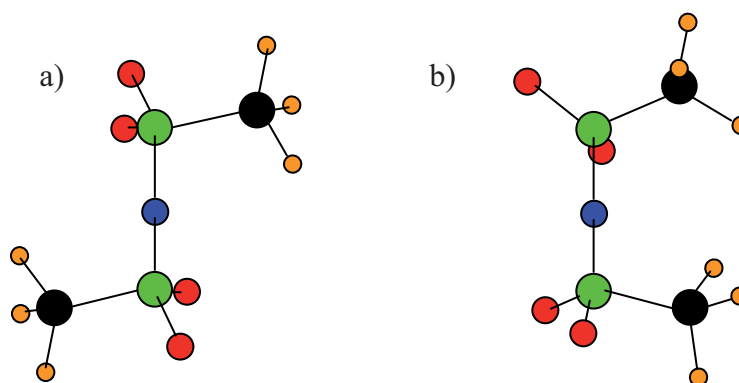
Figure II.35: Projection of the TFSI conformers, a) *transoid C$_2$* ; b) *cisoid C$_1$* from ref 38.

80

II. 8. 5. Li$^+$ solvation in LiTFSI / PMMA binary mixtures

According to Ali *et al*.,[39] the room-temperature conductivity of LiTFSI/PMMA blends increases from $\sim 10^{-7}$ S cm^{-1} at 15 wt%LiTFSI (MMA/Li $\sim$16.3) up to $\sim 10^{-5}$ S cm^{-1} at 20 wt%LiTFSI (MMA/Li $\sim$11.5). Then it increases more slowly and reaches a maximum of 1.25 10^{-4} S cm^{-1} at 35 wt%LiTFSI (MMA/Li $\sim$5.3). At this latter concentration, the system becomes a polymer-in-salt solid electrolyte in which the dipole-dipole interactions between the ester groups of PMMA are shielded by the plasticizing TFSI$^-$ anion.[40] The interaction of Li$^+$ with the C=O group of PMMA has been evidenced, but the composition of the Li$^+$ coordination shell as a function of the concentration is not known.

The Raman spectra of Figure II.36 show that the intense TFSI$^-$ line at 742 cm^{-1} presents a shoulder at 747 cm^{-1} due to anions involved in ion-pairs. A fit has been performed with mixed gaussian/lorentzian profiles having a proportion of lorentzian fixed at 60%.[41] The 747 cm^{-1} band has a negligible intensity for MMA/Li = 32, but ion-pairing effects already appear for the relatively diluted mixture MMA/Li = 19 and they concern 25% of the anions for MMA/Li = 9.5.
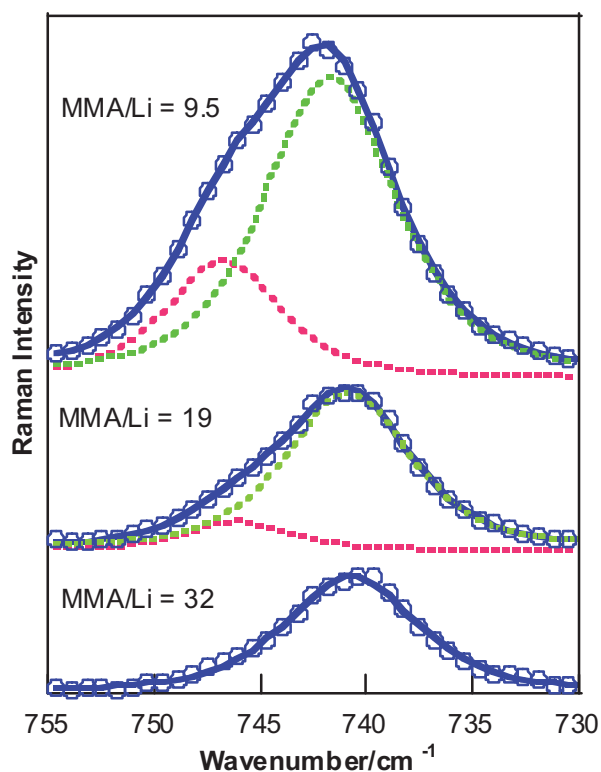
Figure II.36: Raman spectra focussed on the TFSI$^-$ bands at 742 and 747 cm^{-1} of LiTFSI/PMMA blends with composition MMA/Li = 32, 19 and 9.5, fitted as described in the text.

The ATR-FTIR spectra of PMMA exhibit an asymmetric $\nu_{C=O}$ absorption centred at 1724 cm^{-1} (Figure II.28 a); addition of LiTFSI produces a new absorption due to the coordinated C=O groups at 1700-1702 cm^{-1}. These profiles were fitted by two Gaussian components. Using equations (II.13) and (II.14), the number of coordinated C=O per lithium is found to be 3 or 2 for and R_{IR} = 1 or 1.5 respectively (Figure II.37).
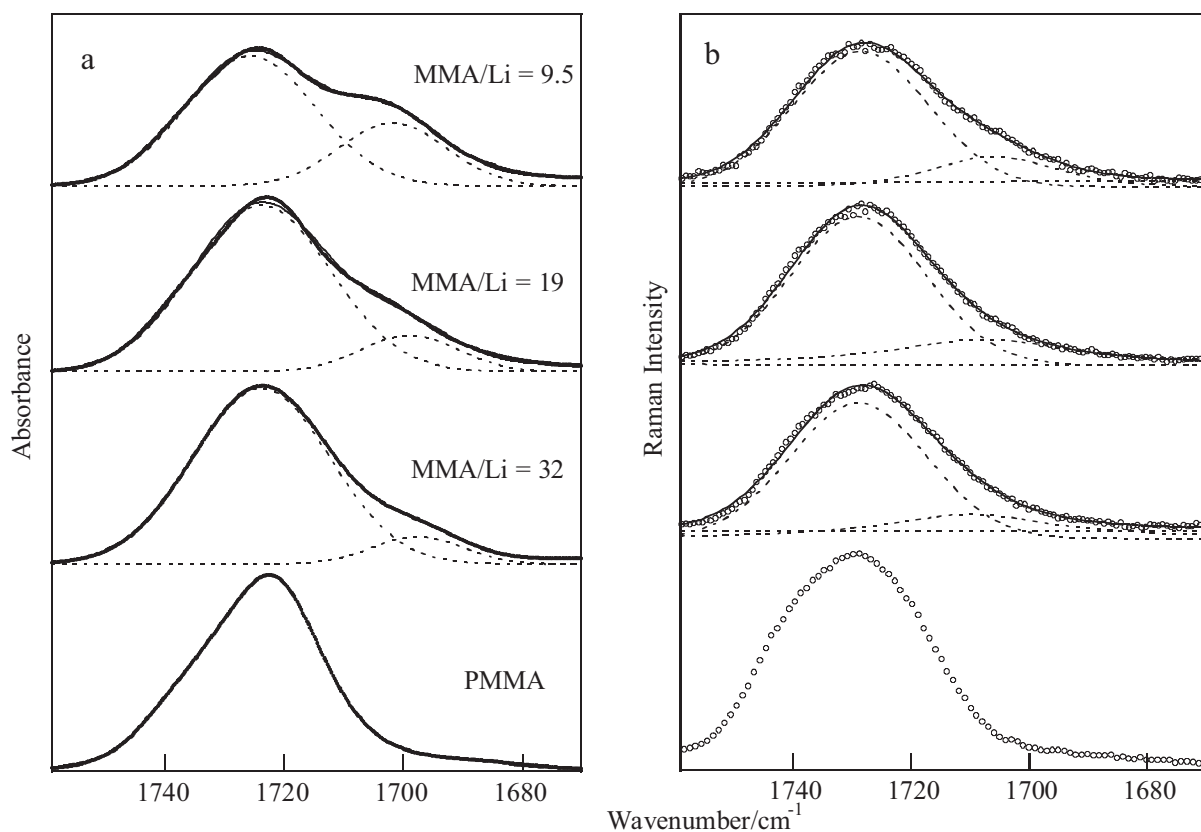
Figure II.37: FTIR-ATR spectra (a) and Raman spectra (b) at room temperature of PMMA and of LiTFSI/PMMA blend with MMA/Li = 32, 19 and 9.5.

This is of course a very rough evaluation based on a reduced number of samples and resulting from approximate values of R_{IR} and from the use of only two Gaussian components in the fitting procedure. This latter hypothesis may be rather restrictive. Indeed, the Raman $\nu_{C=O}$ profiles (Figure II.37 b) do not coincide with the IR ones (Figure II.37 a) and it is not enough to consider different values for the intensity factors R_{IR} and R_{Raman} to explain the observed differences. Much better fits are obtained with three components, but the overlapping between these components and the number of parameters is too high for accurate measurements. Nevertheless, the presence of more than two components cannot be excluded if dipolar coupling between C=O groups is considered. In LiTFSI/PMMA blends, the C=O

oscillators surrounding a lithium ion are submitted to ion-dipole interactions that shift to lower wave numbers, but these oscillators can also interact by coupling of their transition dipoles. This coupling depends on the number and orientation of the C=O groups and can give several modes with different positions and activities in IR and Raman. Dipolar coupling between C=O groups may occur even in the absence of lithium and can explain the different asymmetry of the IR and Raman profiles of pristine PMMA (Figure II.37). Further studies such as polarization studies by Raman or tests of PMMA with different tacticities would be helpful to conclude on this aspect.

Let us just conclude from this first level of analysis that Li^+ is coordinated to 2 or 3 C=O groups and also to a $TFSI^-$ anion for relatively diluted blends (MMA/Li = 19). The results are not accurate enough to specify the geometry of these interactions, but the simultaneous interaction of Li^+ with C=O groups and $TFSI^-$ indicates that binding energies are more or less of the same order of magnitude.

II. 8. 6. Li^+ solvation in LiTFSI / BMITFSI plasticized PMMA membranes

II. 8. 6. 1. Influence of PMMA ratio

For this study, a constant ionic liquid composition $x = 0.23$ was first selected and PMMA content was increased from 0 to 50 wt. %. The number of polymer repeat units per lithium (MMA/Li) was then 1.91, 4.29, 7.36, 11.45, and 17.17 for 10, 20, 30, 40 and 50 wt. % PMMA, respectively. As shown on the Raman spectra of Figure II.38, the population of coordinated anions first markedly decreases from 0 to 30 wt. % PMMA; then, it does not change very much in between 30 to 50 wt.% PMMA although the 748 cm^{-1} component still appears as a shoulder. The presence of an isosbestic point again confirms that the Raman activity of the considered vibration is unchanged from the 'free' to the coordinated states.
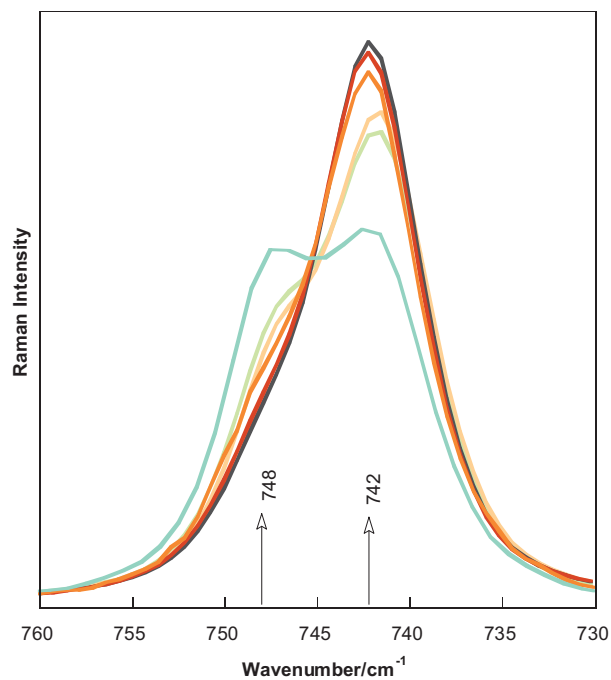
Figure II.38: Raman spectra of PMMA membranes plasticized by $(1-x)$(BMI-TFSI),xLiTFSI with $x = 0.23$. The quantity of PMMA is 0, 10, 20, 30, 40 and 50 wt% by order of increasing intensity at 742 cm^{-1}, respectively. All the spectra have been normalized by integration between 775 and 717 cm^{-1}. A fitting of the two components has been performed using mixed Gaussian/Lorenzian profiles with the proportion of Lorentzian up to 60%, as illustrated in Figure II.39 for 40 wt% PMMA.
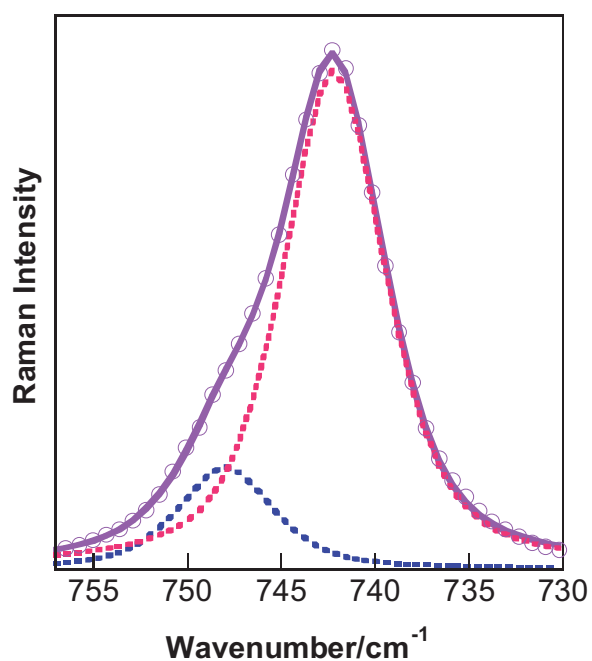
Figure II.39: Raman spectra of PMMA membranes (40 wt %) plasticized by $(1-x)$(BMI-TFSI),xLiTFSI with $x = 0.23$. The two components have mixed Gaussian/Lorentzian profiles with a proportion of Lorentzian up to 60%.

The PMMA/Li interaction can be followed from the IR spectra of the $\nu(C=O)$ stretching vibration of PMMA, as indicated by the ATR-FTIR spectra of the same series of samples (Figure II.40). Indeed, the region of the C=O stretching vibration exhibits the two expected components for the "free" and coordinated C=O groups, located after fitting at 1729 ± 2.5 cm^{-1} and 1712 ± 4 cm^{-1}, respectively as illustrated for one composition in Figure II.40b.
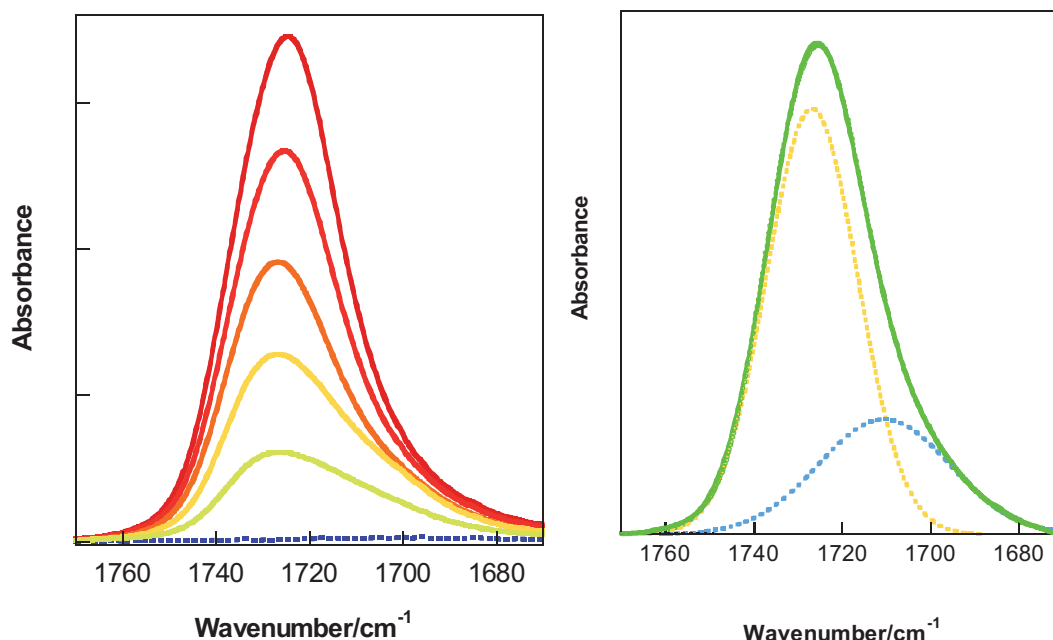
Figure II.40: a) FTIR-ATR spectra at room temperature of PMMA membranes plasticized by $(1-x)$(BMI-TFSI),xLiTFS$_I$ with $x = 0.23$, with increasing quantities of PMMA as follows: 0 (dotted blue line, pure ionic liquid), 10, 20, 30, 40 and 50 wt% from bottom to top.
    b) FTIR-ATR spectra of PMMA membranes (40 wt%) plasticized by $(1-x)$(BMI-TFSI),xLiTFSI with $x = 0.23$. The two components have mixed Gaussian/Lorentzian profiles with a proportion of Lorentzian up to 60%.When the PMMA content increases from 10 to 50 wt%, the component of the 'free' C=O groups is shifted from 1730 to 1726 cm^{-1} and the component of the coordinated C=O groups is shifted from 1715 to 1707 cm^{-1}.

The number of coordinated anions and C=O groups per lithium can be determined from the preceding results using eqs (II.9) and (II.14) and have been plotted in Figure II.41. As previously pointed out, the number of coordinated anions is close to 2 for MMA/Li = 0 since most lithium ions are then involved in [Li(TFSI)$_2$]$^-$ clusters.

When MMA/Li increases, these clusters are quickly destroyed and the coordination number reaches a plateau of about 0.7 for a PMMA content of 30 wt%. At the same time, the number of coordinated C=Os increases rapidly from zero to about 3 when the PMMA content increases from 0 to 30 wt%. The results obtained with $R_{IR} = 1.5$ are reported for comparison. They give a solvation number of about 2.2, but, as previously pointed out, the R_{IR} value is more probably close to 1 and the solvation number close to 3.
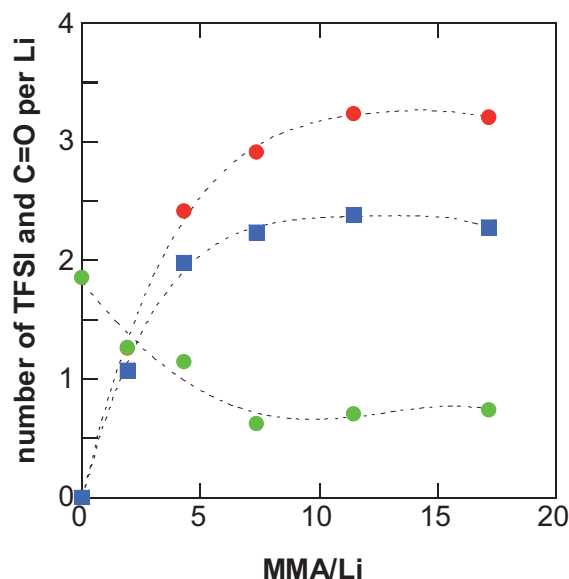
Figure II.41: Population of coordinated anions (●) per lithium and number of coordinated C=O groups per lithium (●: R$_{IR}$ = 1.0, ■: R$_{IR}$ = 1.5) as a function of the number of polymer repeat units per lithium, MMA/Li, for a composition x = 0.23 in (1-x)(BMI-TFSI),xLiTFSI.

We can assume from the above solvation numbers that the lithium does not have a unique solvation shell in the plasticized PMMA membranes. It may for example be coordinated by 3 C=O groups in some sites and by 2 or 3 C=O groups and 1 TFSI$^-$ anion in other ones. The anion is not completely excluded from the solvation shell, which means that the binding energy of the S=O groups of TFSI$^-$ with Li$^+$ is of a comparable order of magnitude with the Li$^+$…O=C interactions.[35] The thermodynamic stability of the membrane may take advantage of the cross-linking effect of the lithium ion.

The changes which take place in the lithium solvation from the pure ionic liquid to the plasticized PMMA membrane are expected to modify the diffusion and conduction mechanisms. Let us recall that in the pure ionic liquids (1–x)(BMITFSI), xLiTFSI, the lithium diffuses mainly within a [Li(TFSI)$_2$]$^-$ anionic cluster. The diffusion of all the ions, including the [Li(TFSI)$_2$]$^-$ anionic cluster, slows down when x increases because the viscosity increases. The addition of PMMA produces a further increase of the viscosity and decreased diffusion for all the ionic species. Self-diffusion coefficients have not been measured in plasticized PMMA, but the conductivity of the membranes, measured as a function of the concentrations and of the temperature (see section II.7) reflects the same evolution.

A few values measured at 293 K are recalled in Figure II.42 to illustrate the strong effect of the PMMA concentration and the comparatively weaker effect of the LiTFSI mole fraction for a given PMMA concentration.
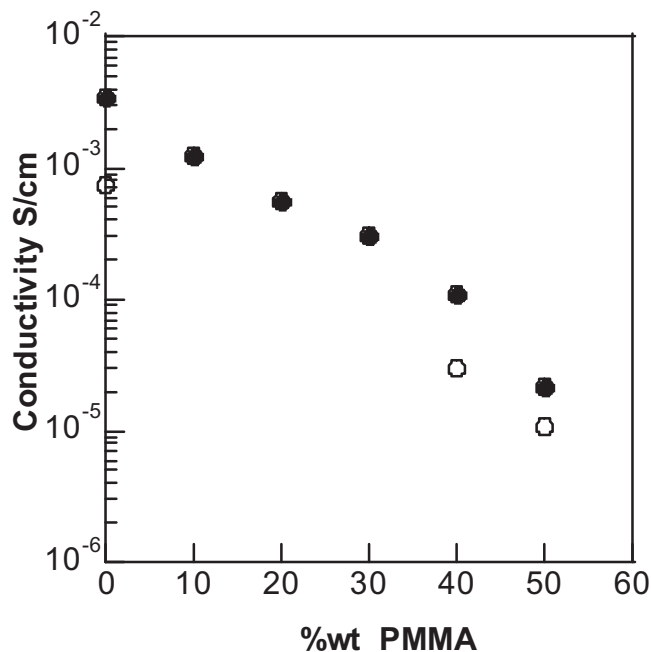
Figure II.42: Conductivity at 293 K of PMMA membranes plasticized by (1-*x*)(BMITFSI), *x*LiTFSI ionic liquids containing LiTFSI mole fractions *x* = 0.03 (filled circle) and 0.23 (open circle).

The conductivity of $3 \ 10^{-5}$ S cm^{-1} at 293 K measured for *x* = 0.23 and *y* = 40 wt. % PMMA is low, but a thin membrane has proved to give good results in an electrochromic device as illustrated in chapter IV. The improvement of the lithium transference number probably compensates the decrease of conductivity, as compared to the pure ionic liquid.

II. 8. 6. 2. Influence of LiTFSI molar ratio

A typical composition used for a plasticized membrane electrolyte in electrochromic devices is *x* = 0.23 and *y* = 40 wt. % PMMA. According to Figure II.41, the lithium ion has reached its maximum possible solvation by TFSI⁻ and PMMA for a composition of PMMA > 30 wt%. The study of LiTFSI molar ratio influence will therefore be performed on membranes with 40 wt% PMMA with LiTFSI concentration from *x* = 0 to 0.37. The populations of "free" TFSI- anions were measured as previously explained based on the typical IR profiles in the $\nu_{C=O}$ region; which are reported in Figure II.43. They present an isosbestic point and their total integrated intensity, measured as a function of *x*, is constant within ± 5%. Furthermore, the intensity of the "free" component is directly transferred into the "coordinated" component. This is a good indication that the two components have similar

intensity factors. Therefore, if theoretical considerations indicate a value of 1.5 for R$_{IR}$,[35] the experimental results strongly suggest a R$_{IR}$ value close to unity.
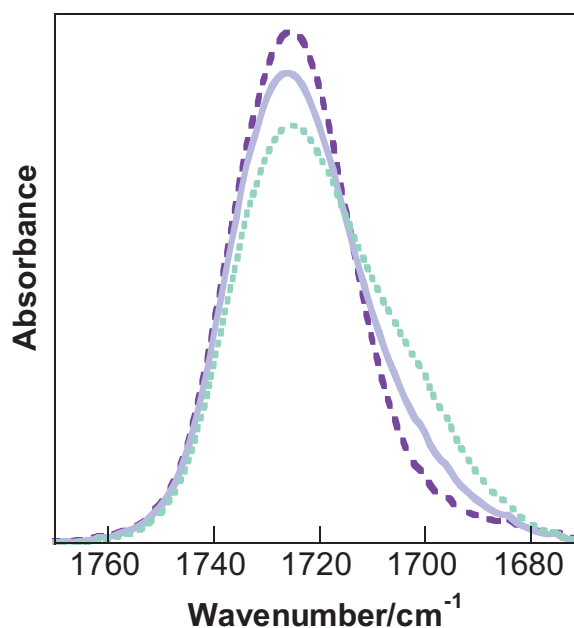
Figure II.43: Infrared spectra in the C=O stretching vibration of PMMA (40 wt%) plasticized by $(1-x)$(BMI-TFSI),x LiTFSI ionic liquids containing LiTFSI mole fractions of x = 0.028, 0.23 and 0.37, by order of decreasing intensity at 1729 cm^{-1} and increasing intensity at 1712 cm^{-1}, respectively.

II. 9. *Diffusion coefficient measured by PGSE-NMR*

Conductivity measurements provide only information on the overall transport of charged species. Raman and ATR IR gave information on the nature of the species in presence. To get information on the diffusion of these species and their transport in the electrolytes several techniques can be applied:

- Method involving the passage of a measured quantity of charge through a cell and subsequent determination of changes in the composition of the electrolyte in the vicinity of the anode and cathode (ex : Hittorf / Tubandt measurements) [42]
- Method following the movement of the constituents as they diffuse through the polymer electrolyte (ex: PGSE-NMR)
- Current fraction measurement (ex: dc polarisation)

In the case of fully dissociated electrolyte all these methods give the same result. On the contrary, as a result of ion association, in the case of associated electrolytes such as ionic liquids, results differ depending on the ability of the method to distinguish or not the associated ions. We decided to use the PGSE-NMR (Li, H and F) method since it gives information on the nature of the species involved. The NMR study has been performed in BMITFSI ionic liquid (not with the BMIPF$_6$) for sake of simplicity; indeed working with BMIPF$_6$ would have introduced an additional anion to be considered in an already complicated mixture.

Diffusion coefficients were measured for liquid electrolytes with x LiTFSI from 0 to 0.36. For more information on NMR technique see appendix A.

II. 9. 1. NMR spectra

II. 9. 1. 1. LiTFSI / BMITFSI solutions

The ^{1}H, ^{7}Li and ^{19}F NMR spectra of 0.03 LiTFSI / 0.97 BMITFSI are given in Figure II.44, Figure II.45 and Figure II.46 respectively.
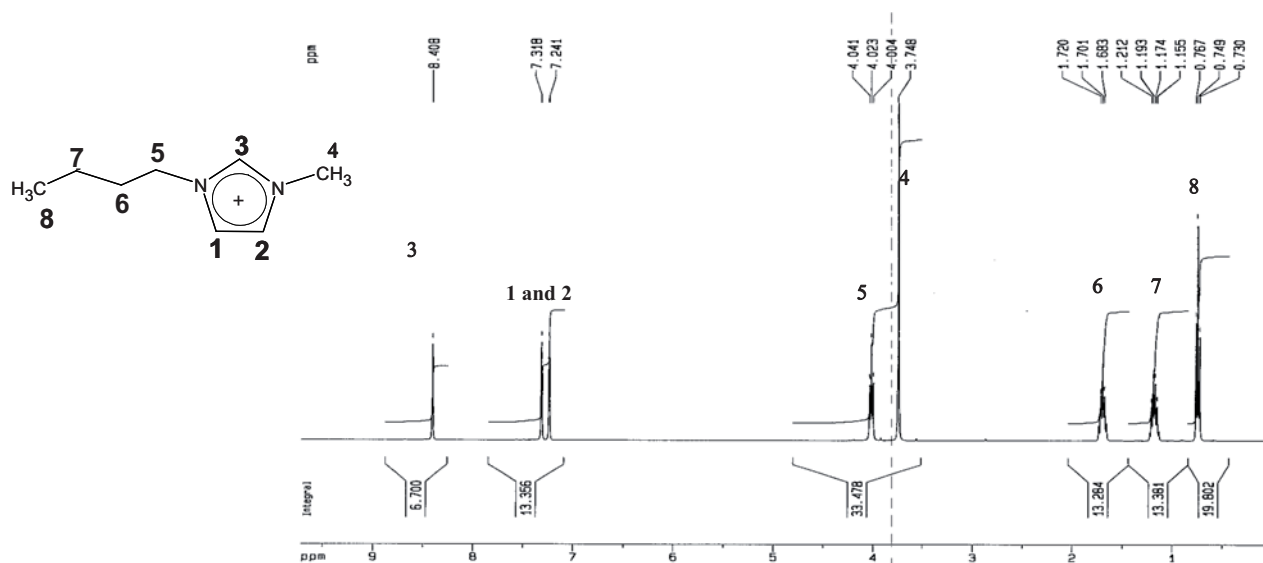
Figure II.44: ^{1}H NMR spectrum of 0.03LiTFSI/0.97BMITFSI in D$_2$O/MeOH, and proton assignation.
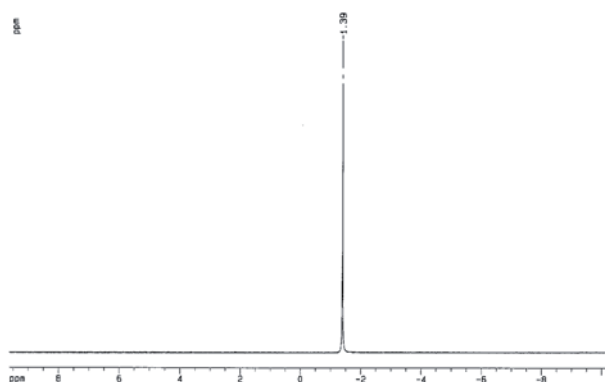
Figure II.45: ^{7}Li NMR spectrum of 0.03LiTFSI/0.97 BMITFSI with reference D$_2$O/MeOH.
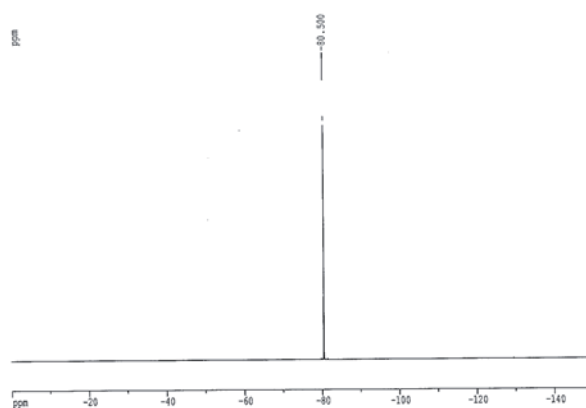
Figure II.46: ^{19}F NMR spectrum of 0.03LiTFSI/0.97 BMITFSI in D$_2$O/MeOH.

In the case of the ^{1}H NMR, different signals are observed corresponding to various proton environments in BMI$^+$ (no H in TFSI$^-$). In the 1-2 ppm region, the protons of the aliphatic chain are detected whereas protons of the aromatic cycle exhibit a signal in the 7-9 ppm region (Figure II.44). In the case of ^{7}Li and ^{19}F, only one signal is observed showing that the different environments of Li$^+$ ("free" Li$^+$ and Li$^+$ involved in clusters) and of F (TFSI$^-$) are not observable on the NMR time scale due to fast exchange between the considered species.

II. 9. 1. 2. PMMA

The NMR spectrum of PMMA in CDCl$_3$ is given in Figure II.47. It demonstrates that the commercial PMMA is atactic (see reference spectrum of an atactic PMMA in appendix D), the substituents (here CH$_3$) are randomly distributed on each side of the chain of polymer.

2
(CH₃)
|
(-CH₂-C-)n
3 |
CO(OCH₃)
1
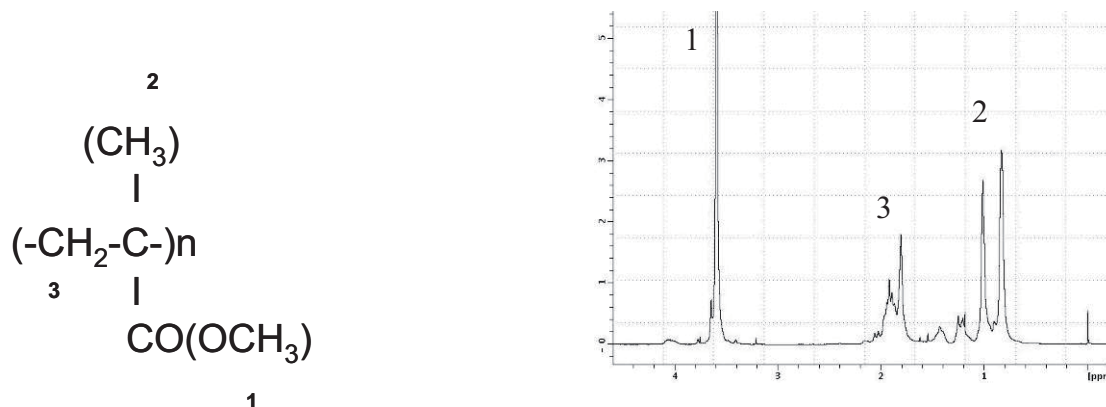
Figure II.47: ^{1}H NMR spectrum of PMMA dissolved in CDCl$_3$. The peak assignation shows the atacticity of the PMMA.

II. 9. 1. 3. LiTFSI/BMITFSI/PMMA

As PMMA is added in the ionic liquid, besides all the peaks of BMI$^+$, peaks characteristic of PMMA appear as a wide band around 3.4 ppm (Figure II.48).
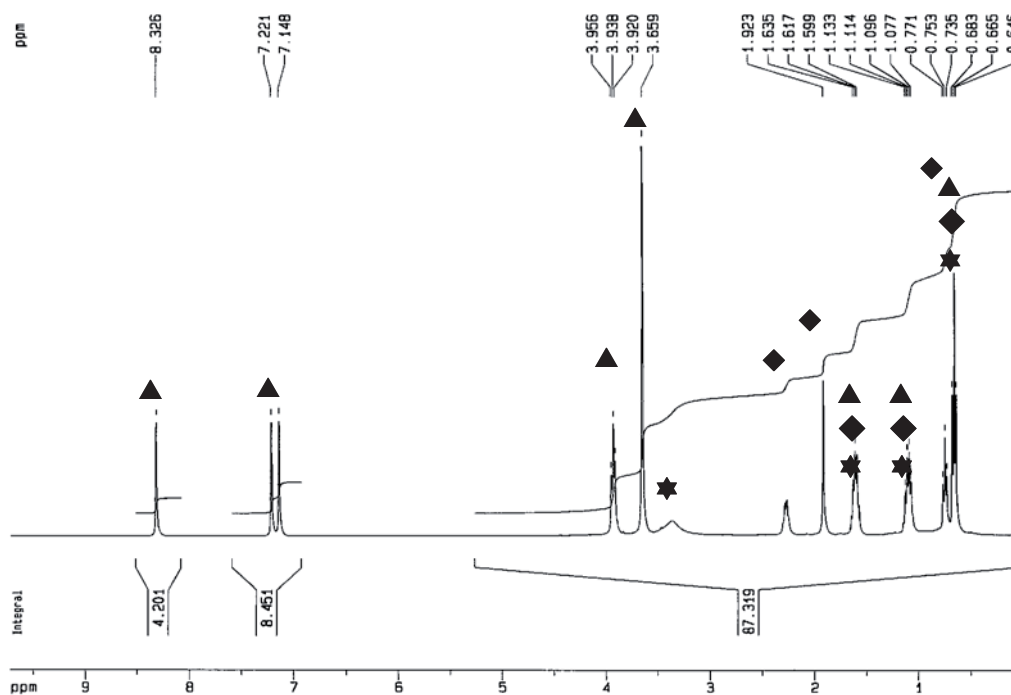
Figure II.48: ^{1}H NMR spectra of 0.3 LiTFSI / 0.97 BMITFSI with 20 wt% PMMA with reference D$_2$O/MeOH at 50°C, ▲ BMI; ✦ PMMA; ◆ Butanone

We could also observe other peaks due to the co-solvent butanone at 0.7, 1.9, and 2.2 ppm. Even after 48h thermal treatment at 70°C under vacuum, this co-solvent couldn't be totally eliminated from the bulk electrolyte. Residual butanone comes from difficulties to

evaporate the solvent in the NMR tubes; the measure of the diffusion coefficients is then not fully accurate as will be discussed later on.

II. 9. 2. Diffusion coefficient in liquid electrolyte LiTFSI/BMITFSI

The diffusion coefficient of the different species can be measured by NMR as far as they give distinct NMR signals. In the case of LiTFSI/BMITFSI mixttures, 3 several species could be distinguished: "TFSI" (^{19}F nucleus), "Li$^+$" (^{7}Li) and "BMI$^+$" (^{1}H). The measure is based on the Pulse Gradient Spin Echo Nuclear Magnetic Resonance (PGSE-NMR) method where the application of a gradient in the magnetic field allows the measure the species displacement.

II. 9. 2. 1. Principle of the diffusion coefficient by Pulsed field gradient NMR (PGSE-NMR)

The principle of PGSE-NMR have been detailed by Stejskal and Tanner[43] and developed by Price[44] about 10 years ago. This method involves the measurements of the attenuation of the intensity of a spin-echo signal resulting from the displacement of nuclear spins after imposition of spatially well-defined gradient pulses. This is a non invasive method which provides a convenient way to measure the self-diffusion of each ionic species in a system provided that the components contain NMR-sensitive nuclei.

The sequence is detailed in Figure II.49. This is a sequence based on a Hahn spin-echo pulse sequence[45] (90°-τ-180°-τ-acq.) commonly used for NMR measurements with an additional rectangular gradient inserted into each τ delay. A homogeneous field Bo is first applied to the system so that the macroscopic magnetization is on the z-axis. Upon application of a 90° radio frequency RF pulse, it rotates to the x-y plane. A gradient pulse of duration δ and magnitude g induces the dephasing of the spins, and then a 180° radio-frequency pulse reverses the precession so that the effect of a second gradient identical to the first (duration δ, magnitude g) is compensated unless the spins have moved in between the two pulses. The

decrease of the signal amplitude with the applied gradient is proportional to the movement of the spins.
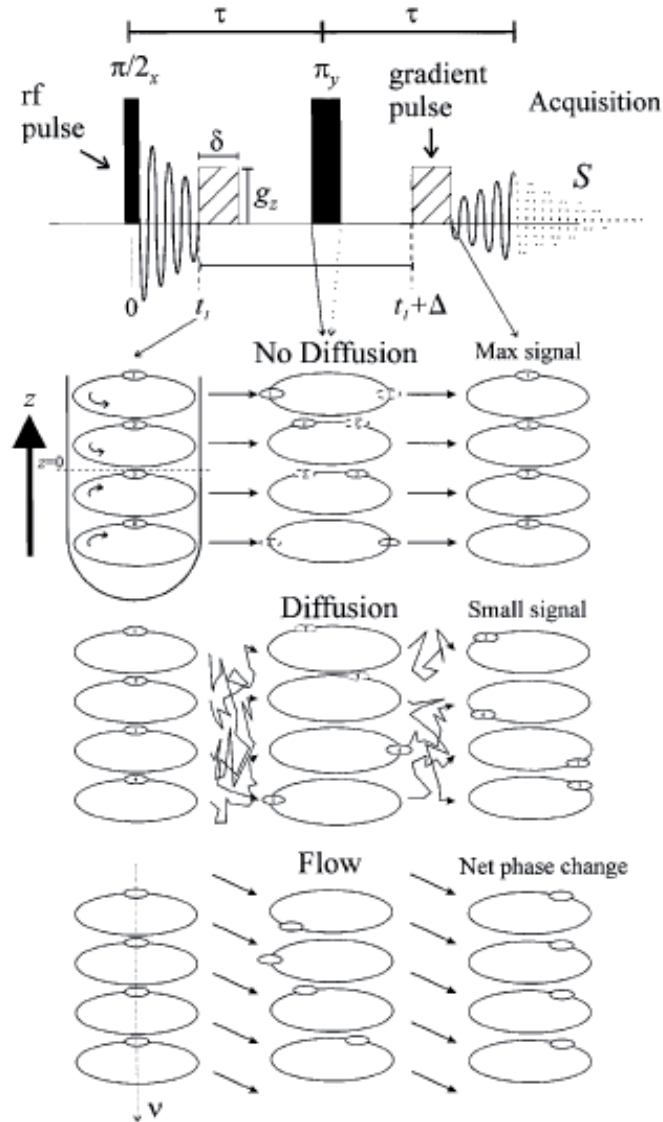
Figure II.49: A schematic representation of how the Stejskal and Tanner or PFG pulse sequence measures diffusion and flow. Reprinted from ref 44.

The echo signal attenuation is related to the experimental parameters by the following equation:

(II.16)
$$\ln(E) = \ln\left(\frac{S}{S_{g=0}}\right) = -\gamma^2 g^2 D \delta^2 \left(\Delta - \frac{\delta}{3}\right)$$

where S is the spin-echo signal intensity and γ is the gyromagnetic ratio, Δ the time between the two pulses, g the magnitude of the pulse and δ the duration of the gradient pulse.

Experimentally, the D value is determined by the slope of the plot $\ln(S/S_{g=0})$ versus $- \gamma^2 g^2$ $\delta^2(\Delta- \delta/3)$.

Data are then plotted on a 2D graph; see an example in Figure II.50. When several peaks are available, the diffusion coefficient is taken as the average value for all the concerned peaks.
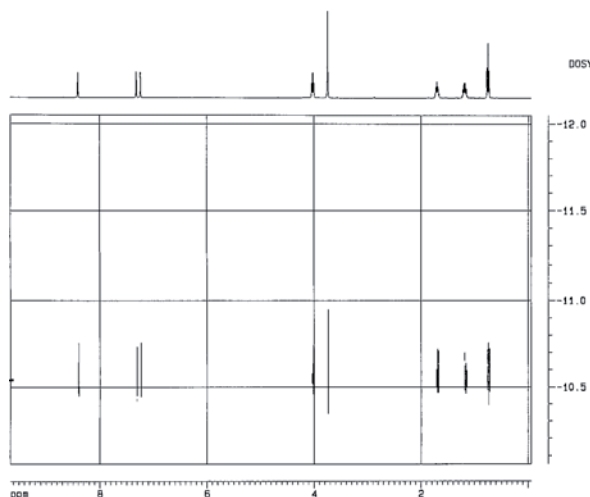
Figure II.50: 2D representation of chemical displacement in X-coordinate and diffusion coefficient (10^y) in Y-coordinate for a LiTFSI/BMITFSI solution (x $_{LiTFSI}$ = 0.03)

II. 9. 2. 2. Measurements of the species diffusion coefficients in LiTFSI/BMITFSI mixtures

II. 9. 2. 2. i. Influence of the Li$^+$ concentration

The diffusion coefficients of the ^{1}H, ^{7}Li and ^{19}F nuclei have been measured as a function of the TFSI$^-$ mole fraction, x, in (1-x)BMITFSI, x LiTFSI mixtures for $0 < x < 0.23$. Results reported in Table II.14 and Figure II.51 indicate that all the diffusion coefficients decrease when x increases, such as the previously described conductivity does. These diffusion coefficients are strongly dependent on the Li$^+$ ion concentration whatever the considered species. This general behaviour is expected from the increase of the viscosity η induced by the addition of LiTFSI.
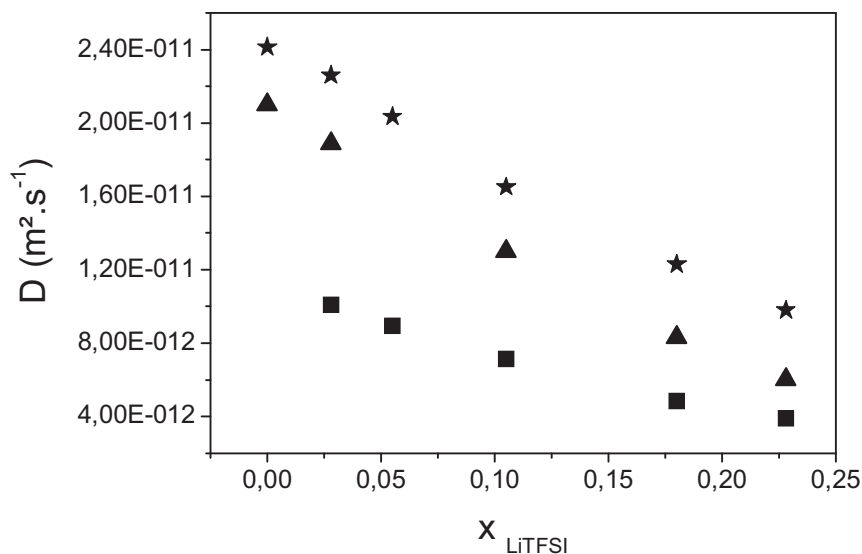
Figure II.51: Diffusion coefficients measured by PGSE-NMR, dependence on the LiTFSI molar ratio at 25°C for: ★ ^{1}H, ▲ ^{19}F, ■ ^{7}Li.

x	D_{Li}	D_F	D_H	$D_F{}^{46}$	$D_H{}^{46}$
0.0		21.1	24.1	21.8	27.4
0.03	10.1	18.9	22.6		
0.06	8.9	16.6	20.5		
0.11	7.1	13.0	16.5		
0.18	4.8	8.3	12.3		
0.23	3.9	6.0	9.8		

Table II.14 : Diffusion coefficients ($\times 10^{-12}$ m^2.s^{-1}) of the ^{1}H, ^{7}Li and ^{19}F nuclei, measured by PGSE-NMR at 298 K for ionic liquids (1-x)BMITFSI, xLiTFSI of variable composition, the value obtained by Tokuda et al. [46] are reported for comparison.

The BMI$^+$ cations carry all the protons and, when x varies, they experience rather constant interactions with the surrounding anions that are either free or coordinated to the lithium. Thus, their ^{1}H diffusion coefficient D_H can be considered as a probe of the global changes occurring in the dynamics of the solution when x and η increase. In other words, D_H is supposed to be proportional to the fluidity 1/η according to the Stokes-Einstein equation:

(II.17)
$$D = kT/c\pi\eta r_s$$

where k is the Boltzmann constant, T is the absolute temperature (K), c is a constant and r_s is the effective hydrodynamic (Stokes) radius.

At $x = 0$, the "free" TFSI$^-$ anions diffuse slightly slower than the BMI$^+$ cations as shown by the respective values $D_F = 21.1 \ 10^{-12}$ and $D_H = 24.1 \ 10^{-12}$ m^2 s^{-1}. These values for

the pure ionic liquid are in reasonable agreement with those measured previously by Tokuda *et al.*[46] (see Table II.14).

The Van der Waals radii of BMI$^+$ and TFSI$^-$ are 0.330 and 0.326 nm, respectively.[46] However, considering the higher amplitude of its conformational flexibility, the TFSI$^-$ anion may have a slightly larger r_s value than the BMI$^+$ cation. The small value found for D_{Li} at high LiTFSI dilution (D_{Li} is about twice as small as D_F and D_H) is again compatible with the diffusion of Li$^+$ within a [Li(TFSI)$_2$]$^-$ cluster (as demonstrated by Raman experiment for $x <$ 0.2) having about twice the r_s value of TFSI$^-$ or BMI$^+$.

All these qualitative observations can be put in a more quantitative form by assuming that the diffusion of the free TFSI$^-$ anions depends on the viscosity of the solution in the same way as that of the BMI$^+$ cations does. One can then infer that the ratio 21.1/24.14 is maintained in the considered concentration domain, *i. e.* that the diffusion coefficient of the free anions as a function of x is simply given by:

(II.18) $$D_{\text{"free" TFSI}} = (21.07/24.14)D_H$$

The measured ^{19}F diffusion coefficient results from the weighted contribution of the free and coordinated anions according to:

(II.19) $$D_F = (1-2x)\, D_{TFSIfree} + 2x\, D_{TFSIcoord}\ \text{ for } x < 0.2$$

In such a way that $D_{TFSIcoord}$ can be evaluated from:

(II.20) $$D_{TFSIcoord} = [D_F - (1-2x)\, D_{TFSIfree}]/2x$$

The values thus determined are added in Figure II.52.
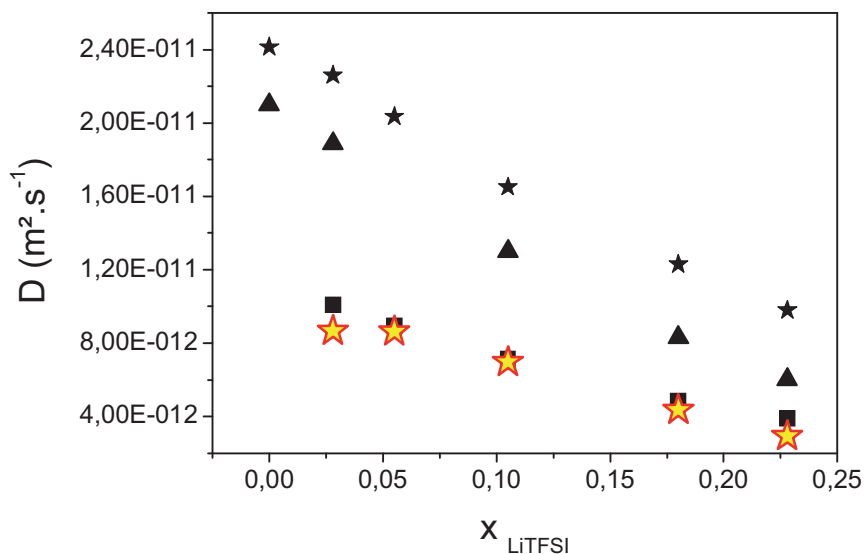
Figure II.52: Diffusion coefficients measured by PGSE-NMR as a function of x in $(1–x)(BMITFSI),xLiTFSI$ ionic liquids at 25°C: black stars: ^1H, triangles: ^{19}F, squares: ^7Li, red stars: ^{19}F diffusion coefficient of the coordinated anions in $Li(TFSI)_2^-$, calculated as explained in the text.

Within experimental errors, $D_{TFSIcoord}$ is equal to D_{Li}, which is a good confirmation that all the lithium ions are involved during sufficiently long times in $Li(TFSI)_2^-$ clusters.

This conclusion seems to be applicable to other ionic liquids based on an imidazolium cation and a fluorinated anion. For example, results obtained by Hayamizu *et al*. on the $(1-x)(EMIBF_4),xLiBF_4$ system gave quite similar behaviours for the self-diffusion coefficients of the ^1H, ^7Li and ^{19}F nuclei as a function of x up to $x \sim 0.2$.[24] At $x = 0$, the EMI^+ cation diffuses slightly faster than the "free" anion ($D_H/D_F \sim 1.2$ at 303 K). Then, the ^{19}F diffusion is found to decrease faster than the ^1H diffusion as a function of x ($D_H/D_F \sim 1.7$ at 303 K and $x = 0.2$), while D_H/D_{Li} at these temperature and concentration is about 3.3. The simple approach given in (II.19) and (II.20), suggests the existence of a $[Li(BF_4)_n]^{(n-1)-}$ anionic cluster with $n \sim 3$.

Another example is provided by Nicotera *et al*.[47] who have measured the ^1H, ^{19}F and ^7Li diffusion coefficients in $(1-x)PYR_{13}TFSI,xLiTFSI$ where PYR_{13} is N-methyl-N-pyrrolidinium. Although the measured values are only available in graphs, it is possible to estimate a ratio of $D_H/D_F \sim 1.1$ at 313 K and $x = 0$, whereas at $x = 0.2$ and 313 K, $D_H/D_F \sim 1.8$ and $D_H/D_{Li} \sim 2.2$. These data are again consistent with a diffusing $Li(TFSI)_2^-$ cluster.

The above evaluations of the lithium solvation numbers by TFSI or BF_4 are very qualitative, but they do indicate that in LiX doped ionic liquids the lithium is coordinated during relatively long enough times (as compared to Raman frequency) in $[Li(X)_n]^{(n-1)-}$ anionic clusters to be measured by NMR (time scale of the NMR: $10^{-9} – 10^{-10}$ s). As the

doping levels are generally low ($x \sim 0.2$) the fraction of current transported by the lithium is also small. Furthermore, the lithium transference number T$_{Li}$ can be defined as:

(II.21) $T_{Li} = \alpha t Li^+ - \chi t LiX_2^- + \delta 2 t Li_2 X^+ + \ldots$

where α, χ, δ, … are the populations of the corresponding ionic species containing Li$^+$ and t denotes the individual transport numbers. Neutral ion-pairs LiX, Li$_2$X$_2$, etc.., of respective populations β, ε etc.., are not included in T$_{Li}$ because they do not contribute to the ionic conductivity. The sum of all these populations is equal to the LiTFSI mole fraction:

(II.22) $x = \alpha + \beta + \chi + \delta + \varepsilon + \ldots$

In the examples described above with X = TFSI$^-$, the LiX$_2^-$ species are predominant and the corresponding - χtLiX$_2^-$ term in (II.21) gives a negative T$_{Li}$. This is a rather pessimistic conclusion for a lithium conducting electrolyte. However, there are many examples in the literature of electrochromic devices or of lithium batteries that work reasonably well with such electrolytes.[48] We will indeed establish that typical electrochromic systems based on PEDOT and Prussian Blue electrodes, undergo highly reversible coloration/bleaching cycles using (1-x)BMITFSI,xLiTFSI ionic liquids with x = 0.1-0.3, but do not work for x = 0. This indicates that the few Li$^+$ ions available in the equilibrium of (II.21) are sufficient to promote the electrochromic process. It can also be inferred that the transport of lithium is not limited to a vehicular mechanism, *i.e.* to a diffusion of the only [Li(X)$_n$]$^{(n-1)-}$ anionic species. MD simulations suggest that an important contribution to the lithium transport comes from the exchange of TFSI$^-$ anions in the first Li$^+$ coordination shell and outer shells.[49] In other words, the Li(TFSI)$_2^-$ cluster is labile and can liberate a Li$^+$ cation in the vicinity of an electrode.

However the electrochromic devices or lithium batteries will perform even better if the lithium transference number is made positive, for example by changing the lithium solvation from Li(TFSI)$_2^-$ to some positive [Li(S)$_n$]$^+$ species. There are indications of the validity of such a strategy in the literature for the lithium intercalation into graphite[26,50] or for the lithium metal plating/striping.[51]

II. 9. 2. 2. ii. Discussion on BMITFSI / LiTFSI interactions

In the pure ionic liquid $(1-x)$(BMITFSI),xLiTFSI for $x < 0.2$, the lithium solvation is essentially insured by two TFSI$^-$ forming [Li(TFSI)$_2$]$^-$ anionic clusters as previously observed for the EMI analogue.[1] The variation of the diffusion coefficients of the ^{1}H, ^{7}Li and ^{19}F nuclei as a function of x can be interpreted in terms of the diffusion of three distinct species: the BMI$^+$ cations that carry all the protons and govern the ^{1}H values; the "free" anions that contribute to the ^{19}F data in proportion to their population $(1-2x)$, and the [Li(TFSI)$_2$]$^-$ anionic clusters that govern both the ^{7}Li and the ^{19}F values, the latter in proportion to the population $2x$ of coordinated anions. This very simple treatment leads to the conclusion that the lithium transference number is negative in $(1-x)$(BMITFSI),xLiTFSI ionic liquids for small x values. It seems that this conclusion can be extended to LiX doped ionic liquids, where X$^-$ (= TFSI$^-$, BF$_4^-$, PF$_6^-$, etc..) is a fluorinated polyatomic anion. Although such electrolytes can be used in electrochemical devices with lithium insertion electrodes, it seems interesting to displace the lithium solvation towards [Li(S)$_n$]$^+$ species by adding appropriate ligands S. During this work, a very detailed PGSE-NMR study of the $(1-x)$(BMITFSI), xLiTFSI system[52] appeared in which the authors infer a solvation of the lithium by three anions in Li(TFSI)$_3$$^{2-}$. They also suggested that 'this anionic form of lithium would not be profitable as a charge-transporting species in lithium batteries. They proposed to relax this unfavorable solvation by adding a solvent or a silica dispersion, in complete agreement with previous conclusion for the $(1 - x)$(EMITFSI), xLiTFSI system.[4] In an even more recent publication[53], the $(1 - x)$(EMITFSI), xLiTFSI system was again investigated by Raman spectroscopy and the authors fully confirm the results and conclusions concerning the formation of [Li(TFSI)$_2$]$^-$ clusters with preferential *cisoid* conformation for the coordinated anions.

II. 9. 2. 3. Molar conductivities: Λ_{EIS} and Λ_{NMR} and ratio of charged species in the electrolytes

The molar conductivity Λ, i.e. the conductivity per mole of compound is obtained both from EIS and from diffusion coefficient measurements. Λ_{EIS}, the molar conductivity determined from EIS measurements, is based on the migration of all the charged species when submitted to an electric field; it is obtained by dividing the conductivity (S.cm^{-1}) by the molar concentration (mol.cm^{-3}). The Nernst-Einstein equation can be used to calculate the molar conductivity from diffusion coefficients that we obtained by PGSE-NMR, Λ_{NMR}. This

equation does not consider any ion association and is based on the assumption that each ion has an activity of unity. It is the conductivity that would be attained by the electrolyte if fully dissociated. In this latter case, the ratio $\Lambda_{EIS}/\Lambda_{NMR}$ is equal to 1. Thus, the ratio $\Lambda_{EIS}/\Lambda_{NMR}$ gives information on the ionic association and/or ionic activity of the considered electrolyte.

The molar conductivity, Λ_{NMR}, is calculated through the PGSE-NMR diffusion coefficients D, using the Nernst-Einstein equation.

$$\text{(II.23)} \qquad \Lambda_{NMR} = \frac{N_A e^2 (D_{cation} + D_{anion})}{kT}$$

where N_A is the Avogadro's number ($6.02 \ 10^{23}$ mol^{-1}), e is the electric charge of each ion (for monovalent ions: e = $1.6 \ 10^{-19}$ C), k is the Boltzmann constant ($1.38 \ 10^{-23}$ J.K^{-1}) and D$_{cation}$ and D$_{anion}$ are the diffusion coefficient for the cations and anions in presence.

This formula is easily applicable in the case of an electrolyte made of a salt (lithium salt) dissolved in a classical electrolyte (such as propylene carbonate). However, when a lithium salt is introduced in the BMITFSI IL, all the species that might form in solution must be considered: BMI$^+$, TFSI$^-$ and [Li(TFSI)$_2$]$^-$ as shown by our Raman experiments (see above) and for other ionic liquids.[4,24] The diffusion coefficient for the global term of 'anion' accounts for both TFSI$^-$ and [Li(TFSI)$_2$]$^-$. The molar conductivity from PGSE-NMR is then:

$$\text{(II.24)} \qquad \Lambda_{NMR} = \frac{N_A e^2 (D_{[Li(TFSI)_2]^-} + D_{TFSI^-} + D_{BMI^+})}{kT}$$

Raman experiments results are used to determine the species involved in NMR diffusion coefficient for each atom (Li, F and H):

$$D_{[Li]} = D_{[Li(TFSI)2]^-}$$

$$D_{[F]} = x_{[Li(TFSI)2]^-} * D_{[Li(TFSI)2]^-} + x_{TFSI^-} * D_{TFSI^-}$$

$$D_{[H]} = D_{BMI^+}$$

and following equation (II.19):

$$D_{[F]} = 2x_{LiTFSI} * D_{[Li(TFSI)2]^-} + (1-2x_{LiTFSI}) * D_{TFSI}$$

The molar conductivity deduced from NMR experiments is then given by eq. (II.25)

$$(II.25) \quad \Lambda_{NMR} = \frac{N_A e^2 \left[D_{[Li]} + \dfrac{D_{[F]} - 2x_{LiTFSI} D_{[Li]}}{1 - 2x_{LiTFSI}} + D_{[H]} \right]}{kT}$$

where x_{LiTFSI} represents the molar fraction of LiTFSI in BMITFSI.

Molar conductivities, Λ_{EIS} and Λ_{NMR} and the molar conductivity ratio, $\Lambda_{\text{EIS}} / \Lambda_{\text{NMR}}$ are listed in Table II.15 for liquid electrolytes (1-x)BMITFSI/xLiTFSI of variable compositions. As already pointed out, in the case of σ plots (EIS), only charged species motion is responsible for conductivity, whereas from D plots (NMR), ions, ion-pairs and neutral aggregates contribute to diffusion values. As the values for LiTFSI-BMITFSI mixtures are all less than unity, this indicates that not all the species can contribute to the ionic conduction. Neutral aggregates are formed and/or strong interactions occur between the ions which tends to decrease their ionic activity.

x	D_{Li}	D_F	D_H	Λ_{NMR} (mS.cm².mol⁻¹)	Λ_{EIS} (mS.cm².mol⁻¹)	$\Lambda_{EIS}/ \Lambda_{NMR}$
0.0		21.1	24.1	1.7	0.9	0.55
0.03	10.1	18.9	22.6	2.0	0.6	0.32
0.06	8.9	16.6	20.5	1.7	0.5	0.31
0.11	7.1	13.0	16.5	1.4	0.5	0.39
0.18	4.8	8.3	12.3	1.0	0.4	0.38
0.23	3.9	6.0	9.8	0.8	0.3	0.37

Table II.15 Diffusion coefficients (x10⁻⁸ cm².s⁻¹) of the different species measured by ¹H, ⁷Li and ¹⁹F nuclei PGSE-NMR at 298 K for ionic liquids (1-x)BMITFSI/xLiTFSI of variable compositions. Molar conductivities are determined by NMR (Λ_{NMR}) and impedance techniques (Λ_{EIS}).
.

Thus we can estimate the percentage of ion aggregates or pairs by (1 - $\Lambda_{\text{EIS}}/\Lambda_{\text{NMR}}$). Here we must point out that the diffusion coefficient given by NMR are average values for the ions and ionic aggregates since their exchange rate is faster than the NMR time scale. The percentage of ionic aggregates obtained is a time average value that we can define as an existence probability of aggregates if we could measure the NMR and the conductivity at the same time scale.

From these data, the pure ionic liquid BMITFSI is a mixture of approximately 55/45 free and associated species which is consistent with the value obtained by Tokuda et al.[46]. This rather low value of the ratio can be explained by two reasons:

- a rather low viscosity of the ionic liquid as compared to IL with still larger cationic species, leading to rather high value of the diffusion coefficient measured by NMR.[54]

- the electron donor ability (Lewis basicity) of the TFSI$^-$ anion responsible for the relatively high interaction between BMI cation and TFSI anion and the formation of aggregates.[46]

As the lithium salt is added the proportion of species that do not take place in the conduction increases as shown by the decrease of $\Lambda_{imp}/\Lambda_{NMR.}$ due to the increase in viscosity and formation of [Li(TFSI)$_2$]$^-$ clusters. Moreover, these clusters are much less mobile than separated species due to their size so that their ionic activity is reduced. However; it is interesting to note that this $\Lambda_{imp}/\Lambda_{NMR}$ ratio remains rather constant over the whole concentration range up to $x=0.23$.

II. 9. 3. Diffusion coefficient in gel electrolytes (LiTFSI / BMITFSI / PMMA)

The diffusion coefficient of the membrane composed of LiTFSI, BMITFSI, and PMMA are measured by PGSE-NMR. A solution of LiTFSI, BMITFSI, and PMMA in butanone is prepared and placed in the NMR-tube. The solvent is then evaporated by heating at 80°C under vacuum during 48h. Once dried, the samples appeared jelly up to 30% PMMA and membrane-like above this PMMA ratio. In practice, the complete evaporation of the solvent could not be achieved in samples with %PMMA higher than 20%, the NMR signal of butanone was still visible. The residual amount of butanone may influence the viscosity of the sample, moreover the homogeneity of the membrane was doubtful (more butanone remaining at the bottom of the tube) so that the obtained results could not be taken into account. For 0 to 20 wt% PMMA, D$_{1H}$, D$_{19F}$ and D$_{7Li}$ are presented in Figure II.53.

Figure II.53: Diffusion coefficients measured by PGSE-NMR as a function of wt% PMMA in $(1-x)$(BMITFSI),xLiTFSI (x=0.03) ionic liquids at 25 °C: ★: ^{1}H, ▲: ^{19}F, ■: ^{7}Li

The addition of PMMA produces a general decrease of the diffusion for all the species because of the increase of the macroscopic viscosity. Moreover, the ratio D_H/D_{Li} changes from 2.3 at 0 wt. % PMMA to 1.4 at 20 wt. % PMMA due to an increase of D_{Li}. Up to 10 wt% PMMA, the diffusion coefficient of BMI^+, $TFSI^-$ and Li^+ are affected in more or less the same order. However, for 20 wt% PMMA, if the diffusion coefficient of BMI^+ follows the same trend, those of Li^+ and $TFSI^-$ do not. In other words, $TFSI^-$ is no more slowed down, relatively to BMI^+, as expected from the fact that PMMA has liberated a large number of anions from the Li^+ coordination. Li^+ itself diffuses relatively faster, as if its local coordination to the C=O groups were labile, or at least less constraining, in terms of diffusion, than the solvation in $[Li(TFSI)_2]^-$.

Further measurements are necessary to confirm and extend these observations, but it seems that the lithium transference number might well be improved in plasticized PMMA since lithium ratio transported by negatively charged clusters decreases.

II. 9. 3. 1. Molar conductivities: Λ_{EIS} and Λ_{NMR} for the gel electrolytes

For the electrolytic membranes LiTFSI/BMITFSI/PMMA, Raman experiments showed that in addition to the species cited above, the Li$^+$ has a tendency to coordinate with the C=O from the PMMA, so that the diffusion coefficients relates to:

$$D_{Li} = x_{[Li(TFSI)2]^-} * D_{[Li(TFSI)2]^-} + x_{Li\,O=C\,said"free"} * D_{[Li\,O=C]}$$

$$D_F = x_{[Li(TFSI)2]^-} * D_{[Li(TFSI)2]^-} + x_{TFSI+} * D_{TFSI^-}$$

$$D_H = D_{BMI^+}$$

There are three unknown parameters: $D_{[Li(TFSI)2]^-}$, $D_{[Li\,O=C]}$ and D_{TFSI^-} so that, with the information at our disposal, the calculus of the Λ_{NMR} is not possible.

II. 10. Conclusion

The study of the electrolytes containing PMMA and ionic liquid BMITFSI or BMIPF$_6$ showed:

- their transparency
- their good ionic conductivity
- their cohesive aspect and their long term stability
- strong interactions between the polymer, the ionic liquid and the lithium salt.

These interactions were observed in detail, with both direct methods (Raman, ITR) and indirect ones (DSC, EIS, measurement of the coefficients of diffusion). Measurements of DSC indeed showed that the presence of a lithium salt and of the PMMA prevented the crystallization of the IL. The major decrease of the conductivity when increasing the fraction of polymer shows that the polymeric matrix is in interaction with the liquid and modifies its properties. Moreover, in the presence of lithium salt (LiTFSI) this effect is even more pronounced, highlighting a strong interaction IL-PMMA relayed by lithium. Raman and IR spectroscopy techniques show that the addition of a lithium salt (LiTFSI) in the BMITFSI generates the creation of ionic pairs [Li (TFSI)$_2$]$^-$ - (for $x_{LiTFSI} < 0.12$), which can be related to

the constancy of charge carriers amount (measurements EIS, VTF model). Measurements of diffusion coefficients (PGSE-NMR) in these liquids show also a decrease of these coefficients with increasing lithium salt concentration, partly due to a higher macroscopic viscosity, as well as to microscopic interactions between the species. For $x > 0.12$, the number of charge carriers increases (EIS) as well as the number of free TFSI$^-$ (Raman). Moreover, when dissolved in PMMA, the lithium ion is coordinated to 2 or 3 C=O groups. Finally the study of the LiTFSI-BMITFSI-PMMA mixtures shows the destruction of the clusters [Li(TFSI)$_2$]$^-$ because there is competition between TFSI$^-$ and the O=C of the polymer.

These measurements gave a negative transference number for lithium; in the LiTFSI-BMITFSI liquids. However the addition of PMMA, even in low proportions (20%) improved this transference number to reasonable values for its use in electrochromic devices. Measurement with the 50% wt% PMMA membrane could not be carried out for practical reasons but it is extremely probable that the effect is even more pronounced. The Raman spectroscopy is able to detect species with very short life times (about the ps.). The frequency of observation of the NMR is slower (400 MHz), and that of the spectroscopy of impedance complexes even slower (1Hz - 1MHz). However the phenomena observed according to these various techniques are in good agreement, showing the long enough life time for the clusters detected by Raman.

The initial aim of the Nanoeffects project was to use flexible electrodes in electrochromic devices in combination with hydrophobic ionic liquids, BMIPF$_6$ or BMITFSI, into which the lithium salt LiTFSI was dissolved. We first considered BMIPF$_6$–based electrolyte mainly due to the cheaper price of BMIPF$_6$ as compared to BMITFSI. Unfortunately, we found that the presence of residual water in the Prussian Blue films (their electrodeposition is made in aqueous media see next chapter) leads to the degradation of the electrolyte. Indeed, hydrofluoric acid (HF) is formed upon reaction of PF$_6^-$ with water.[55] To cope with this problem, the removal of coordinated and non-coordinated water in Prussian Blue was considered. Unfortunately, the annealing of Prussian Blue above 80°C induces cracks in the films which are detrimental with respect to the electrochromic performances of the devices[56]. Only partial removal of water could be achieved by annealing the films at 70°C under vacuum; this treatment could not circumvent the film degradation during the electrochemical cycling in BMIPF$_6$ -based electrolyte (see appendix E for trials of electrodeposition of PB in ionic liquids to avoid the use of water for electrodeposition) .

Due to this lack of compatibility between BMIPF$_6$ and Prussian Blue, **we retained only BMITFSI based electrolytes in the following of the study**.

References

[1] M. Gazard, *Handbook of Conducting Polymers*, vol. 1, **1986**, Marcel Dekker.

[2] M.P. Scott, M. Rahman, C.S. Brazel, *Eur. Pol. J.*, **2003**, 39, 1947

[3] G. Campet, C. Mingotaud; A. Poquet; J.N. Portier, S. Ravaine, *Compositions d'électrolytes, procédé de fabrication et applications électrochimiques,* **2001**, patent FR 2803951.

[4] M. Herstedt, M. Smirnov, P. Johansson, M. Chami, J. Grondin, L. Servant, J.C. Lassègues, *J. Raman Spect.,* **2005,** 36, 762.

[5] T. Fox, G. *Bull. Am. Phys. Soc,.* **1956**, *1*, 123.

[6] E. Nielsen, *Mechanical Properties of Polymers and Composites*, Marcel Dekker, New York, **1975**, Chapter 1.

[7] R. M. Waxler, D. Horowitz and A. Feldman, *Appl. Opt*. **1979,** 18, 101.

[8] P. Bonhôte, A.-P. Dias, N. Papageogiou, K. Kalyanasundaram, M. Grätzel, *Inorg. Chem*., **1991**, 30, 4013.

[9] M. A. B. H. Susan, T. Kaneko, K. Hayamizu, A. NODA, M. Watanabe, *J. Am. Chem. Soc.,* **2005**, 127, 4976.

[10] H. Vogel, *Phys. Z.* **1921,** 22, 645.

[11] G. Tammann, W. Hesse, *Z. Anorg. Allg. Chem.,* **1926,** 156, 245.

[12] G.S. Fulcher, *J. Am. Ceram. Soc*., **1925,** 8, 339.

[13] S. Arrhenius, *Z. Phys. Chem*., **1889,** 4, 226.

[14] W.D. Callister Jr., *Materials Science and Engineering—An Introduction*, fifth ed., **2000,** Wiley, New York, p. 871.

[15] F. Civan, J.J. Weers, *SPE Prod. Facilities,* **2001,** 16, 4, 260.

[16] R. Gilmont, *Chem. Eng. Prog*., **2002,** 98, 10, 36.

[17] K. Monkos, *Curr. Top. Biophys.,* **2003,** 27, 1–2, 17.

[18] P.G.Bruce, *Solid State Electrochem.*, **1995**, ed. Cambridge university press, p. 130.

[19] J.L. Souquet, M. Duclot, M. Levy, *Solid States Ionics*, **1996**, 85, 149.

[20] M. Galiński, A. Lewandowski, I. Stępniak, **2006,** *Electrochim. Acta*, 51, 5567.

[21] D. Turnbull, M.H. Cohen*, J. Chem. Phys.,* **1961**, 34, 120.

[22] M.J. Monteiro, F.F.C. Bazito, L.J.A. Siqueira, M.C.C. Ribeiro, R.M Torresi, *J. Phys. Chem. B*, **2008,** 112, 7, 2102.

[23] D.R. McFarlane, J. Sun, J. Golding, P. Meakin, M. Forsyth, *Electrochem. Commun*., **2000,** 45, 1271.

[24] K. Hayamizu, Y. Aihara, H. Nakagawa, T. Nukuda, W.S. Price, *J. Phys. Chem. B,* **2004**, 108, 19527.

[25] J.C. Lassègues, J. Grondin, D. Talaga, *Phys. Chem. Chem. Phys*., **2006**, 8, 5629.

[26] J.C. Lassègues, J. Grondin, R. Holomb, P. Johansson, *J. Raman Spect.,* **2007**, 38, 551.

[27] P.G. Bruce, C.A. Vincent, *J. Chem. Soc. Faraday Trans*., **1993**, 89, 3187.

[28] Y. Grohens, J. Shultz, R.E. Prud'homme *Int. J. Adhes. Adhes.*, **1997**, 17, 16.

[29] M. Brogly, Y. Grohens, C. Labbe, J. Schulz, *Int. J. Adhes. Adhes.* **1997,** 17, 257.

[30] I. Rey, P. Johansson, J. Lindgren, J.C. Lassègues, J. Grondin L. Servant, *J. Phys. Chem. A*., **1998**, 102, 19, 3249.

[31] R. Holomb, P. Johansson, P. Jacobsson, I. Albinsson and J.C. Lassègues, in preparation.

[32] S. Duluard, J. Grondin, J.L. Bruneel, I. Pianet, A. Grélard, G. Campet, M.H. Delville and J.C. Lassègues *J. Raman Spect.* **2008**, <u>39</u>, 627.

[33] L.J. Hardwick, M. Holzapfel, A. Wokaun, P. Nová, *J. Raman Spect.*,**2007**, 8, 5629.

[34] S.A. Katsyuba, E.E. Zvereva, A. Vidis, P.J. Dyson, *J. Phys. Chem. A,* **2007**, 111, 352.

[35] P. Johansson, M. Edvardsson, J. Adebahr P. Jacobsson, *J. Phys. Chem. ,.* **2003**, 107, 12622.

[36] H.E. Johnson, S. Granick *Macromolecules,* **1990**, 23, 3367.

[37] D.L. Allara, Z. Wang, G.C.Pantano, *Non-Cryst. Solids,* **1990**, 120, 93.

[38] M. Herstedt, W.A. Henderson, M. Smirnov, L. Ducasse, L. Servant, D. Talaga, J.C. Lassègues, *J.Mol. Struct.,* **2006,** 783, 145.

[39] A.M.M. Ali, M.Z.A. Yahya, H. Bahron, R.H.Y. Subban, M.K. Harun, I. Atan, *Mater. Lett*., **2007,** 61, 2026.

[40] Z. Florjańczyk, E. Zygadło-Monikowska, W. Wieczorek, A. Ryszawy, A. Tomaszewska, K. Fredman, D. Golodnisky, E. Peled, B. Scrosati, *J. Phys. Chem. B,* **2004**, 108, 14907.

[41] S. Duluard, J. Grondin, J.L. Bruneel, G. Campet, M.H. Delville and J.C. Lassègues *J. Raman Spect.* **2008**, 39, 1189

[42] Hittorf, W. *On the Migrations of the Ions During Electrolysis*; (1853 to 1859); Edited by W. Ostwald, 2nd. Edition, Part I. **1903,** 49

[43] E.O. Stejskal, *J. Chem. Phys.*, **1965,** 43, 3597.

[44] W.S. Price, *Pulsed-Field Gradient Nuclear Magnetic Resonance as a Tool for Studying Translational Diffusion: Part I. Theory*, in Concepts Magn.Reson., **1997,** 9, 299 ; W.S. Price,

Pulsed-Field Gradient Nuclear Magnetic Resonance as a Tool for Studying Translational Diffusion: Part II. Experimental Aspects, in Concepts Magn. Reson., **1998,** 10, 197.

[45] E.L. Hahn, *Phys. Rev.*, **1950,** 80, 580.

[46] H. Tokuda, K. Hayamizu, K. Ishii, M. A. B. H. Susan, M. Watanabe, *J. Phys. Chem. B,* **2004**, 108, 16593.

[47] I. Nicotera, C. Oliviero, W. A. Henderson, G. B. Appetecchi, S. Passerini, *J. Phys. Chem. B,* **2005**, 109, 22814.

[48] a) B. Garcia, S. Lavallée, G. Perron, C. Michot, M. Armand, *Electrochim. Acta*, **2004**, 49, 4583; b) S. Seki, Y. Kobayashi, H. Miyashiro, Y. Ohno, A. Usami, Y. Mita, N. Kihira, M. Watanabe, N. Terada, *J. Phys. Chem. B*, **2006**, 110, 10228; c) M. Ishikawa, T. Sugimoto, M. Kikuta, E. Ishiko, M. Kono, *J. Power Sources*, **2006**, 162, 658; d) A. Brazier, G. B. Appetechi, S. Passerini, A.S. Vuk, B. Orel, F. Donsanti, F. Decker, *Electrochim. Acta*, **2007**, 52, 4792.

[49] O. Borodin, G.D. Smith, W.A. Henderson, *J. Phys. Chem. B*, **2006**, 110, 16879.

[50] M. Holzapfel, C. Jost, P. Novák, *J. Chem. Soc., Chem. Comm*., **2004**, 2098.

[51] J. Xu, J. Yang, Y. NuLi, J. Wang, Z. Zhang, *J. Power Sources*, **2006**, 160, 621.

[52] Y. Saito, T. Umecky, J. Niwa, T .Sakai, S. Maeda, *J. Phys. Chem. B*, **2007**, 111, 11794.

[53] Y. Umebayashi, T. Mitsugi, S. Fukuda, T. Fujimori, K. Fujii, R. Kanzaki, M. Takeuchi, S.I. Ishiguro*, J. Phys. Chem. B*, **2007**, 111, 13028.

[54] A. Noda, K. Hayamizu, M. Watanabe, *J. Phys. Chem. B,* **2001**, 105, 4603.

[55] P. Scovazzo, J. Kieft, D.A. Finan, C. Koval, D. DuBois, R. Noble, *J. Membrane Science*, **2004**, 238, 1-2, 57.

[56] S.A. Agnihotry, S. Punita, G.J. Amish, D.P. Singh, K.N. Sood, S.M. Shivaprasad, *Electrochim. Acta*, **2006**, 51, 4291.

Chapter III. Electrochromic thin films synthesis and properties in ionic liquid electrolyte: PEDOT, Prussian Blue and Prussian Blue analogue

III. 1. Introduction

Poly(3,4-ethylenedioxythiophene) (PEDOT) and Prussian Blue (PB) are well known electrochromic materials[1] with electrochromic properties that have been found to be interesting for their application as electrochromic materials for Nanoeffects low-cost and low-energy consuming devices. As previously detailed (cf. Chapter I), these properties are:

- large surface deposition
- low energy consuming deposition,
- low deposition temperature compatible with plastic substrates
- high colouration efficiency for PEDOT
- Prussian Blue capacity matched to that of PEDOT (around 3 mC/cm²)
- no residual colouration in the bleached state (OK for PB, improvable for PEDOT)

Our aim is to determine whether these materials can be used in ionic liquid based electrolytes. Following the conclusions of Chapter II on ionic liquid based electrolytes, the chosen electrolyte composition is 0.03 LiTFSI / 0.97 BMITFSI (molar ratio). The electrochemical parameters for complete devices based on PEDOT and Prussian Blue electrochromic materials with such electrolyte will be deduced from the following study. This study will also include experiments performed on a Prussian Blue analogue, InHCF, that is expected to be a nearly transparent electrode[2].

The non colourlessness of PEDOT in the bleached state was addressed within the Nanoeffects consortium and led to great improvements (patent pending), this will not be detailed here.

III. 2. PEDOT

III. 2. 1. Introduction to PEDOT

III. 2. 1. 1. Strategy for the working electrode: interest of PEDOTs

As explained before, PEDOT derivatives have been chosen for their high colouration when gaining electrons: colouration efficiencies around 200 cm²/C are easily obtained[1].

PEDOT also benefits from a fast colour change[1]. Moreover, as most of the poly(thiophene)s, PEDOT is relatively easy to synthesize both chemically and electrochemically, stable in air and easily processable[3,4]. PEDOT exhibits a deep blue colouration in its coloured state and a light blue colouration in its bleached state.

The relation between the PEDOT structure and its electrochromic properties will be detailed.

III. 2. 1. 2. PEDOT general formula

PEDOT is obtained by oxidative polymerization of the monomer 2,3-dihydrothieno[3,4-b]-1,4-dioxin, more often called ethylene dioxythiophene (EDOT) of formula given in Figure III.1A. This molecule can be polymerized either chemically or electrochemically to produce conducting poly(ethylene dioxythiophene) (PEDOT). As-prepared PEDOT is in the oxidized state represented on Figure III.1B, this polymer is conductive as will be explained in the next paragraph.

A   B

Figure III.1: EDOT formula (A) and PEDOT (B) formula in its oxidized form, counter anions are inserted in the structure to ensure electroneutrality.

III. 2. 1. 3. Conductive character of PEDOT: p-doping

Polymers are generally insulating materials, their electronic conductivity remaining lower than 10^{-5} S.cm^{-1}. However, some of them, by gaining or loosing electrons become conductive with conductivities as high as 2,000 S.cm^{-1} [5] (i.e. in the range of the ITO conductivity). For example for PEDOT, conductivities as high as 500-700 S.cm^{-1} or even up to 1,000 S/cm have been published.[6] The redox reactions induce the formation of poly-cations upon oxidation or poly-anions upon reduction in the polymer chain depending on the polymer nature. This results in the presence of charged species on the polymer backbone, leading to polaronic p-type or n-type conductivity (cf. Figure III.2A1). The terms p-doping (oxidation)

and n-doping (reduction) are often used for electronic conductivity enhancement in conductive polymers by analogy with semi-conductors. The p-doping is more frequently observed in polymers due to their low electron affinity, including PEDOT.

In the neutral polymer (Figure III.2A1), the electrons are delocalized along the conjugated backbones through overlap of π-orbitals (Figure III.2A2). This results in an extended π-system with a filled valence band. By removing electrons from the π-system by oxidation ("p-doping"), a charged unit called a polaron is formed and further oxidation leads to the formation of a bipolaron (see Figure III.2B). This increases the p-type conductivity and it also introduces intraband-gap energy levels[7-5-8] .

Figure III.2: Neutral PEDOT formula (A1) and its band gap structure (A2). Bipolaronic species obtained via two-electron oxidation (p-doping): formula (B1) and band gap structure (B2).

Upon deeper oxidation, the bipolaron bands finally merge in the valence and conduction bands and the polymer reaches a metallic-like state. The high electronic conductivity of PEDOT favours the electron transfer rate into the film and the electronic mobility within the film, which is undoubtedly in favour of a fast colour change.

III. 2. 1. 4. PEDOT colour change

Undoped PEDOT has a high conjugation length since the aromatic cycles of the backbone are coplanar (cf. Figure III.3A). Furthermore, the two electrons donating oxygen

atoms coupled to the thiophene ring account for the π-π^* transitions, and contribute to lower the bandgap[9]. Due to that, the π-π^* interband transition takes place and is in the visible range, this leads to a deep-blue colouration[1]. PEDOT doping removes the electronic conjugation, by lowering the number of aromatic rings overlapping (cf. Figure III.3.B). Therefore, the energy needed for interband electronic transitions π-π^* increases; that leads to an increase of the optical transparency in the visible domain. Additionally, bands appear at lower energy (near IR) due to the sub band gap levels appearing due to polaron and bipolaron formation [1,10], they will induce optical absorption in the near infrared domain, as will be shown below (Fig. III-8).

Figure III.3 : Undoped (A) and p-doped (B) PEDOT molecular orbital schematization

PEDOT, as opposed to most of the materials is a rather special material since, the bleached film (p-doped form) is more conductive than the coloured one (neutral form).

III. 2. 1. 5. Electrochemical doping/dedoping of PEDOT

For electrochromic devices, PEDOT films will experiment electrochemically induced doping and dedoping. Electrochemical p-doping of a polymer is schematized in Figure III.4.

- Polymer oxidation at the anode

$$(R)_n \longrightarrow (R)_n^{+\circ} + e^-$$
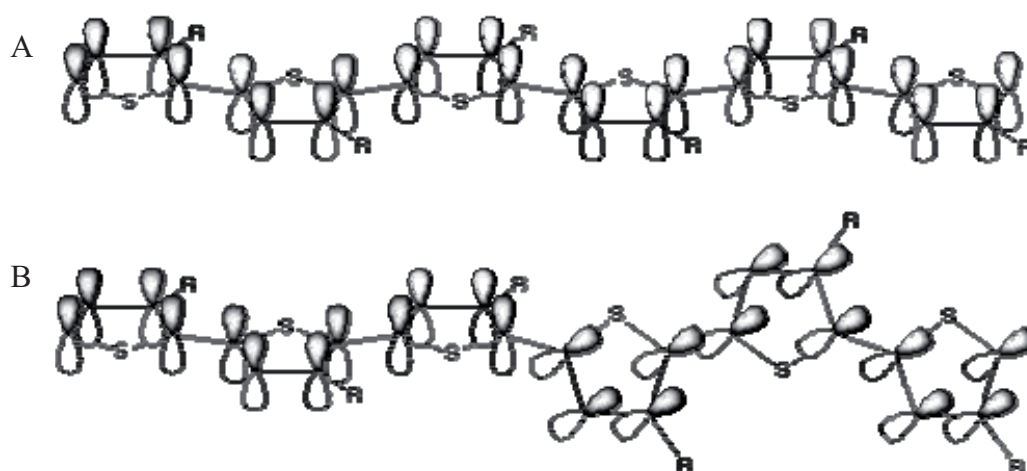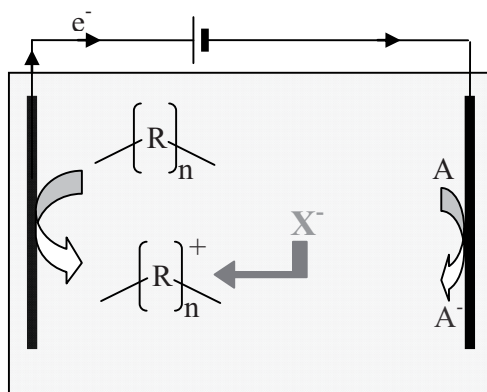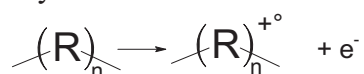
- Auxiliary compound A reduction at the cathode
- Insertion of an anion X⁻ from the solution in the polymer

Figure III.4: Electrochemical p-doping of a polymer $(R)_n$

Oxidation is induced at the PEDOT electrode by applying an oxidative voltage or current. Counter and reference electrodes are added in the circuit. During oxidation of the polymer, either an anion enters into the structure or a cation is withdrawn from it. For PEDOT, it is generally the insertion of an anion that takes place.[11] The inserted species X- can be ClO4⁻, Tos⁻, PF6⁻, BF4⁻ or TFSI⁻. Recent studies have shown the possibility of using an ionic liquid alone, for example devices with BMITFSI (anion: TFSI⁻) have been made.[12, 13] In the case of a PEDOT-PSS (PSS: polystyrene sulfonate) codeposited films, the PSS- is intrinsically attached to the polymer chain and acts as the counter anion.[14,15,16,17] In this case, a cation from the electrolyte is inserted in the film.

III. 2. 1. 6. Polymerization and doping

An important feature is that the electrochemically or chemically prepared PEDOT films are generally obtained in their oxidized (p-doped) state, i.e. both polymerisation and doping are performed in a single step.

III. 2. 2. PEDOT deposition methods

PEDOT deposition can be performed via three main methods: coating of PEDOT dispersions, in-situ chemical polymerization of EDOT in an already deposited layer

containing the precursors and electrochemical polymerization of the monomer. The electrochemically polymerized films and films obtained by the deposition of commercially available PEDOT dispersions that will be presented here were prepared at the ICMCB. The in-situ chemically polymerized films were prepared by Fraunhofer ISC institute.

III. 2. 2. 1. Electrochemical polymerisation

III. 2. 2. 1. i. Principle

PEDOT can be electrochemically polymerized both in organic [18-19], aqueous[20-21-22-23] solvents or in mixtures, for example water-acetonitrile[24]. The deposition in aqueous solvent is beneficial from cost, handling and safety points of view. However, the use of surfactants that have the detrimental side effect of decreasing films conductivity[25] is mandatory since EDOT solubility in pure water is very low. Electrodeposition in organic solutions, such as acetonitrile that we chose in this study, is more favourable (up to 0.15 mol/L)

The electrochemical process offers the possibility of a precise control on the thickness of the deposited films, via control of the passed charge. By this technique, the thickness of the films can be varied from a few Å to many micrometers. However, for large area deposition, the deposits are found inhomogeneous due to the too high sheet resistance of the transparent conductive substrate used as a current collector: the deposition rate decreases as the distance from the current injection increases. Progresses in substrate conductivity are expected to solve this problem (intrinsic increase of material conductivity, deposition of a metallic grid transparent to the eye on the conductive substrate). Another technique consisting in adding a homogeneous prelayer of PEDOT on the conductive substrate was tested (see below III. 2. 7.).

III. 2. 2. 1. ii. Procedure

A solution of 0.1M of tetrabutyl ammonium perchlorate (TBAP), 0.005 M of EDOT in acetonitrile is prepared and used as the electrolyte for the deposition; it contains the precursor reservoir for the electropolymerisation. The deposition is made in a three-electrode cell configuration (cf. Figure III.5).
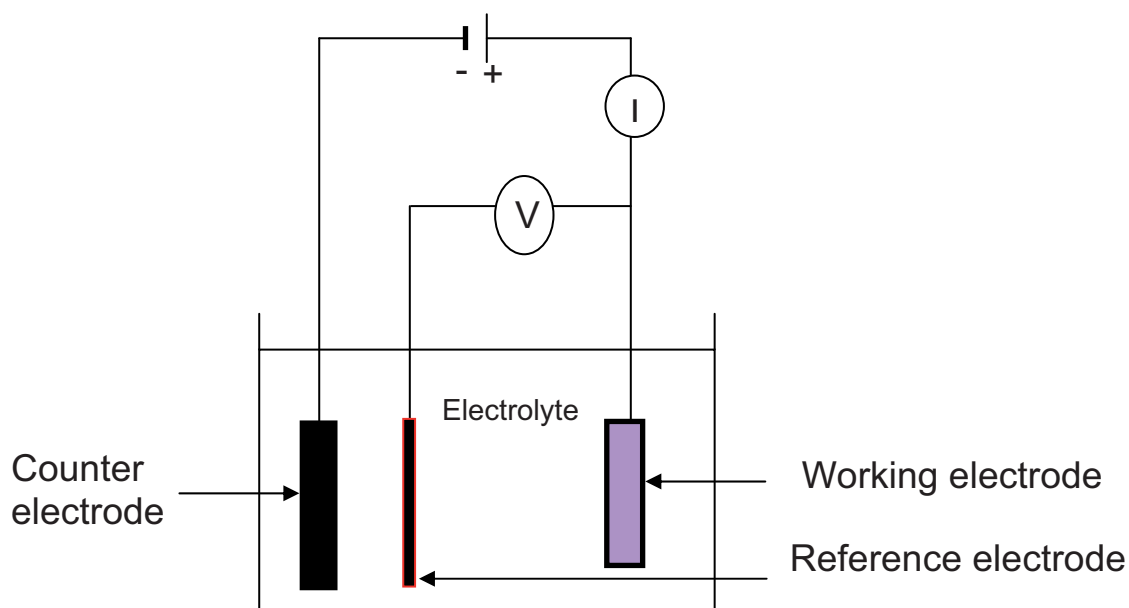
Figure III.5 : Scheme of the electrodeposition cell configuration. The counter electrode needs to be at least as large as the working electrode.

The desired substrate is placed at the working electrode; the counter electrode is a FTO plate and the reference a saturated calomel electrode. An oxidative potential of generally +1.4 V/SCE is applied during the chosen time.

III. 2. 2. 2. In-situ chemical polymerization

III. 2. 2. 2. i. Principle

The polymerization is activated (for example by heating) once the solution containing the precursors is deposited as a thin film on the desired substrate. This solution contains the monomer EDOT and an oxidative agent. It must be used as quickly as possible after preparation and stored at low temperature to avoid early polymerization. A reaction moderator is added in the solution to lower the polymerization rate. After polymerization, the excess of oxidant is removed by rinsing. In-situ polymerization can be made both in organic[26] and in aqueous[27] solutions. Fraunhofer-ISC, which developed this kind of deposition within the Nanoeffects project, works with non-aqueous electrolytes.
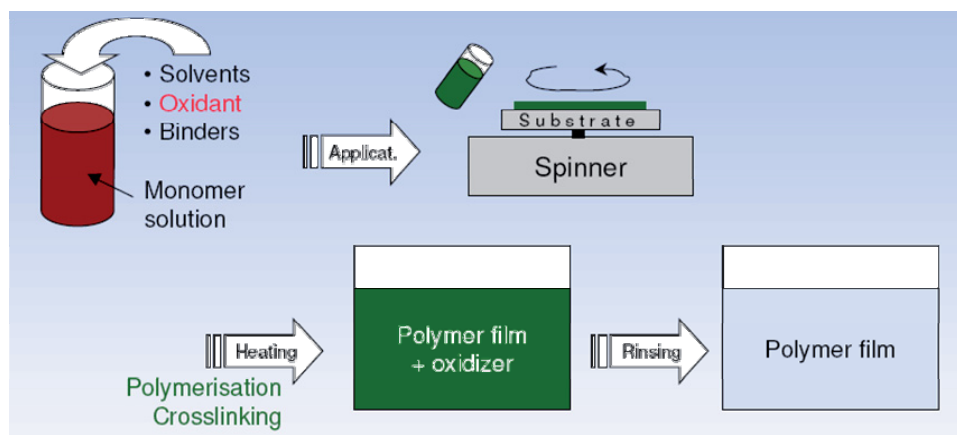
Figure III.6 : In-situ polymerized films preparation (courtesy by Fraunhofer ISC)

In-situ chemical polymerization process can be used with a wide variety of monomers and can be adapted to large surface areas provided adaptation of the deposition method. Moreover, additives, such as a hardener, can be inserted in the films. The rate of polymerization is not easily controllable, and a very precise control of the operating conditions (reaction moderator, temperature) is mandatory to get homogeneous and reproducible coatings.

III. 2. 2. 2. ii. Procedure

The EDOT monomer (Baytron M) is in-situ chemically polymerised on TCO substrates according to the procedure described by Y. Ha et al.[28] 0.625 mmol of moderator base (imidazol, Aldrich) is dissolved in n-butanol (Aldrich, reagent grade) in an ultrasonic bath until getting a clear solution. Afterwards, 2.5 mmol of EDOT and 4.38 mmol of the oxidiser (Fe(OTs)$_3$, Aldrich) are added to the mixture. The solution is filtered on a 0.45 μm membrane. After addition of the oxidative agent, the solution is spin-coated with a KSM Karl-Süss spin coater model RC8 at 600 rates per minute (rpm) for 30 seconds and then at 1200 rpm for 10 seconds. After thermal curing at 120 °C for 20 minutes, the unreacted agents are removed by rinsing in n-butanol and the films dried with compressed air.

III. 2. 2. 3. Coating of PEDOT dispersions

III. 2. 2. 3. i. Principle

PEDOT dispersions were first developed by Jonas et al.[27] who found a route based on oxidative polymerisation of EDOT in the presence of poly(styrene sulfonic acid) (PSSA) and

potassium persulfate (KPS) as oxidative agent. This method is widely used both in aqueous and organic solvents for the commercial production of PEDOT-PSS with variable formulations and particle sizes, under the trademarks Baytron from Bayer and Orgacon from Agfa for example.
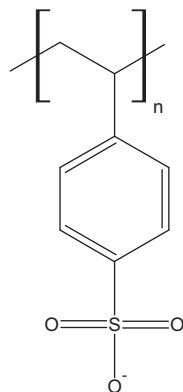
Figure III.7: Polystyrene sulfonate (PSS⁻) formula

Coatings with PEDOT dispersions provide a very simple method for PEDOT films deposition with high homogeneity on large scale substrates. Moreover, the efficient use of environment friendly solvents, ideally water, is demonstrated. However, the presence of resistive additives, for example PSS, is detrimental for the conductivity of the films, the switching time is decreased. Studies at CIDETEC are devoted to select other additives that could be advantageously used.[29]

III. 2. 2. 3. ii. Procedure

Orgacon EP9040 dispersion (PEDOT-PSS in ethanol) from Agfa, is spin-coated on the desired substrate, with the following sequence: 600 rpm, 15 s (deposition of the solution on the substrate), 1,000 rpm for 60s. (homogenization of the layer) and 2,000 rpm for 3 s (removal of the material accumulated at the edges). Most of the solvent is evaporated during the deposition process. A thermal treatment at 100 °C for 5 minutes is then performed to evaporate the remaining solvent and improve the connection between the PEDOT particles. For multilayer coatings, such thermal treatment is realised between each layers.

III. 2. 3. Studied films

The PEDOT-based films that were investigated are listed in Table III.1Table III.1. The area of the coatings is 4 x 5 cm².

Sample	Deposition method	Substrate	Deposition conditions	Counter anion
EP-1	Electrochemical polymerisation	FTO/glass	5 s, 1400 mV	ClO_4^-
EP-2	Electrochemical polymerisation	FTO/glass	10 s, 1400 mV	ClO_4^-
EP-3	Electrochemical polymerisation	FTO/glass	20 s, 1400 mV	ClO_4^-
D-1	Dispersion coating	FTO/glass	4 successive films	PSS^-
ISP-1	In-situ chemical polymerisation	FTO/glass		Tos^-
ISP-2	In-situ chemical polymerisation	ITO/PET		Tos^-

Table III.1 : Summary of the PEDOT samples prepared for the study.

On ITO/plastic substrate, the PEDOT films were much more inhomogeneous than those coated on FTO/glass. For this reason, the PEDOT films obtained by several deposition methods were studied only on FTO/glass substrates. The comparison between the PEDOT layers coated on glass and plastic substrates will be given in the case of the in-situ polymerization only. Moreover, for sake of simplicity, the influence of PEDOT thickness will only be detailed for electropolymerised PEDOT (EP-1, EP-2, EP-3) on FTO/glass.

III. 2. 4. Electrochemical measurements of PEDOT films

III. 2. 4. 1. Electrochemical measurements method

To perform the electrochemical measurements, the PEDOT electrodes are transferred into a deaerated electrolyte, of composition 0.03 LiTFSI/ 0.97 BMITFSI (molar ratio). in a three-electrode electrochemical cell. The substrate used for PEDOT deposition is placed at the working electrode; the counter electrode is a platinum foil and the pseudo-reference electrode is a Ag/AgCl wire. The design of the electrochemical cell allows the in situ measurement of the UV-visible spectrum. The electrochemical studies, except for spectroelectrochemical measurements, were performed in a glove box under inert argon atmosphere with a potentiostat Voltalab 40 and a UV-Visible spectrophotometer Evolution 100 from Thermo.

III. 2. 4. 2. Illustration of the colour change by doping-dedoping

As described above, depending on the level of doping of PEDOT, the colour intensity of the polymer drastically changes. As shown on Figure III.8, the degree of colouration can be finely tuned by the potential applied to the PEDOT electrodes.
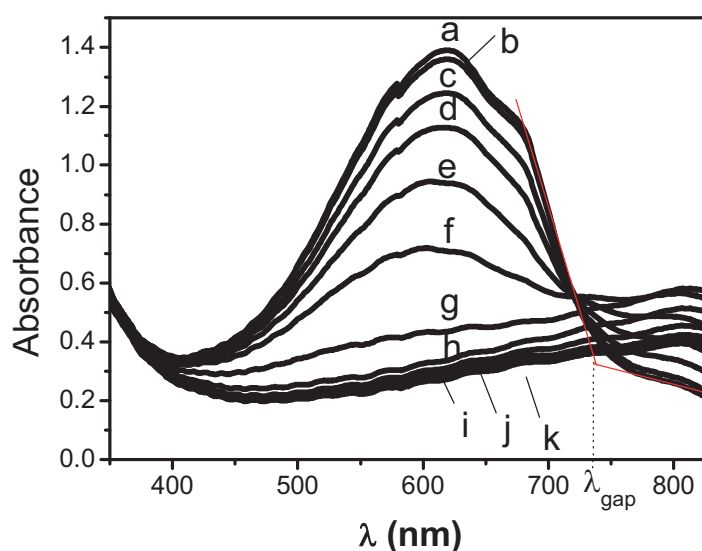
Figure III.8: Absorbance of a PEDOT film depending on the applied potential, in LiTFSI 0.03 (molar ratio) in BMITFSI, pseudo-ref: Ag/AgCl. a) -1.3 V, b) -1 V, c) -0.7 V, d) -0.6 V, e) -0.5 V, f) -0.4 V, g) -0.3 V, h) -0.2 V, i) 0 V, j) 0.2 V, k) 0.3 V, l) 0.4 V, the sample is an in-situ polymerized PEDOT on FTO/glass.

The reduced film of PEDOT is deeply blue coloured with a broad absorption peak at 610 nm (Figure III.8, curve a) due to high conjugation within the polymer, as explained above (III. 2. 1. 4.). The band gap is determined at the maximum absorption wavelength as 1.6 eV. As explained in III. 2. 1. 4. , upon oxidative p-doping, the energy needed for electronic π-π* interband transition increases and a band at 820 nm appears (curves c, d, e, f, g) due to the formation of bipolarons[1]. A residual absorption remains in the visible range, responsible for the pale-blue colouration of the bleached state.

To lower the residual colouration in the bleached state, the thickness of the electrochromic PEDOT films must be optimized depending on the required specifications in order to benefit both from high colouration in the coloured state and minimum residual colouration in the bleached state. This will be detailed in the following chapter III. 2. 5. . A second strategy, addressed by INSTM within the Nanoeffects consortium consisted in modifying the EDOT structure (patent pending), and will not be detailed here.

III. 2. 5. Optimization of PEDOT films thickness

In order to find the best compromise between highly colourlessness of the bleached state and high contrast ratio, PEDOT layers with several thicknesses were prepared and studied. The PEDOT films were obtained by electropolymerisation during different reaction times (5 s for EP1, 10 s for EP2 and 20 s for EP3). The deposition voltage is set at 1.4 V vs. Ag/AgCl. Experiments were performed on highly conductive FTO-coated glass substrates ($R_\square = 13\ \Omega/\square$) in order to specifically study the PEDOT film and not the sum of both layers (TCO + PEDOT film).

III. 2. 5. 1. Coloured states – Bleached states

In-situ transmittance measurements depending on the applied potential were performed on these EP-1,2 and 3 films. The reference for the 100 % transmittance was taken as the glass spectroelectrochemical cell with the electrolyte and the FTO/glass plate inside. Therefore, the transmittance (T) given in Figure III.9 is that of the PEDOT film on its own.
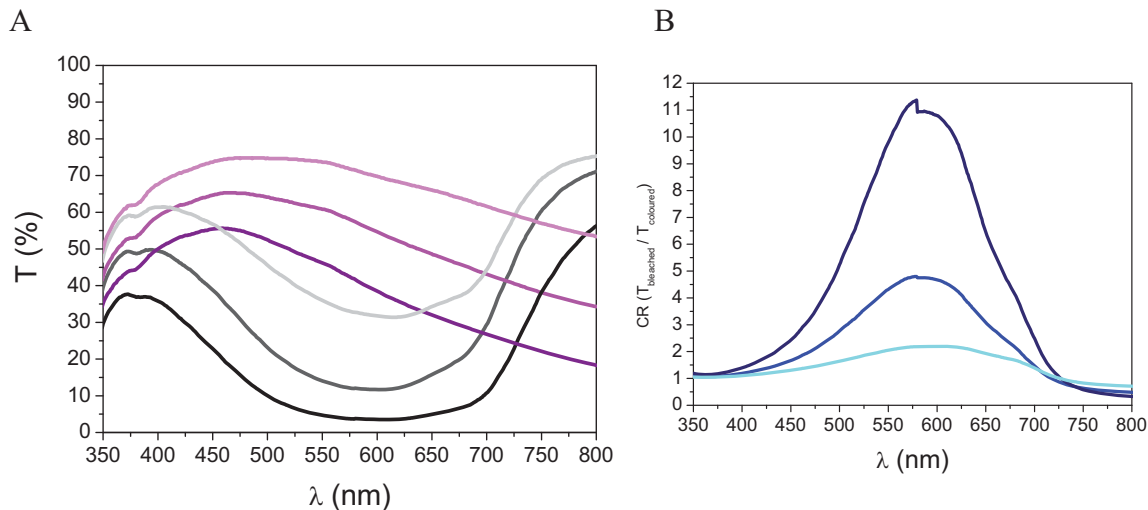
Figure III.9 : A) Transmittance spectra recorded for electropolymerised PEDOT films EP1 (light), EP2 (medium) and EP3 (dark). The pink lines correspond to the bleached state (once oxidised at 1.0 V/$_{Ag/AgCl}$) and the grey lines to the coloured states (once reduced at -1.0 V/$_{Ag/AgCl}$) in 0.03LiTFSI/0.97 BMITFSI (molar ratio) electrolyte. B) Contrast ratio for these films EP1 (light), EP2 (medium) and EP3 (dark)

No major changes in the position of the absorbance bands are observed with increasing film thickness, the only observations concern the level of the absorbance: as the deposition time increases, the colouration in the coloured state increases as well as the residual colouration in the bleached state. In particular, for EP3 (20 s. deposition), the as-

deposited film transmittance is only 40 % at 550 nm (cf. Figure III.9A). The contrast ratio, being very sensitive to high absorbance value, reaches a very high level for the thickest samples (cf. Figure III.9B). The thickness of these films could not be precisely determined, so that the spectroelectrochemical properties dependence will be given as a function of measured film capacities and not film thicknesses.

III. 2. 5. 2. Film capacities

The film capacities in oxidation and in reduction were measured for EP1, EP2 and EP3 films using cyclic voltammetry between -1.0V and +1.0 V vs. Ag/AgCl. The results of surface film capacity (Qs) as a function of the deposition time are given in Figure III.10.
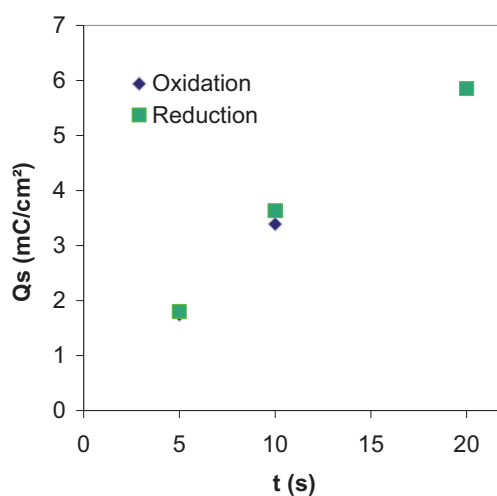
Figure III.10 : Evolution of the film capacities, measured at a constant low current density (15 µA/cm²) between -1.0 V and +1.0 V vs. Ag/AgCl, as a function of the film-deposition time "t" for films EP1 (5 s), EP2 (10 s) and EP3 (20 s)

Capacities up to 6 mC/cm² were obtained. Moreover, the electrochemical capacity of the films linearly increases with the deposition time, as could be reasonably expected. The tuning of the time of the electrochemically induced polymerization allows the preparation of films with a large range of capacities. Attention must be drawn to the fact that a variation of 1s in the deposition time gives rise to a large change in the film capacity (0.4 mC/cm² per second of deposition).

III. 2. 5. 3. Absorbance as a function of film capacity: Beer-Lambert law dependence

The PEDOT films are not reflective because of their polaronic p-type conduction which excludes reflectivity and induces absorption in the NIR. Therefore the absorbance, A,

can reasonably be expressed as A= log (1/T). The dependence of maximum absorbance with the film capacity is given in Figure III.11.
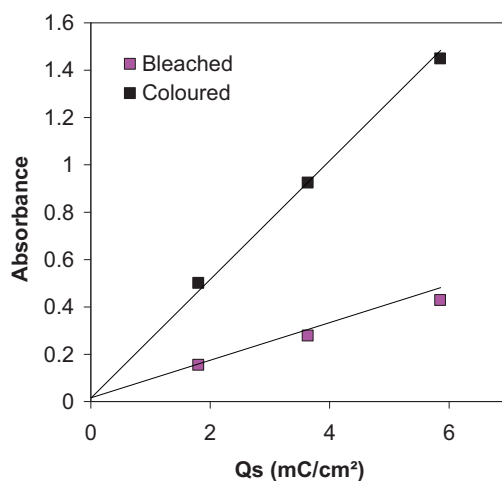
Figure III.11 : Evolution of the films maximum absorbance with the film capacity for the films EP1 (5 s), EP2 (10 s) and EP3 (20 s).

The absorbance due to the residual colouration as well as the coloured films are proportional to the film thickness and follows the Beer-Lambert law.

III. 2. 5. 4. Colouration efficiency

The colouration efficiencies (CE) are calculated using the formula CE= $\Delta A/Q_s$ with ΔA, the difference of absorbance between the bleached and coloured states and Q_s (mC/cm²) the corresponding film electrochemical capacity (cf. III. 2. 5. 2.). The variation of CE with the wavelength is given for each EP1, EP2, and EP3 film in Figure III.12.
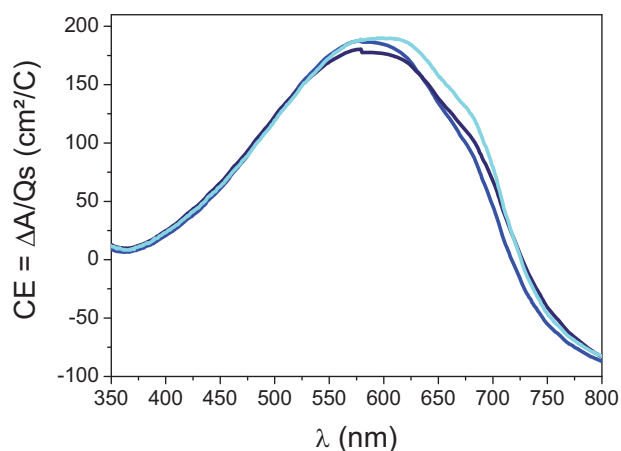
Figure III.12 : Variation of the colouration efficiency with λ as the film capacity increases from 1.8 mC/cm² (EP1, 5 s deposition) to 5.9 mC/cm² (EP3, 20 s deposition)

At the maximum absorbance wavelength (around 580 nm), the CE is about 175-200 cm²/C which is close to the published values (183 cm²/C [30]) As expected, the resulting colouration efficiencies plotted in Figure III.12 overlap with each other for all the electropolymerised films since the CE is an intrinsic parameter of the material.

III. 2. 5. 5. Switching times

The colouration (respectively bleaching) switching time has been measured by calculating the time necessary to get 90 % of the maximum colouration (respectively maximum bleaching) of the PEDOT film (Figure III.13). Measurements were performed at the maximum absorbance wavelength (610 nm). The bleaching potential was taken as +1.0V , whereas the colouring potentials were varied between -0.5 and -1.0 V.

The bleaching is very fast, at the maximum 1 s. is necessary to completely bleach the PEDOT film even for capacities up to 6 mC/cm². The colouration is longer (several seconds). It is indeed a general feature that the cationic polythiophene is easily obtained by p-doping whereas its reduction is more difficult.[6] The oxidation of the polymer corresponds to the formation of electrical cationic charges along the polymer chains; the overall electroneutrality is obtained by incorporating the same amount of anions. The incorporation of the anion upon oxidation of the polymer is easily obtained; on the contrary its extraction from the polymer structure is slow. However, the bleaching potential were rather high (+1V versus +0V to attain the bleached state cf Figure III.8) which could also explain this higher kinetics.
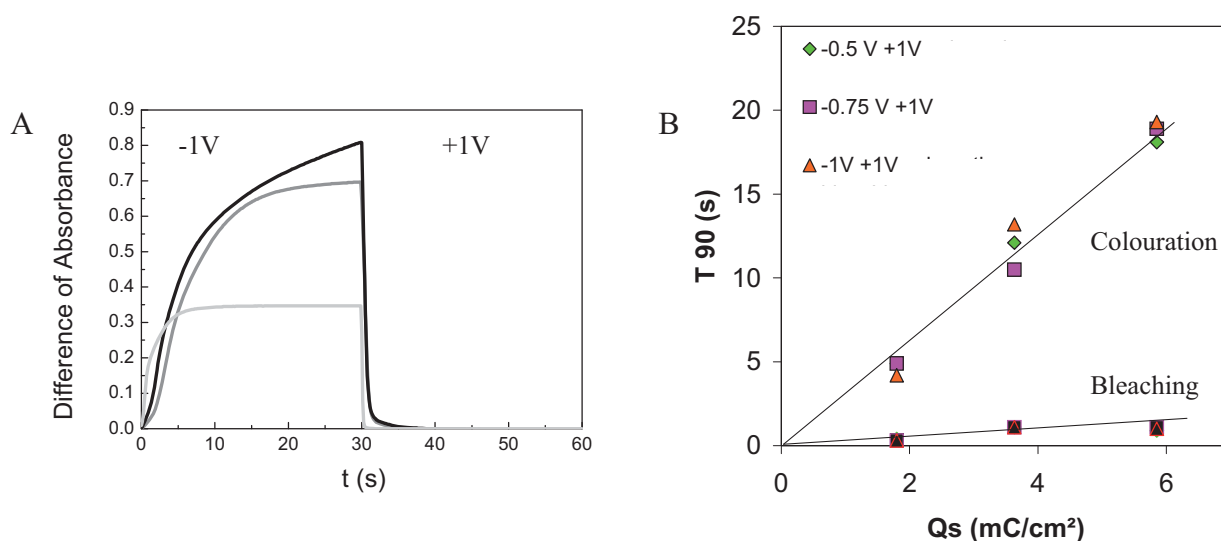
Figure III.13 : A. Difference of absorbance ΔA between the coloured and bleached states with time for -1.0V applied for colouration during the first 30s., followed by 30s at +1V, light : 1.8 mC/cm², medium : 3.6 mC/cm², dark : 5.9 mC/cm². B. Response time to obtain 90 % of colouration or bleaching (T90) as a function of the capacity of the films for different applied potentials in colouration (-0.5 V; -0.75 V and -1.0V), the bleaching potential remains 1.0V, at λ=610 nm.

The switching times are proportional to the film capacities in the studied range of potentials. The time (in seconds) to get 90 % of the colouration/bleaching is 3.1 * Qs (mC/cm²) for the colouration and to only 0.15 * Qs for the bleaching.

III. 2. 5. 6. Conclusion on PEDOT with different capacities

Electropolymerisation of PEDOT allows a fine control of the capacities of the deposited films by simple control of the used charge. Depending on the desired application, the film capacity can be tuned in order to find the best compromise between residual colouration in the bleached state and colouration of the coloured state. Figure III.9 and Figure III.11 give the desired information to make this choice. In our case, a CR around 5 is sufficient so that a deposition time between 5s and 10s is preferred. If higher contrast ratios are required, an increase in the deposition time can be used (CR=11 for 20 s deposition). For all the films, switching times of several seconds in colouration and nearly instantaneous bleaching are obtained, and colouration efficiency is around 200 cm²/C.

However, the film with the lowest capacity (1.8 mC/cm²) shows a transmittance in the bleached state that is still low for some applications (72 % whereas $T_{max} > 90$ % is needed for ophthalmic applications for example). In this case, efforts towards the modification of the EDOT structure are mandatory. Moreover, in the case of in-situ polymerisation, the preparation of very thin PEDOT layers was not possible since this led to inhomogeneous coatings, so that the use of modified EDOT structure is preferred.

III. 2. 6. Comparison of the different deposition routes for PEDOT films.

As stated above, PEDOT films have been prepared via several deposition methods (electropolymerisation, in-situ polymerisation, dispersion coating). Films deposited via these methods on FTO/glass are studied in a deaerated ionic liquid electrolyte, of composition 0.03 LiTFSI/ 0.97 BMITFSI (molar ratio). The PEDOT film is attached to the working electrode of a three-electrodes cell using Ag/AgCl as (pseudo) reference electrode and platinum wire as counter electrode.

III. 2. 6. 1. Level of colouration

The spectroelectrochemical properties of these films were studied using in-situ UV-Visible spectroscopy associated with chronoamperometry and are presented in Table III.2. In order to be able to accurately compare the films, deposits with similar optical properties (ΔA) are studied. However, this revealed to be highly time consuming to set-up the preparation of films with exactly the same properties so that slight deviation in ΔA are authorized: the studied materials namely EP2, D1 and ISP1 (as defined above) have a $\Delta A = 0.9 \pm 0.2$, at maximum colouration wavelength and a residual coloration in the bleached state ($\Delta A = 0.23 \pm 0.04$, Table III.2).

Sample	Deposition method	Capacity (mC/cm²)	ΔA at λ_{max}	A bleached at λ_{max}	Contrast ratio at λ_{max} (CR)
EP2	Electropolymerisation	3.6	0.70	0.26	4.7
ISP1	In-situ polymerisation	3.2	1.09	0.23	12.3
D1	Dispersion coating	7.5	0.97	0.19	9.3

Table III.2: Spectroelectrochemical properties of PEDOT films obtained via several deposition methods: film capacity, delta of absorbance at λ_{max} (wavelength of maximum absorbance), residual absorbance in the bleached state at λ_{max} , contrast ratio at λ_{max} ; for applied potentials -1V/+1V

Films capacities are in the same range of order for ISP and EP films. However, in the case of the dispersion coating higher capacities are needed to attain the same level of colouration. The shapes of cyclic voltammograms and volta-absorptometric curves were studied as detailed below to precise the differences between the three types of films.

III. 2. 6. 2. Cyclic voltammetry and volta-absorptometry

The cyclic voltammograms for each PEDOT are given on Figure III.14 as well as the volta-absorptometric curves (dA/dt = f(V)). Volta-absorptometry measurements consist in recording the evolution of the absorbance first derivative (dA/dt) as a function of the applied potential while a cyclic voltammetry sequence is applied. By comparing cyclic voltammetry and volta-absorptometry, information on the amount of charge that is effectively used for the modulation of the absorbance is obtained. This is also useful to detect side reactions occurring in the system and not linked to the colouration (e.g. electrolyte degradation, water decomposition…).[31]

A. EP2 (Electropolymerisation)
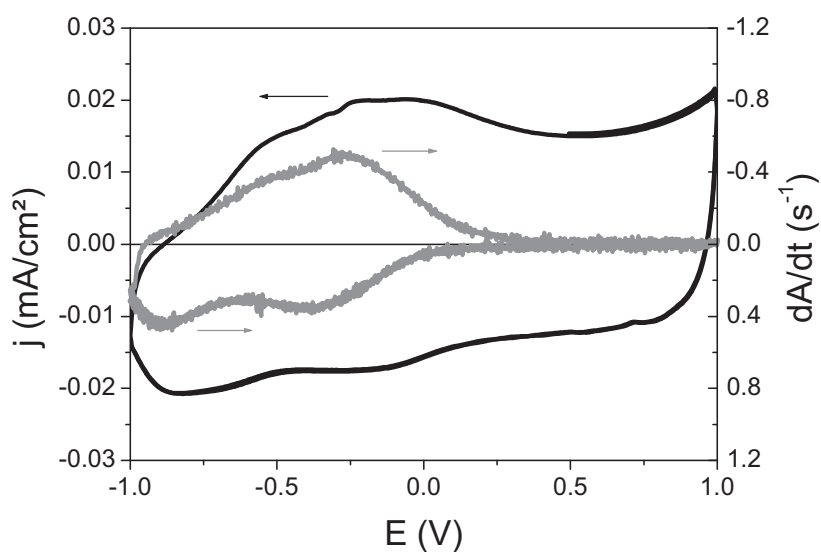
B. ISP1 (In-situ chemical polymerisation)
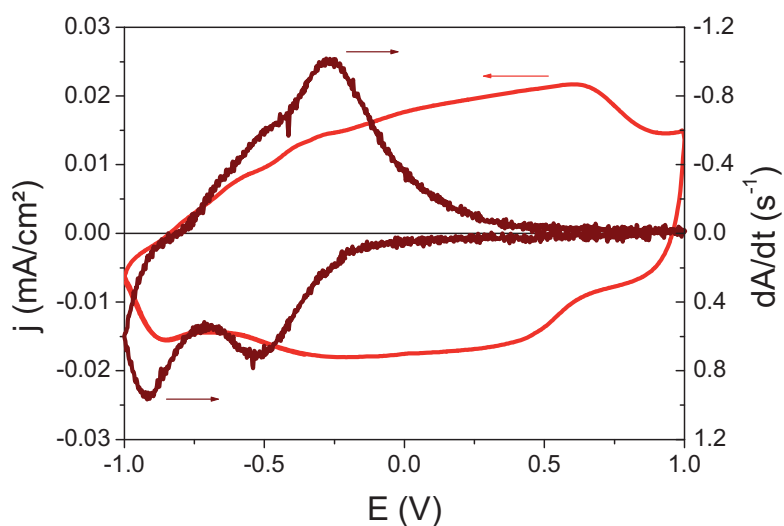
C. D1 (Dispersion coating)
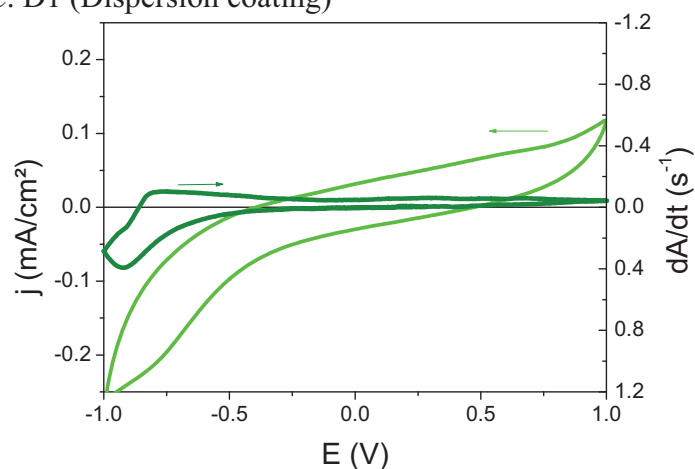
Figure III.14 : Cyclic voltammograms at 500 mV/min, and volta-absorptometry at λ max in 0.03/0.97 molar ratio LiTFSI/ BMITFSI, in a three-electrode cell configuration for electropolymerised PEDOT EP2 (A) in-situ polymerized PEDOT ISP1 (B) , and PEDOT Orgacon D1 (C)

Cyclic voltammogram and volta-absorptometric curves of electropolymerised (EP) and in-situ polymerised (ISP) films are rather similar. For D films, obtained by dispersion coating, the shapes of the cyclic voltammetry and volta-absorptometric curves are different with in particular a ΔA covering the whole studied potential range.

In the case of EP and ISP, the volta-absorptometric dA/dt curves show that the full bleaching is obtained as soon as + 250 mV is applied: application of potential higher than + 250 mV does not induce any additional change in absorbance. However, the observation of the cyclic voltammogram beyond 250mV shows that an oxidative current is measured: the related capacity (about 33% of the total capacity) is not useful for the optical contrast in the visible; above 250 mV, the optical contrast probably occurs in the infra-red region and is related to the decrease (increase) of the concentration of the p-type hole carriers (polarons, bipolarons) during the reduction (oxidation) of PEDOT.

These measurements allow determining which reduction and oxidation potentials would be most appropriate to minimize energy consumption while keeping the optimum optical contrast in the visible. For the electropolymerised film, it is -1.0V / + 0.25V /$_{Ag/AgCl}$; and -1.0V/ +0.5V /$_{Ag/AgCl}$ for the in-situ polymerised for films.

On the contrary, for D1 films (dispersion coating), the sample needs to be cycled over the whole -1.0V +1.0V range to change from its totally bleached state to its totally coloured one. Moreover, as presented in Table III.2, the D1 film capacity must be about twice as high as that of ISP and EP films to get the same colouration.

The values of dA/dt give also some information on the kinetics of the colouration and bleaching: if dA/dt is high the colouration will be fast. As observed on Figure III.14, ISP film benefits from the highest values of dA/dt, followed by EP sample and D sample, which is the slowest. To complete this study, the switching times in real operating conditions (application of potentials) will be presented.

III. 2. 6. 3. Switching times

The dynamic changes of absorbance upon oxidation and reduction were measured for colouring potentials of -1.0V, the bleaching potential being fixed at +1.0V. The switching times of the reactions could be extracted from these experiments by measuring the time for 90% (T90) of colouration or bleaching, they are plotted in Figure III.15.
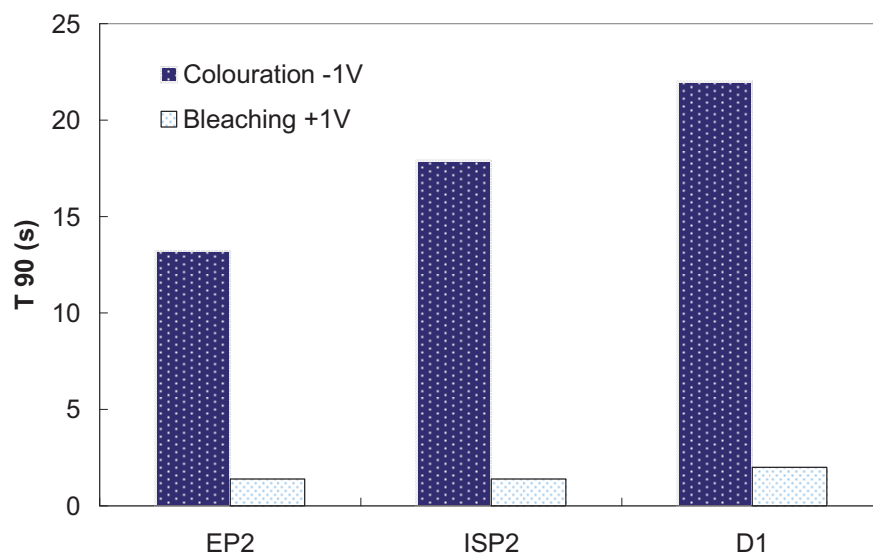
Figure III.15: Colouration and bleaching switching times for the different PEDOT EP, ISP and D for colouration and bleaching potential: -1.0V / +1.0V $_{vs.Ag/AgCl}$

For all the PEDOT layers, the colouration takes much more time than the bleaching (tens of seconds versus 1 to 2 seconds for bleaching). This is a general case for PEDOT films and was discussed in the part on the electropolymerised PEDOT. For the PEDOT-PSS dispersion film (D1), the colouration and bleaching times are longer than for EP and ISP films, illustrating the higher resistivity of the D1 film due to the presence of PSS, which is known as an insulating polymer.

III. 2. 6. 4. Colouration efficiency

The colouration efficiencies of the different PEDOTs are plotted in Figure III.16.
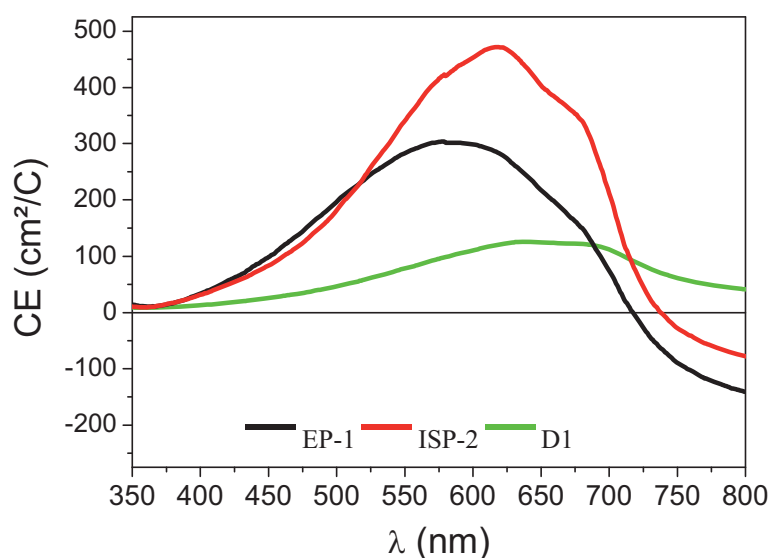
Figure III.16: Colouration efficiency of PEDOT films on FTO/glass

All the samples exhibit a strong blue colouration (wide absorbance around 600 nm). However the absorbance maximum is shifted from 580 nm for EP films to 610 nm for ISP films and 640 nm for the D1 film. Generally, the increase in interband π-π* transition energy is related to a decreases in the conjugation length in the PEDOT chains.[5] Our results suggest that the ordering within the D1 chains is higher (higher conjugation length, lower gap energy) than in ISP and EP films probably due to PSS⁻ anions. Moreover, a shoulder appears on all the samples at 680 nm, due to bipolarons formation as quoted above.

For the EP and ISP samples, in the 700-800 nm wavelength range, the CE is negative. This means that in this part of the spectrum, the coloured material acquires higher absorbance as compared to the bleached state. This appears in the NIR region due to the polaronic conduction.

The ISP film shows the highest colouration efficiencies (CE_{max} = 470 cm²/C), whereas the D sample has the lowest one (CE_{max} = 125 cm²/C), EP film has an intermediate value (CE_{max}= 290 cm²/C). High CE was the reason for the choice of PEDOT films as primary electrochromic materials, so that, as expected, these CE are very high. Another interesting point is that if we take into account the whole range of the visible spectra, the mean value of the CE is still very high due to the broadness of the absorption band.

III. 2. 6. 5. First colouring/bleaching cycles

The absorbance in the bleached and coloured states has been measured for the first cycles of colouration and bleaching of these three types of films. The colouring (-1.0 V) and bleaching (+1.0 V) potentials were applied for about 4 minutes. The absorbance obtained once stabilised has been called A_{stab}. For each cycle, the percentage of A_{stab} has been calculated and is plotted on Figure III.17.

ISP film gradually reaches its maximum absorbance, after 5 cycles its stabilized absorbance value is obtained. On the contrary the EP and D films attain very quickly their maximum colouration level and are totally stabilised after only 2-3 cycles. This observation was also made in cyclic voltammetry sequences for which the ISP films needed at least 20 cycles between -1.0 V and +1.0 V at 100 mV/s to reach their highest ΔA values. The ISP films are prepared via EDOT polymerisation in the presence of an oxidative agent (i.e. reducible agent), this agent is mostly removed by rinsing of the films. However, remaining traces of this product may explain this long formatting time (beyond 5 cycles).

For the bleaching state, the minimum value of the absorbance was obtained as soon as the first oxidative sequence was performed for all the samples.
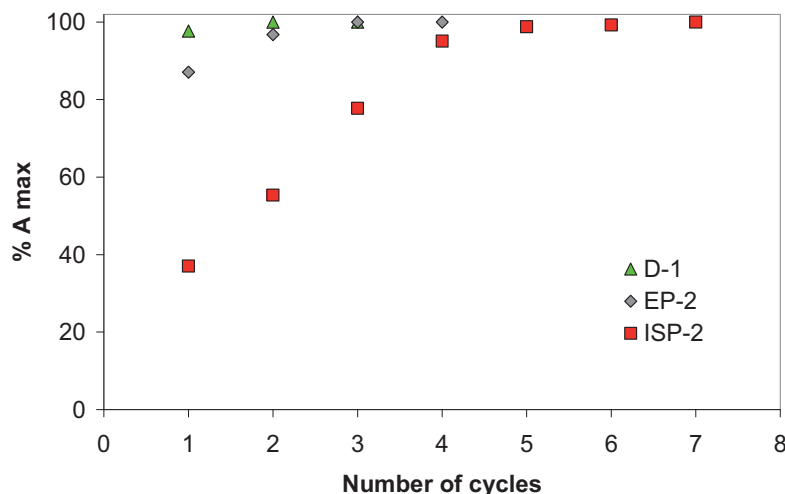
Figure III.17: Evolution of the absorbance with the colouration / bleaching cycles (-1.0 V / +1.0 V) in percent of the maximum absorbance reached at the end of this formatting step.

III. 2. 6. 6. Long term cycling

The long term cycling behaviour has been assessed directly in complete devices for question of time consumption and potentiostat availability (see chapter IV).

III. 2. 7. Improvement of the PEDOT films adhesion and homogeneity

III. 2. 7. 1. Context of the study

PEDOT adhesion on TCO substrate is generally poor. However, in the case of PEDOT-PSS dispersions, the additive that stabilizes the PEDOT particles leads to improved adhesion properties. On the contrary, for both in-situ chemical polymerisation and electropolymerisation, the adhesion remains much lower and delamination or scratches appear very easily.

Two different solutions have been tried to improve the films adhesion on the substrates:

- addition in the formulation of the deposition solution of additives that will promote adhesion of the PEDOT. This work was performed with the in-situ polymerized PEDOT by the ISC-Fraunhofer institute and will not be detailed here. Non confidential details can be found in A. Celik's thesis (by the Fraunhofer ISC).[32]

- prelayer coating before PEDOT electrodeposition: the prelayer will promote the adhesion of the PEDOT film on the substrate. Two pre-layers types have been studied at the ICMCB: very thin PEDOT-PSS dispersion prelayer and mesoporous TiO_2 layer.

III. 2. 7. 2. Procedures of prelayers deposition

III. 2. 7. 2. i. PEDOT-PSS prelayer

The deposition of a pre-layer of Baytron P on the substrate is said to improve PEDOT homogeneity and adhesion.[33] Baytron P dispersion from Bayer was diluted in ethanol (50 Baytron P/50 Ethanol) and coated on the desired substrate. The coating was made with the following sequence: 600 rpm 15 s., 1000 rpm 30s., and then 2000 rpm 2s..

III. 2. 7. 2. ii. Mesoporous TiO2 prelayer

The mesoporous TiO_2 prelayer will act as a host material in which the PEDOT will be electrodeposited protecting it from the peeling. The mesoporous TiO_2 layers have been prepared at CNRS/UPMC UMR 7574 by Eugenia Fernandez from Clément Sanchez's team. A solution containing the TiO_2 precursor, a templating agent, and solvent EtOH and H_2O in the molar proportions $1(1TiCl_4:5EtOH):40EtOH:10H_2O:0.005F127$.[34] The films were deposited by dip-coating, under controlled atmospheric conditions. They were then stored at 70% of humidity during 18h. Afterwards, annealing was performed in three steps: first a heating at 130°C for 24 hours, followed by 3 hours at 350°C and by a step at 500°C for 10 minutes. The TiO_2 maintains its cubic form after the heating step at 350°C, the quadratic structure (anatase) is, as expected, obtained upon a final step at 500°C for 10 minutes.

III. 2. 7. 3. PEDOT deposits on prelayers

The study is performed with electropolymerised PEDOT on FTO/glass 13Ω/□. For comparison, samples without prelayer and samples with prelayer but without PEDOT are also tested (Table III.3).

Sample	Prelayer	PEDOT electropolymerisation conditions
EP2	None	10s,1400 mV
EP2-TiO$_2$	TiO$_2$	10s,1400mV
FTO-TiO$_2$	TiO$_2$	None
EP3	None	20s,1400 mV
EP3-Baytron	Baytron P	20s,1400mV
FTO-Baytron	Baytron P	None

Table III.3: Deposition conditions of the PEDOT for the study of prelayers, the nature of the prelayer and the duration and applied potential for the electropolymerized PEDOT are given

III. 2. 7. 4. Mechanical properties

The addition of a prelayer of Baytron PEDOT-PSS or of TiO$_2$ has been found to improve the adhesion of the electrodeposited PEDOT on the conductive substrate (no quantitative measurement available). The following study aims at looking at the modification in the spectro-electrochemical properties of the films due to this additional layer.

III. 2. 7. 5. Level of colouration

Table III.4 gives the capacities, the difference of absorbance (ΔA) and the colouration efficiencies of the films.

Sample	Capacity (mA/cm²)	ΔA	CE red at λ_{max} (cm²/C)
EP2	3.63	0.68	187
EP2-TiO$_2$	3.79	0.57	156
TiO$_2$	0.65	0.01	0
EP3	5.85	1.03	176
EP3-Baytron	4.81	0.77	159
Baytron	0.05	0.00	0

Table III.4: Capacity, ΔA and colouration efficiency of the samples. Data collected by slow chronopotentiometry between -1.0 V and +1.0 V, in a three-electrode cell with PEDOT at the working electrode, a platinum wire at the counter electrode and a pseudo reference Ag/AgCl.

We can observe that, whereas the Baytron prelayer has nearly no electrochemical activity in the range -1.0V/+1.0V, the TiO$_2$ capacity is about 15% of that of PEDOT. However, none of them impart any additional colouration by itself (ΔA due to TiO$_2$ or Baytron alone is nearly zero). The EP$_2$-TiO$_2$ capacity comes from both TiO$_2$ and PEDOT. If we assume that the TiO$_2$ capacity remains the same as in the case of FTO-TiO$_2$, the capacity of PEDOT itself is only 3.1 mC/cm² (instead of 3.63 mC/cm² in the EP-2 film). Then, the presence of a prelayer of TiO$_2$ leads to a decrease in the amount of PEDOT deposited in the

substrate of about 15%, which is responsible for a decrease in ΔA of 0.11 and in colouration efficiency of 30 cm²/C. In the case of the PEDOT deposited on the Baytron prelayer, the capacity of PEDOT itself decreases a lot (- 22%), whereas the decrease of absorbance is even higher (-34%). The colouration efficiency decreases by 17 cm²/C (9%). To summarize, the presence of the TiO_2 and Baytron prelayers lower slightly the PEDOT colouration but increase the layer adhesion.

III. 2. 7. 6. Switching times

The time to get 90% of the colouration and bleaching, when reduction -1.0 V and oxidation +1.0 V potentials are used are summarized in Table III.5. The colouration time is increased in the case of the TiO_2 prelayer and decreased in the case of PEDOT prelayer. The bleaching is very fast (1 s.) for all the samples. This is in agreement with the fact that the oxidation of polythiophene is known to be easier than its reduction as already discussed above.

Substrate	T_{90} colouration (s)	T_{90} bleaching (s)
EP2	13	1.4
EP2-TiO2	16	1
EP3	19	1
EP3-Baytron	11	1

Table III.5: Switching times T 90, time for 90% of the colouration or bleaching, for the PEDOT films on FTO alone and on FTO + TiO2 or Baytron prelayers.

The switching times remain in the same range of order for all the samples. The presence of a TiO_2 layer leads to a slight increase in the colouration time, whereas the Baytron layer lowers it. For TiO_2 layers, the high surface of contact between the electrolyte and the EC and the semi-conductive character that will facilitate the electron injection in the PEDOT layer film would be in favour of a decrease in the switching time but this is not observed.

III. 2. 7. 7. Conclusion on prelayers

In both cases of TiO_2 and Baytron prelayer, the presence of a prelayer allows increasing the adhesion of the PEDOT on the substrate; however this also leads to a lowering of the colouration efficiencies and ΔA. But the spectroelectrochemical properties of the PEDOT on

prelayer films are still very compatible with the desired application. The switching times remain in the same range of order as for PEDOT films alone.

III. 2. 8. Conclusion on PEDOT

PEDOT layers can be prepared by three methods:

- The electropolymerisation for an easy control the quantity of deposited material; it is however difficult to obtain homogeneous deposits on large surface.

- The polymerization in-situ, which gives rather homogeneous films on large surface; low film thickness is difficult to reach.

- The deposit of PEDOT dispersion which are easy to obtain; but exhibit low reduction potential (problem of stability) and low coloration efficiency.

PEDOT coating on the conducting substrates is problematic in the case of the electropolymerisation and the in-situ deposit. It was improved by the modification of the formulation for the in-situ deposit (cf. Ayse Celik's thesis[32]) or by the deposit of a Baytron P layer or of mesoporous TiO_2 for electrodeposited films. The mode of deposit which provided the best results is polymerization in-situ:

- Deposit on large surface could be performed on large surfaces as opposed to electrodeposited PEDOT

- Working potentials entirely included within the potential range of the electrolyte as opposed to PEDOT-PSS.

- Greater colouration efficiencies than the PEDOT PSS.

Moreover, the chemical modification of EDOT (confidential) allowed a decrease of the residual colouration in the bleached state of the in-situ polymerized polymer.

The in-situ polymerisation method was thus used for the preparation of complete electrochromic systems with large size, as presented in the following chapter (chapter IV). The influence of the conductivity of the substrate will be also studied in this part, with 5*5 cm² samples. A preliminary study on the influence of the percentage of PMMA in the electrolytic membranes on the electrochromic properties of complete systems is also presented in this chapter (the PEDOT used at this time was a dispersion of PEDOT PSS).

III. 3. Counter electrode: Prussian Blue and its analogue

III. 3. 1. Strategy for the counter electrode: interest of PB and analogues.

The choice of the material for an efficient counter electrode must fulfil the following criteria:

- it must be an electroactive material with redox potential located in the electrochemical-stability window of the chosen system (electrolyte, transparent conductive electrodes).

- if electrochromic, the colouration must be anodic since PEDOTs are cathodically colouring.

- a high colourlessness state in the reduced state is required.

- its electrochemical capacity must be at least equal to that of PEDOT (1-3 mC/cm² for the PEDOT layers we use).

Prussian Blue (PB) and one of its analogues, indium hexacyanoferrate (InHCF) are well-known materials[35] and interesting candidates with regards to these criteria[36,37].

Campet *et al*[38] demonstrated the possibility to use Prussian Blue electrodes for electrochromic devices with lithium conducting ionic liquid based electrolytes. The electrochemical behaviours of PB and InHCF in such electrolytes will be further detailed in this work.

III. 3. 2. Brief history of PB and analogues

Prussian Blue compounds have been studied for a long time. Its first synthesis was performed in 1704 in Berlin by Diesbach and Dipple[39]. It was first used as a pigment due to the exceptional intensity and longevity of its colour (Figure III.18). It is extensively used for artistic and industrial applications: watercolour, oil paintings, printing inks, cyanotype photographic process and colorant for papers, plastics, leathers, textiles and cosmetics.

Figure III.18: Cyanotype (Prussian Blue pigment) made by Anna Atkins, a British scientist and photographer, in 1843.

Neff first reported in 1978 the electrochemistry of Prussian Blue films[36]. Various reviews[40,41,42] on PB and related analogues have shown that besides electrochromism, they also have applications in diversified fields such as electrocatalysis, electroanalysis, ion-exchange and ion-sensing[43,44,45,46]. Their photomagnetic properties are also widely studied[47].

III. 3. 3. Formula, structure and electrochromic aspect

Prussian blue is the most known representative of the family of the transition metal hexacyanoferrate compounds with general formula:

$$A_h M'_k [Fe(CN)_6]_l \cdot m \, H_2O$$

where h, k, l, m are stoichiometric numbers, A designates an alkaline metal or a transition metal cation, M' represents a transition metal cation.

These compounds are called Prussian Blue (PB) or 'iron hexacyanoferrate' for M'=Fe.

If M' is different from Fe, these 'metal (M') hexacyanoferrates' are called Prussian Blue analogues[41].

III. 3. 3. 1. Prussian Blue

The blue PB chromophore contains Fe^{3+} and $[Fe(CN)_6]^{4-}$ as established by the CN stretching frequency in the IR spectrum and confirmed using Mössbauer spectroscopy[48]. The distribution of oxidation states is then represented as Fe^{III}-Fe^{II}. The CN bridges allow a partial electron-delocalisation between the iron centres[49].

The chromophore $Fe^{3+}[Fe(CN)_6]^{4-}$ has a negative charge, so that in the solid a cation A must be incorporated to compensate the charge. The nature of the inserted cation A is highly preparation sensitive (conditions of deposition, nature of the deposition solution) and

will evolve upon electrochemical reduction-oxidation cycling depending on the composition of the electrolyte used.

Two extreme cases have been highlighted:

- A=Fe leading to "insoluble" PB (*i*-PB) which is $Fe^{3+}[Fe^{3+}[Fe^{II}(CN)_6]^{4-}]_3$

- A=K leading to "soluble" PB (*s*-PB): $K^+Fe^{3+}[Fe^{II}(CN)_6]^{4-}$

In fact, all the PB forms are insoluble in water, the designation as "soluble" is only due to its easy dispersion, as colloidal particles, in water.

III. 3. 3. 1. i. Prussian Blue structure

The first attempts to determine the chemical formula, oxidation states of the metals and solid state structures for PB type compounds took place in the 1930s with Keggin and Miles, who proposed a face-centred cubic structure with interstitial cations (cf. Figure III.19*(a)*); the latter was deduced from X-ray diffraction patterns of powders[50]. The absolute assignment of the electronic configuration of the different Fe environments was performed in the late 1960s from Mössbauer and magnetic studies that showed that PB contains high spin ferric (Fe^{III}) and low spin ferrous (Fe^{II}) centres[51].

In 1970, Ludi proposed modifications of Keggin's model with the introduction in the structure of defects occupied by H_2O molecules[52]. It is now recognised that PB is the mixed-valence iron(III) hexacyanoferrate (II) compound $Fe_4[Fe(CN)_6]_3 . x H_2O$ (*x*=14-16).

The first single-crystal X-ray diffraction pattern for *i*-PB was reported in 1972 by Buser and Ludi.[53] It crystallized in the $Fe_4[Fe(CN)_6]_3.14 H_2O$ form. For this crystal, it was found that all the strong reflections belonged to the cubic face-centred space group *Fm3m*. However, a deviation from the cubic Fm3m to a *Pm3m* symmetry has been found and shown to depend on the preparation conditions of PB, the distribution of the defects (Fe^{II} vacancies occupied by H_2O molecules) being in a more ordered arrangement for slowly grown crystals. In this latter case one quarter of the Fe^{III} are coordinated by six N-bound CN ligands; the remaining Fe^{III} are coordinated by four N-bound CN and two water molecules and each Fe^{II} is coordinated by six C-bound CN ligands.
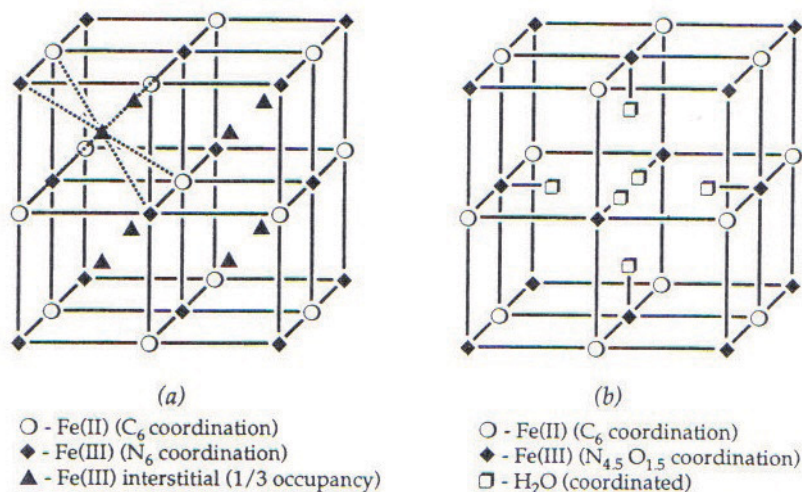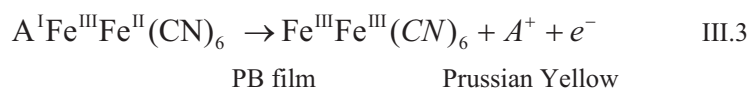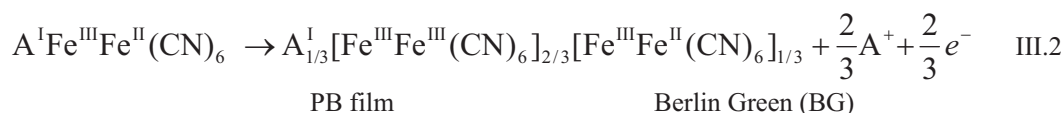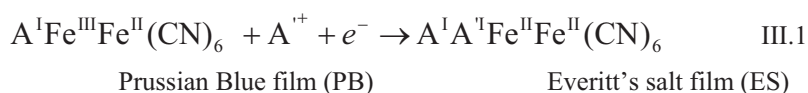
Figure III.19: Schematics representation of the unit cells of Prussian Blue as described by *(a)* Keggin and Miles model and *(b)* Ludi model. Reprinted from ref 35.

Instead of Fe^{3+}, other counter cations can be inserted in the BP structure for $Fe^{3+}[Fe(CN)_6)]^{4-}$ charge compensation : for example Na^+, K^+, Rb^+ or Cs^{+}[54].

III. 3. 3. 1. ii. Electrochromic aspects in Prussian Blue

The Fe^{II}/Fe^{III} Prussian Blue mixed-valence films, when electrochemically reduced (respectively oxidised) give rise to the formation of Fe^{II}/Fe^{II} compound (Everitt's salt) (respectively of Fe^{III}/Fe^{III} (Prussian Yellow)) completely colourless (respectively yellowish) transparent systems following equations III.1 and III.3. An intermediate species is obtained in oxidation, the Berlin Green (III.2) when only part of the A cation is expelled from the structure.

$$A^I Fe^{III} Fe^{II}(CN)_6 + A'^+ + e^- \rightarrow A^I A'^I Fe^{II} Fe^{II}(CN)_6 \qquad \text{III.1}$$

Prussian Blue film (PB) $\qquad\qquad$ Everitt's salt film (ES)

$$A^I Fe^{III} Fe^{II}(CN)_6 \rightarrow A^I_{1/3}[Fe^{III}Fe^{III}(CN)_6]_{2/3}[Fe^{III}Fe^{II}(CN)_6]_{1/3} + \frac{2}{3}A^+ + \frac{2}{3}e^- \qquad \text{III.2}$$

PB film $\qquad\qquad$ Berlin Green (BG)

$$A^I Fe^{III} Fe^{II}(CN)_6 \rightarrow Fe^{III}Fe^{III}(CN)_6 + A^+ + e^- \qquad \text{III.3}$$

PB film $\qquad$ Prussian Yellow

In equation III.1, the charge compensation is performed by insertion of cationic species A'^+; the latter arises from the electrolyte. In fact, exchange between A (initially present in the structure) and A' (present in the electrolyte) occurs during cycling. We observe that, depending on their nature, the cations A and A' can or cannot be reversibly extracted from the structure leading to a reversible or irreversible effect of colouration/bleaching. For example in the exclusive presence of BMI^+ (BMITFSI electrolyte without any salt), BP reduction takes place, showing that BMI^+ is inserted in the BP structure and the film becomes fully bleached. However, its reoxidation is not possible, suggesting that BMI^+ cannot get out of the structure. Consequently, the use of Prussian Blue in BMI^+ based ionic liquid is conditioned to the addition of a salt with smaller cation than BMI^+; we have selected the electrolyte BMITFSI 0.97 / LiTFSI 0.03 (molar ratio) (see chapter II).

III. 3. 3. 2. InHCF

III. 3. 3. 2. i. InHCF structure

Due to the high colouration efficiency of PEDOT and in order to avoid the systematic accommodation of capacities of the two electrochromic layers we aimed at preparing InHCF films because this PB derivative, white in its reduced state and pale yellow in the oxidised one, gives nearly colourless films in either case[37].

The structure of InHCF remains comparable to that of Prussian Blue with indium (III) occupying the Fe^{III} positions[35].

III. 3. 3. 2. ii. Electrochromic aspects in InHCF

The reduction of the transparent $In^{III}Fe^{III}(CN)_6$ gives a slightly yellow coloured $A^IIn^{III}Fe^{II}(CN)_6$ compound with A being a cationic species inserted in the structure to ensure the charge compensation. Further reduction would imply reduction of In^{III} into In^{II}. However, In^{III} has a much lower electron-affinity than Fe^{III}; therefore, the reduction of In^{III} into In^{II} is not possible within the accessible voltage range. Therefore, the following reaction is the only one accessible for InHCF films:

$$In^{III}Fe^{III}(CN)_6 + A^+ + e^- \rightarrow A^IIn^{III}Fe^{II}(CN)_6 \quad \text{(III.4)}$$
$$\text{InHCF} \qquad\qquad\qquad \text{reduced InHCF}$$
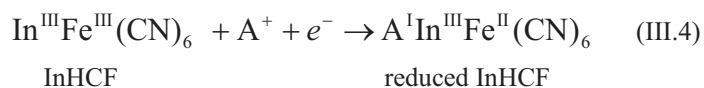
III. 3. 4. PB and InHCF as-deposited films

Among the various methods used to deposit Prussian Blue films[55], the most efficient one, developed by Neff, is the electrodeposition by chronopotentiometry, also called galvanostatic deposition[36,56]. For InHCF, electrodeposition using cyclic voltammetry was preferred to obtain thick enough films[37]. The deposition parameters and the properties of the films will first be given. The electrochemical study will follow in paragraph III.5.

III. 3. 4. 1. PB films

III. 3. 4. 1. i. Electrodeposition of PB

The deposition occurs via the electroreduction of a solution containing iron (Fe^{3+}) and hexacyanoferrate ($[Fe^{III}(CN)_6]^{3-}$) ions in water. Feldman and al. have shown that these two species in solution are in equilibrium with a brown-yellow soluble complex[57] containing Fe^{3+} and $[Fe^{III}(CN)_6]^{3-}$ according to:

$$Fe^{3+} + [Fe^{III}(CN)_6]^{3-} \; \underset{\leftarrow}{\rightarrow} \quad [Fe^{III}Fe^{III}(CN)_6]^0 \quad (III.5)$$

The main electron transfer process during PB electrodeposition is the reduction of this complex to give Prussian Blue.

$$3[Fe^{III}Fe^{III}(CN)_6]^0 + Fe^{3+} + x\,H_2O + e^- \rightarrow Fe_4^{III}[Fe^{II}(CN)_6]_3 \,.\, x\,H_2O \quad (III.6)$$
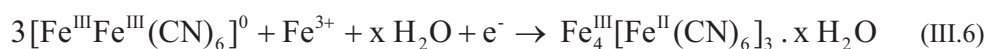
Chronoabsorptometric studies have shown the absence of parasitic reactions since the absorbance of the growing PB film is proportional to the consumed charge[58]. Quartz microbalance studies have been widely used to determine the nature of the inserted cation and the amount of water included in the PB network during deposition[59].

The films can be stored indefinitely. Their level of hydration is variable and depends on ambient humidity[60].

III. 3. 4. 1. ii. Experimental procedure

An equimolar solution of 10^{-2} mol/L of $FeCl_3$ and $K_3Fe(CN)_6$ is prepared with Nanopure deaerated water. Prussian Blue with capacities from 1 mC/cm² to 12 mC/cm² were successfully deposited not only on small (1*2cm²) but also on large substrates (15*15cm²). The substrates are cleaned before use (15 minutes in first ethanol and then water in an

ultrasound bath).The main substrates used were FTO/glass, flexible ITO/PET (Bekaert) and ITO/ophthalmic lenses (Essilor), they are listed in Table III.6, and their sheet resistances reported.

TCO	Substrate	Sheet resistance ($\Omega/\square$)	Supplier
FTO	Glass	13	Solems (F)
ITO	Glass	58	Solems (F)
ITO	PET	45-80	Bekaert (B)
ITO	Ophthalmic lenses	60	Solems-Essilor (F)

Table III.6 : Sheet resistance of the main TCO-substrates used in the study

For some substrates, the experimental conditions have to be adapted in order to prevent damage of the ITO coatings. For example, the heating of the electrodeposited film has to be limited to 60 °C for ITO on ophthalmic lens (see below) in order to avoid cracks of the ITO; less acidic solutions were used for certain ITO-based substrates in order to avoid ITO solubilisation.

The electrodeposition is performed in a three-electrode cell configuration. The conductive substrates, for PB electrodeposition, is placed at the working electrode, the reference is a saturated calomel electrode, and the counter electrode is a highly conducting FTO-glass substrate whose area is larger than that of the substrate. As quoted above, we selected the galvanostatic deposition: a current density ranging between 10 to 40 µA.cm² is applied (see below); the deposition time is calculated in order to get the desired capacity. Once the deposition is performed, the films are carefully rinsed with water and dried with compressed air. The complete dehydration for Prussian Blue films occurs at 150°C [35(p346)]. This temperature is too high for plastic substrates. We therefore chose to perform an identical treatment for all the substrates whatever their nature (glass or plastic substrates as listed inTable III.6): 60°C under primary vacuum for 2h. The samples were then stored in Argon atmosphere of a glove box. Remaining water if any did not disturb the films response as compared to literature data.

Figure III.20 : Prussian Blue films electrodeposited on FTO/glass ($R_{\Omega/\square}$ = 13) with capacities of 3, 6 and 12 mC/cm²

III. 3. 4. 1. iii. PB film thicknesses and surface morphology

The capacity of PEDOT films used for complete devices being around 3 mC/cm², we will now focus our study on PB with this compulsory capacity. These Prussian Blue films have been prepared by applying a current density of tens of µA/cm² during the time necessary to get a capacity of 3 mC/cm² (i.e. 300 s for 10 µA/cm² and 75 s for 40 µA/cm²).

Thickness of the BP films corresponding to 3 mC/cm², deposited on FTO/glass substrates, was measured using SEM (~235 nm) and optical profilometer (~200 nm) (Table III.7). The values deduced from SEM are slightly exaggerated as compared to those deduced from optical profilometer-measurements, probably due to the none fully perpendicular cut of the edges of the Prussian Blue before measurement using SEM.

Current density (µA/cm²)	Time (s)	Expected Capacity (mC/cm²)	Thickness (nm) SEM	Thickness (nm) Optical profilometer
-10	300	3	240	210
-40	75	3	230	190

Table III.7 : Thickness measured using SEM and optical profilometer of Prussian Blue with expected capacity of 3 mC/cm² at different deposition rates (deposition during 300s. and in 75 s. respectively).

In order to evaluate the morphology of the PB films, SEM analysis were made (Table III.8). The samples are crack-free. Grains with diameter around 300 nm for lower deposition current (-10 µA/cm²) and 150 nm for the high deposition current (-40 µA/cm²) are visible. These differences in surface morphology come from the mechanism of nucleation-growth of the PB. In the latter case (fast deposition), the nucleation of PB particles is favoured because

of the higher current density, leading to smaller particles, whereas in the former case, the particles growth is favoured. The size of these particles is in the range of the visible light wavelengths so that diffusion appears. However, when included in complete EC devices, the presence of a liquid (with refractive index closer to that of Prussian Blue than air) on the PB surface highly reduces the diffusion.
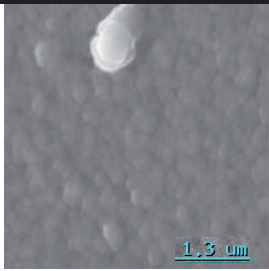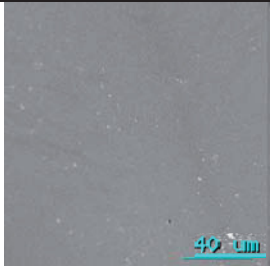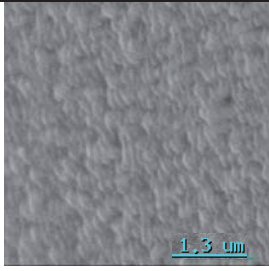
Current density; time	Capacity	SEM images	
-10 µA/cm^2 ; 300 s.	3 mC/cm^2	40 µm	1.3 µm
-40 µA/cm^2 ; 75 s.	3 mC/cm^2	40 µm	1.3 µm

Table III.8 : SEM images of the surface of Prussian Blue films, deposited on FTO/glass substrates with capacity of 3 mC/cm², for different deposition rates (deposition in 300s. and 75 s. respectively)

Higher rate deposition is preferred to obtain lower grain size, but the films with lower deposition rate are less rough. However, the electrochemical and spectro-electrochemical properties of these different films were similar. So that, in the following, the deposition rate is chosen in between these two extreme values (10 to 40 µA/cm²), a value of 20 µA/cm² is generally taken.

III. 3. 4. 1. iv. Influence of the substrate

For the same deposition conditions, the UV-Visible spectra of the PB films deposited on ITO/PET, ITO/glass and FTO/glass are identical, showing that the substrate nature and sheet resistance are not critical. This could be reasonably expected since the depositions occurred at constant current density, so that the same amount of charge is given in all cases.

III. 3. 4. 2. InHCF films

III. 3. 4. 2. i. Electrodeposition of InHCF

Indium hexacyanoferrate films are generally prepared by potential cycling[61,62] in a solution containing $InCl_3$ and $K_3Fe(CN)_6$ since the synthesis via static current has been found to be inefficient. The electrodeposition takes place during the negative scans as In^{3+} interacts with the $[Fe(CN)_6]^{4-}$ species, produced by reduction of the $[Fe(CN)_6]^{3-}$ species; this aspect will be depicted below.

III. 3. 4. 2. ii. Experimental procedure

Solutions of 10^{-2} mol/L $InCl_3$, 10^{-2} mol/L $K_3Fe(CN)_6$ and 1 mol/L KCl are prepared by separately dissolving the salts in deaerated nanopure water. The solutions are mixed just before electrodeposition. The substrates are cleaned before use (first 15 minutes in ethanol in an ultrasound bath, then 15 minutes in water in an ultrasound bath). The substrates used are listed in Table III.9. To study the influence of the substrate sheet resistance on the amount of InHCF material deposited, ITO with sheet resistance from 24 $\Omega/\square$ to 124 $\Omega/\square$ were also considered.

TCO	Substrate	Sheet resistance ($\Omega/\square$)	Supplier
FTO	Glass	13	Solems (F)
ITO	Glass	24, 39, 58, 124	Solems (F)
ITO	PET	45-80	Bekaert (B)
ITO	Ophthalmic lenses	60	Solems-Essilor (F)

Table III.9 : TCO-substrates used in the InHCF study

The substrate is placed at the working electrode of the above quoted three electrode cell. Cyclic voltammetry between 0.2 to 1.3 V/SCE at 100 mV/s, is applied for a given number of cycles starting from the equilibrium potential of the solution (0.18 V/SCE), with a first scan towards oxidation. Once the deposition is performed, the films are rinsed with water and dried with compressed air.

III. 3. 4. 2. iii. Evolution of the cyclic voltammograms during deposition

For InHCF, the electrodeposition was performed via repeated cyclic voltammetry (Figure III.21). The $[Fe^{III}(CN)_6]^{3-}$ species present in the electrodeposition solution are reduced at the working electrode during the negative scan, a negative current peak at 0.7 V/SCE is observed. The formed species $[Fe^{II}(CN)_6]^{4-}$ reacts with the In^{3+} in solution to give a solid film of InHCF in its reduced form: $In^{III}Fe^{II}(CN)_6$. The film is then oxidized during the positive scan so as to form $In^{III}Fe^{III}(CN)_6$ that will be further reduced during the following negative scan. Additional $[Fe^{III}(CN)_6]^{3-}$ species in solution will also be reduced leading to the subsequent growth of the InHCF film[63].
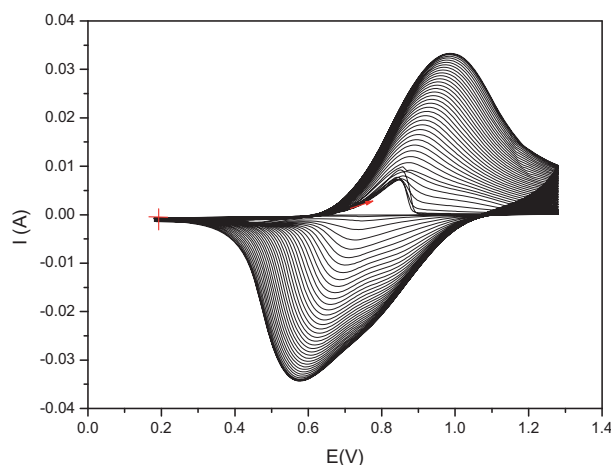

Figure III.21: Electrodeposition of InHCF on FTO/glass by cyclic voltammetry at 100 mV/s between 0.2V and 1.3 V/SCE, counter electrode FTO/glass, 50 cycles, 4*5 cm².

The first oxidative scan shows a sharp wave at 0.8 V/SCE i.e. 1.1 V/ENH probably due to Fe^{II} impurities contained in the Fe^{III} starting material salt. This peak was observed with all the substrates. The oxidation peak progressively shifts towards a higher potential because of the InHCF film formation and its less conductive character causing a potential drop. As expected, this phenomenon is also observed in reduction (negative current, Ep = 0.6 V/SCE). A careful examination of the curve shows that the reduction wave is not the single one; the shape of the curve reveals the presence of a second electrochemical reaction occurring around 0.8 V/SCE. As already mentioned, the most intense wave corresponds to the reduction of $[Fe^{III}(CN)_6]^{3-}$ in solution to give $[Fe^{II}(CN)_6]^{4-}$, that reacts with In^{3+} giving the film $In^{III}[Fe^{II}(CN)_6]$. During the positive scan $In^{III}[Fe^{II}(CN)_6]$ is oxidized into $In^{III}[Fe^{III}(CN)_6]$. The reverse negative scan shows the reductions of both the Fe^{III} ions present in the soluble $[Fe^{III}(CN)_6]^{3-}$ species and in the $In^{III}[Fe^{III}(CN)_6]$ film, leading to the observed curve in the cathodic region (Figure III.21).

III. 3. 4. 2. iv. Influence of the substrate

Strong differences in the deposited films capacities (measured by the area of the last oxidative scan of deposition) are observed depending on the substrate used as shown on Figure III.22. The highest electrochemical capacities are obtained when deposition is performed on FTO/glass, whereas capacities are 4 to 6 times lower for deposition on ITO/PET and on ITO/glass.
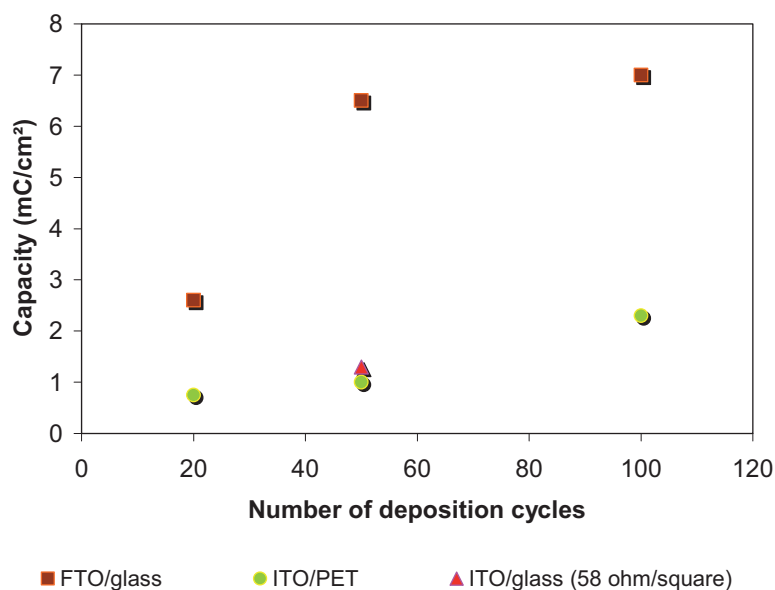

Figure III.22 : Variation of the film capacity (measured by the area of the last oxidative scan during the deposition process) for FTO/glass, ITO/PET and ITO/glass substrates with the number of deposition cycles at 100 mV/s. The counter-electrode is an FTO/glass plate, the reference is a saturated calomel electrode (SCE).

At first, as the sheet resistance of FTO (13 $\Omega/\square$) is much lower than that of ITO/PET and ITO/glass (45-80 and 58 $\Omega/\square$ respectively), an effect of the substrate sheet resistance could reasonably be considered. Indeed, the potential drop in the TCO film would diminish the potential 'seen' by the solution and, therefore, lower the deposited amount. However, we will show in the next paragraph that it is in fact the transparent conductive layer nature which is determinant.

III. 3. 4. 2. v. Influence of the substrate sheet resistance

In order to check the impact of the sheet resistance on the electrochemical deposition of InHCF, the above quoted deposition conditions were performed (50 cycles) on various

ITO/glass substrates exhibiting different sheet resistances from 24 to 124 $\Omega/\square$ (provided by SOLEMS company). The same study could not be performed on ITO/PET substrates because PET with sheet resistance lower than 40 $\Omega/\square$ results in fragile ITO deposits (due to their too high thickness, larger than 300 nm), and the presence of cracks which may influence the results. Figure III.23 shows the cyclic voltammetry of the obtained InHCF films as well as the variation of their capacity with sheet resistance.
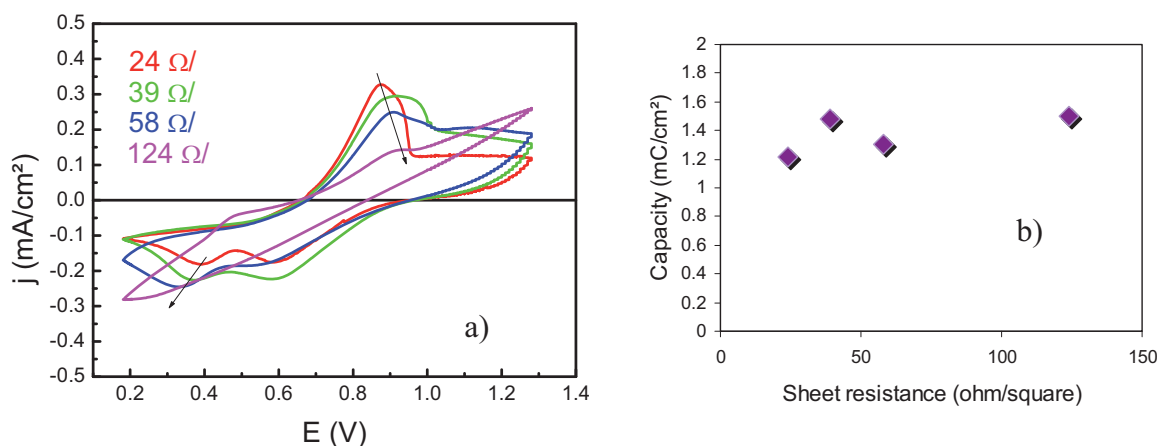

Figure III.23: Electrodeposition of InHCF on ITO substrates on glass with different sheet resistances (24 to 124$\Omega/\square$). a) Last electrodeposition voltammetric cycle (50th); b) capacities measured from the area of the cyclic voltammogram on the last deposition cycle.

Some changes appear in the cyclic voltammogram. Two reduction waves are observed for substrates with sheet resistance from 24 to 58 $\Omega/\square$ (as encountered for deposition on FTO) but they are more separated. For higher sheet resistance (124 $\Omega/\square$), a broad wave is observed. Moreover, the oxidation peak shifts towards higher potentials as the sheet resistance increases which is related to the increase in potential drop within the TCO layer, as quoted above.

However, the capacities are not strongly affected and remain constant, in the range of 1 to 1.5 mC/cm². Therefore, unexpectedly, the influence of the substrate sheet resistance cannot explain the large differences in capacities observed between FTO/glass and ITO/PET and glass (Fig. III.5). The influence of the substrate surface roughness of the TCO should then be taken into account: FTO prepared via chemical vapour deposition (CVD) being much rougher than ITO films exclusively prepared via sputtering as observed on AFM images.[64] Consequently, InHCF is more easily attached on FTO and is then not released in solution.

III. 3. 4. 2. vi. InHCF films optical properties; influence of thickness and surface morphology

The transmission spectra for deposition of InHCF with two deposition conditions are presented in Figure III.24.

UV-Visible spectra for InHCF films deposited with 50 deposition cycles on ITO/PET show an unrealistic transmittance higher than 100% even after baseline and reflection corrections. In fact, this reveals that the deposition of InHCF on the ITO film makes it even smoother, InHCF filling the cavities of the surface of the ITO film (ITO on PET is rougher than ITO on glass due to lower thermal treatment). This lowers the light diffusion of the surface. As the number of deposition cycles increases from 50 cycles to 100, the transmittance slightly decreases but remains very acceptable. The same phenomenon is obviously observed on FTO/glass (FTO having a rougher surface than ITO/glass, as shown above). Samples deposited on ITO/PET present a transparent aspect up to 100 deposition cycles, and up to 150 cycles on FTO/glass.
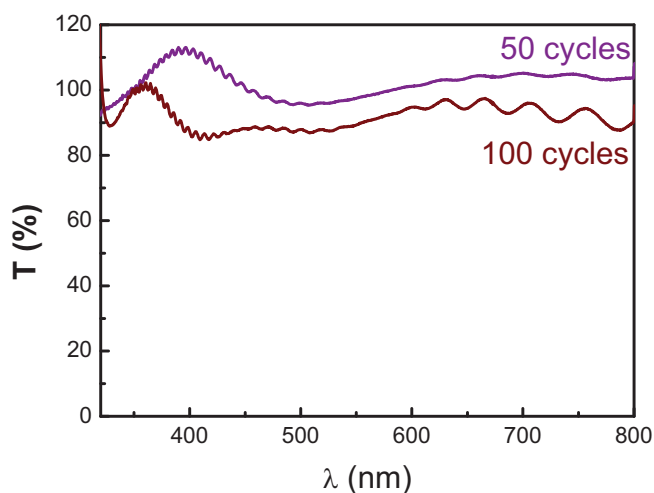
Figure III.24: Transmittance of as-deposited InHCF thin films on ITO/PET depending on the number of deposition cycles (50 and 100 cycles).

However for higher number of deposition-cycles, the sample becomes hazy. This diffusion is related to the surface roughness of the InHCF film that increases with the number of cycles. It is not a volume phenomenon since in such a case films with higher capacity (i.e. higher thickness) would be more hazy than films with lower capacity and we observe, that depending on the substrate, films with capacity of 6.5 mC/cm² (deposition on FTO/glass, 150 cycles) appear less hazy than those at 2 mC/cm² (ITO/PET, 100 cycles). SEM images were made on a transparent film corresponding to 150 cycles on FTO/glass, and show a slightly rough surface (Figure III.25).
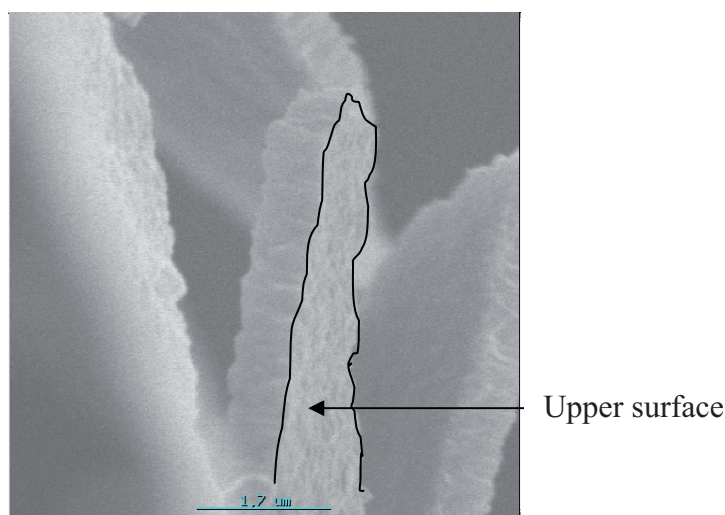
Figure III.25 : SEM images of the surface of InHCF films deposited by cyclic voltammetry for 150 cycles on FTO/glass, cracks on the InHCF films have been intentionally made to observe the surface and the side of the film, 6.5 mC/cm².

The thickness of the InHCF layer was evaluated at approximately 650 nm with this SEM picture. Mechanical and optical profilometers were unsuccessful due to the soft and transparent nature of the InHCF layer.

III. 3. 5. Electrochemical and electrochromic properties

III. 3. 5. 1. Prussian Blue

After having described the preparation of the films and some of their physical properties, we will now present their electrochemical and electrochromic behaviour in ionic liquid based electrolytes. As explained before, we will now focus on Prussian Blue films with capacity around 3 mC/cm² i.e. the maximum necessary for the complete devices with PEDOT primary electrochromic material.

III. 3. 5. 1. i. Absorbance spectra

The variation of the absorbance in the visible range (350-800 nm) has been measured for Prussian Blue films at different applied potentials in LiTFSI 0.03 / BMITFSI 0.97 electrolytes. Figure III.26a presents the visible spectrum of the as obtained 3 mC/cm² film on FTO/glass at 0.5V potential (curve a) as well as those recorded (spectra b to h) during reduction from 0.5 V to -1V/Ag/AgCl.

The large $Fe^{II}Fe^{III}$ intervalence band with a maximum absorbance at 715 nm, progressively decreases with consumption of Fe^{III}. Figure III.26B illustrates the same behaviour upon oxidation with potentials from 0.5V to 1.3V.
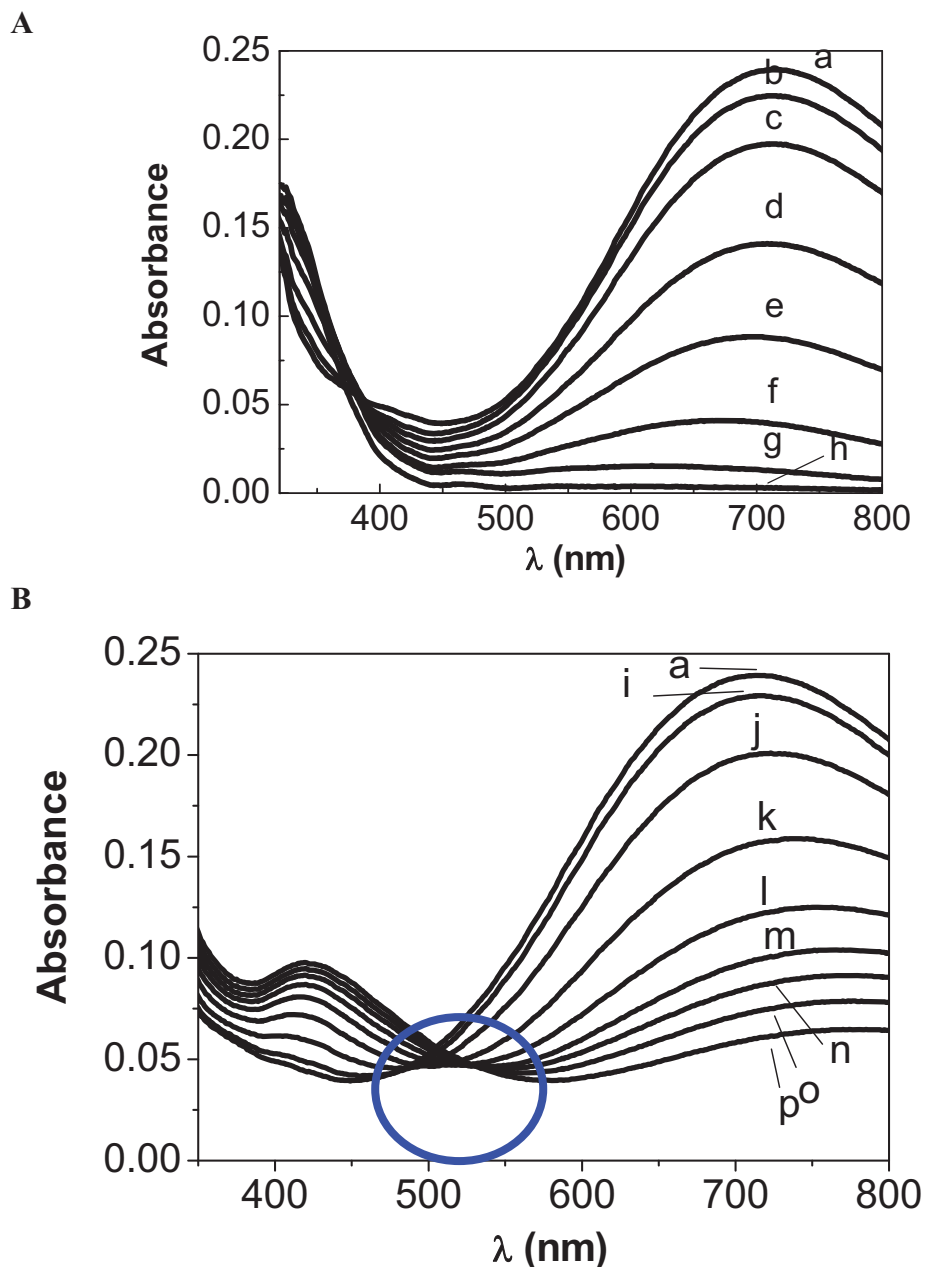

Figure III.26: Absorbance of a Prussian Blue film at 3 mC/cm² on FTO/glass for different applied potential, ref Ag/AgCl, CE=Pt wire. A: Reduction of Prussian Blue: a)0.5V, b) 0.3V, c)0.2V, d) 0.1V, e) 0V, f) -0.1V, g) -0.2V, h) -1 V; B: Oxidation of Prussian Blue: a) 0.5V, i) 0.6V, j) 0.7V, k) 0.8V, l) 0.9V, m) 1V, n) 1.1V, o) 1.2V, p) 1.3V.

As seen on Figure III.26 A, the reduction of PB is completed at -1.0 V and the reduction product, $Fe^{II}Fe^{II}$ or Prussian White is completely colourless and transparent (curve h). An isosbestic point is observed, which is the characteristic of a change of absorbance with

only two species, Prussian Blue and Prussian White in accordance with the following equation:

$$A^I Fe^{III} Fe^{II}(CN)_6 + A^{'+} + e^- \rightarrow A^I A^I Fe^{II} Fe^{II}(CN)_6 \qquad III.1$$
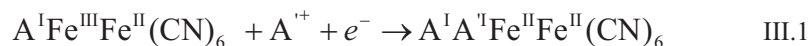
The product of its oxidation (Figure III.26 B) is first green (curves j to o) and remains slightly yellowish even at high oxidative potential (+1.3 V, curve p). For intermediate potentials, from 0.7 V to 1.0 V (curves j to m) , the presence of more than two species may be inferred since no precise isosbestic point was found, the presence of Prussian Blue, Berlin Green and Prussian Yellow is probable.

III. 3. 5. 1. ii. Colouration / bleaching with dynamic change of potential

For comparison with PEDOT, the volta-absorptometry and cyclic voltammetry have been simultaneously performed for Prussian Blue, at 500 mV/min, at 720 nm (Figure III.27).
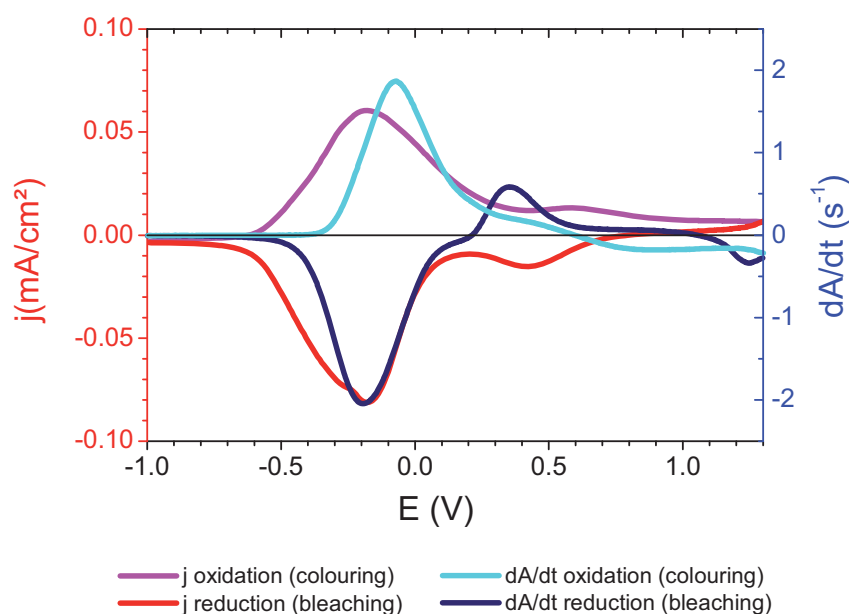

Figure III.27: Cyclic voltammetry at 8.3 mV/s, j = f(V) on the left axis and cyclic volta-absoptometry dA/dt = f(V) at 720 nm on the right axis for Prussian Blue on FTO/glass at 3 mC/cm², reference electrode CSE, counter electrode FTO/glass.

Let first consider the -1V/0.2V region. As explained above, the absorbance of PB films decreases as reduction of PB towards PW takes place: this is characterized by the negative dA/dt at 720 nm as the potential moves from 0.2V to -1.0V. A following oxidation of PW from -1.0V to 0.2V, is concomitant with a dA/dt positive: the films colours (in blue), PB is formed. As the potential further increases (0.5V to 1.3V), it arises in the region of production

of BG by oxidation of PB, the absorbance derivative becomes negative as the blue component of the colouration decreases and the yellow one increases (cf. Figure III.26B, curves a, i, j, k, l, m, n, o, p).

In addition to these information, that were in fact already accessible from Figure III.26, volta-absorptometry is a powerful tool to determine whether the change in colouration and the reduction (or oxidation) of the film are concomitant. As a reminder, in the case of PEDOT, in a certain range of potential (dependent on the nature of the PEDOT), oxido-reduction takes place in the film without any visible colouration (absorption occurs in the NIR region). In the case of Prussian Blue, such a discrepancy in the two phenomena is not observed, the colouration change being directly proportional to the number of produced blue chromophores.

III. 3. 5. 1. iii. Film capacities

Cyclic voltammetry measurements were performed between -1.0 V and 0.50 V and the film capacities were deduced from the anodic or reduction peak areas. The plot of measured capacities with respect to the theoretical capacities (Figure III.28), exhibits a good agreement and shows the reliability of the electrodeposition method to control the amount of deposited material.
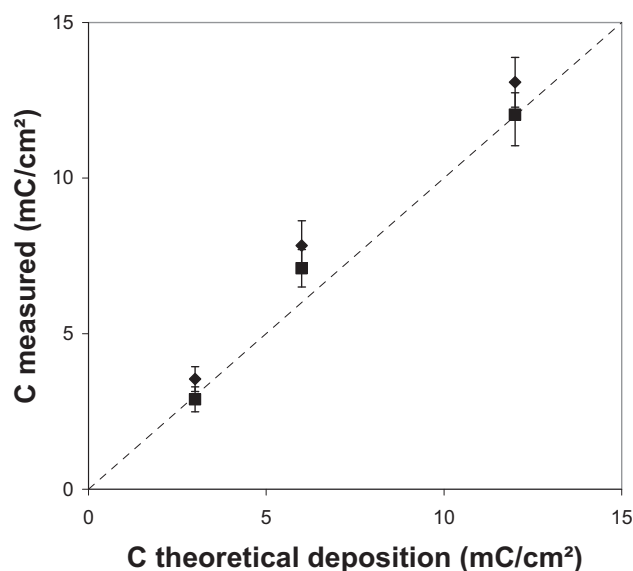

Figure III.28: Capacities of Prussian Blue films measured by cyclic voltammetry at 100 mV/min in LiTFSI 0.03 / BMITFSI 0.97 as a function of the theoretically deposited capacity. ■ oxidation ♦ reduction

III. 3. 5. 1. iv. Colouration efficiency

The redox system $Fe^{II}Fe^{II}$ (colorless)/$Fe^{III}Fe^{II}$ (blue) will be used all along the following studies. The colouration efficiency at different wavelengths is presented in Figure III.29. It is obtained from visible spectra recorded at 0.5 V/Ag/AgCl and -1.0 V/Ag/AgCl respectively. Its maximum value is 78 cm²/C, which is classical for inorganic materials and in the same range of order as the values reported in the literature for Prussian Blue in other electrolytes (e.g. 88.8 cm²/C for K^+ electrolyte[65]).
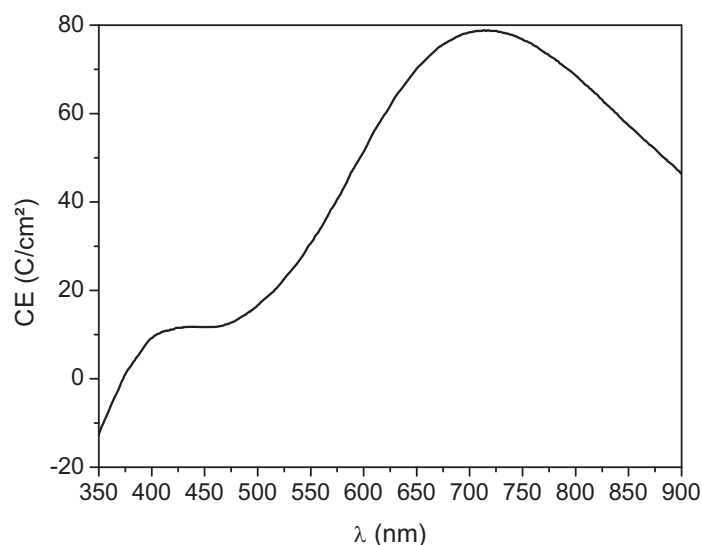

Figure III.29 : Colouration efficiency of PB for the transition PB – PW (Everitt's salt), UV-Visible spectra and chronoamperometry curves were recorded at the same time in a three-electrode cell (Ref: Ag/AgCl; CE: Platinum wire, electrolyte: LiTFSI 0.03 / BMITFSI 0.97). The electrical potentials were maintained during the whole measurement.

III. 3. 5. 2. InHCF films

The properties of InHCF films in ionic liquid electrolytes will be detailed hereafter. Our aim was to use InHCF films as transparent and nearly colourless counter electrodes with high enough electrochemical capacity.

III. 3. 5. 2. i. Absorbance spectra

The absorbance spectra were recorded while applying different potentials to the InHCF film. They are reported on (Figure III.30) for a film with a 5 mC/cm² capacity. The film is rather absorbing due to the surface roughness of the InHCF film as already explained. However, this film was selected to show that even for rather thick film the colour change is limited. The as-deposited film is slightly yellow, with an absorbance essentially situated in the blue region (curve f), and exhibits the same visible spectrum as that oxidised at 1.3V (oxidised state of InHCF). During reduction, the film becomes even more colourless (curve a).
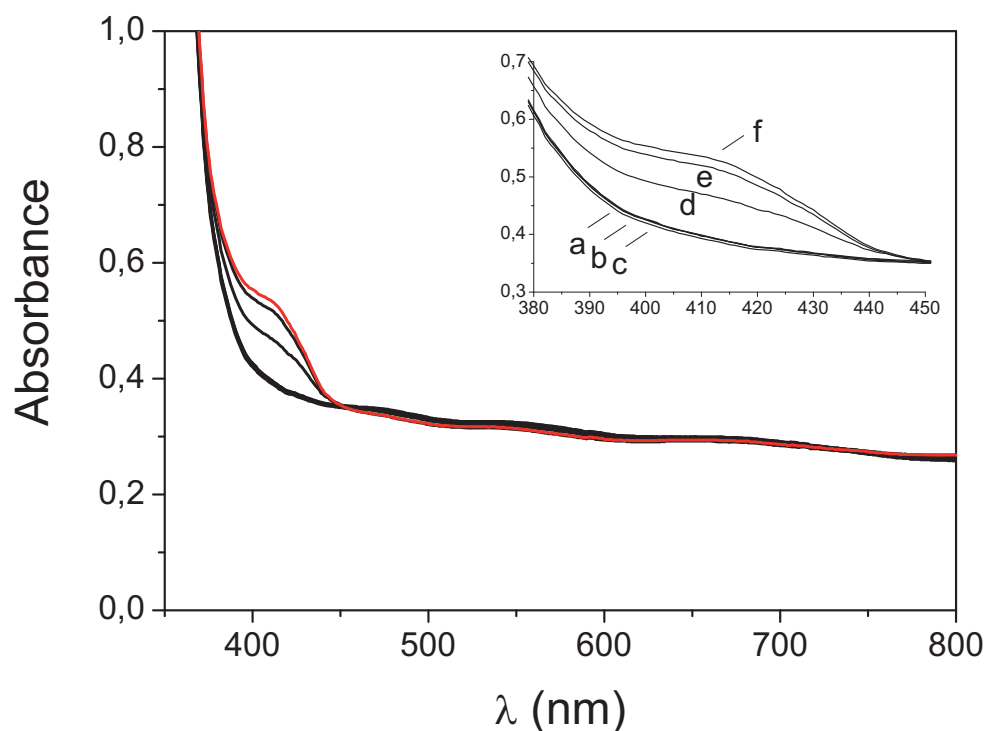

Figure III.30: Spectroelectrochemistry of the InHCF thin film of 5 mC/cm² on ITO/Orma, measure of the absorbance as a function of the applied potential, ref: Ag/AgCl, counter electrode : Pt foil; a)-1.0V, b) -0.5V, c) 0.0V, d) 0.5V, e)1.0V, f) 1.3V (as-deposited).

The films to be used in complete devices will have a capacity around 1-2 mC/cm². For them, the absorbance will be decreased by a factor 5 to 2.5 as compared to the film at 5 mC/cm². The remaining colouration will be extremely low (as shown on the as-deposited films of Figure III.24).

III. 3. 5. 2. ii. Colouration and bleaching with dynamic change of potential

As for PEDOT and Prussian Blue, volta-absorptometry has been performed. Colouration and current density evolution evolve in parallel (Figure III.31).
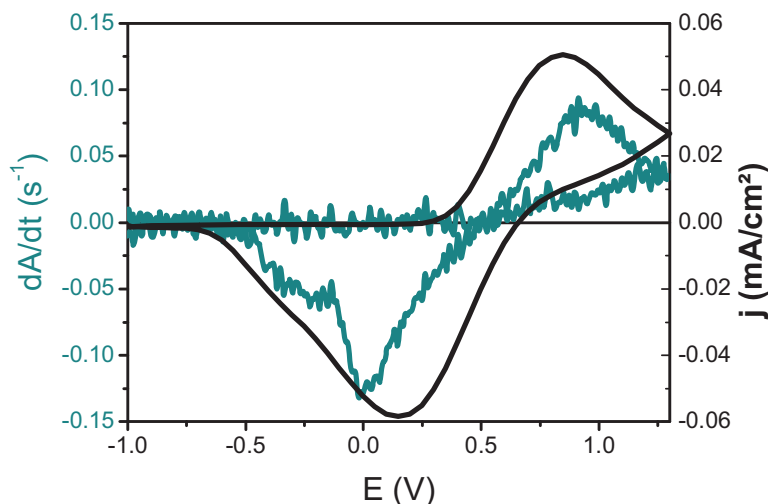

Figure III.31: Volta-absorptometry of a 5 mC/cm² InHCF deposited on ITO/Orma at 8.3 mV/s at 420 nm.

A rather low signal to noise ratio and a very low dA/dt (compare to BP) confirm the overall transparency of this type of layer.

III. 3. 5. 2. iii. Film capacities in BMITFSI/LiTFSI electrolyte.

The electrochemical capacities of the InHCF films on ITO/PET, FTO/glass, ITO/Orma (Essilor) and IZO (Indium Oxide doped with Zinc, ICMCB) on PET, were measured by cyclic voltammetry in LiTFSI 0.03/BMITFSI 0.97. Their values depend on the number of deposition cycles and on the substrate nature as illustrated in Figure III.32. The most visible phenomenon is that the capacities seem to vary linearly with the cycling number whatever the substrate nature.
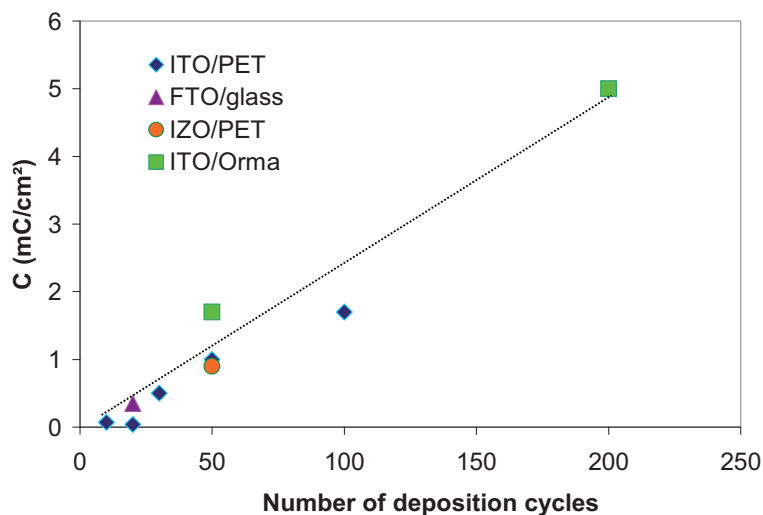
Figure III.32: Capacity measured by the area of the cyclic voltammetry at 8 mV/s in LiTFSI 0.03/BMITFSI 0.97 peak for InHCF deposition on ITO/PET, FTO/glass, ITO/Orma as a function of the number of deposition cycles at 100mV/s for 5 cm² sample.

As opposed to PB films, these films exhibit much lower capacities (around 70% less) than those they have for their very last deposition cycle (cf as-deposited InHCF films study: III. 3. 4. 2. iv.). To explain this result, we need to take into account the nature of the cation (Li$^+$) but also that of the anion; here the TFSI$^-$ steric hindrance is much higher than that of the Cl$^-$ present in the deposition solution. The use of smaller anions is expected to increase the available capacity of this InHCF films. However, this study shows that capacities in the range of 1-2 mC/cm² are reached in 0.03 LiTFSI/ 0.97 BMITFSI after 50-100 deposition cycles and even up to 5 mC/cm² after 200 deposition cycles; this is highly sufficient to foresee their use as complementary electrodes of PEDOT.

III. 3. 6. Conclusion on PB and InHCF counter-electrodes

Prussian Blue could be deposited on large substrates by electrodeposition. Its colouration efficiency (around 78 cm²/C) is rather high, it will give a slight additional colouration to the PEDOT based EC devices. In other devices, Prussian Blue could also be used as primary electrochromic material. In addition to these measurements, preliminary studies of the diffusion coefficients in PB are given in appendix F.

InHCF shows interesting properties as nearly colourless counter electrode. For capacities in the range of 1-2 mC/cm², the as-deposited films are transparent and show only a very slight yellow colouration when reduced. Its deposition on large substrate were not demonstrated.

III. 4. Conclusion

This study showed that Prussian Blue and one of its analogues InHCF can be used as counter-electrodes in conjunction with PEDOT working electrode, in LiTFSI/BMITFSI electrolytes.

BP, InHCF and PEDOT films were always obtained in their oxidized form. The possibility to obtain one of the two electrodes in the reduced state would simplify a lot the preparation of complete EC devices. However, attempts to prepare them in the reduced state, by stopping the electrodeposition after a negative scan, were systematically unsuccessful; the films were re-oxidized in the electrodeposition solution.

The use of InHCF as colourless electrode for ECDs is very promising but unfortunately couldn't be done in the timescale of this thesis.

Concerning the possibility to prepare such materials on an industrial scale, PEDOT dispersions are already deposited at large scale (Agfa) and the industrialisation of the deposition of in-situ polymerized PEDOT is expected for the close future. For Prussian Blue, the electrodeposition technique can be well adapted to large scale deposition, the preparation of Prussian Blue film from an ink composed of nanoparticles of Prussian Blue in the presence of a surfactant, has been evidenced by Hara et al.; it is also promising for industrial applications[66,67]. We can infer that large scale preparation of InHCF film could be made in the same way.

Our Nanoeffects partners INSTM and Fraunhofer ISC in charge of the modification of the PEDOT in order to decrease the remaining blue colour of PEDOT succeeded to diminish it in an appreciable amount. This is an important point for the preparation of ophthalmic electrochromic devices for which a fully colourless bleached state is needed.

The modification of PEDOT towards more neutral colour is still under study.

For the devices studied in the next chapter, we will focus our attention on systems based on PEDOT as the main electrochromic layer combined with PB layer, each of them exhibiting a 3 mC/cm² capacity. In this range of capacities Prussian Blue films are indeed, totally crack-free and give an additional blue colouration in the coloured state. A theoretical colouration efficiency of 250 cm²/C (78 (BP) + 175 (PEDOT)) is expected for the EC devices based on these two materials, which is within the highest values for ECD.

A preliminary study of the influence of the percentage of PMMA in the electrolytic membranes on the electrochromic properties of complete systems will be presented in this

chapter (studies carried out with PEDOT PSS). The influence of the conductivity of the substrates will also be studied on samples using in-situ polymerised PEDOT. Eventually, the study of large complete devices (15*13 cm²) was performed with PEDOTs obtained by in-situ polymerisation.

References

[1] P.M.S. Monk, R.J. Mortimer, D.R. Rosseinsky, *Electrochromism and electrochromic devices,* **2007**, Cambridge University Press (ed.).

[2] N.R. de Tacconi, K. Rajeshwar, R.O. Lezna, *Chem. Mater.,* **2003**, 15, 3046.

[3] J.Roncali, *Chem. Rev.,* **1992**, 92, 711.

[4] G.Barbella, M. Melucci, G. Sotgiu, *Adv. Mater.,* **2005**, 17, 1581.

[5] M. Gazard, *Handbook of Conducting Polymers*, vol. 1, **1986**, Marcel Dekker.

[6] S. Kirchmeyer, K.J. Reuter, *J. Mater. Chem.*, **2005**, 15, 2077.

[7] J.L. Bredas, G.B. Street, *Acc. Chem. Res.,* **1985**, 18, 309.

[8] B. Scrosati, *Prog. Solid State Chem.,* **1988**, 18, 1.

[9] Q. Pei, G. Zuccarello, M. Ahlskog, O. Inganăs, *Polymer,* **1994**, 35, 7, 1347.

[10] H. Neugebauer, *J. Electroanal. Chem.,* **2004**, 563, 153.

[11] P. Hou, D. Han, Z. Wang, G. Yang, X. Xu, L. Niu, *Synth. Met.,* **2007**, 157, 18-20, 779.

[12] W. Lu, A. G. Fadeev, B. Qi, E. Smela, B. R. Mattes, J.Ding, G. M. Spinks, J. Mazurkiewicz, D. Zhou, G. G. Wallace, D. R. MacFarlane, S. A. Forsyth,; M. Forsyth, *Science,* **2002**, 297, 983.

[13] W. Lu, A. G. Fadeev, B. Qi,; B. R. Mattes, *Synth. Met,.* **2003**, 139, 135.

[14] M. Lefebvre, Z. Qi, D. Rana, P. G. Pickup, *Chem. Mater.,* **1999**, *11*, 262.

[15] F. Jonas, W. Krafft, B. Muys, *Macromol. Symp.,* **1995**, *100*, 169.

[16] M. Lefebvre, Z. Qi, D. Rana, P. G. Pickup, *Chem. Mater.* **1999**, *11*, 262.

[17] F. Jonas, W. Krafft, B. Muys, *Macromol. Symp.* **1995**, *100*, 169.

[18] M. Dietrich, J. Heinze, G. Heywang, F. Jonas, *J. Electroanal. Chem.,* **1994**, 369, 87.

[19] C. Kvarnström, H. Neugebauerm, S. Blomquist, H.J. Ahonen, J. Kankare, A. Ivaska *Electrochim. Acta,* **1999**, 44, 2739.

[20] A. Lima, P. Schottland, S. Sadki, C. Chevrot, *Synth. Met,.* **1998**, 93, 33.

[21] Z. Qi, P.G. Pickup, *J. Chem. Soc.,Chem. Commun.,* **1998**, 2299.

[22] A.J. Downard, D.J. Pletcher, *J. Electroanal. Chem.,* **1986**, 206, 139.

[23] N. Sakmeche, S. Aeiyach, J.J. Aaron, M. Jouini, J.C. Lacroix, P.C. Lacaze, *Langmuir,* **1999**, 15, 7, 2566.

[24] E.V. Ovsyannikova, M.Y. Grosheva, V.V. Topolev, S.V. Timofeev, L.P. Bobrova, F. Jonas, S. Kirchmeyer, A.D. Aliev, N.M. Alpatova, *Russian Journal of Electrochemistry* **2004**, 40, 8, 825.

[25] D. Han, G. Yang, J. Song, L. Niu, A. Ivaska, *J. . Electroanal. Chem.,* **2007,** 602, 24.

[26] G. Heywang, F. Jonas, *Adv. Mater.,* **1992**, 4, 2, 116.

[27] F. Jonas, W. Kraft, B. Muys, *Macromol. Symp.,* **1995**, 100, 169.

[28] Y. Ha, N. Nikolov, S. Pollack, J. Mastrangelo, B. Martin, R. Shashidhar, *Adv. Funct. Mater.,* **2004**, 14, 615.

[29] R. Marcilla, E. Ochoteco, C. Pozo-Gonzalo, H. Grande, J.A. Pomposo, D. Mecerreyes, *Macromolecular Rapid Communications* **2005**, 26, 14, 1122.

[30] J. Dyer, L. Aubrey; J.R. Reynolds, *Electrochromism of conjugated conducting polymers.* Handbook of Conducting Polymers (3rd Edition) **2007**, 1, 20.

[31] Kulesza, Journal of solid state electrochemistry, 1: 88-93 (19971997)

[32] A Celik, PhD Thesis, Fraunhofer ISC, Germany 2008

[33] X. J. Wang, K. Y. Wong,. *Thin Solid Films* **2006**, 515, 4, 1573.

[34] E.L. Crepaldi, G.J. de Soler-Illia, D. Grosso, F.Cagnol, F. Ribot, C. Sanchez, Journal of the American Chemical Society **2003**, 125, 32, 9770.

[35] K.R. Dunbar, R.A. Heintz, *Prog. Inorg. Chem.,* **1997**, 45.

[36] V.D. Neff, *J. Electrochem. Soc.,* **1978**, 125, 886.

[37] S.J. Dong, Z. Jin, *Electrochim. Acta,* **1989**, 34, 1749.

[38] G. Campet, C. Mingotaud; A. Poquet; J.N. Portier; S. Ravaine, *Compositions d'électrolytes, procédé de fabrication et applications électrochimiques* , patent FR2803951, **2001**.

[39] Diesbach, **1704**, cited in Gmelin, *Handbuch der Anorganischen Chemie* **1930**, Deutsche Chemische Gesellschaft, , 59, Eisen B, 671.

[40] K. Itaya, I. Uchida, V.D. Neff, *Acc. Chem. Res.,* **1986**, 19, 162 ; and references therein.

[41] P.M.S. Monk, R.J. Mortimer, D.R. Rosseinsky, *Electrochromism: Fundamentals and Applications*, **1995**, VCH; and references therein.

[42] N.R. De Tacconi, K. Rajeshwar, R.O. Lezna, *Chem. Mater.,* **2003**, 15, 3046.

[43] J.A. Cox, R.K. Jaworski, P.J. Kulesza, *Electroanalysis,* **1991**, 3, 869.

[44] A.A. Karyakin, *Electroanalysis,* **2001**, 13, 813.

[45] R. Konchi, *Crit. Rev. Anal. Chem.,* **2002**, 32, 79.

[46] F. Ricci, G. Palleschi, *Biosens. Bioelectron.,* **2002**, 21, 79.

[47] *Magnetism : Molecules to Materials V.* , chapter 9: Magnetic Prussian Blue Analogs, **2004,** WILEY-VCH.

[48] A.K. Bonnette,jr., J.F. Allen, *Inorg. Chem.,* **1971**, 10, 1613.

[49] B. Mayoh, P. Day, *J. Chem. Soc. Dalton Trans,.* **1974**, 846.

[50] J.F. Keggin, F.D. Miles, *Nature,* **1936**, 137, 577.

[51] A. Ito, M. Suenaga, K.Ono, *J. Chem. Phys.,* **1968**, 48, 8, 3597.

[52] A. Ludi, H.U. Güdel, M. Rüegg, *Inorg. Chem.* **1970**, 9, 2224.

[53] H.J. Buser, D. Schwarzenbach, W. Petter, A. Ludi, *Inorg. Chem.*, **1977**, 16, 2704.

[54] D.R. Rosseinsky, H. Lim, H. Jiang, J.W. Chai, *Inorg. Chem.,* **2003**, 42, 6015.

[55] A) Electroless deposition: Y. Yano, N. Kinugasa, H.K. Yoshida, K. Fujino, H. Kawahara, *Proc. Electrochem. Soc.*, **1990**, 90, 125; B) Sacrificial anod method: K.-C. Ho, *Proc. Electrochem. Soc.*, **1994**, 94, 170; C) Extensive redox cycling of hexacyanoferrate(II) containing solutions: H. Gomathi, G.P. Rao, *J. Appl. Electrochem.*, **1990**, 20, 454; D) Embedding of micrometer-sized crystals into electrode surface: F. Scholz, B. Meyer, in *Electroanalytical Chemistry: A series of Advances*, **1998**, vol.20.

[56] K. Itaya, T. Ataka, S. Toshima, *J. Am. Chem. Soc.,* **1982**, 104, 4767.

[57] B.J. Feldman, O.R. Melroy, *J. Electroanal. Chem.,* **1987**, 234, 1-2, 213.

[58] G.J. Cheng, S.J. Dong, *Electrochim. Acta,* **1987**, 32, 1561.

[59] I. Ho, H. Lee, H. Yang, Kwak, *J. Electrochem. Commun.,* **2001**, 3, 6, 274.

[60] D.R. Rosseinsky, J.S.Tonge, *J. Chem. Soc. Faraday Trans.*, **1987**, 1, 83, 245.

[61] a) P.J. Kulesza, M. Faszynska, *J. Electroanal. Chem.*, **1988**, 252, 461; b) P.J. Kulesza, M. Faszynska, *Electrochim. Acta,* **1989**, 34, 1749.

[62] Z. Jin, S.J. Dong, *Electrochim. Acta,* **1990**, 35, 1057.

[63] Goncalves, R.M.C., Kellawi, H., Rosseinsky, D.R., *J. Chem. Soc., Dalton Trans.,* **1983**, 991.

[64] I. Saadeddin, PhD Thesis, ICMCB, France, **2007**.

[65] D.R. Rosseinsky, A. Glidle, *J. Electrochem. Soc.,* **2003**, 150, 9, C641.

[66] M. Yamada, M. Arai, M. Kurihara, M. Sakamoto, M. Miyake, *J. Am. Chem. Soc.*, **2004,** 126, 9482.

[67] S. Hara, H. Tanaka, M. Tokumoto, T. Kawamoto, M.Yamada, M. Miyake, M. Kurihara, M. Sakamoto, *IME7 proceedings*, **2006**, 52.

Chapter IV. Complete devices: set-up and characterization

_____

IV. 1.*Introduction*

Complete devices are prepared with electrochromic layers of PEDOT and Prussian Blue separated by ionic liquid based electrolyte. The method of preparation has been progressively improved in collaboration with the Nanoeffects consortium partners, especially ISC, Solems, Essilor and HydroQuébec. The objective is to demonstrate the feasibility of this technology to prepare large surface area ECD devices.

First, major considerations concerning the set-up of these complete devices will be explained then the detailed procedure of preparation will be presented. The influence of the electrolytes gelification (PMMA addition) and of the TCO substrate resistivity on the electrochromic behaviour of the systems will be detailed with finally the properties of the optimized devices.

IV. 2. *Preparation of complete devices*

As explained before, as-prepared electrochromic PEDOT and Prussian Blue layers are in their oxidised state, so that the preparation of a complete device must include a step of reduction of one of the two layers. This chapter will explain the specificities of our system and will detail the whole sequence of EC device preparation.

IV. 2. 1. Specificity of the PEDOT-Prussian Blue system

IV.2.1.1. Preparation in the bleached or in the coloured state

The working principle of an ECD relies on the complementary redox reactions of two materials: one is oxidised at one electrode while the other is simultaneously reduced at the other electrode. So that when preparing a device, the two electrochromic layers must be in two different redox states (reduced and oxidised respectively).

As -deposited PEDOT and Prussian Blue, as-well as PEDOT derivative and InHCF, are prepared in the oxidised state (see chapter III). So that the complete devices preparation sequence requires either the reduction of PEDOT and the system will be prepared in the oxidised state for PB and reduced state for PEDOT i.e. in the coloured state, or the oxidation

of PEDOT and reduction of Prussian Blue and the system will be prepared in the reduced state for PB and oxidised state for PEDOT i.e. in the bleached state (Figure IV.1).

As-deposited PEDOT and PEDOT derivatives are in an oxidised state, but they are not fully oxidised. If the preparation in the bleached state is chosen, Prussian Blue must be reduced but PEDOT must also be fully oxidised to gain an as colourless as possible bleached state. The preparation in the coloured state is more favourable since only the PEDOT layer is to be coloured before assembly. Moreover, the coloured state of PEDOT is more stable in open atmosphere than the bleached state of Prussian Blue, and this is favourable for the preparation in the coloured state.
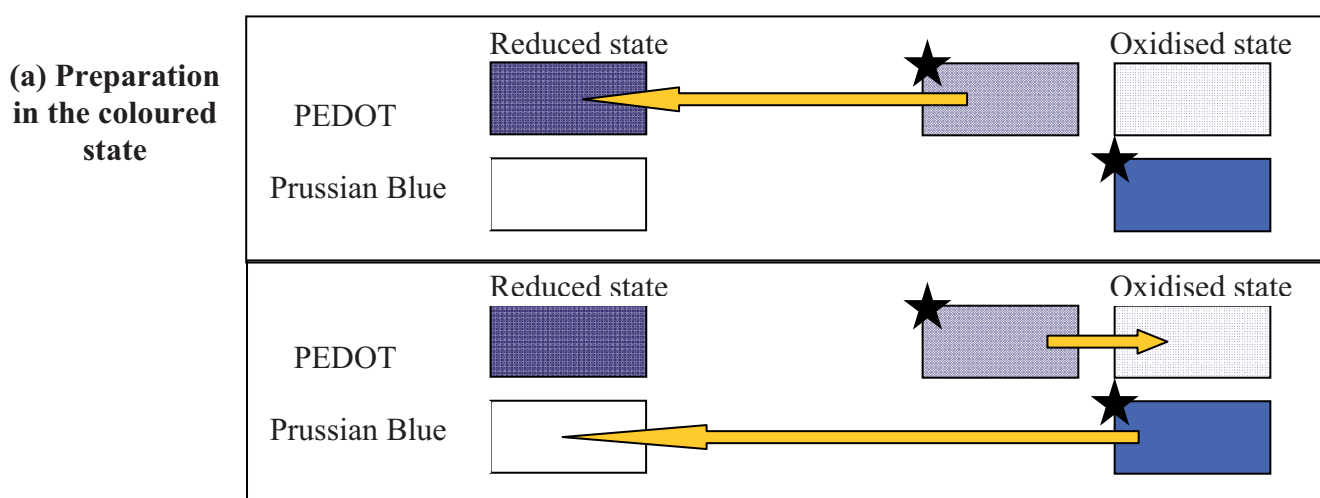
Figure IV.1: PEDOT and Prussian Blue colour in the as-deposited states (★) and their fully oxidised and fully reduced states. The arrow show the necessary steps to set up the device in the coloured state (a) and in the bleached state (b)

To simplify the device preparation, a set-up in the coloured state has been chosen. This choice will require particular attention to capacities balance of the materials as detailed below.

IV.2.1.2.Materials capacities balance

For devices prepared in the bleached state, the capacity matching between the two electrochromic layers is not required: the device benefits from a fully bleached state in any case, the material with the lowest capacity will determine the level of colouration of the device.

On the contrary, for the preparation of the devices in the coloured state, the materials must be chosen carefully in order to have the possibility to fully bleach the device. Indeed, a

completely colourless and transparent bleached state is mandatory for the some applications (in particular ophthalmic lenses). To achieve this requirement, one of the solutions would be to have Prussian Blue and PEDOT films with identical capacities. However, as demonstrated by voltabsorptometry (see III.3.3.2), PEDOT layers overall capacity includes both a colouration effective part and a non colouration effective part (about 33% of the total for the ISP sample). So that there is a certain tolerance in the capacity of the Prussian Blue layer: it can be between 77% and 100% of PEDOT total capacity (cf Figure IV.2). We generally chose 90%.

This choice of a Prussian Blue with 90% of PEDOT capacity allows to use a part of the non colouring PEDOT as an intermediate zone to ensure both high capacity of the complete device (too low BP capacity would result in low capacity for the complete device and low colouration) and full bleaching of PB (too high PB capacity would result in not fully colourless device in the bleached state).
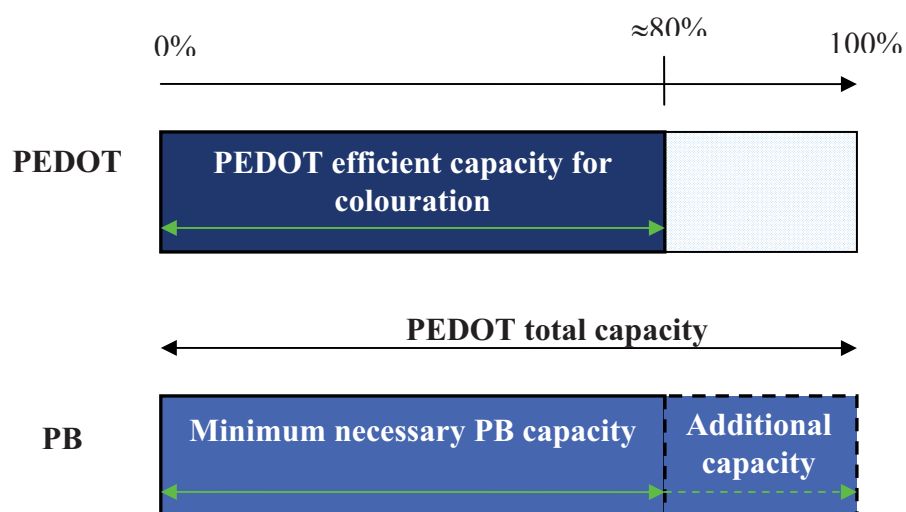

Figure IV.2 : PEDOT and Prussian Blue efficient capacity for colouration: for PB the whole capacity leads to colouration whereas for PEDOT it is only a part of it As-deposited PEDOT is slightly coloured (partly reduced). PB capacity must be chosen in between 77% and 100% of PEDOT capacity.

IV.2.1.3. Interface between the layers

Special attention must be given to the quality of the interface in between the different layers. In the case of plasticised polymeric membrane, the possibility to soften the membrane

(for example by heating around or above the Tg) gives more fluidity at the interface in order to have a better penetration of the electrolyte in the active material. Heating of the devices after lamination of the layers onto each other is performed in order to strengthen the interface This has been shown to be efficient for the 40% PMMA membranes. For the 50% PMMA membrane, the Tg is too high and the membrane was not enough soften at temperature compatible with plastics (T<70°C for ITO/Orma substrates), the colouration of the ECD was not homogeneous.

IV.2.1.4. Electrical contacts

The design of the electrical contacts is highly important since it determines the geometry of the electron injection in the electrochromic layer. For TCO substrate exhibiting a low conductivity, a metallic conductor is added around the electrochromic area to improve the electronic injection in the device. Conductive tapes (copper and silver), conductive pastes (silver paste) or sputtered metals (nickel depositions proposed and prepared by Solems) have been used for this purpose.

Another solution consists in adding on the TCO an invisible metallic grid in order to enhance the conductivity; this solution was not tested in our study.

IV.2.1.5. Sealing of the devices

Due to side chemical and electrochemical reactions with water and oxygen, devices must be carefully sealed. In our case, the use of a relatively hydrophobic solvent (ionic liquid with TFSI$^-$ anion), is expected to lower water entrance in the devices, this has been tested by testing the cycle life of a device that was not sealed (Figure IV.3).
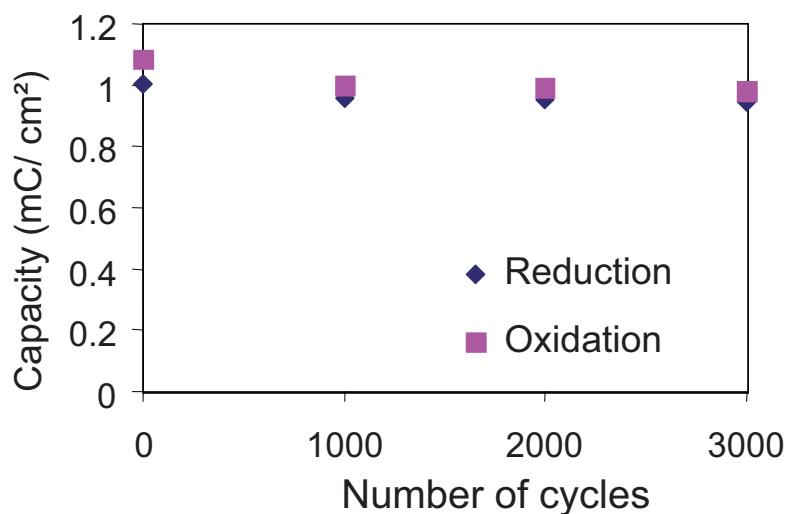
Figure IV.3 : Variation of the capacity of the device with the number of cycles measured by chornoamperometry while applying -0.5V / +1.0V.

Without any sealing, this device shows a loss of only 5% of colouration properties after one year at rest. However, the cycling stability target for Nanoeffects is 10^5 cycles, and the long term stability is required in terms of years (minimum 2 years for ophthalmic applications, 10 years for buildings and cars), so that higher standards of sealing are crucial.

The sealing was then improved by using a scotch tape that lower the environmental influence on the device (oxygen, water …). However, more effective sealing would be more beneficial.

IV. 2. 2. Sequence of device preparation

Devices were prepared according to the following sequence (Figure IV.4 to Figure IV.9):

1) Deposition of the PEDOT film on a conductive substrate such as ITO/PET

Figure IV.4 : Photo of a PEDOT on ITO/PET prepared at ISC (11*15cm² active surface)

2) Measurement of the PEDOT capacity in the liquid electrolyte
3) Deposition on a conductive substrate, such as ITO/PET, of a PB film of the desired capacity (generally 90% of PEDOT overall capacity).
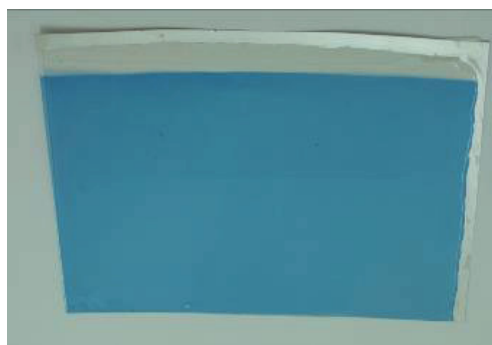

Figure IV.5 : Prussian Blue deposited on ITO/PET at 90% of PEDOT capacity

4) Deposition of the membrane electrolyte on PB

Figure IV.6 : Electrolytic membrane deposited on the Prussian Blue layer

5) Electrochemical reduction (colouration) of PEDOT in a three electrodes cell filled with 0.03 LiTFSI / 0.97 BMITFSI liquid electrolyte.

6) Manual lamination of coloured PEDOT on the stack electrolyte/BP/ITO/PET

Figure IV.7: Application (manual lamination) of coloured PEDOT on the electrolyte/Prussian Blue stacks.

7) Hot-pressing of the PEDOT layer on the stack membrane electrolyte/PB

Figure IV.8 : Hot-pressing of the whole stack under vacuum at 80°C for at least 2h.

Metallic
deposition
(tape,
paste,
sputtered
layer) on
ITO/PET

As-deposited
PEDOT

As-deposited
Prussian Blue

Scotch-tape
as spacer

Deposition of the
electrolytic membrane
(doctor-blade, spin-
coating)

Colouration
of
PEDOT
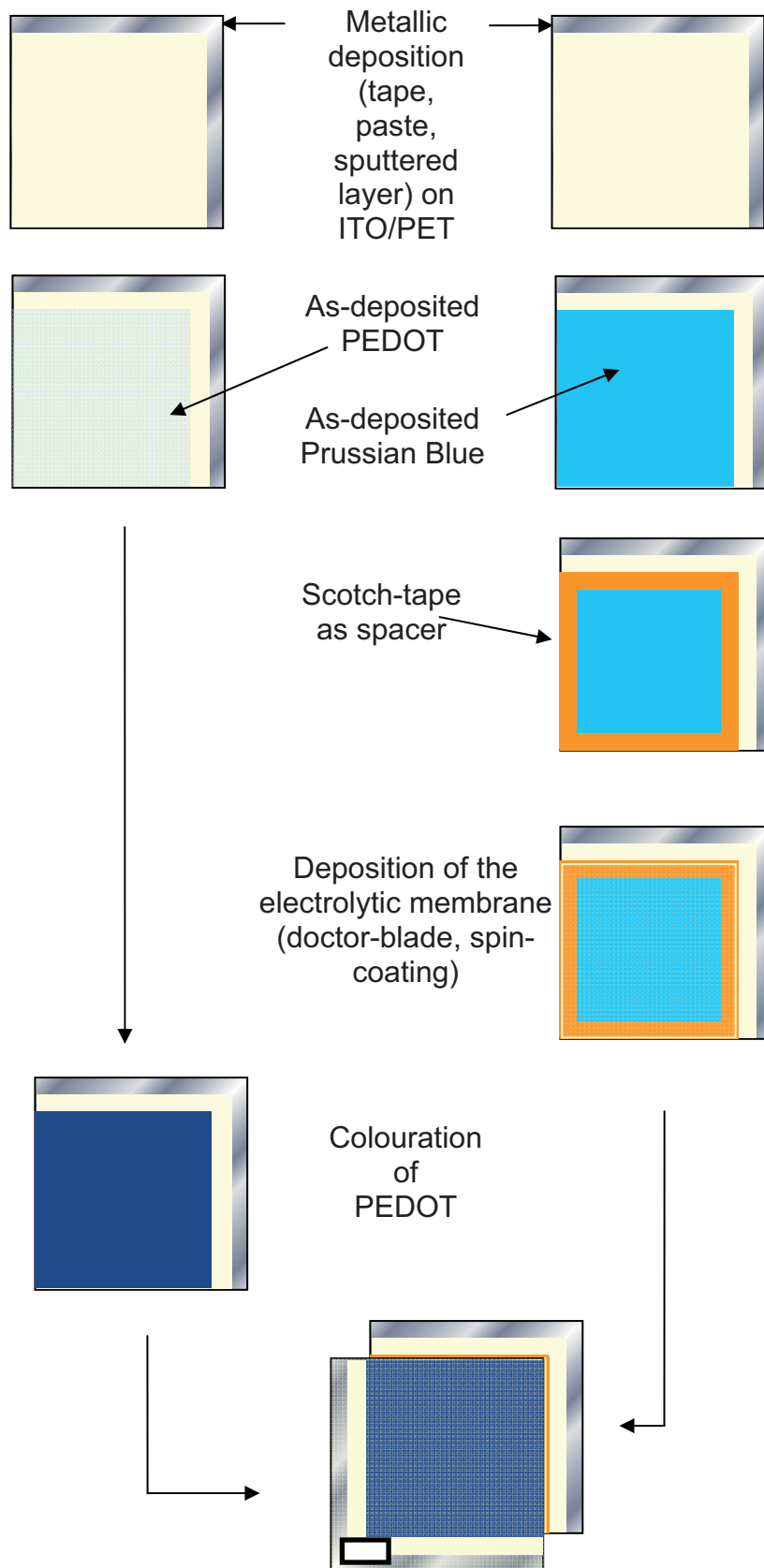
Figure IV.9 : Illustration of the preparation sequence

IV. 3. *Influence of PMMA ratio of the membrane electrolyte*

IV. 3. 1. Nature of the devices used for the study and context of the study

PMMA membranes plasticized with 0.03LiTFSI/0.97BMITFSI solution were used as electrolytes with 50%, 60% 70% ratios of the IL electrolyte solution. PEDOT-PSS coatings (as D-1 sample in part III) were placed in front of PB layers. Both layers were deposited on 5*5 cm² FTO glass substrates with 4*5cm² active area. The aim was to study both the mechanical behaviour of the gel or membrane electrolytes (presented in part II) and the spectroelectrochemical properties of the resulting devices depending on the percentage of PMMA. At the moment of this study, we used PEDOT-PSS films instead of in-situ polymerised PEDOT that was afterwards identified as the best candidate for large devices.

IV. 3. 2. Spectro-electrochemical properties of a device with 30wt% PMMA

Figure IV.11 shows the variation of absorbance of such a device at various applied potentials. The absorbance centred at 660 nm covers a large range of the sun light visible spectrum with a dark blue colour in the coloured state (Figure IV.11). Despite a slight residual colouration in the bleached state due to the PEDOT (see Figure III.8), the device shows a high ΔA (0.71) and a CE of 290 cm²/C, essentially due to the PEDOT contribution.

1V   -1V

Figure IV.10 : Bleached (1V) and coloured state (-1V) of a -complete device with electrolytic membrane based on 70% LiTFSI 0.03 / BMITFSI 0.97 and 30 wt% PMMA, on FTO/glass with PEDOT PSS and PB electrochromic films.
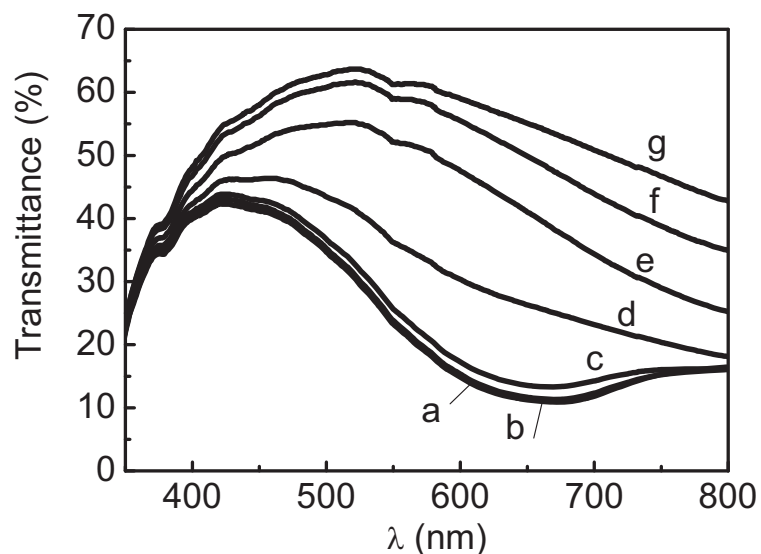
Figure IV.11 : UV-Visible spectra during spectroelectrochemical study of a complete device (30 wt% PMMA/ 70wt% 0.03 LiTFSI- 0.97 BMITFSI), in the 400-800 region as a function of the applied potential. Transmittance measured at. a) -1.8 V, b) -1.5 V, c) -1.0 V, d) -0.5 V, e) 0.0V, f) 0.5 V, g) 1.0 V, air is taken as the reference.

The spectro-electrochemical properties were determined by applying a fixed potential during 30 s. and measuring meanwhile the ΔA of the complete device.
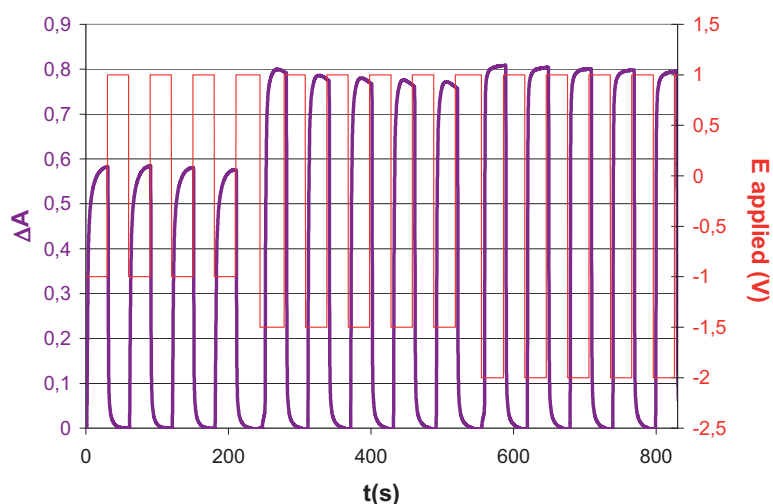

Figure IV.12: Spectroelectrochemistry of the following complete device:
Glass/ FTO/ PEDOT Orgacon / electrolytic membrane : 70% 0.03 LiTFSI/ 0.97 BMITFSI, 30% PMMA / BP / FTO/Glass, measure of the ΔA while applying colouring and bleaching potentials.

The delta of absorbance, kinetics and cycling behaviour for complete EC devices with wt% PMMA from 30 to 50 wt% were extracted from these measurements as described below.

IV. 3. 3. Influence of wt% PMMA on absorbance and kinetics

Even if the ΔA of the device between the two states decreases with increasing PMMA ratio (Figure IV.13), the kinetics for colouration and bleaching at the maximum absorbance wavelength (660 nm) (Figure IV.15) remain nearly constant. The colouration and bleaching times defined by the time necessary to reach 90% of the maximum colouration or bleaching are 5s. and 2s. respectively.
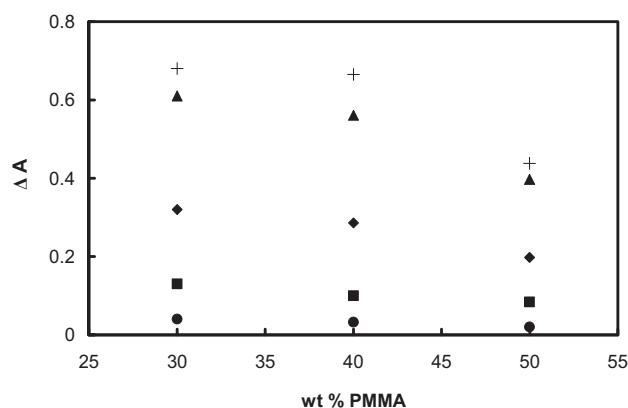

Figure IV.13 : Variation of the difference of absorbance (ΔA)between coloured and bleached states at 660 nm (ΔA=0 at E=1V) with different PMMA ratios at various applied potentials: (●) 0.5V; (■) 0.0V; (♦) -0.5V (▲) -1.0V; (+) -1.5V.
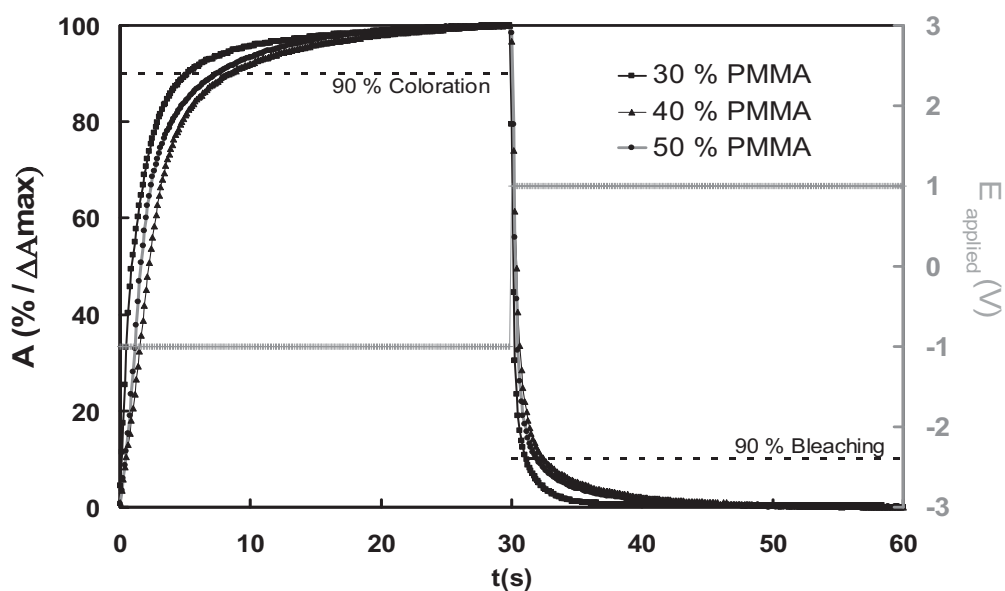

Figure IV.14 : Kinetics of colouration and bleaching at 610 nm when switching the potentials at -1.0V for colouring and +1.0V for bleaching.

176

IV.3.3.1. Influence of wt% PMMA on long term cycling

Long term cycling was performed by chronoamperometry (5 s) in the -1.0 V / +1.0V range (Figure IV.15). A delay of 5s. was used in order to insure that the system reached 90% of each electrochromic state.

After a first period of formatting over the 200 first cycles, the capacities remain nearly constant (<3 % decrease between 200 and 1000 cycles). For all the devices, the loss of ΔA after these 1000 cycles was around 15%, which is very promising since no protecting sealing was used. Moreover, after 4 months shelf live, the systems exhibited very high electrochromic stability (ΔA loss less than 1% after 4 months).
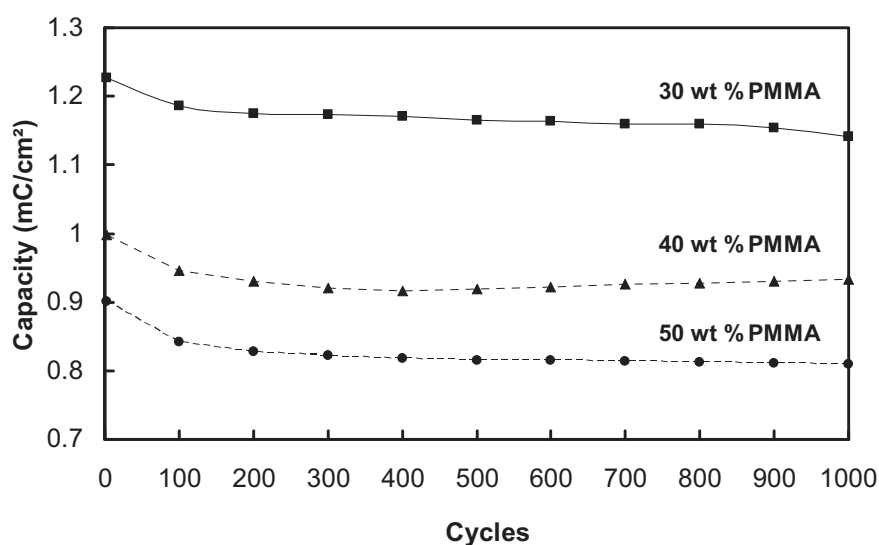

Figure IV.15: Variation of the capacity during cycling at -1V 5 s +1V 5 s. of devices with 30 to 50 % PMMA in 0.03 LiTFSI / 0.97 BMITFSI

IV. 3. 4. Conclusion on wt% PMMA influence

Complete devices using ionic liquid (0.03 LiTFSI / 0.97 BMITFSI) based polymer membrane electrolytes have demonstrated efficient electrochromic properties and long term stability both under cycling (up to 1000 cycles) and at rest (4 months). The incorporation of PMMA in the electrolyte gives rise to adhesive and nearly solid membranes. These membranes have many advantages: (i) they lead to leakage-free, moisture-free and short circuit-free solid-state devices (ii) they can adapt their shape to any kind of substrates including curved and very flexible ones. Further studies are under investigation to fully understand the lithium motion in the electrolyte and in the electrochromic materials. The use

of other type of PMMA (longer chains, in situ polymerized) is expected to lead to interesting results in terms of conductivity and mechanical behaviour.

IV. 4. *Influence of the substrate conductivity*

IV. 4. 1. Context of the study

The resistivity is an intrinsic property of a material. The resistivity of the transparent conducting oxides (TCOs), which act as current collectors, must obviously be as low as possible. As quoted above, ITO and FTO are the main commercially available TCOs. For ITO, the resistivity reaches 5.10^{-4} Ω.cm when it is deposited by sputtering on glass followed by annealing in air at 350°C for at least two hours; the resistivity of ITO reaches only 10^{-3} Ω.cm when sputtered on PET without further annealing. For FTO, the resistivity reaches its lowest value (5.10^{-4} Ω.cm) when it is deposited by CVD on glass followed by annealing at 450°C for at least four hours in order to achieve appropriate high crystallinity needed for low resistivity, therefore, for the moment conductive FTO could not be deposited successfully on PET. We will use thin layers of these conducting materials. The square resistance (also called 'sheet resistance') of the films (resistivity divided by the thickness), which must be as low as possible, will decrease as the film thickness increases. However, TCOs are not fully transparent and become fragile as the thickness increases so that a compromise has to be found.

The following studies were performed in order to determine the performances of the complete devices depending on the sheet resistance of the TCO. The background idea was to determine whether the Nanoeffects consortium had to work on the improvement of TCO layers sheet resistance on plastics or not.

Substrates with different square resistance were provided by Solems : ITO from 24 to 124 $\Omega/\square$ on glass of 5*5cm². PEDOT-ISP films were prepared by the Fraunhofer-ISC. Prussian Blue ones were electrodeposited at ICMCB. The electrolytic membranes were made with 0.03 LiTFSI / 0.97 BMITFSI with 30 wt% PMMA added.

IV. 4. 2. Spectroelectrochemical properties

The absorbance of the complete electrochromic devices prepared with the different conducting substrates (5*5cm²) was measured while applying a voltage step -0.5V 30 s. / +1.0V 30 s. (Figure IV.16).
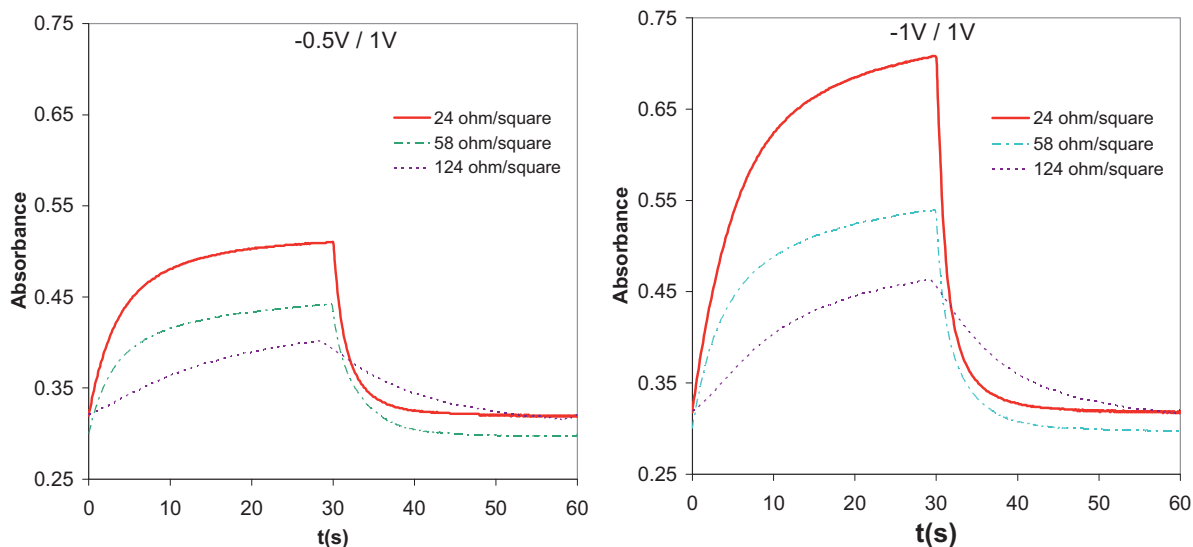
Figure IV.16 : Variation of the absorbance with time for EC devices prepared with conducting substrate of sheet resistance 24, 58 and 124 Ω/□ : colouration at -0.5V (left) and at -1.0V (right) for 30 s. followed by bleaching at 1.0V the next 30 s..

The absorbance delta between the bleached and coloured states increases as the sheet resistance of the substrate decreases. In the range -0.5V to -1.0V, the application of a higher potential in reduction allows to reach higher values of absorbance. This is much more visible for the device with 24 Ω/□ ITO.

As expected the charge needed to colour the films (area under the I=f(t) curve) also increases as the reduction potential is increased from -0.5V to -1.0V (Figure IV.17).
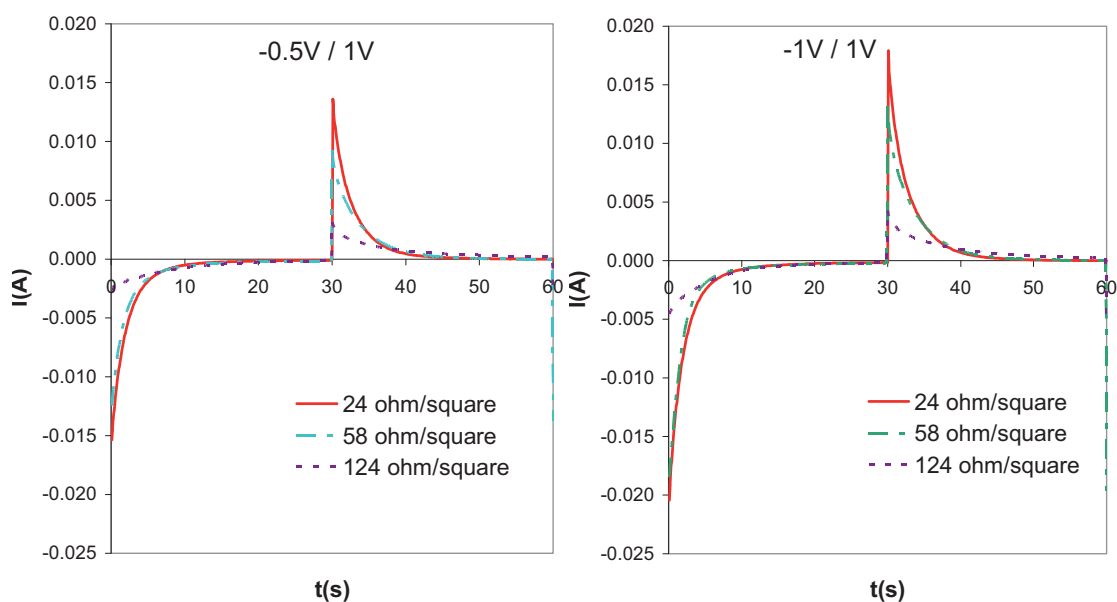

Figure IV.17 : Variation of the current consumed by the device with time for EC devices prepared with conducting substrate of sheet resistance 24, 58 and 124 Ω/□ : colouration at -0.5V (left) and at -1.0V (right) for 30 s. followed by bleaching at 1.0V the next 30 s..

As a rough approximation, the potential drop within the TCO layer is equal to the product of the resistance of the device by the current passing through it. The samples are squared and the electrical contacts are facing each other so the resistance (in ohms) of the device is equal to the square resistance of the film (in ohm/square). The I*R values are given for the devices with different ITO conductivities in Figure IV.18.

Except the first seconds, the potential drops are higher for devices with more resistive ITO. For example, a potential drop of 0.1V remains after 10s. of colouration and bleaching potentials for the device with ITO at 124 $\Omega/\square$. The colouration being highly dependent on the potential applied (see Figure IV.11), a decrease in absorbance around 0.05 would be expected for this potential drop. The observed absorbance drop is however higher than expected (see Figure IV.16).
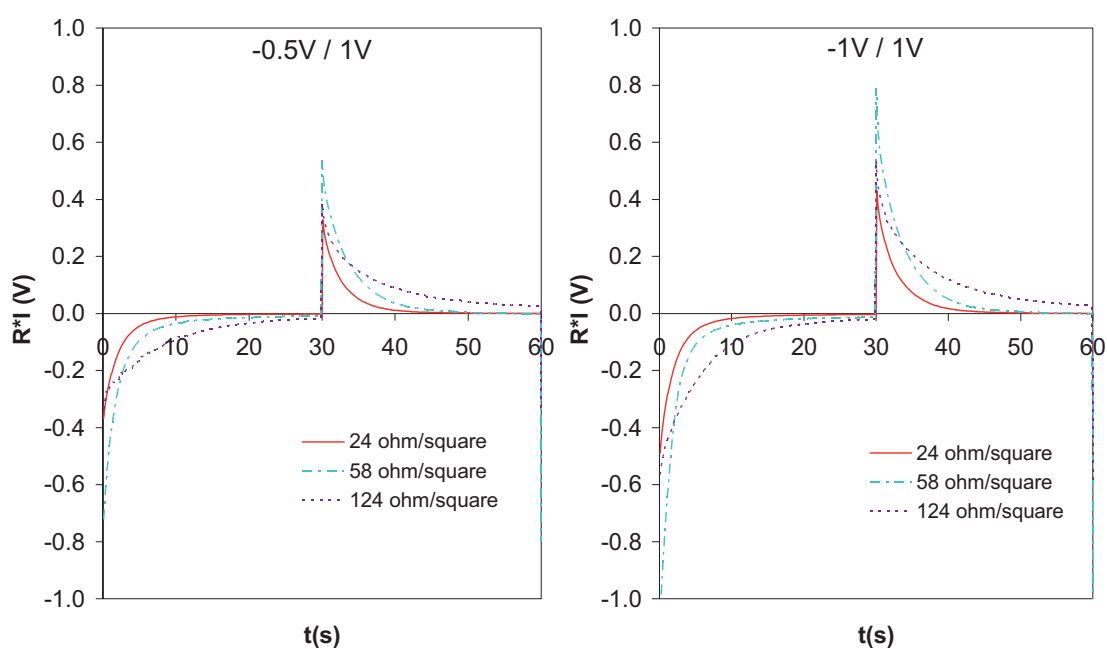

Figure IV.18: Variation of the product of the resistance of the device by the current passing through it with time for EC devices prepared with conducting substrate of sheet resistance 24, 58 and 124 $\Omega/\square$: colouration at -0.5V (left) and at -1.0V (right) for 30 s. followed by bleaching at 1.0V the next 30 s..

The time for 90% of colouration or bleaching has been extracted from Figure IV.16 and are given in Figure IV.19 a) for colouration and Figure IV.19b) for bleaching.
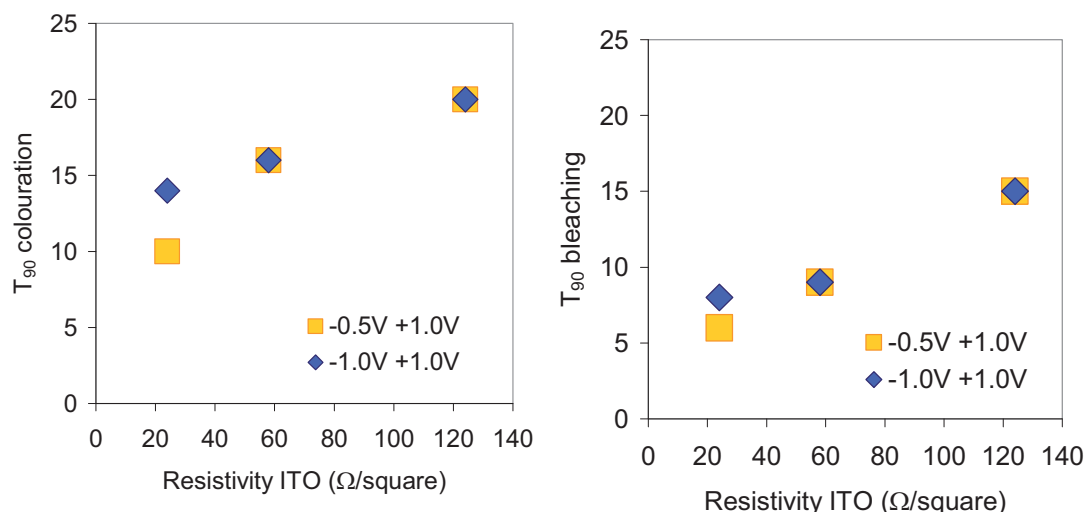
Figure IV.19 : a) Time for 90% of colouration b) Time for 90 % bleaching, of EC devices prepared with conducting substrate of sheet resistance 24, 58 and 124 $\Omega/\square$: colouration at -0.5V and at -1V.0 for 30 s. followed by bleaching at 1.0V the next 30 s.

As the ITO resistivity increases, the colouration and bleaching times slightly increase. The higher resistance of the ITO layer is responsible for a slowing in the kinetics of the devices both in colouration and bleaching. As expected due to the results on PEDOT layers (chapter III), the bleaching is faster than the colouring.

Moreover, for ITO resistivity higher than 58 $\Omega/\square$, the colouration and bleaching times become independent on the potential applied (-0.5V to -1.0V).

IV. 5. *Long term cycling*

Nanoeffects project was dedicated to the preparation of large scale electrochromic devices. At the end of the project, 12*15 cm² active area devices were prepared with an optimized formulation (PEDOT formulation made by INSTM and ISC, BP and ionic liquid based electrolyte formulation by ICMCB) (Figure IV.20).
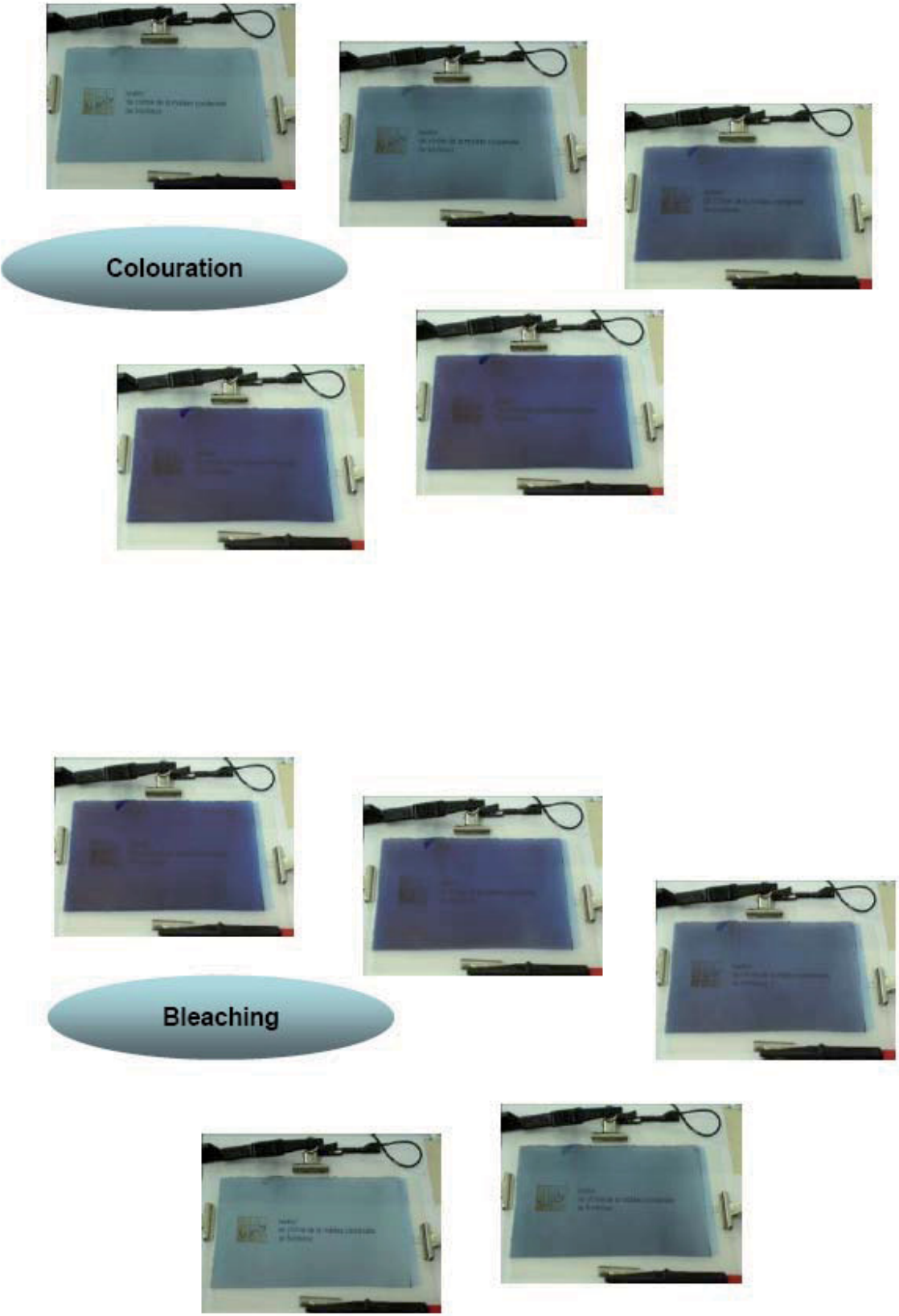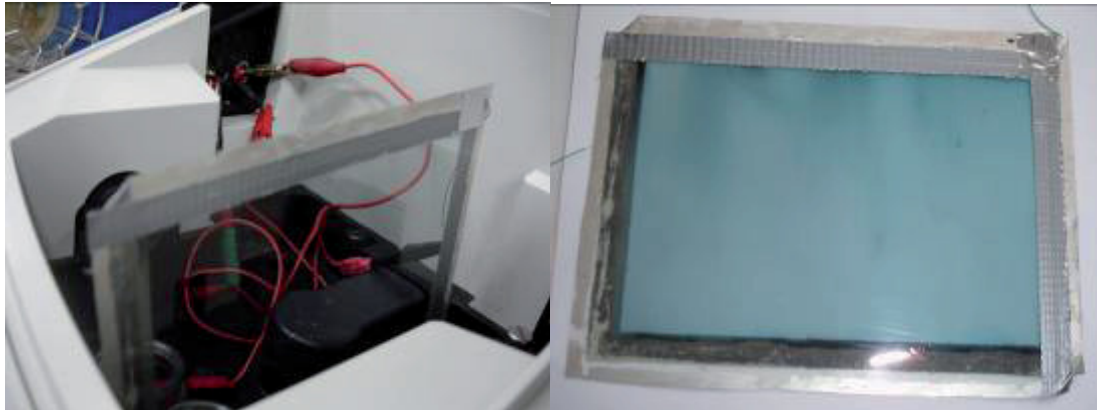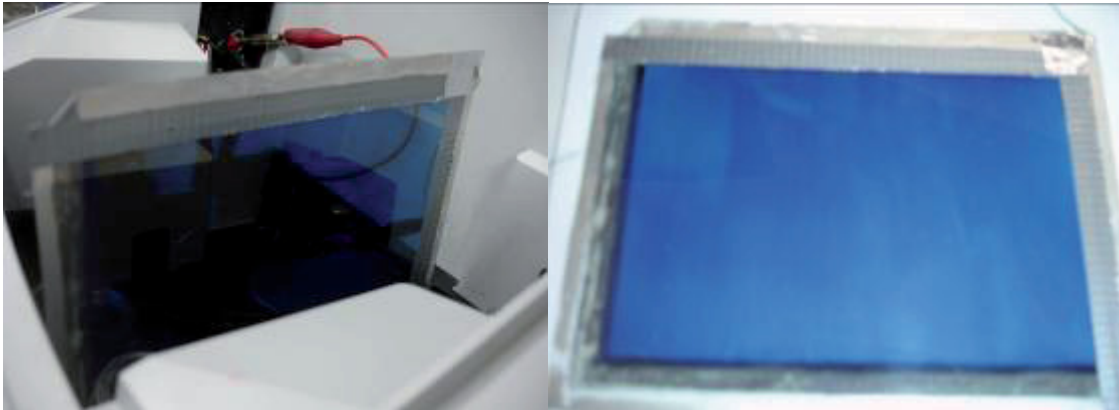
Figure IV.20 : Bleached to fully coloured state of the complete device (and reverse) , showing the control of light shading with potential.

The device has been sealed on the edges with a very resistant scotch tape.
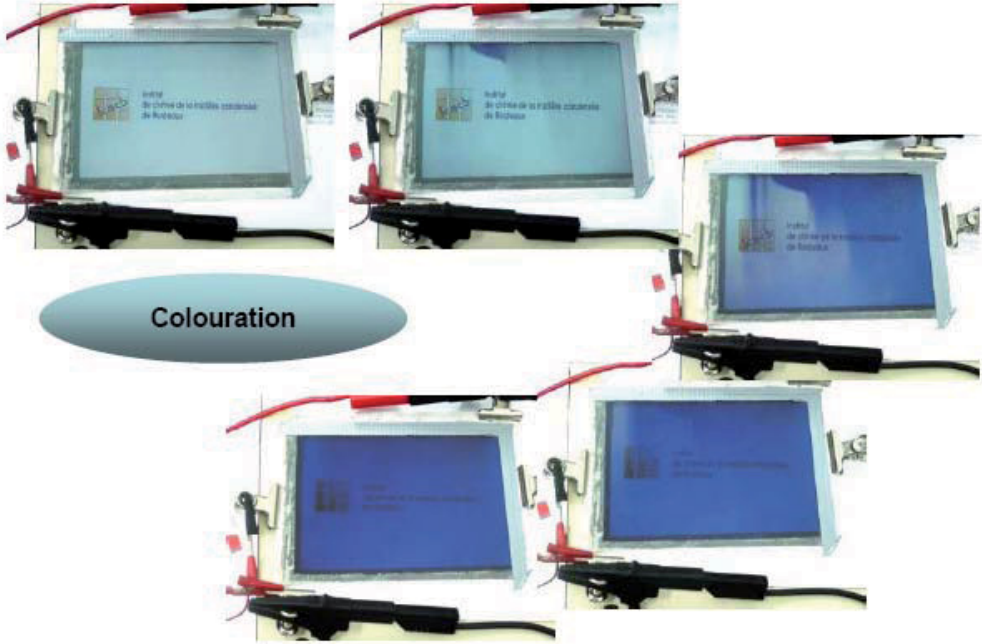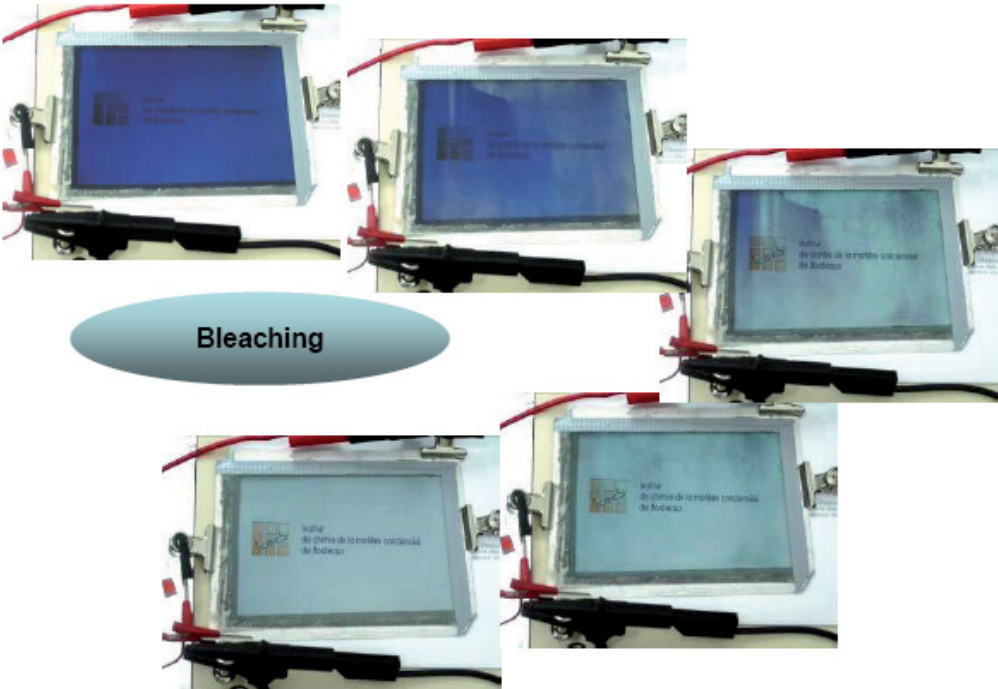

Bleached state

Coloured state

Figure IV.21 : Bleached and coloured state of the complete device, on the left view of the spectrophotometer installation for transmission measurements.

This complete device was scanned over more than 21 000 cycles (average capacity of 1.36 mC/cm²) to check the long term stability on large size area systems (Figure IV.23).
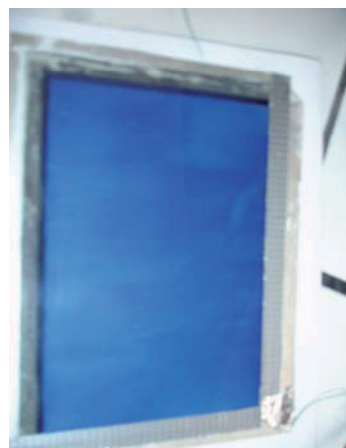
a) Bleached to coloured states after 450 cycles between +1.0V and -1.3V
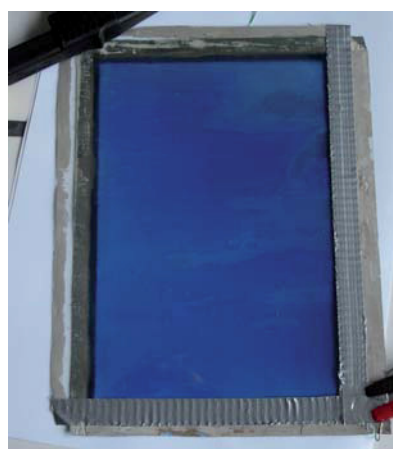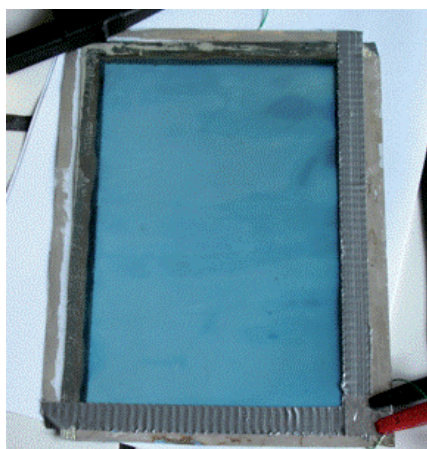

b) Coloured to bleached states after 450 cycles between +1.0V and -1.3V

Figure IV.22 : Back and forth coloration of the complete device, after 450 cycles.

a) Bleached and colored states after 2 600 cycles between +1.0V and -1.3V

b) Bleached and colored states after 21 000 cycles between +1.0V and -1.3V

Figure IV.23 : Bleached and fully coloured state of the complete device, after 2600 and 21 000 cycles.

Some defects are detectable which can be attributed to manual set-up. However chrono-amperometry studies showed the homogeneity and relative stability of such a system with 21000 cycles corresponding to a long term testing of 6 years and 10 switches a day (ophthalmic specifications: 3 years stability) (Figure IV.24).
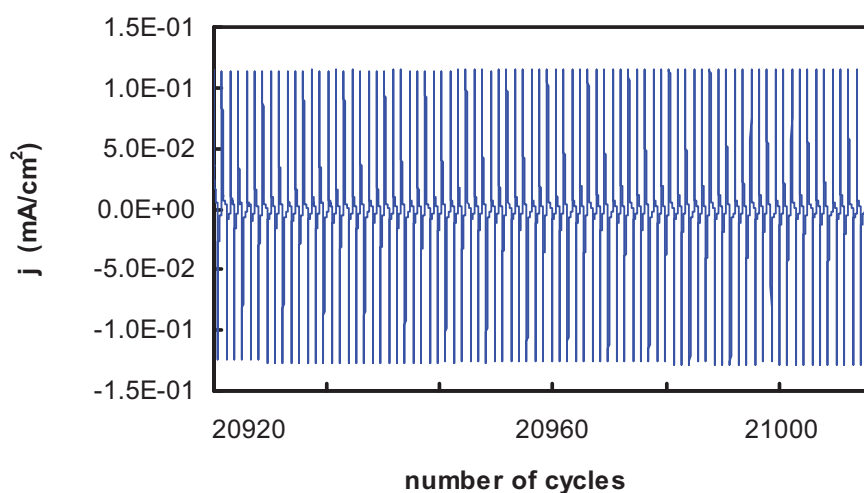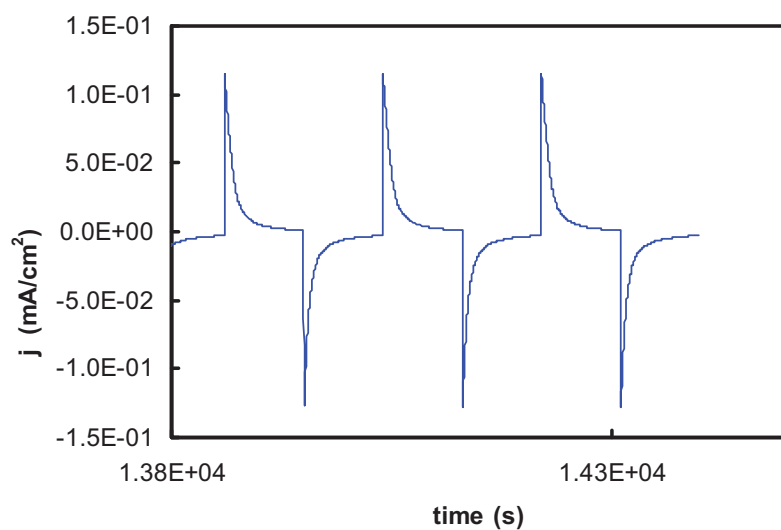
Figure IV.24 : Last chronoamperometric cycles of a large device scan between +1.0V (90s) and -1.3V (90s).

This system exhibited the following visible spectra (Figure IV.25) and coloration efficiencies (Figure IV.26) as well as contrast ratios (Figure IV.27) for cycles n° 1, 450, and 21000.

Figure IV.25: UV-Visible spectra during spectroelectrochemical study of a complete device with 12*15 cm² active area in the 400-800 region as a function of the applied potential. Transmittance measured at -1.3 V for the colouration and +1.0 V for the bleaching after 10, 450 and 21000 cycles.
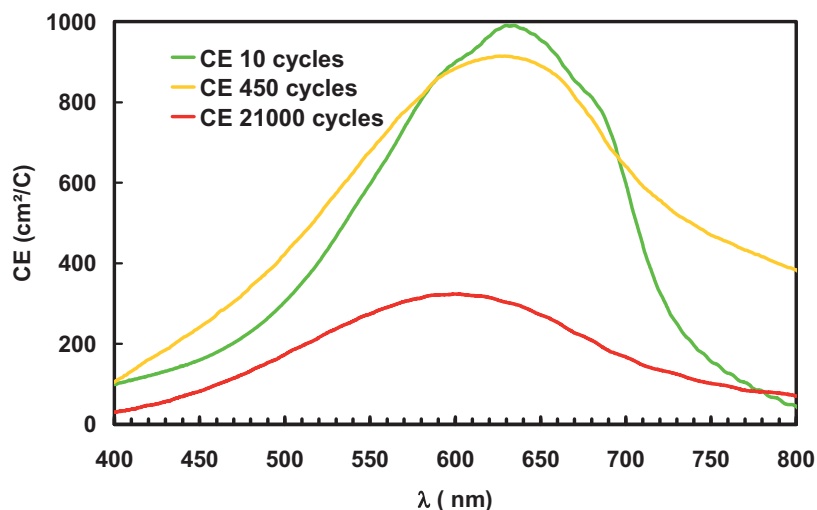
Figure IV.26 : Colouration efficiencies of a complete device with 12*15 cm² active area in the 400-800 region as a function of the applied potential. The absorbance measurement were performed at -1.3 V for the colouration and +1.0 V for the bleaching after 10, 450 and 21000 cycles.

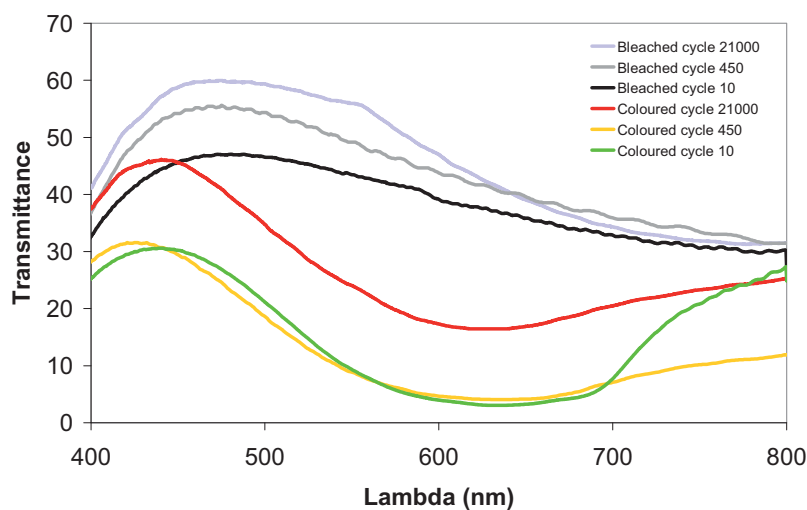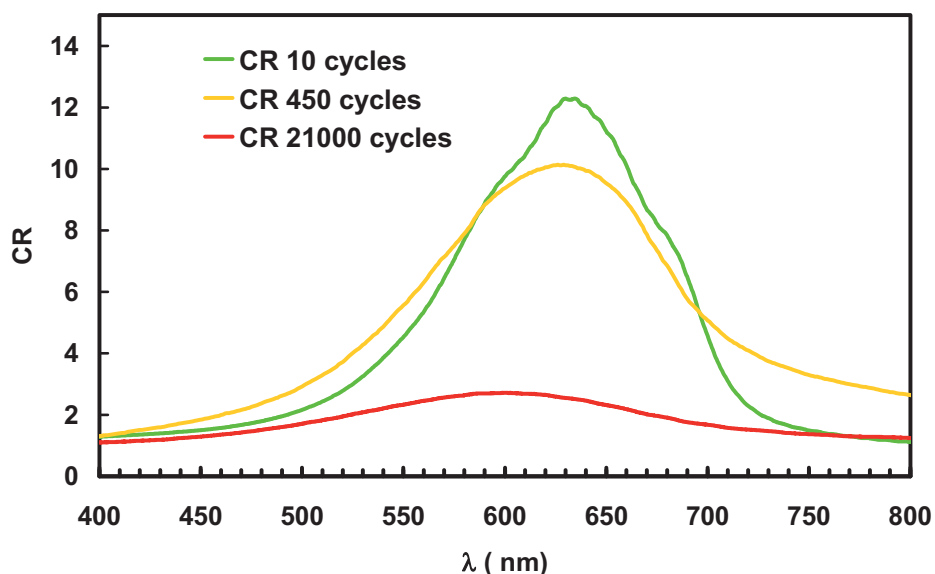Figure IV.27 : Contrast ratio of a complete device with 12*15 cm² active area in the 400-800 region as a function of the applied potential. The absorbance measurement were performed at -1.3 V for the colouration and +1.0 V for the bleaching after 10, 450 and 21000 cycles.

The transmittance remains stable up to 450 cycles in both coloured and bleached states. Then a decrease is observed and after 21000 cycles the system is around four times less efficient than originally. The contrast ratio is directly linked to the transmittance so that its decrease is expected. On the contrary, the colouration efficiency is an intrinsic parameter of the materials, its decrease with the number of cycles shows that electrochemical reactions that consume current without giving any colouration occur. These reactions may come from the entrance of electroactive agents in the device (e.g. water, oxygen …) or from the fact that the

187

PEDOT has shifted to a more oxidized state (no colouration but current consumption as explained in IV.2.1.2).

These devices show rather good properties even though they were prepared manually. The use of industrial processes to prepare the electrochromic films, electrolytic membranes and the full device (for example by roll-to-roll method) would lower the quantities of defaults and increase the life time. Improvements of the sealing would undoubtedly be also very beneficial.

IV. 6. *Conclusion*

The increase in both PMMA ratio and resistivity of the TCO layer has an influence on the spectroelectrochemical properties of the devices. More precisely, the ΔA is decreased in both cases and, concerning the kinetics, whereas PMMA ratio from 30 to 50 % does not have much influence, an increase in ITO resistivity (from 24 to 124 $\Omega/\square$) decreases the kinetics with an increase from 5 s. to 15 s. for bleaching and from 10s. to 20 s. for colouration times.

The devices show rather large decrease in the performances with long term cycling. However, their properties are very promising for lab-scale prepared devices. Their preparation on an industrial scale would lead to huge improvements in the quality of the films, of the interface between the layers and of the sealing that will ensure a much better life time.

The transmittance in the bleached state has been improved thank to modification in the EDOT structure . The use of a colourless counter electrode, such as InHCF, would be also of interest, but could not be tested in full devices.

An optimisation in the whole stack transmittance would also arise from the matching of the optical indexes of the layers, this was not addressed within this project.

General conclusion and perspectives

The aim of the present work was to determine whether ionic liquid based electrolytes could be used in electrochromic devices and which performances were obtained. The studied ionic liquids were 1-butyl-3-methylimidazolium hexa-fluorophosphate (BMIPF$_6$) and 1-butyl-3-methylimidazolium bis (trifluoromethanesulfonyl) imide (BMITFSI) both known to have a rather hydrophobic character. The electrochromic compounds tested were poly(3,4-ethylenedioxythiophene) (PEDOT), Prussian Blue (PB) and indium hexacyanoferrate (InHCF).

BMIPF$_6$ did not match our expectations with regards to device stability due to hydrofluoric acid formation in contact with remaining water in Prussian Blue films (annealing was limited to 70°C because of the used substrate (ITO/Orma)). On the contrary, such problems were not encountered with BMITFSI.

The jellification of the electrolyte was performed with poly (methyl methacrylate) (PMMA). Complete devices were prepared with these jellified electrolytes and PEDOT and PB as electrochromic materials.

Electrolyte formulation

The optimization of the electrolyte formulation concerned the choice of the lithium salt and PMMA concentrations.

Interactions between BMITFSI and PMMA have been highlighted by the strong decrease in ionic mobility of the IL when in contact with PMMA (strong decrease in conductivity). Raman and ATR-IR studies gave more information on the interactions occurring in the BMITFSI/PMMA/LiTFSI electrolytes, by showing that :

- ionic pairs [Li(TFSI)$_2$]$^-$ are formed when LiTFSI is added in BMITFSI
- one lithium cation is linked to 2-3 C=O of the PMMA in PMMA/LiTFSI blends

the addition of PMMA in LiTFSI/BMITFSI liquid electrolytes leads to the destruction of some ionic pairings [Li (TFSI)$_2$]$^-$ due to competition between TFSI and C=O for the complexation of Li$^+$.

These results show the high compatibility of the ionic liquid BMITFSI and the polymer PMMA, still increased with LiTFSI addition. This ensures the stability of the electrolytic membrane (no phase separation).

In liquid LiTFSI/BMITFSI electrolytes, the transference number for lithium is negative. The lithium clusters are attracted by the positive electrode which is rather detrimental to PB

reduction by lithium insertion. This is however not fully limitative since it doesn't prevent the complete devices functioning, lithium clusters reach the negative electrode by diffusion and clusters scission at the electrode give the necessary free lithium ions. Moreover, as soon as PMMA is added (even for ratio as low as 20%), the transference number reaches reasonable value for the use of these electrolytic membranes in electrochromic devices.

The addition of LiTFSI in BMITFSI is mandatory for the functioning of Prussian Blue. This is however responsible for a slight decrease in conductivity. A formulation of 0.03 LiTFSI / 0.97 BMITFSI were shown to be a good compromise for electrochromic functioning.

Electrochromic material deposition and electrochromic properties

The aim of the scan in material preparation methods were to determine which method was the most appropriate for the preparation of large scale films with no defects and high mechanical resistance. The different deposition methods were electrodeposition (PEDOT, PB and InHCF), in-situ polymerization (for PEDOT only) and deposition of polymer dispersion (for PEDOT only). Finally, for the preparation of up to 20*20cm² samples, electrodeposition has been found the most suitable for Prussian Blue and in-situ polymerization for PEDOT films.

PEDOT, Prussian Blue and InHCF were tested in LiTFSI 0.03 / BMITFSI 0.97 liquid electrolytes. Their electrochromic properties did match with the results obtained in the literature in more classical solvents. Modified PEDOT, with better colourlessness in the bleached state, were prepared by partners of the project. We tested them in this electrolyte and obtained also positive results (not presented here). InHCF transparent electrodes are of interest to simplify the preparation of complete devices since the precise matching between the colouration of the two electrodes is not necessary any more, we showed that InHCF can be used in such ionic liquid based electrolytes.

Complete devices

Complete devices were prepared to validate the use of ionic liquid based electrolytes in such electrochromic devices and to have a better knowledge of the influence of different parameters (PMMA content in the electrolyte, substrate conductivity) on the electrochromic

properties. Both an increase in PMMA content (20 to 50%) and an increase of substrate resistivity (24 to 124 $\Omega/\square$) lead to a decrease in ΔA but the kinetics of the device is much more affected by ITO resistivity than PMMA ratio.

Finally, complete devices with a 15*13 cm² active area, a colouration efficiency of 250 cm²/C and switching times of 30s.were obtained. The devices showed a blue colouration. Their long term cycling showed a good stability for the 450 first cycles, a decrease was then observed. Sealing improvements are expected to lead to highly improved stability.

Perspectives

The usefulness of ionic liquid based electrolytes jellified with PMMA for electrochromic devices has been demonstrated, as well as the mechanical and long-term stability of such membranes. The complete devices with PB and PEDOT show interesting electrochromic properties, however the cycling stability is to be improved (100 000 cycles expected for ophthalmic application for example). Working on the sealing is primordial for the long term stability of such electrochemical devices.

Following the positive results obtained during Nanoeffects (high colouration efficiency, low switching times, nearly colourless bleached state and interesting routes to get a neutral colour), the European commission will support the four years Innoshade program mostly dedicated to the improvement of the neutral colour and to the up-scaling of these devices.

APPENDIX

_____

APPENDIX A. Characterization methods.

A. 1. *Electrochemical Impedance Spectroscopy (EIS)*

A. 1. a Basic Aspects

Electrochemical impedance spectroscopy method was initially used by Gerischer et Mehl[1] and Weiniger et Breiter[2] for the study of adsorbed species on electrodes. This method is based on the fact that electrochemical processes occurring at the electrodes (charge transfer, diffusion of species, insertion, etc.) can be modelled using equivalent electrical circuits. When the electrochemical cell is constituted of an electrolyte, sandwiched in between two current collectors, the equivalent circuit can often be averaged in the high frequency domain by a parallel RpCp circuit. Rp represents the average electrolyte resistance from which the overall electrolyte conductivity can be deduced. Rp corresponds to the extrapolation in the low frequency domain of the impedance with the x-axis (annexe).

The impedance of the electrochemical cell can be measured by applying an alternative signal (current or potential) on the electrochemical cell and measuring the associated response (potential or current). By modulating the applied signal frequency from high frequencies to low frequencies, the different electrochemical phenomena from the quickest to the slowest can be scanned. The confrontation between experimental data and model electrical circuits allows determining parameters such as proper resistance, diffusion and charging transfer coefficients. .

The amplitude of the applied signal is chosen small enough to remain in the pseudo-linear behaviour range, so that the response is a signal with the same frequency as the excitation signal; only its phase changes.

In the case of an applied sinusoidal potential signal, given by:

$$E(t) = E_0 \cos(\omega t) \qquad \text{(Eq. 1)}$$

The answer signal will be:

$$I(t) = I_0 \cos(\omega t + \Phi) \qquad \text{(Eq. 2)}$$

The impedance is calculated as the potential over the current intensity:

$$Z(t) = \frac{E(t)}{I(t)} = \frac{E_0 \cos(\omega t)}{I_0 \cos(\omega t + \Phi)} = Z_0 \frac{\cos(\omega t)}{\cos(\omega t + \Phi)} \qquad \text{(Eq. 3)}$$

This can be noted in complex notation:

$$Z(t) = Z' - jZ'' \quad \text{with} \quad Z' = Z_0 \cos\Phi \text{ and } Z'' = Z_0 \sin\Phi \qquad \text{(Eq. 4)}$$

A usual representation of the impedance is the Nyquist's plot, which consists in reporting in the complex plan –Z" as a function of Z'.

The equivalent electrical components for the most common electrochemical process are given below:

- **Solution internal resistance R_p**: takes into account the ions type, their concentration, the temperature and the geometry of the cell. We have reported above that the conductivity of the electrolyte is given by:

$$\sigma = \frac{d}{R_p A}$$

- **Double layer capacity C_{dl}**: it represents the pseudo-capacitor of several Angstroms width which is created at the electrode-electrolyte interface and due to charge accumulation.

- **Charge transfer resistance R_{ct}**: it measures the kinetics of the electronic charge transfer, namely the kinetics of reduction or oxidation of the species at the electrode.

- **Warbürg impedance**: gives information on the ion diffusion through the electrode. For diffusion in an infinite thickness film, it is given by:

$$Z_w(\omega) = \frac{RT}{C\, n^2 F^2 A \sqrt{j\omega D}} \qquad \text{(Eq. 5)}$$

where ω is the pulsation of the signal, R is the ideal gas constant (8.314 Jmol^{-1}K^{-1}), T the temperature in K, C the species concentration in the electrolyte (mol.cm^{-3}), n the number of exchanged electrons, F the Faraday constant (F = 96 500 C), A the active area (cm²) and D the diffusion coefficient of the species (cm^2/s). In the Nyquist diagram, it is represented by a 45° slope.

The Nyquist diagram of an electrolyte sandwiched between two stainless-steel blocking electrodes (for which the Warburg impedance must not be considered,) is given in Figure A.1. The equivalent electrical circuit consists in one resistance Rp, one capacitance Cp associated in parallel (the product Rp Cp being the relaxation time, namely the time required for the mobile species of the electrolyte to jump from one site to the neighbouring equivalent one) and a capacitance Cd associated in series with the parallel Rp-Cp configuration; Cd represents the accumulation of the mobile species in the electrolyte at the blocking electrodes which occurs at low frequencies of the excitation signal. Therefore, the Nyquist plot is

composed of a circle at high frequencies due to the RpCp circuit and a ca pacitive vertical slope at low frequencies (see Figure A.1).
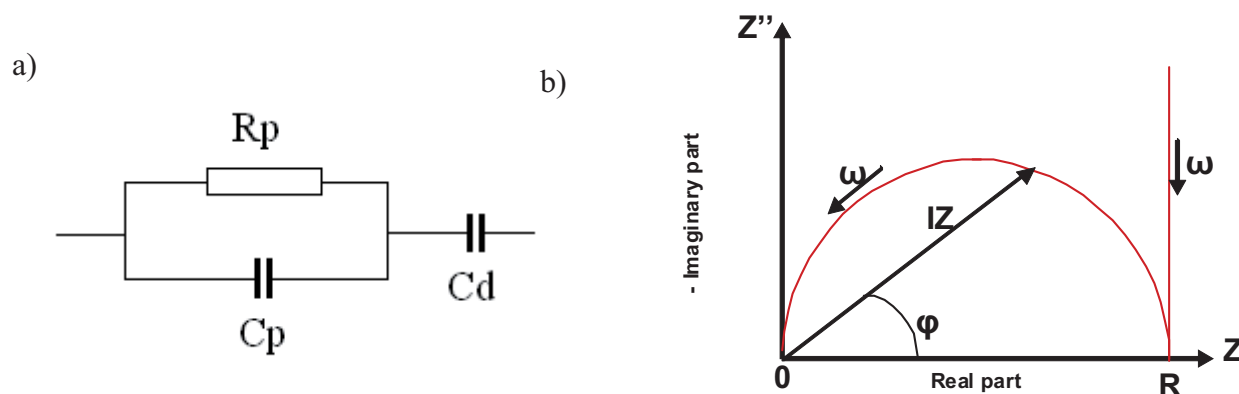
a)

b)

Figure A.1 : RpCp electrical circuit with Cd capacity from blocking electrode (a) and Nyquist plot associated (b)

A. 1. b Technical Aspects

EIS measurements on electrolytes are performed with a HP 4194A Impedance/Gain Phase analyser. The temperature is measured by a platinum resistance thermometer connected to a Keithley 195A digital multimeter. Frequencies range from 100 Hz to 15MHz is scanned by measuring the impedance in 200 points per decades of frequencies with 16 measures for each point. The potential amplitude of the entrance signal is 200 mV, the sample is not polarized ($E_{mean} = 0V$).

The electrolyte is placed in a two electrode cell, the electrodes being metallic blocking electrodes.

In the case of liquid electrolytes, the liquid is placed in a cell made of two pieces of brass of diameter 2 cm with an internal diameter of 1.8 cm. A constant space of 500 microns in between the two electrodes is ensured by a rigid PTFE O-ring (cf. Figure A.2a)).

In the case of membranes, the electrolyte solution is deposited by doctor blade on the stainless steal plate. A PTFE O-ring (t = 100 μm, external diameter = 2 cm, internal diameter = 1.8 cm) is placed on top of the membrane to avoid short circuits between the two metallic electrodes. After butanone evaporation, the second stainless steel plate is placed on top of the electrolyte. The assembly is then heated at 70°C under vacuum until being stuck together.

The current collector is made of brass; a system with a spring ensures a good electrical contact between the cell and the current collector.
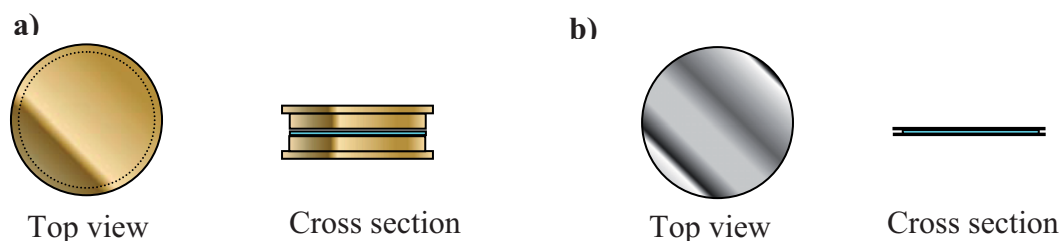
Figure A.2: Schematic view of the two electrode cell used for EIS measurement for liquid electrolytes (a) and membranes (b)

A. 2. Nuclear Magnetic Resonance spectroscopy (NMR)

A. 2. a Basic aspects

When placed in a magnetic field of strength B, a nucleus with a non zero net spin can absorb a photon. The frequency υ of the absorbed photon depends on the gyromagnetic ratio γ of the nucleus.

$$\upsilon = \gamma\ B \qquad \text{(Eq. 6)}$$

NMR can only be performed if the natural abundance and gyromagnetic ratio of the studied isotope abundance are high enough to be detected. The nuclei of interest in this study are listed below.

Nuclei	Unpaired protons	Unpaired neutrons	Net Spin	Abundance	γ (Hz/G)
^{1}H	1	0	$^1/_2$	99.99	4258
^{19}F	1	0	$^1/_2$	100	4008
^{7}Li	3	4	$^3/_2$	92.41	1656
^{13}C	0	1	$^1/_2$	1.07	1071

The particle can undergo a transition between two energy states by absorption of the photon. The energy E of a photon is related to its frequency υ by Plank's constant (h= 6.626 .10^{-34} J s).

$$E = h\ \upsilon \qquad \text{(Eq. 7)}$$

In NMR, the quantity υ is called the resonance frequency or Larmor frequency. The energy of the photon to cause a transition has to be equal to the difference of energy between the two spin states, before and after transition, i.e.

$$E = h \, \gamma \, B \qquad \text{(Eq. 8)}$$

The proportions of nuclei and in the upper level (N^-) and in the lower energy level (N^+) are given by the Boltzmann statistic:

$$N^-/N^+ = e^{-E/kT} \qquad \text{(Eq. 9)}$$

where E is the energy difference between the two spin states, k is the Boltzmann constant (k = $1.3805 \cdot 10^{-23}$ J K^{-1}), and T the temperature in Kelvin.

The NMR signal results both from the transition from lower energy level to upper energy level and from the reverse transition. The NMR is a sensitive enough spectroscopy to be able to detect very small population differences between these states.

, The magnetic field B experimented by the nucleus depends on its chemical surroundings

$$B = B_0 - \sigma \, B_0 = (1 - \sigma) \, B_0 \qquad \text{(Eq. 10)}$$

where σ is the shielding constant.

Electron donor groups induce a high concentration of electron around the nucleus, a magnetic field opposed to the applied field is generated which causes a shielding of the signal (shift towards low frequencies). On the contrary, electron withdrawing groups induce a deshielding. An anisotropy (preferred conformation, double bonds…) can also induce shielding and deshielding zones in the molecule.

A. 2. b   Mutual diffusion, self-diffusion

The perpetual and irregular movement, referred as Brownian motion of the particles, first observed by Robert Brown in 1827 and governed by Fick's empiric laws demonstrated later on by Albert Einstein, is the basis mechanism for diffusion[3]. Two kinds of diffusion are to be considered: self-diffusion and mutual diffusion. Diffusion is a process of transport driven by an external force field that can come for example from a concentration, temperature

or pressure gradient. Self-diffusion characterizes the random walk of the particles in a liquid at the thermodynamic equilibrium; the particles have an equal opportunity of taking up any point in the total space of the liquid. On the contrary mutual diffusion is a measure of the transport of matter occurring i.e. when the thermodynamic equilibrium of the solution is not reached, upon concentration gradient for example. From a practical point of view, mutual diffusion, also known as chemical diffusion, interdiffusion or transport diffusion, is the most important effect in the description of the transport of matter in many physical and chemical processes.

Experimentally, the value of D is determined by the slope of a plot $\ln(S/S_{g=0})$ versus $- \gamma^2 g^2 \delta^2(\Delta- \delta/3)$ via PGSE experiments. The PGSE technique is described in the manuscript.

A. 2. c PGSE: technical aspects

The pulse parameters are: Δ=150ms and δ=10ms for F, and 5 ms for H and 15 ms for Li. For Li and H PGSE-NMR, a 400 MHz JEOL (from CESAMO laboratory) and … for (from IECB laboratory).

The use of an external reference was mandatory since the diffusion coefficient measurements are sensitive to the presence of other species added in the studied system (changes in viscosity, interactions…). D_2O/MeOD (v:v 50:50) was placed in a sealed tube and was used as a reference.

Liquid electrolytes were placed directly in the NMR tube in addition to the sealed tube with MeOH-D_2O reference in it.

For membrane electrolytes, the membrane solution in butanone were placed in the NMR tube and butanone was then slowly evaporated (T increased slowly from 40°C to 70°C and then put under vacuum). The reference tube were then placed in the membrane in the NMR-tube, if necessary the membrane solution was heated up.

A. 3. Raman and ATR-IR spectroscopy

For the study of the interactions taking place inside the liquid and membrane electrolytes, Raman and Attenuated Reflectance Infra-Red spectroscopies have been used. Raman spectroscopy takes information from diffracted light, IR spectroscopy from absorbed light. The vibrational transitions observed in infrared (IR) and Raman spectra appear in the 10^4-10^2 cm^{-1} region. They generally originate from vibrations of nuclei constituting the molecule. According to quantum mechanics, a vibration is IR-active if the dipole moment is changed during the vibration and is Raman-active if the polarisability is changed during the vibration. In general vibrations are strong in Raman if the bond is covalent (C≡C, C=C, P=S, S-S) and strong in IR if it is ionic (O-H, N-H). Inspection of IR and Raman spectra for a large number of compounds showed that a common group exhibits its group vibrations in the same region regardless of the rest of the molecule. These group frequencies have been measured for a number of inorganic and organic compounds, giving rise to empirical spectroscopic tables.

A. 3. a Raman spectroscopy

A.3.a.1) Basic aspects

The phenomenon Raman has been discovered by Sir Chandrasekhra Raman in 1928.

Raman spectroscopy consists in irradiating a sample with an intense laser beam in the UV or Visible region (υ_0). The resulting scattered light is of two types:

- the Rayleigh scattering, strong, at υ_0
- the Raman scattering, weak (10^{-5} of the incident beam), at $\upsilon_{0 \pm} \upsilon_m$ where υ_m is a vibrational frequency of the molecule.

The incident light (electromagnetic wave) has an electric field strength (E) that fluctuates with time (t) according to the equation:

$$E = E_0 \cos (2\pi \, \upsilon_0 \, t) \qquad\qquad (Eq. \; 11)$$

where E_0 is the vibrational amplitude.

The irradiation by this light, produce an electric dipole moment. For a diatomic molecule the expression of this dipole moment P is:

$$P = \alpha \, E = \alpha \, E_0 \cos (2\pi.\upsilon_0 \, t) \qquad\qquad (Eq. \; 12)$$

where α is the polarizability.

If the molecule is vibrating with a frequency υ_m, the nuclear displacement q is written:

$$q = q_o \cos 2\pi . v_m t \qquad \text{(Eq. 13)}$$

For small amplitude of displacement the polarisability is a linear function of the displacement, so:

$$\alpha = \alpha_0 + \left(\frac{\partial \alpha}{\partial q} \right)_0 q_0 + ... \qquad \text{(Eq. 14)}$$

The electric dipole for the diatomic molecule is given by:

$$P = \alpha_0 E_0 \cos 2\pi v_0 t + \left(\frac{\partial \alpha}{\partial q} \right)_0 q_0 E_0 \cos 2\pi v_0 t \cos 2\pi v_m t \qquad \text{(Eq. 15)}$$

$$P = \alpha_0 E_0 \cos 2\pi v_0 t + \frac{1}{2} \left(\frac{\partial \alpha}{\partial q} \right)_0 q_0 E_0 \left[\cos\{2\pi(v_0 + v_m)t\} + \cos\{2\pi(v_0 - v_m)t\} \right] \qquad \text{(Eq. 16)}$$

The first term represents the dipole radiation at frequency v_0 (Rayleigh scattering), while the second term corresponds to the Raman inelastic light scattering of frequency $v_0 + v_m$ (anti-Stokes) and $v_0 - v_m$ (Stokes). The population at $v=0$ (ground state) is much larger than that at $v=1$ (first excited level) (Maxwell-Boltzmann distribution law) so that the Stokes intensity is higher than the Anti-Stokes one under normal conditions (see Figure A.3).
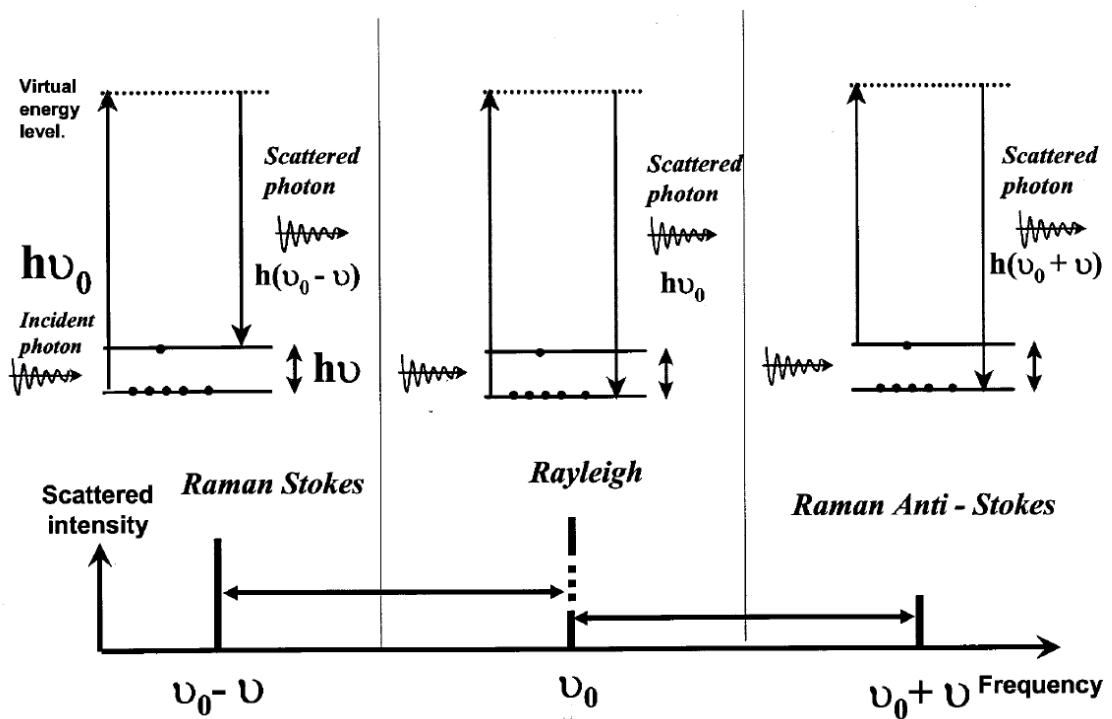

Figure A.3: Rayleigh, Stokes and Anti-Stokes scattering

The Raman technique is non invasive and non destructive, and needs only a small amount of compound since the probe diameter is about 1 micron.

But one has to be careful on the facts that the use of a powerful laser source may cause local heating or photodecomposition of the studied material and that some compound fluoresce when irradiated by a laser beam which disturb the spectra collection.

A.3.a.2) Technical aspects

Raman spectra were recorded, as previously described[4], at room temperature with a Labram 1B Jobin-Yvon spectrometer, an incident wavelength of 632.8 nm and a resolution of 3 cm^{-1}.

Under those conditions no fluorescence were detected for our materials.

A. 3. b IR spectroscopy

A.3.b.1) IR spectroscopy: basic aspects

By infrared spectroscopy, the absorption of infrared light by the sample as a function of the frequency is measured. The energy absorbed by the molecule at each vibration transition is given by:

$$\Delta E = h\upsilon \qquad (Eq. 17)$$

The intensity of IR absorption is governed by the Beer-Lambert law:

$$I = I_0\, e^{-\varepsilon c d} \qquad (Eq. 18)$$

A.3.b.2) Attenuated Total Reflectance (ATR) - FTIR spectroscopy

One of the strength of the IR technique is the possibility to analyse a wide range of solid, liquid or gas. The use of Attenuated Total Reflectance device is very beneficial especially for thin films. The signal is enhanced due to IR beam multiple reflections on the sample.
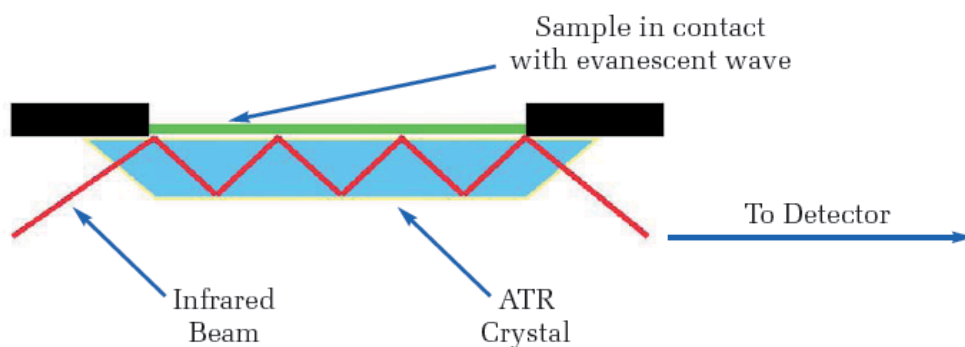
Figure A.4 : Total internal reflection at the interface between the ATR crystal and the sample. Depth of penetration of the evanescent wave is approximately 1 μm

A.3.b.3) ATR-IR: technical aspects

The membrane solution is deposited on a stainless steal plate. The butanone is evaporated by heating at 70°C under vacuum for minimum 8h. Some butanone remained so that the experiments were remade with dichloromethane instead of butanone. The membranes are transferred into a Linkam TMSG600 stage flushed with argon and equipped with a glass window in order to remain in an air and moisture free atmosphere.

The ATR-IR spectra are recorded using a Nicolet Nexus spectrometer with a resolution of 4 cm^{-1} and a single reflection diamond ATR system (Specac). Several spectra are accumulated; they are limited to ~600 cm^{-1} at low wave numbers by the diamond transparency. No correction of the wavelength on the penetration depth is applied because the quantitative measurements are performed on very narrow spectral regions.

A. 4. UV-Visible spectroscopy

The UV-Visible spectra of the membranes, sandwiched between two transparent substrates, were measured between 300 and 1100 nm with a UV-Vis-NIR spectrophotometer CARY / 5E with a resolution of 1 nm and a speed of 200 nm/min . The substrates were either glass or FTO/glass.

The membrane in solution in the co-solvent was deposited on one substrate. Once the co-solvent was evaporated (by heating at 70°C under vacuum), the second substrate was placed on top of the membrane; then, a second heating step (70°C under vaccum) was performed, without intentionally pressing, until the two glass plates were stuck together.

A. 5. X-Ray diffraction

XRD measurements are performed with a PAN analytical X'Pert MPD with Bragg-Bentano geometry from 5 to 80° in two-theta, the resolution is of 0.02. The detector is an X'Celerator. The acquisition time is 30 minutes / diagram.

The membrane solution is cast on the aluminium sample holder and the co-solvent is evaporated.

A. 6. Differential Scanning Calorimetry

DSC measurements are performed with a ThermoAnalysis DSC Q100 at the LCPO laboratory.

About 10 mg of the dried membrane is placed in an aluminium sample holder. The reference is an empty sample holder. The samples are quenched at -150°C and then heated up to 100°C at a heating rate of 10°C/min.

APPENDIX B. Conductivity of solutions of salt in molecular solvents

The addition of salts in ionic liquids such as BMITFSI and BMIPF6 leads to a decrease in the ionic conductivity of the mixture as described in the manuscript.

The general behaviour in of addition of lithium salt in molecular solvent mixtures is given here for comparison (see Figure B.1). The global conductivity first increases while increasing the amount of the salt, as the amount of free ions increases. However, as the ion concentration increases, the viscosity also increase and the ions dissociation becomes more difficult. The conductivity reaches a maximum and then decreases with a further increase in the salt concentration[5]
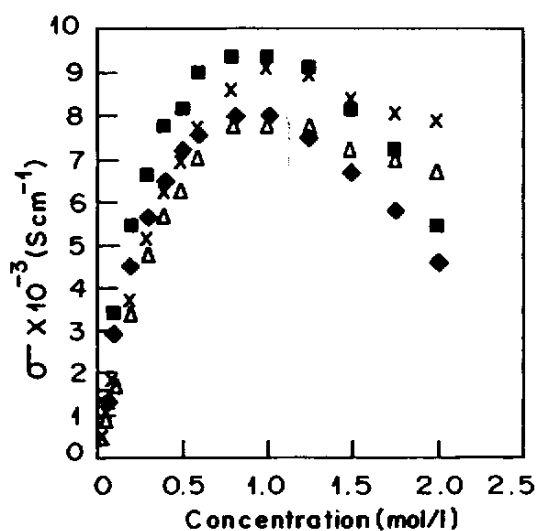

Figure B.1 : Evolution of the conductivity at 25°C as a function of LiClO$_4$ and LiN(CF$_3$SO$_2$)$_2$ concentration in PC($\blacklozenge$,Δ) and PC+EC($\blacksquare$, ×), respectively. Reprinted from reference 5

APPENDIX C. BMIPF$_6$

C. 1. Thermo-mechanical characterisation

C. 1. a DSC measurements

Differential Scanning Calorimetry measurements were also performed on BMIPF$_6$ based electrolytic membranes.

C.1.a.1)   Effect of the PMMA addition in BMIPF$_6$/LiTFSI/ PMMA membranes

The DSC diagrams for 10 to 40 wt% of PMMA in a LiTFSI in BMITFSI molar fraction x=0.04 are given on Figure C.1.
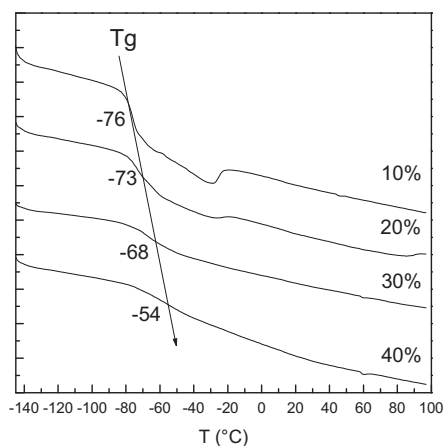

Figure C.1 : Evolution of the DSC curves with increasing PMMA wt% from 10 to 40 in xLiTFSI/(1-x)BMIPF$_6$ x = 0.04.

C.1.a.2)   Effect of the LiTFSI addition in BMIPF$_6$/LiTFSI/PMMA membranes

The LiTFSI ratios were changed from 0.01 to 0.04 and PMMA wt% varied from 0 to 40%. The DSC diagram with increasing LiTFSI concentration at fixed PMMA ratio are very similar to those of BMITFSI based membranes and present only one glass transition. The evolution of the glass transition with LiTFSI concentration is very small and within the experimental error as shown in Figure C.2.
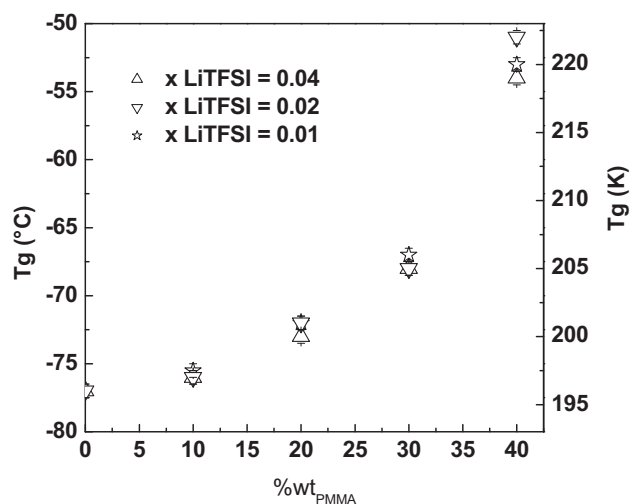
Figure C.2: Evolution of the glass transition temperature of the membranes containing $x = 0.01$ to 0.04 LiTFSI in BMIPF$_6$ with respect to the PMMA weight percentage (from 0 to 40%).

The variation is slow up to 40% and follows the same trends as for the LiTFSI/BMITFSI system.

C. 2. *Ionic conductivity of the electrolytes*

Electrochemical Impedance Spectroscopy (EIS is used to measure the overall conductivity of a of the electrolytic media, whatever its state: liquid, gel or membrane. This can be performed at different temperatures and gives rise to thermodynamic characteristics of the system. The data presented here concerns the LiTFSI/BITFSI/PMMA membrane.

The ionic conductivities will be presented for the following systems:

- liquid electrolytes:
    - BMIPF$_6$ with x $_{LiTFSI}$ = 0.002, 0.01, 0.02
- membrane electrolytes :
    - BMIPF$_6$ / PMMA (0, 30, 40 wt%)
    - BMIPF$_6$ / x $_{LiTFSI}$ = 0.01, 0.02, 0.04 / PMMA (20, 30, 40 wt%)
    - BMIPF$_6$ / x $_{LiTFSI}$= 0.002 / PMMA (0, 20, 30, 40 wt%)

C. 2. a) Ionic conductivities of liquid ionic liquid based electrolytes

The measurements have been performed under moisture free atmosphere in the 20°C to 65°C temperature range. LiTFSI molar fractions from 0.002 to 0.02 have been tested. The dependence of the ionic conductivity on the LiTFSI molar fraction is given in Figure C.3.
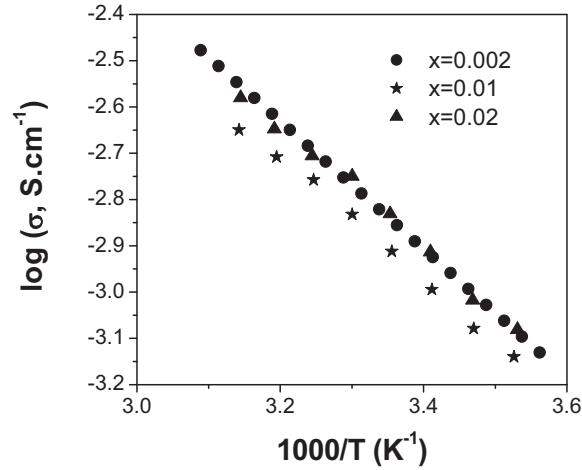

Figure C.3 : Temperature dependence of the conductivity σ in the range -30°C - +60°C for BMIPF$_6$ solutions with LiTFSI molar fractions: ● 0.002 ; ★ 0.01 ; ▲ 0.02.

The ionic conductivity of pure BMIPF$_6$ is around 3.77 10^{-3} S.cm^{-1} at RT. As the lithium salt concentration increases, the ionic conductivity slightly decreases however the differences are rather low and maybe in the experimental error since the Li salt ratio remained low (Table C.1).

x LiTFSI (molar ratio)	Tg (°C)	Tg (K)	σ (S.cm^{-1}) T=30°C	σ_0 (S.cm^{-1})	B (K)	T$_0$ (K) (Tg-50)	R²
0	-77	196	0.00377	0.31	795	146	0.999
0.002	-77	196	0.00175	0.27	772	146	0.998
0.01	-77	196	0.00117	0.21	765	146	0.999
0.02	-77	196	0.00147	0.2	757	146	0.999

Table C.1: Conductivity data for BMIPF$_6$ with various amounts of LiTFSI, Tg values are deduced from DSC measurements.

C. 2. b) Ionic conductivities of BMIPF$_6$/PMMA membranes

We undertook a study of the ionic conductivity of pure BMIPF$_6$/ PMMA membranes in which no lithium salt had been added (Figure C.4) to compare with the conductivity of the pure BMITFSI.
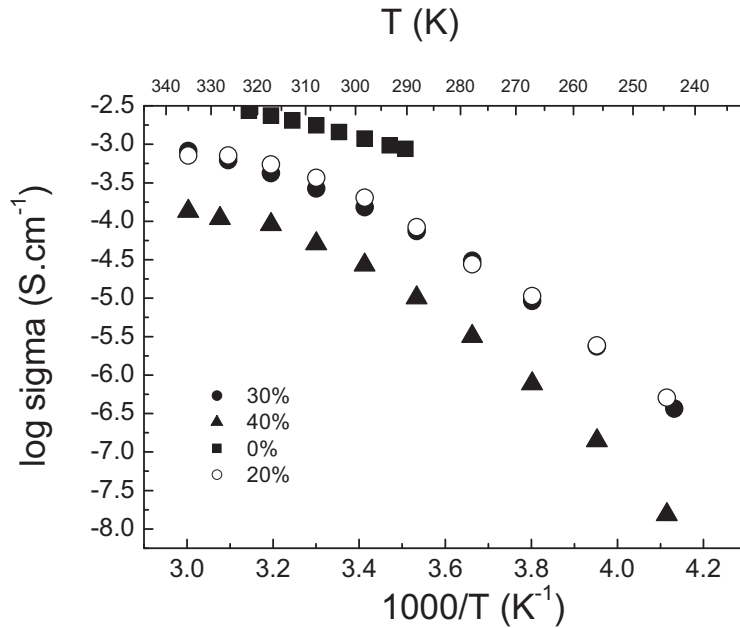

Figure C.4 : Temperature dependence of the conductivity σ for pure BMIPF$_6$ electrolytes with PMMA wt%: ■ 0%; o: 20%, ● 30%; ▲ 40%.

% PMMA	Ionic liquid	x LiTFSI	Tg (K)	σ (S.cm^{-1}) T=30°C	σ membrane / σ liquid (%)	σ$_0$ (S.cm^{-1})	B(K)	T$_0$ (K)	R²
0	BMIPF$_6$	0	196	0.00377	100	0.31	795	146	0.999
20	BMIPF$_6$	0	201	0.00037	9.8	8.76	1548	151	0.995
30	BMIPF$_6$	0	205	0.00027	7.1	1.93	1328	155	0.997
40	BMIPF$_6$	0	222	0.00005	1.3	1.13	1335	172	0.999

Table C.2: Conductivity of ionic liquid jellified by PMMA, ratio σ $_{membrane}$/σ $_{liquid}$, VTF data : σ$_0$, B, T$_0$

The conductivity decreases with increasing PMMA ratios as expected. The charge carriers number shows by its variation the effect of charge separation of the PMMA as

observed for the BMITFSI case. The energy of activation increases characterizing the interaction in between the polymer and the ionic liquid (Table C.2) (Figure C.5).
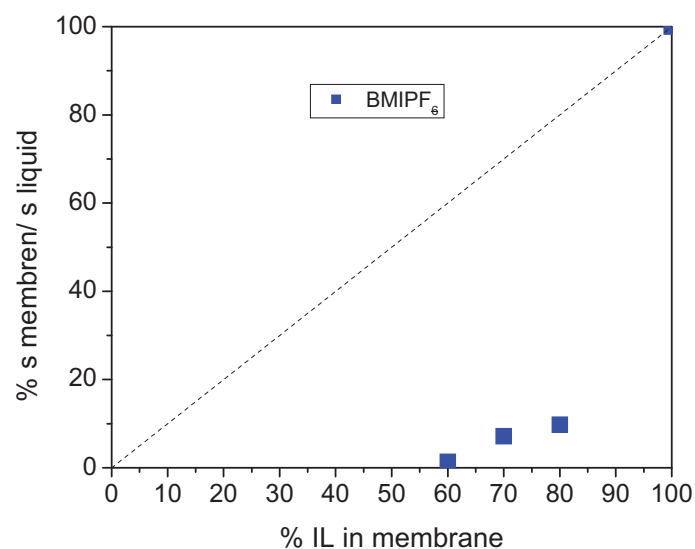

Figure C.5: Evolution of $\sigma_{membrane}/\sigma_{liquid}$ as compared to the wt% of liquid in the membrane

C. 2. c) Ionic conductivities of LiTFSI/BMIPF$_6$/PMMA membranes

C.2.c.1) Influence of LiTFSI concentration

BMIPF$_6$/LiTFSI systems have only be studied for low LiTFSI molar ratio (x_{LiTFSI} from 0 to 0.04), due to LiTFSI low dissolution in BMIPF$_6$. In these conditions, no influence of the LiTFSI concentration over the imposed range (due to the lithium salt insolubility) on the ionic conductivity is observed for PMMA from 20 to 40wt % as can be seen on Figure C.6, Figure C.7and Figure C.8.
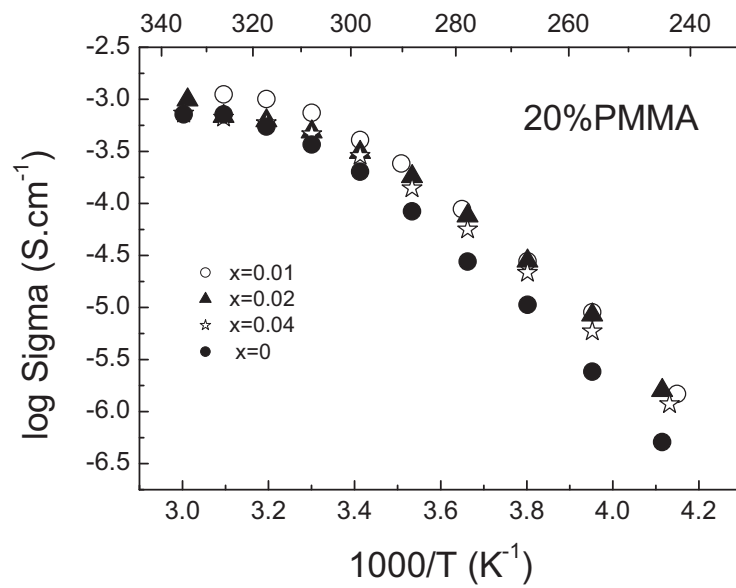
Figure C.6: Temperature dependence of the ionic conductivity σ for BMIPF$_6$ electrolytes with 20 wt% PMMA and LiTFSI molar ratio: ● 0.00, ○ 0.01, ▲ 0.02, ☆ 0.04.
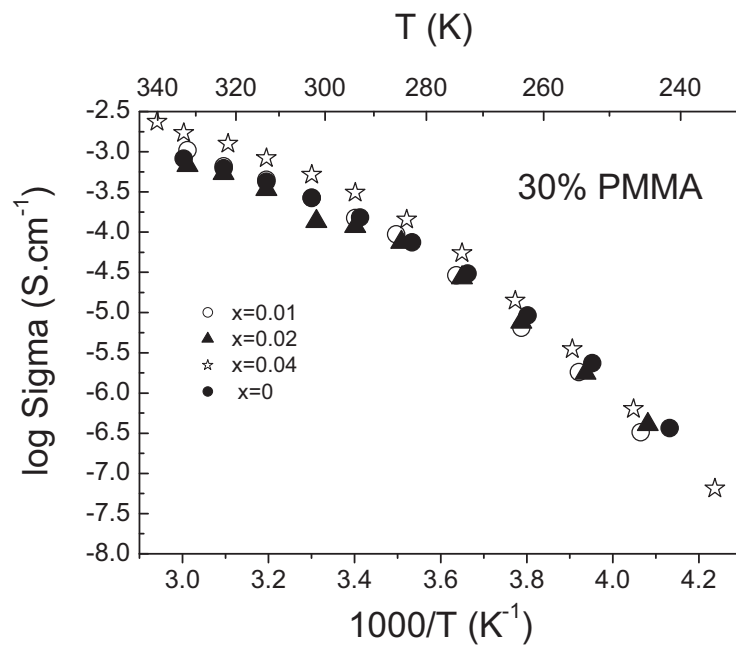

Figure C.7: Temperature dependence of the ionic conductivity σ for BMIPF$_6$ electrolytes with 30wt% PMMA and LiTFSI molar ratio: ● 0.00, ○ 0.01, ▲ 0.02, ☆ 0.04
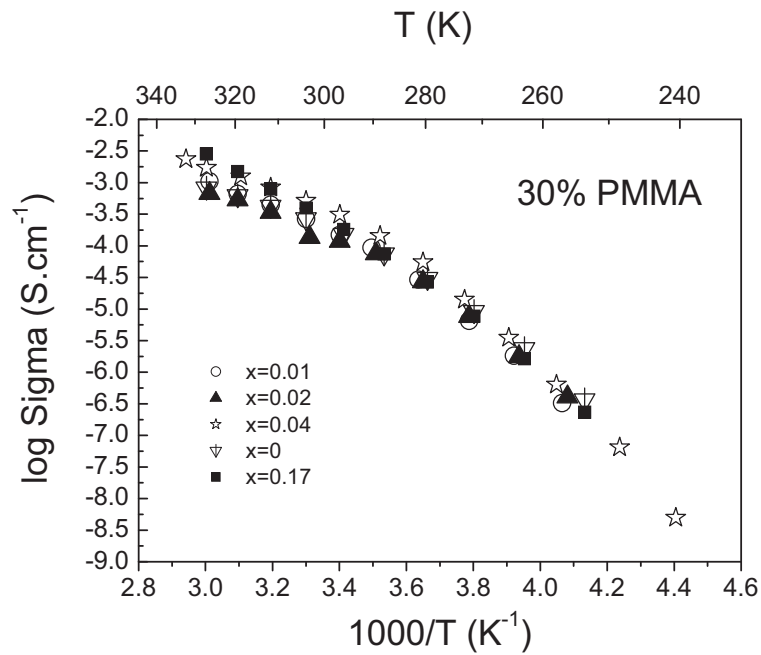
Figure C.8 : Temperature dependence of the ionic conductivity σ for BMIPF$_6$ electrolytes with 40wt% PMMA and LiTFSI molar ratio: ● 0.00,○ 0.01, ▲ 0.02, ☆ 0.04
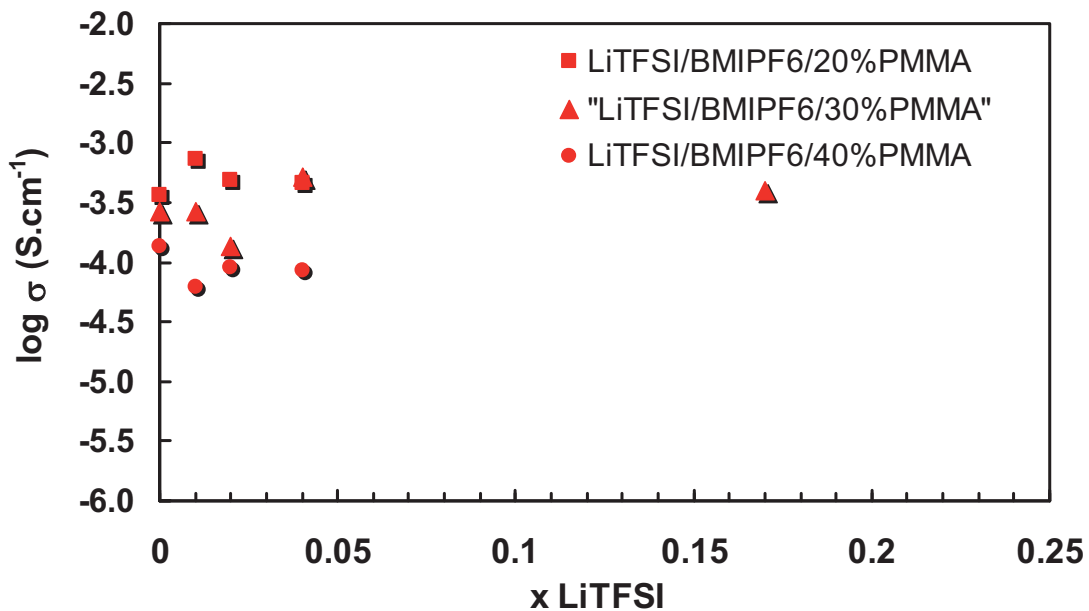

Figure C.9: Evolution of the ionic conductivity of the BMIPF6/PMMA membranes with the molar ratio of LiTFSI at 20 °C of:, ■ BMITFSI + 20 wt% PMMA, ▲ BMITFSI + 30 wt% PMMA; ●BMITFSI + 40 wt% PMMA.

C.2.c.2) Influence of PMMA ratios

The influence of PMMA ratio is presented for the membranes with x_{LiTFSI}= 0.01 in BMITFSI (Figure C.10). The same evolutions are observed for different x_{LiTFSI} ratios, results are gathered in Table C.3.
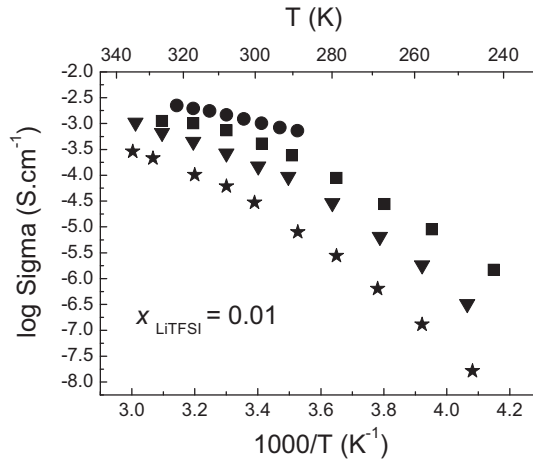

Figure C.10: Temperature dependence of the ionic conductivity σ for $BMIPF_6$ electrolytes with LiTFSI molar ratio of 0.01 and PMMA wt%: ● 0%; ■ 20%; ▼ 30%; ★ 40%

				X				
% PMMA	Ionic Liquid	x_{LiTFSI}	T_g	σ (S.cm^{-1}) T=30°C	$σ_0$	B	To	R²
0	$BMIPF_6$	0.01	196	0.00117	0.21	765	146	0.999
20	$BMIPF_6$	0.01	201	0.00037	5.7	1377	151	0.999
30	$BMIPF_6$	0.01	205	0.000265	6.54	1506	156	0.999
40	$BMIPF_6$	0.01	222	0.0000611	1.31	1334	170	0.999
0	$BMIPF_6$	0.02	196	0.00147	0.2	757	146	0.999
20	$BMIPF_6$	0.02	201	0.00037	1.52	1229	151	0.999
30	$BMIPF_6$	0.02	205	0.0001352	6.54	1360	156	0.999
40	$BMIPF_6$	0.02	222	0.0000933	2.11	1376	170	0.999
20	$BMIPF_6$	0.04	201	0.00037	3.18	1353	151	0.999
30	$BMIPF_6$	0.04	205	0.0005176	8.00	1446	156	0.993
40	$BMIPF_6$	0.04	222	0.00002089	2.69	1364	170	0.999
30	$BMIPF_6$	0.17	205	0.0003963	19.49	1593	156	0.999

Table C.3: Conductivity of LiTFSI/$BMIPF_6$ jellified by various PMMA ratios, VTF data: $σ_0$, B, T_0 for x = 0.01.

APPENDIX D. PMMA tacticity

Tacticity (from the Greek 'taktikos': relating to order) is the relative stereochemistry of adjacent chiral centres within a macromolecule6. The regularity of the macromolecular structure influences the degree to which it has crystalline or amorphous long range order. The knowledge of the tacticity of a polymer helps understanding for example the mechanical properties of a polymer or the way it interacts with other molecules or solvent.

Two adjacent structural units in a macromolecule constitute a diad; a diad can be *meso* (same conformation of the asymmetric centers) or *racemo* (opposite conformation of the two asymmetric centres) as shown in
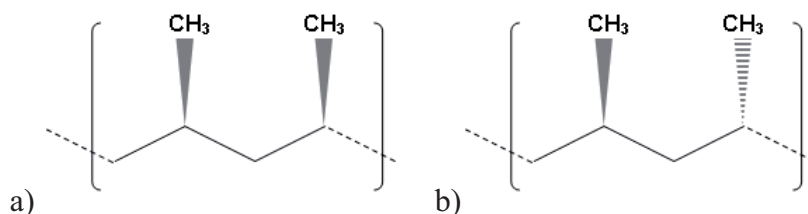

Figure D.1: An example of a) *meso (m)* and b) *racemo (r)* diads in a polypropylene molecule.

In isotactic macromolecules, all the substituents are located on the same side of the backbone, the structure of the polymer is a succession of *meso* diads. Isotactic polymers are usually semicrystalline and often present a helix configuration.

Figure D.2 : Isotactic polymer, succession of *m* diads (triad: *mm*)

In syndiotactic macromolecules, the substituent have alternate positions along the polymeric backbone, it is a succession of *racemo* diads (*rr*)

Figure D.3 : Syndiotactic polymer, succession of *r* diads (triad: *rr*)

On the contrary in atactic polymers, the substituents are randomly placed along the polymer backbone. In this case a percentage of meso triads (*mm*), racemo triads (*rr*) and heterotriads (*rm*) can be measured.

Figure D.4: Atactic polymer, random succession of *mm, rr, rm* triads

Tacticity can be measured using 1H ou 13C NMR (Figure D.5), by integration of the peaks corresponding to the different diads and triads. [7] Other techniques sensitive to tacticity include X-Ray powder diffraction, secondary ion mass spectroscopy[8] (SIMS), FTIR spectroscopy[9]

In our case the PMMA was identified as being atactic by NMR, however the percentage of the different diads was not measured precisely.
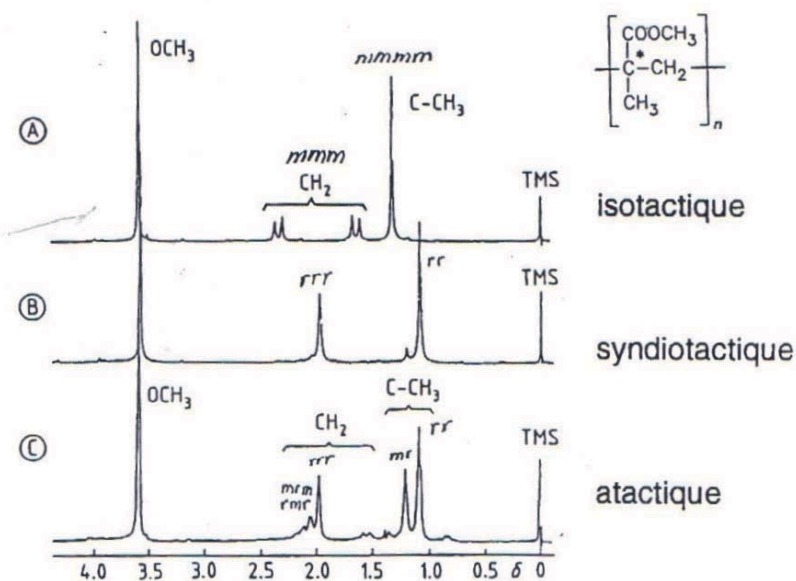

Figure D.5: 1H RMN spectra at 220MHz. Solution of poly(methyl methacrylate) in o-dichlorobenzene at 100°C.

APPENDIX E. PB electrodeposition in ionic liquid

The Prussian Blue electrodeposition is classically performed in water. However, as explained in the manuscript the remaining water (even in a very small amount since the BP films have been thermally treated under vacuum) makes it impossible to use $BMIPF_6$ as electrolyte (formation of HCl). Moreover, the presence of remaining water in the complete device is detrimental for the long term cycling of the devices. The preparation of BP in dry conditions has been tested in collaboration with Solvionic (Toulouse). The first trials consisted in dissolving the classical precursors of PB ($K_3Fe(CN)_6$ et $FeCl_3$ 6 H_2O) in the BMITFSI ionic liquid. This method revealed unproductive, so that special precursors were prepared by Solvionic.

E. 1. First trials with BMITFSI

The first trials consisted in dissolving $K_3Fe(CN)_6$ et $FeCl_3.6$ H_2O in BMITFSI. The solubility of these products is rather low in BMITFSI but a concentration of 10^{-2} M could be attained. However, the mixing of the two solutions led to a green precipitate, probably composed of Berlin green, or mixture of Berlin Green with Prussian Blue (Figure E.1). The heating at 60°C 2h and then 80°C 1h was not efficient to improve the dissolution. In any case, electrodeposition did not work.
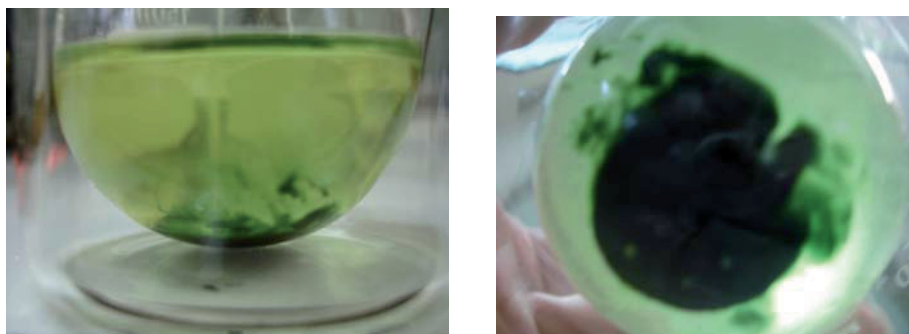

Figure E.1: **Mixture $K_3Fe(CN)_6$ + $FeCl_3.6H_2O$ in BMITFSI**

E. 2. Modification of the precursor by Solvionic

Several routes were tested by Solvionic:

- Preparation of BMIFeCl$_4$ by mixture of BMICl and FeCl$_3$.6H$_2$O : mixture become biphasic (BMIFeCl$_4$ and H$_2$O)

- Preparation of BMIFeCl$_4$ by mixture of BMICl and dry FeCl$_3$: monophasic, dissolution of K$_3$Fe(CN)$_6$ not obtained

- Mixture of BMICl and K$_3$Fe(CN)$_6$:no réaction. Addition of FeCl$_3$: obtention of a blue-green biphasic paste

Electrodeposition from these dispersions were unsuccessful.

Trials of deposition using spin-coating were also unsuccessful, the films prepared are not homogeneous, PB particles are visible on the surface.

Electrochemical bleaching of these inhomogeneous films was not possible, this can be attributed to the fact that PB is not well attached to the electrode but rather present as aggregates
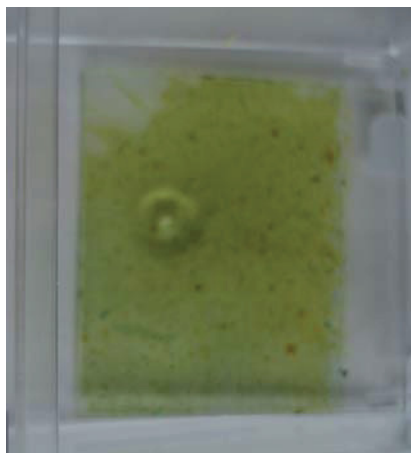

Figure E.2: Example of deposition using spin coating, 1000 pm, 30s.
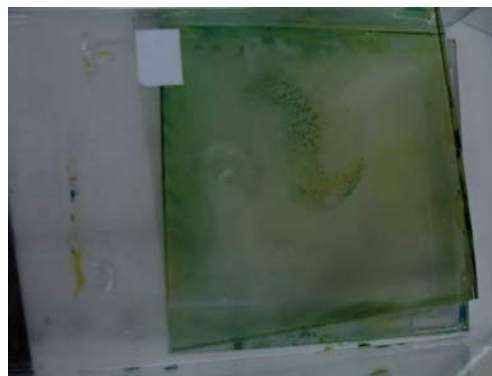

Figure E.3: Unsuccessful trial of electrochemical bleaching (counter-electrode: FTO, pseudo-reference electrode: Ag/AgCl), potential applied up to -2V.

These trials were mostly unsuccessful however, they showed that:

- Possibility to prepare BP particles
- Control of the reaction condition could lead to smaller particles that could be used for example as an ink.

APPENDIX F. Kinetics of the colouration reaction of BP by EIS

Information on the kinetics of the colouration reaction are obtained by Electrochemical Impedance Spectroscopy (EIS). With this method, the inspection of the contributions of charge transfer and diffusion of species phenomena is possible as EIS is able to distinguish phenomena with different kinetic constants. Their dependence upon applied potential is also available showing phenomena occurring at the electrodes and their evolution as the colouration process progresses.

F. 1. Equivalent circuit

EIS can distinguish depending on their time constants the different phenomena occurring at the electrode: charge transfer, diffusion in the liquid, diffusion in the solid.

As compared to the equivalent circuit for an electrolyte between two blocking electrodes that we used for the measurement of ionic conductivity of an electrolyte (cf. part II: Electrolyte); for insertion electrodes, the Randles circuit has to be completed with a term taking into account the diffusion of the species into the film. The equivalent circuit and then the Nyquist diagram are modified. This later consists in a semi-circle, a vertical slope as for blocking electrodes case with an additional slope, with an angle of 45°, called Warburg slope, linked to the diffusion of the species. Depending on the time constant of the several phenomena the position of each element in the Nyquist diagram can move.

F. 2. Experiments

Prussian Blue with a 3 mC/cm² capacity were deposited on FTO/glass via classical electrodeposition. Two Prussian Blue deposited on FTO were placed in a 0.03 LiTFSI/ 0.97 BMITFSI electrolyte, one being the working electrode the other the counter electrode. The pseudo-reference electrode is a Ag/AgCl wire. The impedance is measured at different applied potential with a Voltalab 40. The frequency varies from 100 kHz to 50 mHz.

F. 3. Results

For the PW/PB transition (oxidation of PW) the EIS spectra show two distinguishable shapes depending on the applied potential. It consists in a semi-circle with a vertical slope for potentials in between -600 mV and -200 mV. This is characteristic of a kinetics limited by the charge transfer, the diffusion of the species does not limit the oxidation kinetic. On the other hand, before -600mV and after -200mV and until the end of the transition PW to PB, a Warburg slope appears. This is characteristic of a diffusion phenomenon. The diffusion of the inserted species is only the limiting step when the potential are far from the E_0 potential of the redox couple PB/PW.

In the range of frequency of the Warburg, the slope of the $Im(Z)=f(w^{-1/2})$, is equal to the prefactor A_w, linked to the diffusion coefficient by the formula[10]:

$$A_w(\Omega.s^{-1/2}) = \frac{V_m \, dE/dx}{(2D)^{1/2}.F.S}$$

with V_m the molar volume, $V_{m \, Prussian \, Blue} = 677 \, cm^3/mol$[11], S the geometrical surface in cm², dE/dx (in V) the slope of the electrochemical isotherm for a given x, F=96485 C/mol.

So that :

$$D = \left(\frac{V_m}{\sqrt{2}.F.S} \frac{dE}{dx} \frac{1}{A_w} \right)^2$$

The EIS have been performed on the Prussian Blue films at 3 mC/cm² on FTO/glass. The voltage have been varied from -700 mV to + 250 mV. To calculate dE/dx for the different insertion molar ratio x, the equilibrium potential – composition curve was measured by chronopotentiometry at 1 µA/cm² (Figure F.1).
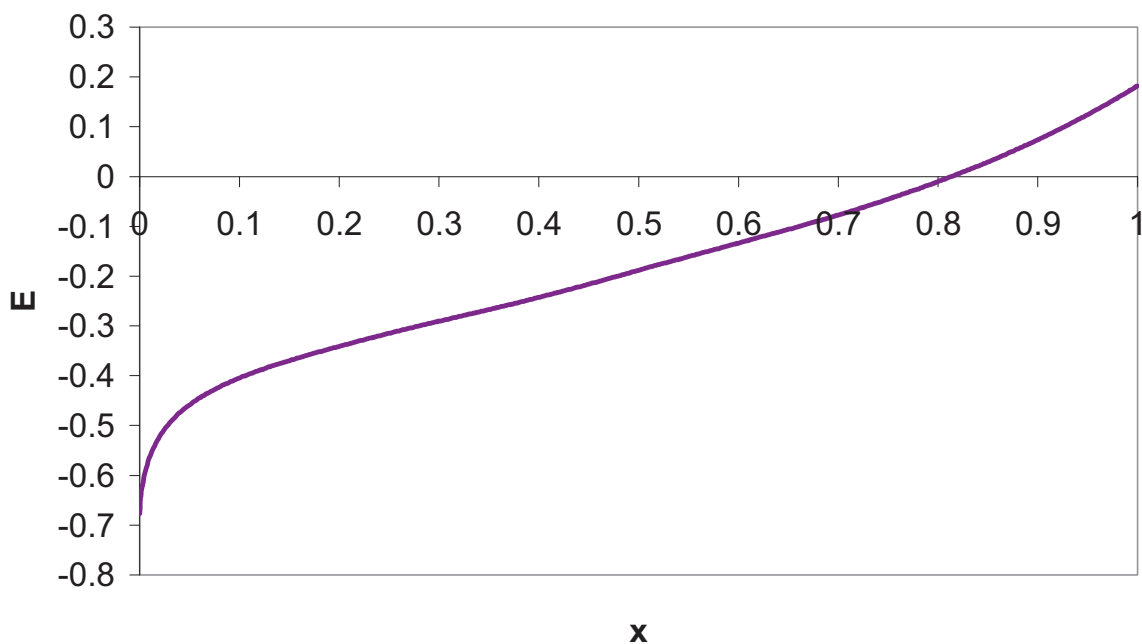
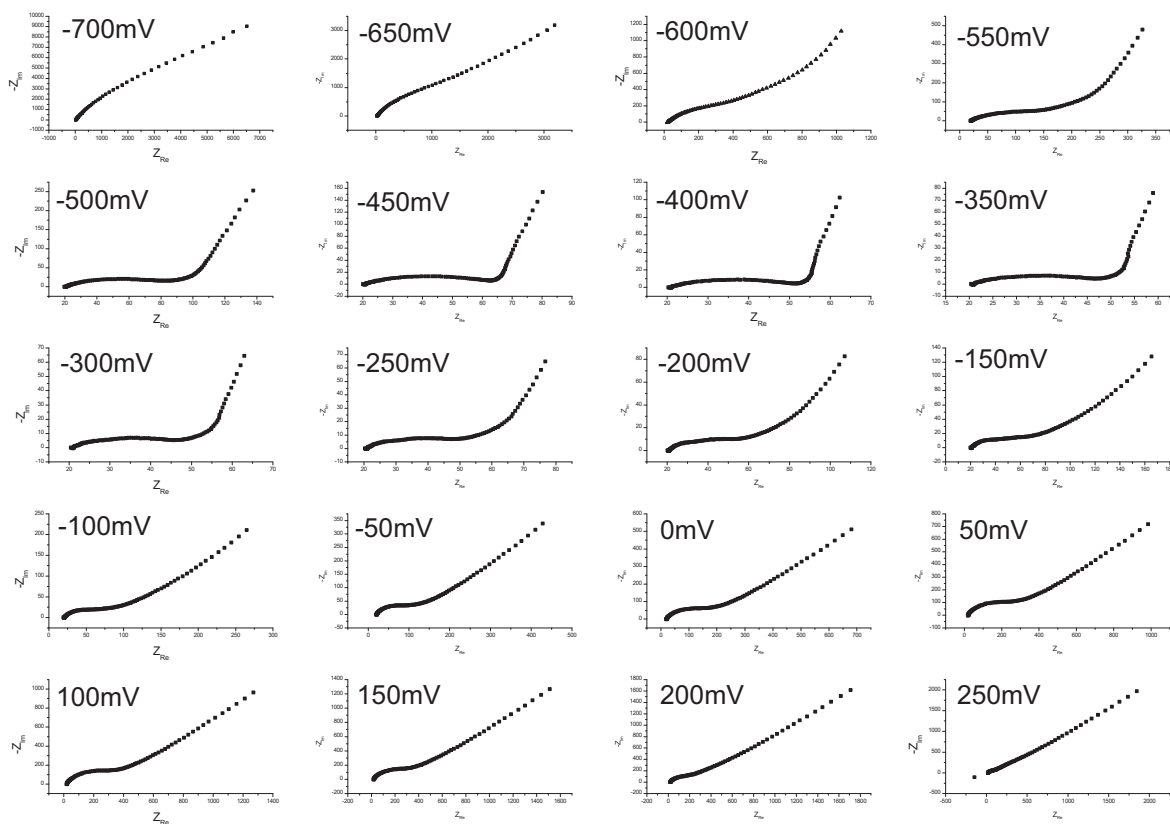Figure F.1: Chronopotentiometric curves for the first oxidation at low current density (1 µA/cm²) of PB 3 mC/cm² in a 0.03 LiTFSI/ 0.97 BMITFSI.

Figure F.2 : EIS spectra of a Prussian Blue film at 3 mC/cm² on a FTO/glass electrode. The potential increases from – 700mV to + 250 mV.

As shown by EIS measurements both electronic transfer and diffusion occur during the colouration of PB. The diffusion phenomenon, characterized by a Warburg slope (45°) appears more clearly when the potential is lower than -600mV or higher -200mV. In these regions the diffusion coefficient in the Prussian Blue material can be measured. The diffusion coefficients are plotted as a function of the applied potential in Figure F.3.
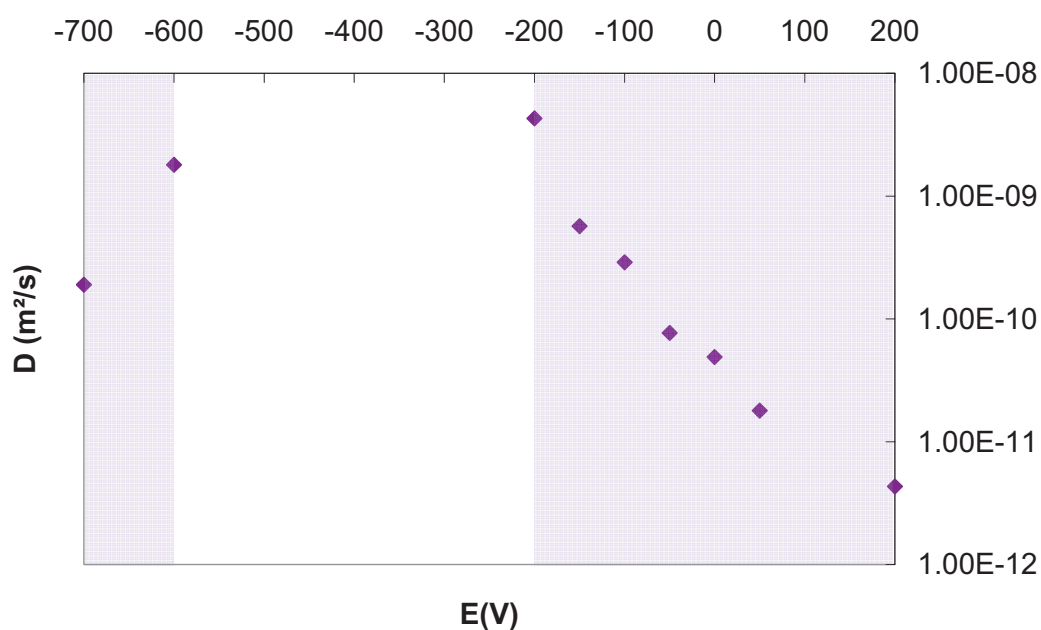

Figure F.3: Diffusion coefficient measured by EIS on a Prussian Blue sample at 3 mC/cm² on FTO/glass in 0.03 LiTFSI / 0.97 BMITFSI electrolyte. The purple zones correspond to the range of potentials for which the EIS spectra show diffusion Warburg slope.

This preliminary study made with Prussian Blue in LiTFSI 0.03 / BMITFSI 0.97 electrolyte shows the potentiality of the EIS method in the study of the diffusion phenomenon within Prussian Blue or its analogues. The measure of the diffusion coefficient in PB when changing the nature of the solvent as well as the nature or concentration of the salt would help to understand the insertion mechanism. For example, we have observed that with BMITFSI alone, the reduction of PB to PW is not reversible; EIS study would be interesting for a better understanding of this phenomenon.

References

[1] H. Gerischer, W. Mehl, Z. *Electrochem.*, **1955**, 59, 1049.

[2] J. L. Weiniger, M. W. Breiter, *J. Electrochem. Soc.*, **1964**, 111, 707.

[3] J. Kärger, Diffusion under confinement, *Sitzungsbericht der Sachsischen Akademie im Hirzel-Verlag*, **2003.**

[4] M. Herstedt, M. Smirnov, P. Johansson, M. Chami, J. Grondin, L. Servant and J. C. Lassègues, *J. Raman Spectrosc.*, **2005**, 36, 762 ;

[5] M. Deepa. et al., *Solid States Ionics*, **2002,** 152-153, 253.

[6] R.J. Young, *Introduction to polymers*, **1991.**

[7] Wu, Ting Kai et al. *Macromolecules* **1977**, *10*, 529.

[8] X. Vanden Eynde et al. *Surf. Interf. Anal.* **1997**, *25*, 41.

[9] J. Dybal, et al. *Macromolecules,* **1990**, *23*, 1301.

[10] S. Franger, S. Bach, J. Farcy, J.-P. Pereira-Ramos, N. Baffier, *Electrochim. Acta* , **2003**, 48, 891.

[11] R. Birdwhistell, *J. Chem. Educ.*, **1992**, 69, 473.

Titre : Etude et mise au point de membranes électrolytiques à base de liquides ioniques pour systèmes électrochromiques flexibles

Résumé :

L'électrochromisme est le changement réversible de couleur d'un matériau lors de son oxydation ou de sa réduction électrochimique. Cette thèse porte sur l'étude d'électrolytes à base de liquide ionique ($BMIPF_6$ et BMITFSI), de sel de lithium (LiTFSI) et de polymère (PMMA) et sur la préparation de systèmes électrochromes à base de ces électrolytes et du PEDOT, du Bleu de Prusse ou d'InHCF comme matériaux électrochromes. La conduction ionique mesurée par EIS, les analyses thermo gravimétriques, les spectroscopies IR et Raman et la mesure des coefficients de diffusion informent sur les interactions entre les espèces dans l'électrolyte. Les matériaux électrochromes (PEDOT, BP, InHCF) sont ensuite étudiés dans un électrolyte modèle LiTFSI 0.03 / BMITFSI 0.97. Enfin, des systèmes électrochromiques flexibles sont réalisés et leur propriétés de coloration et de cyclage étudiées.

Mots clés :

• Electrochromisme   • Liquides ioniques • Electrolyte gélifié • PEDOT • Bleu de Prusse

---

Title : Study and set-up of ionic liquid based electrolytic membranes for flexible electrochromic devices**.**

Abstract :
Electrochromism is the reversible colour change of a material upon electrochemical oxidation or reduction. This thesis will focus on the study of ionic liquid (BMIPF6 and BMITFSI), lithium salt (LiTFSI) and polymer (PMMA) based electrolytes and on the preparation of electrochromic devices with PEDOT, Prussian Blue or one of its analogues InHCF, as electrochromic materials. The measurement of ionic conductivity by EIS, thermo-gravimetric analysis, IR and Raman spectroscopy and measurement of diffusion coefficients of these electrolytes highlight the interactions between the different species of the electrolyte. Electrochromic materials (PEDOT, BP, InHCF) are then studied in a model electrolyte (LiTFSI 0.03 / 0.97 BMITFSI), their electrochromic properties are detailed. Finally, flexible electrochromic devices are made and their properties of colouration and cycling are presented.

Keywords :

• Electrochromism   • Ionic liquid   • Jellified electrolyte   • PEDOT   • Prussian Blue